DEVELOPMENT OF PHOSPHATE BASED BIOACTIVE GLASSES DOPED WITH TRANSITION METAL IONS FOR BONE REGENERATION

THESIS

SUBMITTED IN PARTIAL FULFILMENT OF THE REQUIREMENTS FOR THE AWARD OF THE DEGREE OF

Doctor of Philosophy

IN

PHYSICS

BY

M. MOHAN BABU

(Roll No: 701444)

Under the supervision of

Dr. P. SYAM PRASAD

DEPARTMENT OF PHYSICS
NATIONAL INSTITUTE OF TECHNOLOGY
WARANGAL-506004, (T. S.), INDIA

MARCH – 2020

DECLARATION

This is to declare that the work presented in the thesis entitled **"Development of phosphate based bioactive glasses doped with transition metal ions for bone regeneration"** is a bonafide work done by me under the supervision of **Dr. P. Syam Prasad,** Associate Professor in the Department of Physics and was not submitted elsewhere for the award of any degree.

I declare that this written submission represents my ideas in my own words and where others ideas or words have been included; I have adequately cited and referenced the original sources. I also declare that I have adhered to all principles of academic honesty and integrity and have not misrepresented or fabricated or falsified any idea/data/fact/source in my submission. I understand that any violation of the above will be a cause for disciplinary action by the Institute and can also evoke penal action from the sources which have thus not been properly cited or from whom proper permission has not been taken when needed.

Date: (M. Mohan Babu)

Place: NIT Warangal Roll Number: 701444

NATIONAL INSTITUTE OF TECHNOLOGY, WARANGAL

CERTIFICATE

This is to certify that the work presented in the thesis entitled **"Development of phosphate based bioactive glasses doped with transition metal ions for bone regeneration"** is a bonafide work carried out by **Mr. M. Mohan Babu** under my supervision and was not submitted elsewhere for the award of any degree.

Date:
Place: NIT Warangal

Dr. P. Syam Prasad
Associate Professor
Research supervisor

Acknowledgements

I would like to express my sincere heartfelt gratitude to my research supervisor, Dr. P. Syam Prasad, Associate professor, department of Physics, NIT Warangal for his constructive guidance, relentless encouragement and his love of research motivated me throughout the duration of my research study and moreover for the inspiration he provided to ensure the completion of this work. His expertise, availability to discuss ideas and willingness to give of his knowledge were instrumental. For this, I will be eternally grateful.

I express my sincere thanks to the Director, National Institute of Technology, Warangal, for having given me the opportunity to carry out the work and allowing me to submit the work in the form of thesis.

I express my sincere thanks to CSIR-UGC (JRF), New Delhi for the fellowship support.

I express my sincere thanks to Prof. K. V. G. Reddy, Head, Department of Physics, NITW, for his valuable suggestions and support.

I express my sincere thanks to Former Heads of Department of Physics, NITW, for their valuable help and support.

I sincerely thank members of the Doctorial scrutiny committee Prof. K. V. G. Reddy, Prof. Sonawane Shirish Hari, Dr. P. Abdul Azeem, for their valuable suggestions at every stage of my research work.

I am very much thankful to Dr. Rajendra Kumar Singh for helping me with cell culture studies in his laboratory at the National Research Foundation (NRF) of the Republic of Korea and I am extremely thankful to Dr. Prakash Saudagar and his group for helping me with antibacterial test in the Department of Biotechnology, NIT Warangal for allowing to work in his lab.

I am extremely thankful to Dr. P. Venkateswara Rao, Associate professor, Department of Physics, University of the West Indies, Mona Campus, Jamaica for his continuous support during my entire research work.

I take this opportunity to express my gratitude to Prof. D. Dinakar and Prof. M. Sai Shankar, Prof. Ramana Reddy, Prof. L.R.G. Reddy, Prof. R.L.N Sai Prasad, Dr. B. Sobha, Dr. S. Roy, Dr. K. Thangaraju, Dr. Kusum Kumari, Dr. D. Paul Joseph, Dr. V. Jayalakshmi, Dr.

Haranath, Dr. Rakesh Kumar Department of Physics, National Institute of Technology Warangal for their valuable advice, encouragement and moral support in my career.

I express my thanks to Prof. Raja Vishwanathan NIT Warangal for their help during my research work.

With all happiness I acknowledge the cheerful assistance rendered by all my research colleagues Dr. S. Rajkumar, Dr. V.Himamaheswara Rao, Dr. P.V.N. Kishore, Rama Rajan, Dr. Ashish Kumar, Harikrishna, Gnaneswar, Buchaiah, Purushotham Reddy, and other co-research scholars for their munificent support.

I would also like to thank Mr. Srinivas, Ravinder, Narender and Mrs. Ramya, Technicians, NIT Warangal for their help to record XRD patterns, TG-DTA and SEM-EDX spectra of my samples.

I am happy to express my heartfelt thanks to my friends M.Naresh Kuamr, A. Laxman, K. Anil, B. Raju, J. Bheemaraj, Dr. P. Mahesh, P. Madhukar, P. Rajender, Sruthi Durge, Satyanarayana, for their support and encouragement during the entire course of my research.

I am very thankful to my life partner J. Sumalatha and my brother M. Venkatesh, for their motivation and encouragement. It would not have been possible for me to enter my research journey without their motivation, cooperation and encouragement.

My gratitude goes to my beloved family members who with all their patience, prayers and faith in the almighty, waited all these long years to see me reach this stage. Their blessings and care always gave me fresh energy and gusto to do something more with perfection.

I always remember and cherish the encouragement and inspiration provided by my mother, all my friends and well-wishers during the course of my research work.

Date: **M.MOHAN BABU**

Dedicated to

…..My parents

And

MY Wife

Preface

Bioactive glasses and glass ceramics are most prominent materials for application in the repair and regeneration of damaged soft and hard tissues. These glasses have potential to solve the answer transplantation problems which occurred due to shortage of living tissues and organs available. In general, these bioactive materials undergo specific surface reactions with the tissues and form a HAp layer when implanted into the body. Moreover, this HAp layer is similar to the mineral constituent of bone. This layer acts as an interface and forms a strong bond between the implant and tissue. The thickness and strength of HAp layer depends on the chemical composition of glass matrix chosen. Bioactivity is a measure of the capacity of material to form apatite layer when the material is in contact with physiological body fluid *in vitro*. It is also confirmed from *in vitro* bioactivity that the material can show potential bioactivity *in vivo* environment. The first bioactive glass composition was successfully generated by Larry Hench and his co-workers in the 1970s. Various clinically approved bioactive glasses like 45S5, 58S and some silica based glasses are used effectively for bone and dental applications. Most of the available commercial bioglasses contain high amount of silica. These silica rich glasses have the potential to develop long term implants to replace hard and soft tissues in vivo due to their in soluble nature. However, the long term interaction of silica locally and systemically is not yet understood completely and raises questions about the long-term reaction *in vivo*. Most of the clinical reports established that the glasses with a high amount of silica and high network connectivity were accepted by the human body but the rate of degradation was very low and the glass remnants were present in the patient's body for more than 14 years.

As an alternative to rarely absorb SiO_2 based glasses which rarely absorb for tissue repair, P_2O_5 based glasses were developed by many researchers because of their unusual properties such as lower melting temperature, lower transition temperature, higher thermal expansion coefficient, higher electrical conductivity, higher degradability, higher biocompatibility and lower chemical durability. Among the phosphate based glasses, the calcium containing phosphate glasses shows high bioactivity. Moreover, these glasses are the best suited for bone bonding due to the chemical composition which is very close to the natural bone phase.

Motivation and objectives of the work

In general, phosphate based glasses have poor mechanical strength, high dissolution and poor chemical durability when compared with silicate and borate based glasses, which limits their applications. The control over degradation rate and improvement of mechanical properties can be obtained by adding intermediate network modifiers such as transition metal oxides (Ca^{2+}, Na^{+}, Zn^{2+}, Mg^{2+}, Sr^{2+} and K^{+}). The incorporation of these elements modifies the phosphate network and subsequently affects the degradation properties. The rate of degradation can be selectively controlled by varying the amounts of constituents incorporated into glass.

In view of this, it is proposed to investigate the influence of four transition metal oxides viz., ZnO, TiO_2, Al_2O_3 and ZrO_2 trailed in the calcium phosphate based glass system in order to improve the structural, and mechanical properties along with biological properties such as biocompatibility, bioactivity, cytotoxicity, cell viability and antibacterial activity suitable for the development of novel bone regenerated implant materials.

The main objective of the present study is to develop bioactive glasses by melt quenching technique and study the effect of transition metal oxides (ZnO, TiO_2, Al_2O_3 and ZrO_2) as a replacement for CaO and the resulting impact on structural, physical, mechanical properties and *in vitro* bioactivity, Cell viability and proliferation of $8ZnO–22Na_2O–24CaO–46P_2O_5$ bioglass system for generation of resorbable implant material for bone repair and regeneration applications.

The experimental studies carried out are:

(i) Densities of prepared glasses were measured by employing Archimedes principle using Xylene as an immersion liquid.

(ii) The mechanical properties such as hardness and fracture toughness were measured to know the structural compactness.

(iii) The analysis of various thermal parameters such as glass transition temperature (Tg), crystallization temperature (Tc), melting temperature (Tm), thermal stability (ΔT) and Hruby's criterion (H) of the glass system was carried out to understand the structural transformations at different temperatures.

(iv) XRD study was performed to confirm the amorphous/crystalline nature of the prepared samples as well as the formation hydroxyl apatite layer (HAp) over glass surface post immersion in simulated body fluid (SBF).

(v) FTIR spectroscopic studies were used to investigate the various functional and structural groups in the glass before and after immersion in SBF.

(vi) SEM study was performed to obtain the surface morphology of glass samples and EDS analysis reveals elemental compositions of the glass samples.

(vii) The measurement of weight loss of glasses provides the information about the dissolution kinetics and insight about dissolving a certain amount of glass in SBF solution.

(viii) pH evaluation confirms the suitability for cellular activity and bone formation of the prepared bioglasses.

(ix) The cytocompatibility and cell Proliferation analysis by using *rMSCs* cells provided the *in vitro* biological activity of the bioglass samples before they were tested *in vivo* as bone regenerative implant.

(x) The antibacterial study against *Escherichia coli* (E. coli) and *Staphylococcus aureus* (S. aureus) and *Pseudomonas aeruginosa* (P. aeruginosa*)* bacteria gives the information about the exhibition of antibacterial activity of as-developed glasses.

The research work presented in this thesis is divided into seven chapters and the outline of each chapter is presented below

CHAPTER-I outlines the general introduction, scope and importance of the present work. It comprises in particular of fundamentals of various bioglass materials, importance of phosphate based bioglasses, influence of transition metal ions on the structural, and mechanical properties of such glasses and *in vitro* bioactivity when incorporated to phosphate glass network and a detailed review on previous literature reports suggesting the suitability of phosphate based bioglasses for application in bone regeneration implant applications.

CHAPTER-II describes in detail various methods such as fabrication of transition metal ions doped phosphate bioglasses by melt quenching technique, density by Archimedes method for calculation of various physical parameters, preparation of simulated body fluid (SBF), conditioned media for cell culture and agar diffusion disc method for antibacterial assy. Along with different experimental techniques employed for the characterization of formation of crystalline hydroxyl apatite layer (HCA) on the glass surfaces by XRD, FTIR, SEM-EDS tests, pH, degradation, TG-DTA and vickers micro hardness tests, were employed and are explained in detail. The description of the apparatus used and the detailed principles and procedures of the experimental measurements were also included.

CHAPTER-III reports the synthesis of ZnO incorporated P_2O_5 based bioglasses and also presents the results and discussions on structural, thermal and in vitro bioactivity studies with varying ZnO content in the glass composition. The density and oxygen molar volume are found to increase and the molar volume and oxygen packing density are decreased with increase of ZnO concentration. The increase in density clearly indicates the presence of more ionic nature of P–O–Zn bonds than P–O–P bonds in glass network, which leads to compactness of the glass structure. The glass transition temperature (Tg) increases with increase in content of ZnO up to 8 mol% and then decreases for higher concentration of ZnO. The increase in Tg can be due to increasing aggregation effect of ZnO on the glass network and slow mobility of large Zn^{2+} ions, which lead to more rigidity of glass network. The values of stability (ΔT) increases from 111.26 °C to 121.19 °C and Hruby criterion (H) increases from 0.4319 to 0.5154 with the addition of ZnO, which clearly points to high stability and good glass forming tendency of all glasses. Vickers micro hardness and toughness values of as-prepared bioglasses increase, with increasing ZnO content is due to the expansion of glass network in harmony with increase in the bond length or inter-atomic spacing between the atoms. Zn^{2+} ions enter interstitially in the glass network to form more P–O–Zn linkages by breaking P–O–P bonds. These, in turn reduce the number of nonbridging oxygens (NBO's) and increase cross-linking density, compactness and rigidity of the glass network. In the present as-prepared glasses, Z8 had highest Hv and K_{IC} values. Correlation between the presence of additional intensity reflections from XRD, intensity of absorption bands of FTIR, change in surface morphology of SEM and ratio of Ca and P values from EDS was determined after incubation periods of 3, 7, 14and 21days in SBF, strongly confirming the development of rich HAp layer with incubation time. The addition of ZnO to glass network, enhances the crystallization of the $CaO–P_2O_5$ layer by creating a large number of OH^- ions required for conversion of amorphous layer to crystalline HAp layer through SBF solution as $Zn(OH)_2$. Unlike, previous results on ZnO doped glasses, the present system of glasses were subjected to controlled degradation behaviour and stable pH variation very close to the value of physiological fluid (pH 7.4) with increase in ZnO content and incubation time, which this might be due to a fixed percentage of CaO and the presence of high content of P_2O_5 and is replaced with a small amount of ZnO in the chosen glass matrices. Enhanced cell proliferation and cytocompatibility indicate that release of Zn^{2+} ions was controlled effectively in all glass samples. Superior antibacterial activity is also detected, which is due to synergistic 'contact-killing' effect of Ca^{2+} and Zn^{2+} release. In summary, Zn^{2+} positively affects cellular response and antibacterial activity, providing an attractive bone filler alternative.

CHAPTER-IV presents results and discussions with regard to the influence of structural, mechanical, and biological properties of titanium incorporated zinc phosphate based glasses for orthopaedic implants. The density, glass transition temperature and mechanical strength of the as-developed glasses increase with increase in TiO_2 content which is attributed to cross link densification of glass structure formed by strong P–O–Ti bonds. In vitro studies confirmed the development of rich crystalline HAp layer on samples with incubation time (3, 7, 14 and 21days) and increase in content of TiO_2 by up to 0.6 mol% in SBF. The glass samples became more resistant to hydration, indicating reduced dissolution rate and pH values. Moreover, controlled degradation with increase in Ti^{4+} was observed. The high cell attachments and biocompatibility were noticed by cell proliferation and cytotoxicity tests conducted using CCK-8 method on rMSCs cells. Furthermore, inhibition of bacteria species growth was significant with increase of TiO_2, which confirmed good antibacterial activity of glasses. The results implied that there was no inhibitory effect on HAp layer formation which is useful for generation of new bone tissues. Among all TiO_2 doped samples, 0.6 mol% glass showed highest mechanical strength, controlled pH and degradation behaviour along with *in vitro* bioactivity and is suitable for *in vivo* evaluation for bone resorbable implant development.

CHAPTER-V reports the synthesis and study of aluminum doped phosphate based bioactive glasses and the influence of Al_2O_3 on structural and bioactivity behavior of phosphate glasses. The results showed that the density and micro hardness of glass samples increases with increasing Al_2O_3 content due to strengthening of glass structure by increasing bond strength of P–O–Al ionic linkages. Sample Al10 is showed highest mechanical strength among all samples. The formation of a rich HCA layer on the surfaces of samples immersed in SBF solution enhanced with incubation time and also with the content of Al_2O_3 up to 6 mol% of alumina and then decreased slightly, as confirmed from XRD, FTIR, SEM and EDS analysis, which indicates good bioactivity in as-prepared samples. Besides, the bioactivity is also confirmed by a decrease in pH values and controlled dissolution of bioglasses in SBF with Al_2O_3. Moreover, the HCA layer formed might remain longer time on these phosphate glasses due to controlled decrease in solubility by the inclusion of alumina. The growth of rMSCs cells on glass samples indicates the enhancement in cell viability and cell proliferation. The biocompatibility of Al6 (6 mol% Al_2O_3) is significantly higher compared to remaining glasses. Moreover, it is observed that the rate of cell proliferation of Al6 improved after culturing it for 72h. Out of all samples A6 showed enhanced bioactivity and high mechanical

strength. So the glass sample (6 mol% Al_2O_3) can effectively stimulate bone growth and can also be appropriate for the development of bone repair resorbable implants.

CHAPTER-VI reports the fabrication and study on HAp layer formation, cytocompatibility, *rMSCs* proliferation, structural and mechanical properties influenced by small quantity of ZrO_2 incorporation on $8ZnO–22Na_2O–24CaO–46P_2O_5$ bioglass system. The results obtained revealed that the physical properties such as density and mechanical strength raise with increasing content of ZrO_2, which is attributed to the establishment of new P–O–Zr bonds. The XRD, FTIR, and SEM-EDS results after immersion in SBF for various time periods strongly confirms the development of rich hydroxyapatite layer over the as-synthesised glass surfaces. It is found that layer formation enhances with immersion time and ZrO_2 content also gives up by 0.5 mol%. The controlled degradation rate and stable pH variations showed the release of Ca^{2+} and Zr^{4+} ions required for thick HAp layer. In addition, the growth of rMSCs cells on the surface of all bioactive glasses increases significantly, which shows enhancement in cell proliferation and biocompatibility. Moreover, these glasses cannot exhibit any toxic effects on *rMSCs* cells evaluated by CCK-8 assay. Furthermore, ZrO_2 doped phosphate bioglasses showed better antibacterial effect against three strains *E. coli*, *S.aureus* and *P. aeruginosa* subsequently, among all glasses Zr.5 (0.5 mol% ZrO_2) bioactive glass is owing to enhanced bioactivity with better mechanical strength and antibacterial activity; hence this would be suitable for development of clinical implants.

CHAPTER VII presents a brief summary and conclusions drawn from investigations carried out on structural, thermal, and mechanical properties, degradation behaviour, pH evaluation and biological properties such as cytocompatibility, cell proliferation and antibacterial activity on calcium phosphate glasses doped with transition metal oxides ZnO, TiO_2, Al_2O_3 and ZrO_2.

Table of Contents

List of Table

List of Figures

List of Abbreviations

Abbreviation	Description
HAp	Hydroxyapatite
HBP	Human Blood plasma
SBF	Simulated Body Fluid
HCA	Carbonated Hydroxyapatite
XRD	X-Ray Diffraction
FTIR	Fourier Transform Infrared
KBr	Infrared grade-Potassium bromide
SEM	Scanning Electron Microscopy
EDS	Energy Dispersive X-Ray Spectroscopy
DTA	Differential thermal analysis
TG	Thermo Gravimetric
rMSC	Rat mesenchymal stem cell
CCK-8	Cell counting kit
α-(MEM)	Minimum essential medium
E. coli	Escherichia coli
S. aureus	Staphylococcus aureus
P. aeruginosa	Pseudomonas aeruginosa
OD	Optical density
Hv	Vickers hardness
K_{IC}	Fracture toughness
ΔT	Thermal stability
Tg	Glass transition temperature
Tc	Crystallization temperature
Tm	Melting temperatures
H	Hruby's criterion

Chapter - 1

Introduction and Review of Literature

In this chapter, an introduction to biomaterials, and defining their necessary and scope, along with the aim of the current work, has been presented. In particular, the features of bioactive materials, bioactive glass, and structure of glass, mechanism of bioactivity and physico-chemical and biological properties of such materials have been described. Several clinical applications of in vitro bioactivity and bioglasses have also been discussed, along with insights into the category of phosphate glasses, a detailed literature review of which takes care of the nuances of the field of study. The main objectives and outcomes of the current thesis are also given at the end of this chapter.

1. Introduction

Bioactive materials typically need to be biomimetic, eliciting a distinct biological response, thanks to their specific interaction with biological matrices and cell/tissue micro environments. These materials are used to support or fully capture the working of living tissues in the human body and also suitable to replace damaged or dysfunctional tissues and organs, partially or completely either natural (biopolymers like chitosan, alginate, hyaluronic acid, etc., proteins like collagen and fibrin, complete matrices like bovine bone mineral matrix) or synthetic (polymers, ceramics, metals and composites), based on the starting materials that are used for their synthesis and characterization. According to materials science, a biomaterial is an essential material possessing highly desirable characteristics such as biocompatibility, bioactivity, biodegradation and sufficient mechanical strength (for being relevant in biomedical areas to possess, for instance, osteoconduction/osteogenesis ability). In other words, biomaterials are defined as natural or artificial substances [1-4]. The basic requirements for potential biomaterials suitable for various biomedical applications are shown in Fig.1.1.

Considerable research has been conducted already over the past two decades to modulate existing materials for medical applications and the development of novel materials. The success of biomaterials in healthcare applications is absolute and is based on biocompatibility, immunological reactions, host response and cell biomaterial interaction [5]. In addition, these materials are necessary for the body to be compatible with their behavior in different cases. It is well known that these organs and tissues have improved greatly the quality of life over the past 50 years and prolonged the average life span significantly, which has led to increased interest in biomaterials research [6,7]. Moreover, it is very essential to know the structure, functions and various properties of biomaterials, in order to enhance the quality of human health by re-establishing the function of bodily active tissues and organs. Thus, the subject of biomaterials can be divided into three aspects of biologically active materials, implants, and their interactions with the human body [8]. Over the past few decades, there has been a lot of innovative efforts from molecular chemistry and biology, to understand basic concepts such as breakthrough kinetics, bio accessibility and synthesis techniques to develop potential biomaterials [9,10], which has been very promising in the field of biomaterials and biomedical engineering. Later, in the 1980s and 1990s, researchers focused on the various bioactive materials development that could induce an appropriate biological response, particularly at the interface of host tissue and biomaterials.

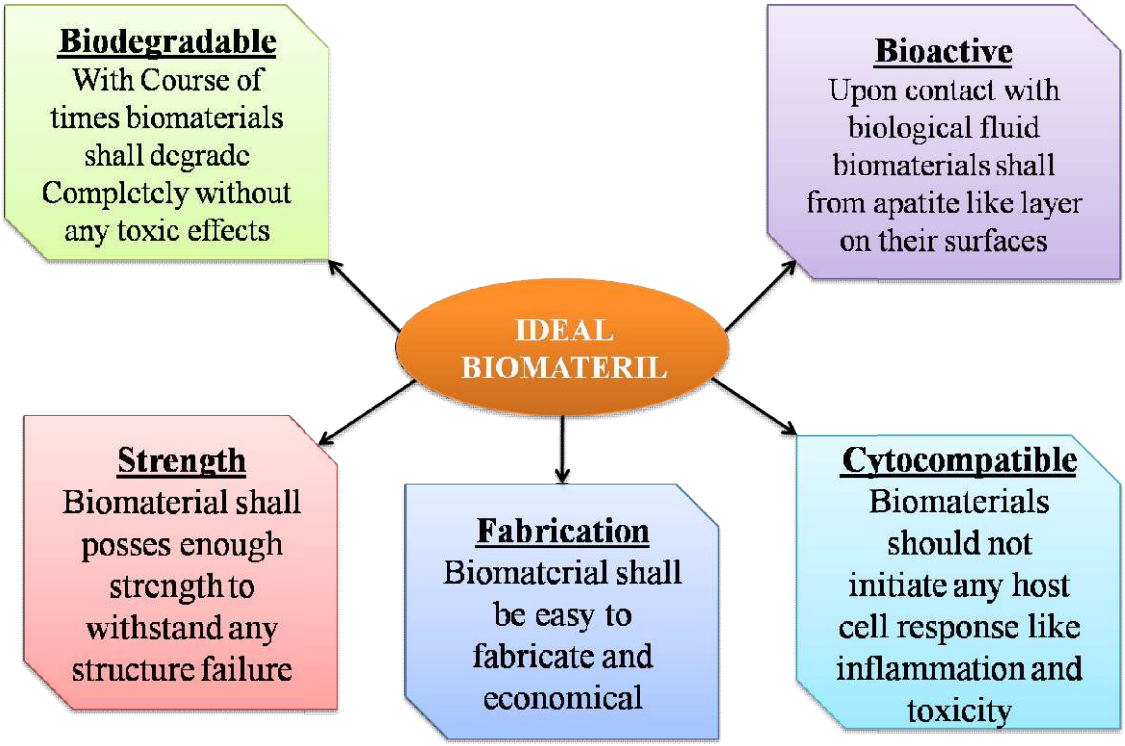

Fig. 1.1 Requirements of potential biomaterials (Kaur, 2017)

Biomaterials are usually attached to host tissues by interfacial bonding or bioactive fixation [11,12]. Bioactive bonding is due to chemical reactions between the interface of the bioactive material and human tissues, including the liquid connective tissue, namely blood. These chemical reactions cause strong bonds between implants and the host tissues. Bone regeneration and tissue reactivity success of bioactive materials depend on their behavior in biological systems and attachment to the surrounding tissues. Bioactive systems, resulting from biomaterials response, can be classified based on their tissue attachment, such as being resorbable, bioactive, porous, or inert; the description and examples of this are précised in Table 1. [11,12].

Biomaterials science is an interdisciplinary area that draws heavily on concepts and inspiration from many branches of science, including biology, chemistry, materials, mechanical engineering and medicine. Biomaterials have been developed for a wide range of use in the medical field, which in turn, requires a comprehensive understanding of the above disciplines. There are three major categories of materials in this field, classified as first, second and third-generation biomaterials, in relation to the period of their development [11,12].

Table 1. Types of tissue attachment of biomaterials

Type of implant	Type of attachment	Example
Resorbable	Replacement with tissues	Tricalciumphosphate, Polylactic acid (PLA)
Bioactive	Interfacial bonding with Tissues (bioactive fixation)	Bioactive glasses, HA, bioactive glass-ceramics
Porous	In-growth of tissues into pores (biological fixation)	Hydroxyapatite (HA), HA coated porous metals
Inert	Mechanical interlock (Morphological fixation)	Metals, alumina, Zirconia, Polyethylene (PE)

1.1 Classification of biomaterial systems

Bioactive systems can be defined as a specific biological response process that leads to the bond between tissue and matter. This has led to the development of materials that can interact with the body to stimulate the desired response from the body tissues. In research on bioglass, the dissolution of materials and the formation of HAp membranes are commonly used as a common indicator of bioactivity of bioglass in the case of *in vitro* assays. The response of the biological system, particularly cell proliferation and growth, is commonly used as an indicator to the extent of bioactivity of bioglass in the case of *in vivo* assays.

1.1.1 Bioinert materials

Bioinert materials belong to first-generation bioceramics and have those characteristic symptoms that the body accepts with minimal interaction with the physical environment. Bioinert systems have no adverse effect on the implant environment, but they fail to stimulate effective biological processes, like osteogenesis, osteoinduction and osteoconduction. Bioinert materials made of metals such as zirconium, aluminium, stainless steel and polymer such as polyethylene fall into this category, possessing abrasion resistance and used mainly for dental and orthopaedic applications [13,14].

1.1.2 Bioactive materials

These come under the second generation of bioceramics and are defined as the formation of bioactive bonding those results due to chemical reactions between the interface of the bioactive material and human tissues. The bone-like membrane and the material made of hydroxyapatite (HAp) exhibit rapid reactions that lead to good chemical bonding. These

chemical reactions cause strong interfacial bonds between the implants and the tissue [15]. These materials are designed to attach themselves to living tissues by forming chemical and biological bonds in the premature stages of implantation. Bone regeneration and tissue reactivity success of bioactive systems depend on their behavior and attachment to surrounding tissues. Bioactive glasses and bioactive glass ceramics are examples of bioactive materials. Fig. 1.2 shows the applications of bioglass/ceramics within the human body and their biomedical importance [8]. For the moment, with regard to amorphous bioactive materials, silicate-based glasses have become increasingly popular with enhanced interactions with hard bone and soft neighbouring tissues [6,16].

1.1.3 Bioresorbable materials

The third generation of biomaterials is defined by their special properties in replacing damaged tissue with fresh healthy tissue. Given a chance that such materials enter the living organism, they gradually disappear over time in the biological system. Some examples of resorbable biomaterials such as tricalcium phosphate ($Ca_3(PO_4)_2$) and Polylactic acid $(C_3H_4O_2)_n$ (with degradable, resorbable and absorbable properties). These materials enter into the body slowly and steadily, before they finally disappear, when they are replaced by completely new tissues. Moreover, these materials can be replaced by bone and tissue cells for an explicit period of time by reacting and dissolving in the bodily fluid [17].

1.1.4 Porous materials

Porous bioactive systems are better than inert bioactive materials due to their biological fixation to tissues through the pores. Pores are very helpful in the growth of veins and tissues inside the implant, through which nutrition can also be sent to the cells. Examples are aluminium implant for hip replacement and hydroxyapatite (HAp) coated metallic implants. In this case, mechanical bonding is obtained by bone growth in the pores, which have diameters >100 μm [18]. An increased interfacial region interaction among the implants and then an increase in resistance of the tissues to the movement of the device mark their characteristic mode of action. Their mechanical strength is not the same as that of bulk materials. However, porous materials do not last long after implantation. Due to corrosion, exposure of a large surface area to body fluids further reduces their strength, thereby affecting the properties of bioactive systems. Biomaterials impact human lives through a multitude of applications, thus promising a bright future for the field. There are a number of pharmacies and manufacturing companies investing in the production, enlargement, and commercialization of new biomaterial products. Nowadays, the field of biomaterials has

rapidly evolved for coming up with various biomedical applications. This includes cases where the biomaterials have already opened a large range of medical equipment for skin, bone and dental repair, artificial arteries, organ replacement, nerve conduction tubes, mechanical heart valves, stents and pacemakers, and orthopaedics in addition to tissue engineering applications, all of which improve the quality of human life worldwide [8,19-21]. Such materials must be capable of eliciting a suitable host tissue response in a particular situation and is considered one of the most prominent features of biomaterials, which is biocompatibility. A biocompatible material must have at least an immune response and had better not interfere with blood flow [22].

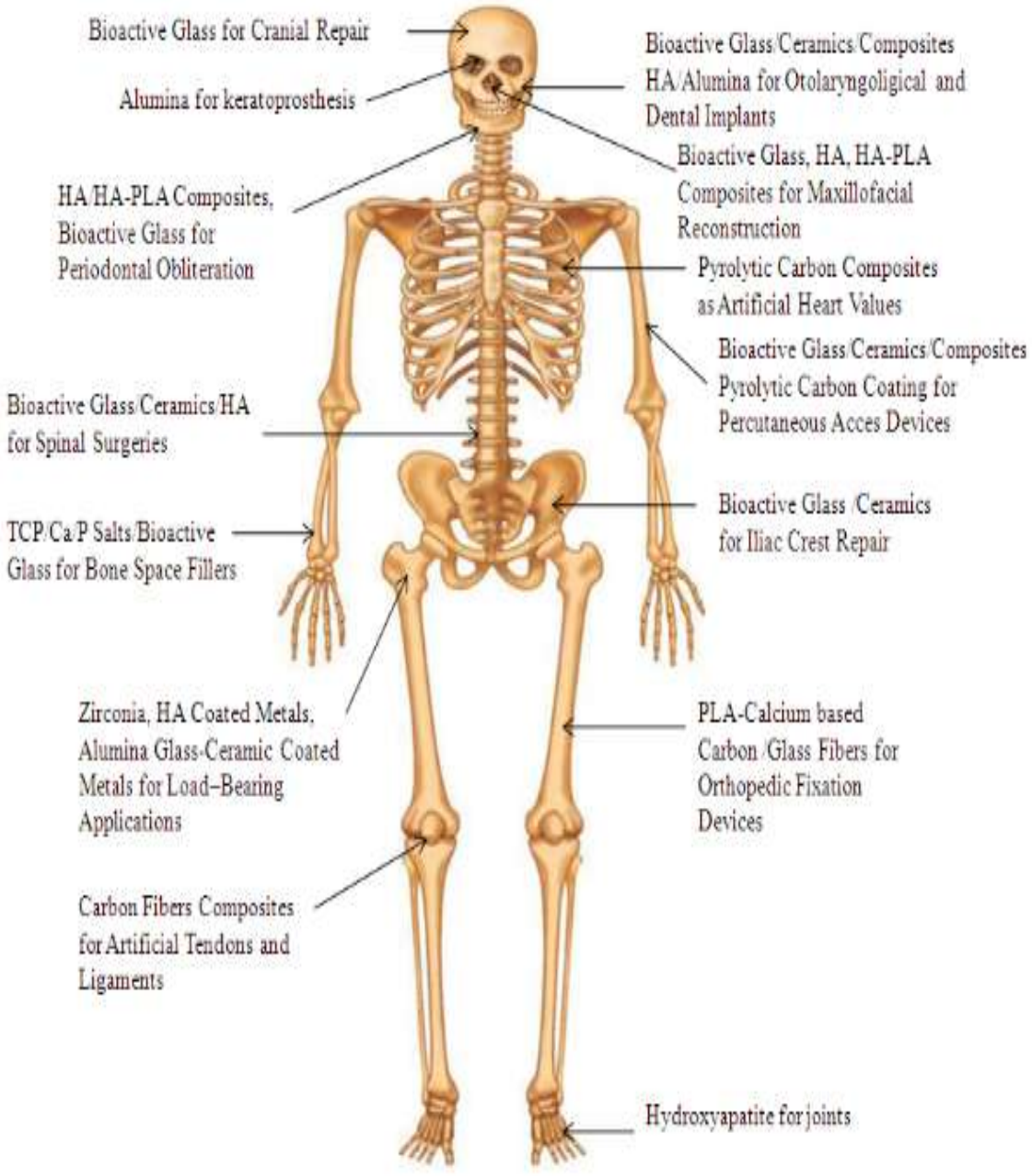

Fig. 1.2 Applications of various bioactive materials within the human body (Kaur, 2017)

1.2 Bioactive glasses

Bioactive glasses are a special type of biomaterials which offer specific biological actions and precise surface reactions once they come into contact with body tissues. The necessity for the development of novel bioactive materials with extraordinary properties has guided research in the area of bioactive glass fabrication. Bioglasses promise better benefits over conventional biomaterials and find use in tissue engineering, such as grafting, augmentation, repair and regeneration of both hard and soft bone tissues etc., and these applications are possible because of their outstanding properties: resorbable, osteoproductive, osteoconductive and osteoinductive behavior [23]. These glasses release ions into the local environment, thereby initiating a variety of biological responses [24]. Silicate based bioglasses are the most appropriate bioactive glass materials, that are extensively employed in non-load bearing applications and are likely to form these tissues with explicit clinical features, primarily for tissue regeneration applications [16,24].

L.L. Hench et al., developed the first bioglass (45S5), which is a SiO_2 based bioactive glass [6] and this comes under the category of second-generation biomaterials, it shows the formation of bone-like apatite layer at the implant of tissue interface [25]. The Hench bioglass is composed of various oxide materials in weight percent of 45% SiO_2, 24.5% Na_2O, 24.5% CaO and 6% P_2O_5. The capacity of the bioglass to form thin hydroxyapatite (HAp) over the surface when immersed in simulated body fluid (SBF) is often considered a sign of its bioactivity [26]. *In vitro* bioactivity is presumed to be an indication of the bioactive potential of materials *in vivo* [27]. The bioactivity rate of bioglass varies, depending on the surface properties of bioglass containing chemical components proportions and makes it easier for the tissue to absorb any biomaterials in several ways [6,28] and the molecular proportions of the calcium and phosphorous oxides are almost similar in all constituents in the bones. Fig. 1.3 shows the phase diagram representing different glass-forming regions.

Bioglass shows high levels of bioactivity in the middle region (region A) named the border of bioactive bone-bonding. The constituent properties of bioglass form a rapid bond with the bone and it simultaneously interact with collagen, thereby bonding with soft tissues [12,29]. In C region, bioglass becomes a recyclable element so that they disappear in the body in about a month. Due to technical limitations, bioglass has never been fitted in D region. Bioactive glasses are highly promising biomaterials and show excellent bioactivity and biocompatibility when interacting with bone and tissue by forming a HAp membrane potential at the interface of the material [6]. This high reactivity is their main advantage for

applications in periodontal repair and bone strengthening. Bioactivity is examined by studying the formation of rich Ca and P layer by soaking the glasses in different SBF solutions.

Since 1969, the domain of bioactive glasses is slowly evolving and has become a landmark in tissue engineering and regenerative medicine. Many researchers and scientists are involved in the research and development of a variety of glass systems for biomedical applications. A glass always has been at the center of some significant innovations that have led to a revolution in various aspects of human life.

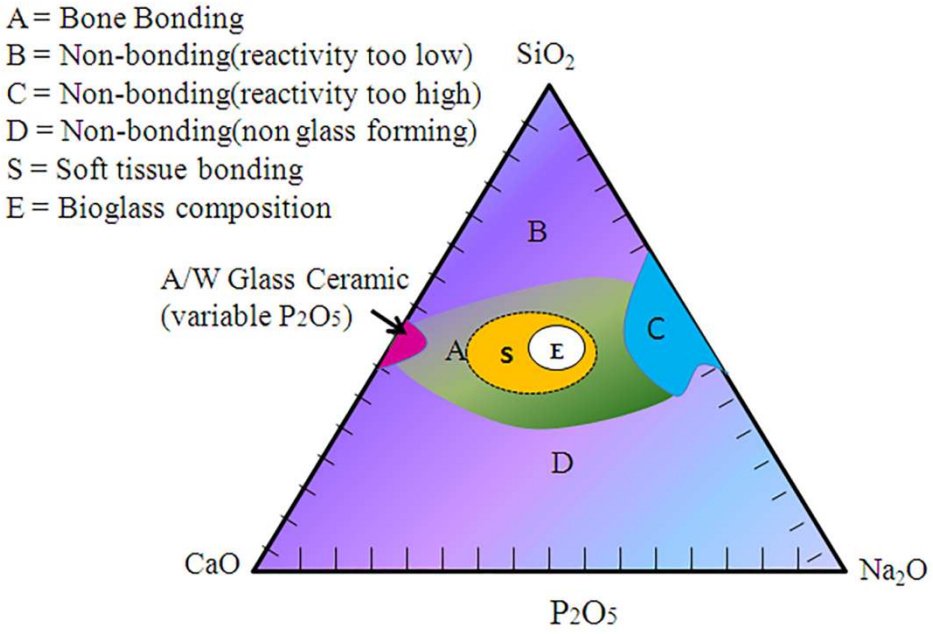

Fig. 1.3 The glass-forming region by phase diagram (L. L. Hench, 1998).

The special focuses on the development of various bioglasses and their glass-ceramics have been received due to the unique characteristic features.

The rapid surface reaction characteristic of bioglass leads to direct attachment to tissues to form a strong chemical bond [30].

(i) The glasses have comparatively low softening temperatures, which is an added advantage considering that ceramic particles can be easily bonded while filling micropores is also easily achieved during sintering.

(ii) The properties can be easily altered by making glass composition suitable for medical applications.

(iii) They exercise great control over chemical and biological bonding reactions with tissues [31].

In recent years, bioactive glass is a novel material that opens up a new research area in natural sciences and medicine, in view of their ability to react with host tissues and promote a

strong bonding, chemically at the interface to the natural bone. The ability to form a tight chemical bond with the living bone is a result of modification of the surfaces comprising precipitation of calcium and phosphorous rich layer. The human bone is made of composite minerals, namely collagen and calcium phosphate. The calcium phosphate-containing carbonate is the major constituent, while magnesium (Mg), sodium (Na), fluoride (F) and other trace elements are minor constituents present in the bone minerals.

1.3 The use of glass as bioactive material

The term "glass" evokes different meanings and images in different parts of the globe. According to the Indo - European base, the word glass refers to any object that is shining, glowing, or glazing while glass is also known as *vitreous*, which is a Latin term. It is defined as "an inorganic product of fusion which has been cooled to a rigid condition without crystallizing," to use the definition given by the American Society for Testing Materials (ASTM) data base [32].

The origin of the discovery of the glass remains unclear, but it needs emphasizing that glass was among the first materials synthesized by mankind several thousand years ago. It was long before glass became an object of scientific research. This was in 1830 that the properties of glass were studied by Faraday. Glasses are produced from melting raw materials, this having been the process for thousands of years. Ancient glass objects made by mankind were discovered at the time of excavation in Egypt and are dated approximately 3000 BC [33,34]. The methods employed for the manufacture of glass had already been known to Mesopotamians by 4500 BC [33]. The structure of glass can best be described as a continuous random network. Glasses can be designed in a variety of shapes and sizes with a great homogeneity, from miniature and delicate fibers of huge glass-lined reactors and equipment. Ancient civilizations in Egypt, China, and India made use of biomaterials for reconstructing damaged body parts. Glass materials present several benefits over crystalline materials in that they boast unique structure and have desirable thermodynamic features. Innovative categories of bioglass have been identified and these play a very restorative role in medicine (biomaterials), energy conversion and in plenty of other fields [37]. Glass science thus embraces a range of features seen as desirable in material science, thereby demanding extensive knowledge in various fields of physics, chemistry and mechanics for any potential researcher.

Glass is an amorphous material, that is, a non-crystalline solid that shows transformation behavior. A glass can thus be defined as "an amorphous material with no long-range order of atoms, lacking periodic atomic structure and exhibiting a region of glass transformation behavior" [34,35] as shown in Fig.1.4. These glass manners are in the temperature range and it is also called the transition region of the glass. Any materials, inorganic, organic, or metallic, formed by any technique, which exhibits glass transformation behavior is a glass.

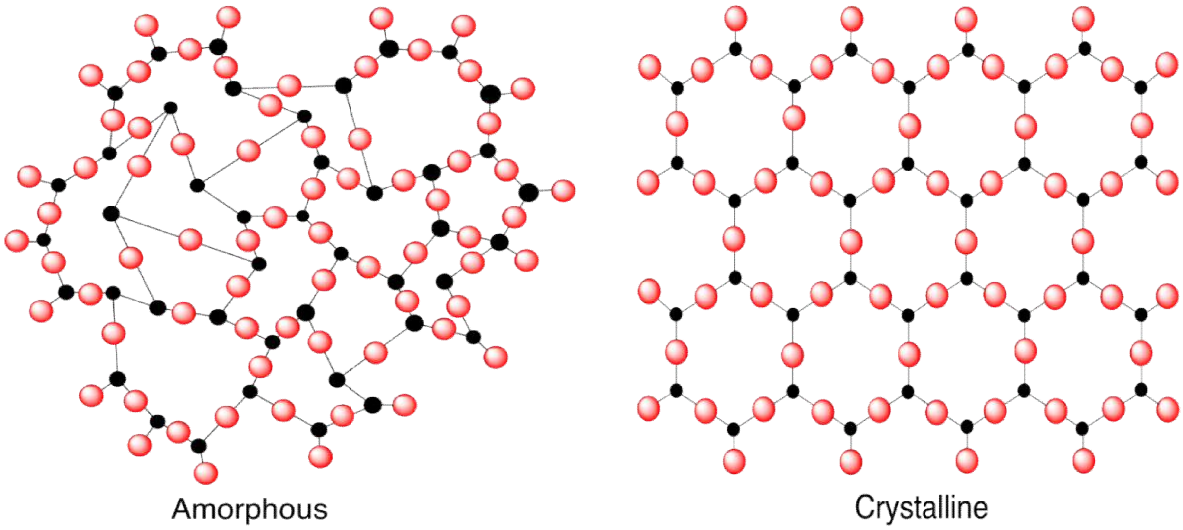

Fig. 1.4 Schematic representation of the amorphous and crystalline nature of glass materials in two-dimensional.

There are major processes involved in producing glass: the melting quenching technique and the sol-gel process. Glass is essentially non-crystalline material generated from a super-cooled liquid, i.e. the disordered structure of the liquid freezes into solid on account of drastically rapid cooling (or quenching). In this transformation, the fluid properties gradually become solid-state properties. Glass is readily one of the most flexible, easy to use and versatile materials, making it a point to retain all properties together. The current research is particularly relevant in the field of telecommunication and biomedical applications.

The melt that can form a glass maintains its liquid-like structure as a super cooled liquid under the melting point of the crystal, then becoming a brittle, and then elastic glass upon further cooling. The transformation of the glass-forming and melting process is illustrated in Fig.1.5. Traditionally glass transformation behavior is discussed based on enthalpy or through volume versus temperature representations.

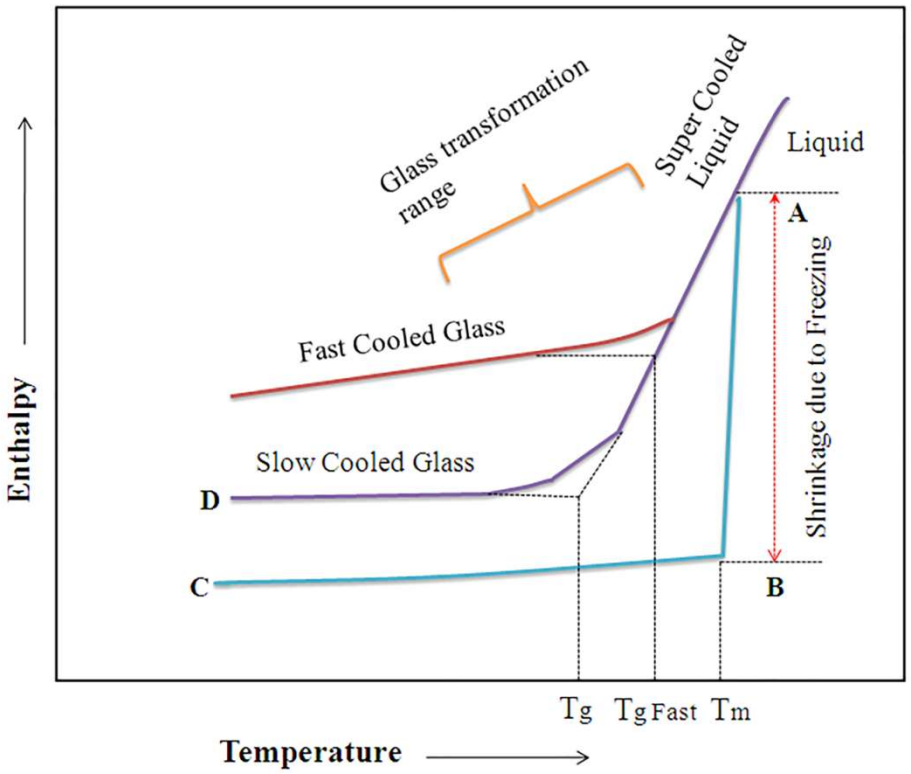

Fig. 1.5 The schematic diagram shows changes related to heating and cooling in the system responsible for the formation of glass.

Glass transformation temperature is usually measured through graphs recorded in thermal analysis or the dilatometer of the glasses. The transition of glass specimen from viscous melt to frozen bulk glass is labelled "glass transition" where the concomitant temperature may be regarded as "glass transition temperature (Tg)". The reversible action, from a bulk glass of liquid melt takes place when a glass is heated to a temperature beyond that of Tg. The transition is on account of an increase in viscosity of liquid melt where it changes depending on the cooling rate of the liquid melt. Therefore, even if the chemical composition is the same, the Tg of glass varies with the cooling rate of the melt. The variation in temperature and enthalpy which illustrates cooling behavior at the time of formation of the glass from liquid to bulk sample is shown in Fig. 1.5. When a substance in a molten state at a temperature higher than its melting temperature (Tm) is cooled below Tm, the atomic structure of the melt reports a change.

The usual slow cooling of a substance from its molten temperature to a temperature lower than the melting temperature permits the atoms to arrange themselves in a long-range periodic order, resulting in the conversion of the material into a crystalline state. Enthalpy changes abruptly as shown in Fig. 1.5. Where with any further cooling, enthalpy registers decrease because of the heat capacity of the crystal. However, if the liquid is cooled at a rate

faster than the melting temperature such that it attains a temperature below melting temperature, avoiding crystallization, a super cooled liquid is formed and on further cooling, the atoms continue to rearrange themselves. Viscosity reports a gradual increase and soon after becoming too large to allow complete arrangement for a stable liquid structure.

1.4 Types of bioactive glasses

Over the past four decades, the main challenges of bioglass tissue engineering are related to the design and development of materials and their bioresorbability after handling their function, so that the tissue can be rebuilt to its natural form. Therein lies our main concern regarding the systematic study of bioactive glass. There has been great research to develop silicate, borate, and phosphate bioactive glasses for biomedical applications. During the process, trace elements are added to obtain the desired properties in the glass matrix. From the compositional aspect of glasses, the chemical composition is chosen depending on the glass making process and the required application of the prepared glass. Some of the reported bioactive glasses and their structural components are described as follows. This chapter describes the basic structural arrangements of three groups of glasses used as biomaterials: silicate glasses, phosphate glasses, and borate glasses, and structural variations control the properties of glass.

1.4.1 Silicate bioactive glass

Bioactive Glass, designated as 45S5, is the most widely investigated glass for biomedical applications. Silica-based bioactive glasses are used in various forms and for a variety of clinical applications [36,6]. Silicon plays an important role in bone mineralization along with gene activation. The first man-made biomaterial silicate glass, 45S5 was found in 1969. The composition of the original bioglass (45S5) is as follows: 45% SiO_2, 24.5% CaO, 24.5% Na_2O, and 6% P_2O_5. SiO_2 is the main content and glass-forming agent in these glasses (L.L.Hench et al.,1969s). Similarly, L.L.Hench et al. found that some glasses are biocompatible and show bone-binding ability. Silica-based (45S5) composition enhances the secretion of vascular endothelial growth factor *in vitro*. Hydroxyapatite is believed to be the best biocompatible replacement material for biomedical applications. Silica-glass is used as a host material, combining calcium and phosphorus to fix broken bones. The literature has reported on two different compositions of bioactive glasses [37], namely melt-derived (45S5) and sol-gel derived (58S) bioglasses. Dissolved-derivative bioglasses show far lower surface area compared to sol-gel derived bioglasses, as reported in *in-vitro* dissolution of both 45S5 and 58S bioglasses [37]. Based on bioactive studies conducted at SBF, reactive oxide on these

bioglass surfaces encourage bioactivity to form strong bonds with living bone tissue. The peculiarity of bioactive glass is that the major part of the bone is hydroxyapatite (HAp) or $Ca_{10}(PO_4)_6(OH)_2$, *in vivo;* with simulated body fluid [38] it gets formed on the glass surface when in contact with the body fluid (SBF) *in vitro* [39,40]. The ionic and covalent property of the Si–O and Si–O–Si bond is preferred for the formation of $(SiO_4)^{4-}$ tetrahedron in both crystalline and glass silica. The substitution of silicon for synthetic hydroxyapatite is underway in several research groups. Furthermore, they concluded that 45S5 bioactive glass composition has the potential to form new bone tissue. In various *in vitro* analysis, they briefly described the reasons for the presence of carbonated hydroxyapatite phase on the 45S5 bioactive glass surfaces [39,40].

1.4.2 Borate bioactive glass

Borate-based glasses have been fabricated to answer the needs of a variety of scientific and engineering applications. In the borate glass system, the melting of the composition rich in B_2O_3 shows high viscosity and a conspicuous tendency for the formation of glass. Since the invention of glasses, borate-based glasses have been very useful for optical and engineering applications. Recent researches [41,42] have amply proved that silica free alkaline borate glasses also exhibit bioactive behavior. Day et al., explored in 2003 [42] and then studied in depth the characteristic features of borate glasses for possible use in biomedical applications [43,44].

For the past two decades, borate glasses have been used in medical applications as bioactive implant material [45]. It has been recognized that borate-based glasses are important ingredients in the healing of chronic wounds. Though borate-based glasses are useful biological materials, few reports are available in the literature [46-49] which detail their numerous advantages. The borate equivalents of silicate-based bioglasses can be rapidly converted to HAp. Manupriya et al. studied the *in vitro* bioactivity and degradation of soda-lime borate glasses immersed in simulated body fluid [49]. The possible bioactivity of borate glasses, because of the low chemical durability, and the modified soda lime silicate becomes faster and more fully hydroxyapatite than L.Hench patent bioglass (45S5) when kept in a diluted potassium phosphate solution instead of SBF. These glasses have been revealed to serve as a substrate for release in the treatment of bone infection [50,51]. Boron plays a potential stimulating agent for bone tissue engineering [52]. Moreover, borate glasses intended for use as implant materials in the human body and attached to living tissues must have reasonable solubility. This is because of the main structural unit of the borate network

(BO_3) is the chains of trihedron or BO_3 triangles [53]. They cannot form a fully three-dimensional structure, and as a result, [BO_3] has a lower cross-linking density.

1.4.3 Phosphate bioactive glass

Phosphate-based glasses happen to be inorganic polymers based on tetrahedral phosphate ion, which form a link to generate a three-dimensional network [54]. In other words, Phosphate glasses have a simple tetrahedral structure, similar to a polymer-based on [PO_4] groups, whose structure is usually described using Q^n terminology, where n represents the number of oxygen atoms that bridge the [PO_4] tetrahedron [54,63,64]. This Q^n terminology is developed for silicate-based glass. The same principle applies to phosphates, but here the bridge to tetrahedron represents the number of oxygen atoms [55]. The presence of any particular Q^n species depends on the cation constitution in the glass composition. The three-dimensional network (Q^3) species are the only phosphate group in the phosphate network that boasts high link, due to the conversion of Q^3 into Q^2 species when adding metallic cations such as Li^+, Na^+ and K^+ [54]. The equivalent of concentrated ions as cations is Q^2 species and is named meta-phosphate composition [56]. Since this ion forms only on oxygen bridges, it is known as a chain terminator, which produces just phosphate dimers or pyrophosphate, which is the only species present, and the number of ions changes to Q^1 when increasing the number of cations to Q^0 species and orthophosphate [56]. Considering that the primary component of phosphate-based glasses are very hygroscopic, the presence of low amounts of water promotes its crystallization [57]. As mentioned earlier, phosphate-based glasses can completely dissolve in aqueous media and offer real benefits for various biomedical applications.

Phosphate glass has been investigated for more than one hundred and fifty years [58,59]. These glasses display very high transmission in the ultraviolet region, low thermo physical coefficient, and large emissions compared to silicate glasses [58,59]. Although P_2O_5 is one among four classic Zachariasen glass-forming oxides, the nature of glass, applications, research, and development happens to be limited thanks to its hygroscopic nature [59,60]. Phosphate glasses are attractive because of their low melting temperature, low viscosity, and high thermal expansion coefficient [59]. Phosphate glass materials have the potential to be used as biomaterials because their chemical composition is close to that of the bone [61]. Kasuga et al., [62] reported calcium phosphate glass materials in the pyrophosphate region. Furthermore, glass-ceramics play an important role in their ability to form Ca–P apatite in SBF.

1.5 A brief review of phosphate-based bioactive glasses in medical applications

Phosphate-based glasses are an attractive option in that they promise a controllable degradation rate from varying their chemical compositions, thereby giving rise to easily metabolizable degradation components in the body. At the same time, phosphate-based glasses are indeed a wise choice to encapsulate drug molecules as this is one sure way to diminish the drug dose needed and effectively combat the side effects associated with particular drugs.

Studies on ZnO–Na_2O–CaO–P_2O_5 bioglass are relatively few in comparison with phosphate-based glasses. A concise review of some of the latest updates related to the present work on phosphate-based bioactive glasses and metal ions doped glasses

Franks et al., [63] prepared ternary P_2O_5–CaO–Na_2O glasses having an almost linear dissolution rate in the aqueous medium, the degradation rate of which can be managed ably through subtle variations in composition. These glasses show markedly severe degradation rate and are eminently suited for biomedical applications as imaging contrast agents and drug delivery systems. In another study, Abou Neel et al., [64] have developed successfully quaternary phosphate-based glass system P_2O_5–CaO–Na_2O–TiO_2 with up to 15 mol% TiO_2 by the melt-quench route. They studied the effect on glass degradation, and physical, surface and biological properties with TiO_2 incorporation. The dispersal of Ti^{4+} ions was also determined using inductively coupled plasma mass spectroscopy (ICP-MS). The results showed that enhancement in the biological activity with the increase in the content of TiO_2.

Navarro et al., [65] examined the effect of titanium addition on P_2O_5–CaO–Na_2O glass systems and observed in the process the inclusion of titanium to P_2O_5–CaO–Na_2O glass systems can enhance the glass-forming ability and chemical durability of these glasses. To add to this, it came through that incorporation of TiO_2 into phosphate-based glasses not only brings down the solubility of the glasses in question but also lowers crystallization tendency thanks to the formation of cross-links between TiO_4 and TiO_6 structural groups and phosphate tetrahedra.

In other studies**,** Franks et al., [66] looked into the solubility of quaternary glasses in P_2O_5–CaO–MgO–Na_2O system. In such quaternary glasses, replacing CaO with MgO managed to reduce solubility as well as changes in pH at longer periods precisely on account of smaller ionic radius of magnesium. Knowles et al., [67] developed quaternary phosphate-

based glasses in the P_2O_5–CaO–K_2O–Na_2O system and K_2O was used as Na_2O substitutes with the concentration of 0 to 25 mol%. The results revealed an increase in solubility with increasing K_2O content following the larger ionic radius of potassium vis-à-vis sodium that brings about a larger disrupting effect on the structure, while simultaneously weakening the network.

Rajendran et al., [68] synthesized P_2O_5–Na_2O–CaO–TiO_2 glass system, with different TiO_2 contents and fixed P_2O_5 (45 wt%) and CaO (24 wt%) by employing the normal melting and annealing technique. They carry out the dissolution behavior of the prepared bioactive glasses with distilled water. Along with ultrasonic velocities, attenuation and elastic properties of the different glasses also studied to reveal the structural changes taking place in the glass system. The obtained results showed that the solubility of the undoped glass is higher than the titanium-containing glasses. In other words, the rate of dissolution the phosphate glasses decreases with an increase in TiO_2 content.

Rajkumar et al., [69] prepared and characterized zirconia doped phosphate-based glasses using the normal melt quench technique. The observed results revealed that all glass samples exhibit the formation of hydroxyapatite (Ca-P) rich layer on the surface, 0.75 mol% of ZrO_2 containing glass processing higher bioactivity, and elastic moduli out of all the prepared samples. Moreover, the formation of NBO network by the breaking of P–O–P bonds into the P_2O_5 glass network is noticed. These results concluded that after the optimization of choosing glass composition might be suitable for biomedical applications.

Ahmed et al., [70] have fabricated the Iron-phosphate glass fibers based CaO–Na_2O–Fe_2O_3–P_2O_5 system and characterized by considering the thermal, dissolution rates, diameter, and biocompatibility studies. Fe_2O_3 was added in traces 1–5 mol%, substituting it for Na_2O mol%. The results brought to light a decrease in dissolution rates for bulk glass and glass fibers, simultaneously with an increase in CaO mol%, along with an increase in Fe_2O_3 mol%. It was discovered that iron-phosphate glass fibers containing 4–5 mol% Fe_2O_3 were adequate for cell attachment to achieve proliferation and differentiation. Ahmed et al., [71] began to study phosphate-based glass in $40P_2O_5$–25CaO–20MgO–$15Na_2O$ system which recorded good cellular response and Hasan et al., [72] studied the system $45P_2O_5$–16CaO–24MgO–$11Na_2O$–$4Fe_2O_3$, which also showed good cytocompatibility and proved its worth in fiber drawing.

Agata Łapa et al., [73] manufactured novel gallium/cerium-doped phosphate-based glasses and phosphate glass fibers 18MgO–10CaO–24Na_2O–45P_2O_5–3Ga_2O_3 mol% and 18MgO–10CaO–24Na_2O–45P_2O_5–3CeO_2 mol% by the melt quenching and melt-spinning method. They studied the degradation behavior, cytocompatibility, and antibacterial potential of the prepared glasses. The results revealed that adding Ga lowers dissolution behavior of phosphate glass fibers, wherein both Ce-PGF and Ga-PGF permit controlled release of ions that show antibacterial properties. Besides this, the presence and controlled release of ions having therapeutic and antibacterial characteristics generates a wound dressing which shows the capability to reduce the growth of Gram-positive bacteria in half, while ensuring non-toxic behavior towards mammal cells.

Kheshen et al., [74] looked at three bio-phosphate glass-specimens with and sans Al_2O_3 addition to shed light on their bioactivity tendencies towards SBF biological solution. The results pointed out that Al_2O_3 exercises a significant impact on the ability of bioglass to form a hydroxycarbonate apatite layer on its surface. That layer was detected by FTIR spectra, SEM micrographs, and EDS pattern. Also, the influence of Al_2O_3 on the mechanical properties was subjected to investigation by measuring the hardness of glass samples, which predictably increased following the addition of Al_2O_3. The thermal expansion coefficient came down by increasing Al_2O_3 percent in bioglass samples.

Kokubo et al., [75] preparation methods revealed the mechanism of formation of the surface apatite layer while also bringing to light changes in ion concentration of SBF fluid with the immersion of glass and glass-ceramics. It has been observed from the above results that the dissolution of Ca and P ions from bioactive glass and glass ceramics has an important role to play in the formation of an apatite layer on the surface.

Takadama et al., [76] revealed the mechanism of apatite formation on bioactive titanium metal *in vitro* employing SEM and EDS studies. Apatite formation on metal may be readily identified by soaking the metal surface in SBF. The metal after immersion in SBF results in the exchange of Na^+ ions from the surface of sodium titanate (produced by NaOH and heat treatment of Ti metal with H_3O^+ ions) in the fluid to form Ti–OH groups on the surface. Amorphous calcium phosphate layer takes shape with a low Ca/P atomic ratio after long soaking time in SBF, which ends up stabilizing into a bone-like crystalline apatite.

1.6 Motivation and Scope of current work

An important feature of phosphate-based glasses is their ability to be used as tools for muscle or nerve repair in soft tissue engineering. To enable hard tissue engineering, phosphate glasses finds use as bone tissue regenerative materials as bulk or as powders mixed with polymers. Phosphate glasses have been comprehensively studied as for the controlled release of antibacterial ions, such as silver, copper, zinc, and gallium, using 3D structure of muscle tissues [77]. The bioactive silicate-based glasses as biomedical implants are a happy choice with a long history. Most of the available commercial bioglasses contain a high amount of silica. These silica rich glasses after potential to develop long term implants to replace hard and soft tissues in vivo due to the insoluble nature. However, the long term interaction of silica locally and systemically is not yet understood completely as also issue about the long-term reaction in vivo [7,8]. Most of the clinical reports proved that glasses with a high amount of silica and high network connectivity were observed by the human body but the rate of degradation was rather low and the glass remnants were present in the patient's body for more than 14 years [9,10]. As an alternative to absorbing SiO_2 based glasses for tissue repair, P_2O_5 based glasses were developed by many researchers because of their unusual properties such as lower melting temperature, lower transition temperature, higher thermal expansion coefficient, higher electrical conductivity, higher degradability, higher biocompatibility and lower chemical durability [11,12]. Among phosphate-based glasses, the calcium-containing phosphate glasses show high bioactivity. Moreover, these glasses are best suited for bone bonding due to chemical composition which is very close to the natural bone phase [13]. In general, phosphate-based glasses have high dissolution and poor chemical durability when compared with silicate and borate-based glasses, which limits the applications.

Considerable work has focused on phosphate-based glasses in P_2O_5–CaO–Na_2O system, which appears to be a fine option for tissue engineering applications with a more controllable degradation rate, in which the presence of bioglass is only necessary to support short-lived cells/tissues [70,78]. The control over degradation rate and improvement of chemical durability can be obtained by adding intermediate network modifiers such as transition metal oxides (Ca^{2+}, Na^{+}, Zn^{2+}, Mg^{2+}, $Sr^{2+,}$ and K^{+}) [14,15]. The incorporation of these elements modifies phosphate network and subsequently affects degradation properties. The rate of degradation can be selectively controlled by varying amounts of constituents incorporated into the glass [15]. Moreover, the metal ions doped bioglasses are expected to have a higher mechanical strength than base glasses, which would offer high strength Phosphate based bioglass suitable for load-bearing applications without losing bioactivity.

The primary motive of the study was finding relevant applications in cellular and tissue engineering exploiting processes such as cell proliferation and bone formation [63,78,79]. A survey of the literature showed that there is ample scope of work in these exciting and application orientation materials. After a careful survey of the literature, it was decided to study phosphate based bioactive glasses derived from the following four glass compositions:

(i) xZnO–22Na_2O–24CaO–(54-x)P_2O_5 (x = 2, 4, 6, 8 and 10 mol%).

(ii) 8ZnO–22Na_2O–(24-x)CaO–46P_2O_5–$x$$TiO_2$ (x =0.2, 0.4, 0.6, 0.8 and 1mol%)

(iii) 8ZnO–22Na_2O–(24-x)CaO–46P_2O_5–$x$$Al_2O_3$ (x = 2, 4, 6, 8 and 10 mol%)

(iv) 8ZnO–22Na_2O–(24-x)CaO–46P_2O_5–$x$$ZrO_2$ (x = 0.1, 0.3, 0.5 and 0.7 mol%)

In view of this, it was also proposed to investigate the influence of four transition metal oxides viz., ZnO, TiO_2, Al_2O_3 and ZrO_2 trailed in calcium phosphate-based glass system in order to improve structural, and mechanical properties along with biological properties such as biocompatibility, bioactivity, cytotoxicity, cell viability and antibacterial activity which are suitable for the development of novel bone regenerated implant materials.

1.7 Schematic representation of the proposed work:

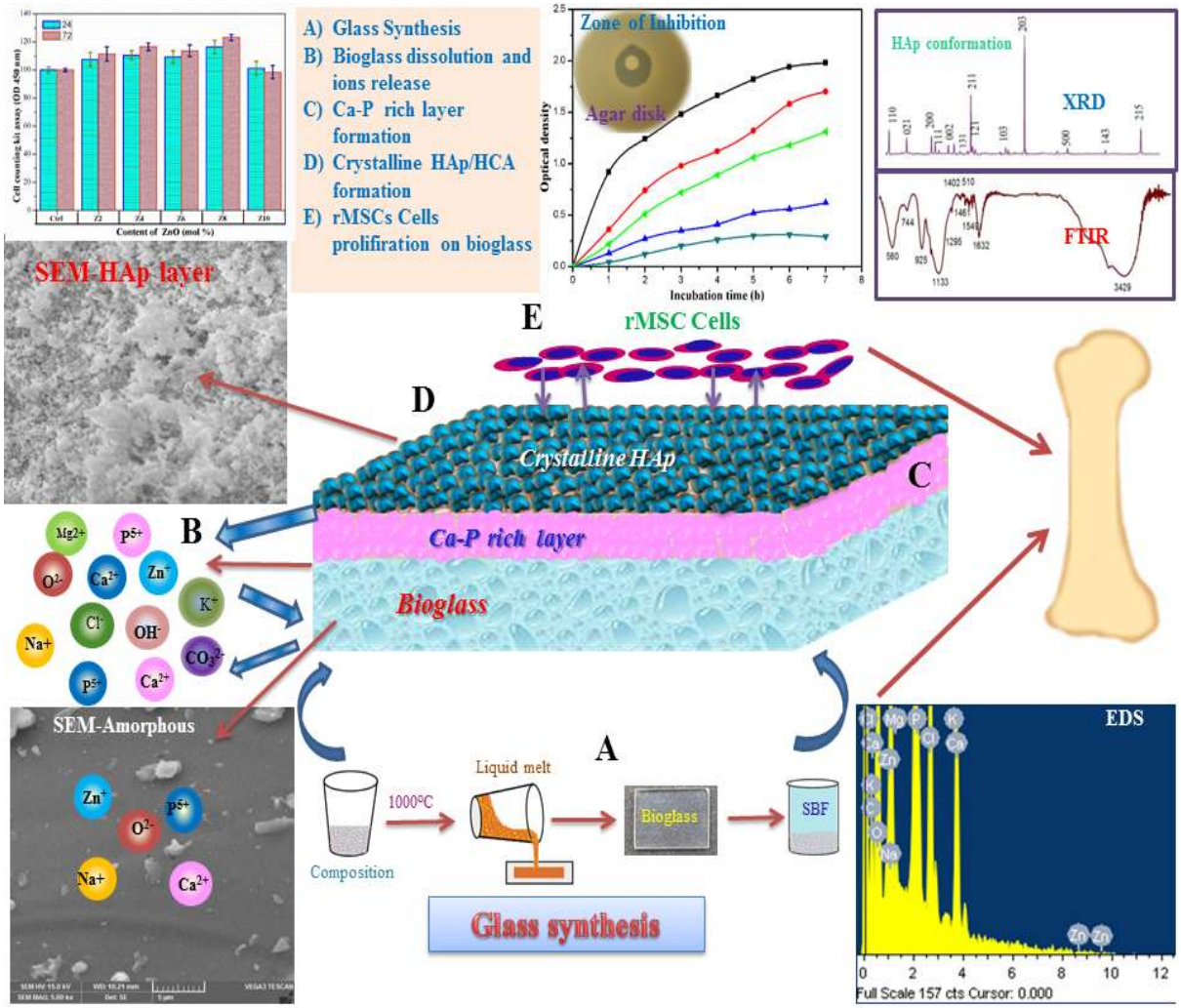

1.8 The main objectives of the present thesis work

i) To optimize the composition of phosphate-based glass, which is considered to be a bone regenerative material.

ii) To improve physico-chemical properties and mechanical strength, in terms of various transition metal oxides ions added.

iii) To study the *in vitro* bioactivity of developed glasses in simulated body fluid employing various characterization techniques.

iv) To gauge the cytocompatibility, cell proliferation and antibacterial assays of bioglasses suitable for *in vivo* clinical applications.

References

[1] G. Kaur, Bioactive Glasses, Springer Nature-2017.

[2] G. Kaur, G. Pickrell, N. Sriranganathan, V. Kumar, D. Homa, Review and the state of the art: sol-gel or melt quenched bioactive glasses for tissue engineering, J. Biomed. Mater. Res. B. Appl. Biomater. 104 (6) (2016) 1248–75.

[3] Minardi, B. Corradetti, F. Taraballi et al., Evaluation of the osteoinductive potential of a bioinspired scaffold mimicking the osteogenic niche for bone augmentation, Biomaterials, 62 (2015)128–37.

[4] J. Park, Bioceramics: properties, characterizations, and applications, New York: Springer-2008.

[5] B. Basu, D. S. Katti & A. Kumar, Advanced Biomaterials: Fundamentals, Processing, and Applications-2010

[6] L. L. Hench, Bioceramics, J. Am. Ceram. Soc. 81(7) (1998)1705–1728.

[7] L. L. Hench, Bioceramics a clinical success, Am.Ceram. Soc. Bulletin, 77 (7) (1998)67–74.

[8] R.S. Joon Park, Lakes, Biomaterials an Introduction, Springer-2007.

[9] J. Chevalier, L. Gremillard, Ceramics for medical applications: a picture for the next 20 years. J. Eur. Ceram. Soc. 29 (2009) 1245–55.

[10] L. L. Hench, J. K. West, The sol-gel process, Chem Rev. 90 (1990) 33–72.

[11] S.F. Hulbert, L. L .Hench,' D. Forbers,L. S. Bowman, History of bioceramics. Ceram. Int. 8 (1982) 131–140.

[12] L.L. Hench, Bioceramics: From Concept to Clinic, J. Am. Ceram. Soc. 74 (1991)1487–1510.

[13] R. L. Hentrich, H. G. Stein, G. A. Graves, & P. K. Bajpai, An Evaluation of Inert and Resorbable Ceramics for Future Clinical Orthopedic Applications, Am. Ceram. Soc. Bulletin, 48 (1969) 801–805.

[14] J. B. Park, J. D. Bronzino and Y. K. Kim, Biomaterials Principles and Applications, CRC Press, Boca Raton, USA. (2003) 21–53.

[15] T. Kokubo, H. M. Kim, M. Kawashita, Novel bioactive materials with different mechanical properties, Biomaterials, 24 (2003) 2161–2175.

[16] L. L. Hench & J. Wilson, Bioceramics. Mrs Bulletin, 16 (1991) 62–74.

[17] M. Vallet-regi, Ceramics for medical applications, J.Chem. Soc–Dalton Transactions, (2001) 97–108.

[18] S. F. Hulbert, J. C. Bokros, L.L. Hench, J. Wilson and G. Heimke, High Tech Ceramics, Elsevier, Amsterdam, The Netherlands (1987)189–213.

[19] G. Kaur, OP. Pandey, K. Singh, D. Homa, B. Scott, G. Pickrell, A review of bioactive glasses: their structure, properties, fabrication, and apatite formation, J. Biomed. Mater. Res. Part-A. 102 (2013) 254–74.

[20] QZ. Chen, SE. Harding, NN. Ali, AR. Lyon, Boccaccini A. Biomaterials in cardiac tissue engineering: ten years of research survey, Mater. Sci. Eng. R-Rep. 59 (2008) 1–37.

[21] H. Shin, Jo S, AG. Mikos. Biomimetic materials for tissue engineering, Biomaterials, 24 (2003) 4353–64.

[22] J. L. Cook, N. Williams, J. M. Kreeger, J. T. Peacock & J. L. Tomlinson, Biocompatibility of three-dimensional chondrocyte grafts in large tibial defects of rabbits, Am. J. Veter. Res. 64 (2003) 12–20.

[23] I. Ahmed, C.A. Collins, M.P. Lewis, I. Olsen, J.C. Knowles, Processing, characterisation and biocompatibility of iron-phosphate glass fibres for tissue engineering, Biomaterials, 25 (2004) 3223–3232.

[24] L. L. Hench, & J. Wilson, Surface-active biomaterials, Science, 226(4675) (1984)630–636.

[25] L. L. Hench & J. M. Polak, Third-generation biomedical materials, Science, 295 (2002) 1014–1017.

[26] T. Kokubo, S. Ito, Z. T. Huang, T. Hayashi, S. Sakka, T. Kitsugi, Ca, P-rich layer formed on high-strength bioactive glass-ceramic A-W, J. Biomed. Mater. Res. 24 (1990) 331–343.

[27] P. Ducheyne, Bioceramics: material characteristics versus in vivo behavior, J. Biomed. Mater. Res. 21 (1987) 219–236.

[28] L.L. Hench, R.J. Splinter, W.C. Allenand, T.K. Greenlee, Bonding mechanisms at the interface of ceramic prosthetic materials, J. Biomed. Mater. Res. 2 (1972) 117–141.

[29] S. B Cho, F. Miyaji, T. Kokubo, K. Nakanishi, N. Soga & T. Nakamura, Apatite formation on silica gel in simulated body fluid: effects of structural modification with solvent-exchange, J. Mater. Sci: Mater. Med. 9 (1998) 279–284.

[30] T. Kokubo, T. Kitsugi, T. Yamamuro, Solutions able to reproduce in vivo surface-structure changes in bioactive glass-ceramic A-W^3, J. Biomed. Mater. Res. 24 (1990) 721–734.

[31] T. Yamamuro, Bioceramics, New York: Elsevier, (1995) 123–127.

[32] Am. Soc. Testing Mater., ASTM C 162-56, ASTM stand. Part 13, 1965.

[33] H.G. P. faender, Schott Guide to Glass, Champan& Hall, London, 1996.

[34] H. Scholze, Glass Nature, structure, and properties, Springer-Verlag New York, 1991.

[35] E. EI-Meliegy, R. van Noort, Glasses and Glass Ceramics for Medical Applications, springer-2012.

[36] L.L. Hench, R.J. Splinter, W.C. Allen, T.K. Greenlee,Bonding mechanisms at the interface of ceramic prosthetic materials, J. Biomed. Mater. Res. 5 (1971) 117–141.

[37] P. Sepulveda, J. R. Jones & L. L. Hench, Characterization of melt-derived 45S5 and sol-gel-derived 58S bioactive glasses, J. Biomed. Mat. Res. 58 (6) (2001) 734–740.

[38] L. L. Hench, The story of Bioglass, J. Mater. Sci. Mater. Med. 17(2006), 967–978.

[39] O.H. Anderson, I. Kangasniemi, Calcium phosphate formation at the surface of bioactive glass in vitro, J. Biomed. Mat. Res. 25 (1991)1019–30.

[40] L.L. Hench, J.M. Polak, Third-Generation Biomedical Materials, Science, 295 (2002) 1014–1017.

[41] M N. Rahaman, W. LIang, D E. Day, N W. Marion, G C. Reilly, J J. Mao, Preparation and bioactive characteristics of porous borate glass substrates, Ceram. Enggg. & Sci. Proceed. 26, 3 (2005) 1–10.

[42] D.E. Day, J.E. White, R.F. Brown, K.D. McMenamin, Transformation of borate glasses into biologically useful materials, Glass Technol. 44 (2003) 75–81.

[43] W. Jia, X. Zhang, S. Luo, X. Liu, W. Huang, M.N. Rahaman, Novel borate glass/chitosan composite as a delivery vehicle for teicoplanin in the treatment of chronic osteomyelitis, Acta Biomater. 6 (3) (2010) 812–819.

[44] M. Brink, T. Turunen, R. Happonen& A. Yli-urpo, Compositional dependence of bioactivity of glasses in the system Na_2O–K_2O–MgO–CaO–B_2O_3–P_2O_5–SiO_2, J. Biomed. Mat. Res. 37 (1996)114–121.

[45] O. H. Andersson, G. Liu, K. Kangasniemi & J. Juhanoja, Evaluation of the acceptance of glass in bone. J Mater Sci: Mater Med. 3(2) (1992) 145–150.

[46] J. Ning, A. Yao, D. Wang, W. Huang, H. Fu, X. Liu, X. Zhang, Synthesis and in vitro bioactivity of a borate-based bioglass, Materials Letters, 61(30) (2007) 5223–5226.

[47] H.S. Ryu, J.K. Lee, J.H. Seo, H. Kim, K. S. Hong, D. J. Kim, S.S. Chung, Novel bioactive and biodegradable glass ceramics with high mechanical strength in the CaO–SiO_2–B_2O_3 system. J. Biomed. Mat. Res. Part A, 68 (1) (2004) 79–89.

[48] W. Huang, DE. Day, K Kittiratanapiboon & M. N. Rahaman, Kinetics and mechanisms of the conversion of silicate (45S5), borate, and borosilicate glasses to hydroxyapatite in dilute phosphate solutions. J Mater Sci: Mater Med. 17 (7) (2006a) 583–596.

[49] K. Manupriya, S Thind, K. Singh, V. Kumar, G. Sharma, D. P. Singh & D. Singh, Compositional dependence of in-vitro bioactivity in sodium calcium borate glasses, J. Phy. Chem. Sol.70 (8) (2009) 1137–1141.

[50] X. Zhang, W. Jia, Y Gu, W. Xiao, X. Liu, D. Wang, N. Zhou, Teicoplanin loaded borate bioactive glass implants for treating chronic bone infection in a rabbit tibia osteomyelitis model, Biomaterials, 31 (22) (2010) 5865–74.

[51] W. Jia, X. Zhang, S. Luo, X. Liu, W. Huang, M. N. Rahaman, J. Wang, Novel borate glass /chitosan composite as a delivery vehicle for teicoplanin in the treatment of chronic osteomyelitis, Acta Biomaterialia, 6 (2010) 812–819.

[52] F. H. Nielsen, Is boron nutritionally relevant? Nutrition Reviews, 66 (4) (2008) 183–191.

[53] P. Pernice, S. Esposite, A. Aronne, V.N. Sigaev, Structure and crystallization behavior of glasses in the $BaO–B_2O_3–Al_2O_3$ system, J. Non-Cryst. Solids, 258 (1999) 1–10.

[54] R. K. Brow, Review: the structure of simple phosphate glasses. J. Non-Cyst. Solids, 263&264 (2000) 1–28.

[55] E. A. Abouneel, D. M. Pickup, S. P. Valappil, R. J. Newport & J. C. Knowles, Bioactive functional materials: a perspective on phosphate-based glasses, J. Mate. Chem. 19 (2009) 690–701.

[56] S. W. Martin, Ionic Conduction in Phosphate Glasses, J. Am. Ceram. Soc. 74 (8) (1991) 1767–1784.

[57] R. K. Brow, R. J. Kirkpatrick & G. L. Turner, The Short-Range Structure of Sodium-Phosphate Glasses .1. Mas Nmr-Studies, J. Non-Cyst. Solids, 116 (1990) 39–45.

[58] Graham, Research on the arsenates and phosphates and modification of phosphoric acid, Philosophical Transactions of the Royal Society. 123, (1833) 263–284.

[59] J.H. Campbell, T.I. Suratwala, Nd doped phosphate glasses for high energy /high peak power laser, J. Non-Cyst. Solids, 263 & 264 (2000) 318–341.

[60] J.E. Shelby, “Introduction to glass science and technology”, 2nd Edition, RS.C.

[61] K. Franks, I. Abrahams, G. Georgiou, J.C. Knowles, Investigation of thermal parameters and crystallization in a ternary $CaO–Na_2O–P_2O_5$ based glass system, Biomaterials, 22 (2001) 497–501.

[62] T. Kasuga, Bioactive calcium pyrophosphate glasses and glass ceramics, Acta

Biomaterialia, 1 (2005) 55–64.

[63] K. Franks, I Abrahams & J. C. Knowles,. Development of soluble glasses for biomedical use Part I: In vitro solubility measurement. J.Materia.Sci.-Materia. in Medic. 11**(**2000) 609–614.

[64] E. A. Abou Neel, W. Chrzanowski & J. C Knowles, Effect of increasing titanium dioxide content on bulk and surface properties of phosphate-based glasses. Acta Biomaterialia, 4 **(**2008) 523–534.

[65] M. Navarro, M.P. Ginebra, J. Clement, S. Martinez, G.Avila& J.A. Planell, Physicochemical degradation of titania-stabilized soluble phosphate glasses for medical applications. J.Amer.Cera. Soci. 86 **(**2003a) 1345–13.

[66] K. Franks, V.Salih, J. C. Knowles, & I. Olsen, The effect of MgO on the solubility behavior and cell proliferation in a quaternary soluble phosphate based glass system. J.Materia.Sci.-Materia. in Medic.13 (2002) 549–556.

[67] J. C. Knowles, K. Franks, & I. Abrahams, Investigation of the solubility and ion release in the glass system K_2O–Na_2O–CaO–P_2O_5. Biomaterials, 22 **(**2001) 3091–3096.

[68] V. Rajendran, A.V. Gayathri Devi, M. Azooz, F.H. El-Batal, Physicochemical studies of phosphate based P_2O_5–Na_2O–CaO–TiO_2 glasses for biomedical applications, Journal of Non-Crystalline Solids 353 (2007) 77–84.

[69] G. Rajkumar a, S. Aravindan b, V. Rajendran, Structural analysis of zirconia-doped calcium phosphate glasses, Journal of Non-Crystalline Solids 356 (2010) 1432–1438.

[70] I. Ahmed, C.A. Collins, M.P. Lewis, I. Olsena, J.C. Knowles, Processing, characterisation and biocompatibility of iron-phosphate glass fibres for tissue engineering, Biomaterials 25 (2004) 3223–3232.

[71] I. Ahmed, A. Parsons, A. Jones, G. Walker, C. Scotchford, C. Rudd, Cytocompatibility and Effect of Increasing MgO Content in a Range of Quaternary Invert Phosphate-based Glasses, J. Biomater. Appl. 24 (2010) 555–575

[72] M.S. Hasan, I. Ahmed, A.J. Parsons, G.S. Walker, C.A. Scotchford, Material characterisation and cytocompatibility assessment of quinternary phosphate glasses J. Mater. Sci. Mater. Med. 23 (2012)2531–2541.

[73] Agata Łapa, Mark Cresswell, Ian Campbell, Phil Jackson, Wolfgang H. Goldmann, Rainer Detsch, Andrew Parsons, Ifty Ahmed and Aldo R. Boccaccini, Ga and Ce ion-doped phosphate glass fibres with antibacterial properties and their composite for wound healing application, J. Mater. Chem. B, 7 (2019) 6981–6993.

[74] A.A. El-Kheshen, F.A. Khaliafa, E.A. Saad, R.L. Elwan, Effect of Al_2O_3 addition on bioactivity, thermal and mechanical properties of some bioactive glasses, Ceram. Inter. 34 (2008) 1667–1673.

[75] T. Kokubo, H. Kushitani, C. Ohtsuki, S. Sakka, T. Yamamuro, Chemical reaction of bioactive glass and glass-ceramics with a simulated body fluid, J. Mater. Sci. Mater. Med. 3 (1992) 79–83.

[76] H. Takadama, H.M. Kim, T. Kokubo, T. Nakamura, TEM-EDX study mechanism of bone like apatite formation on bioactive titanium metal in simulated body fluid J. Biomaed. Mater. Res.57 (2001) 444–448.

[77] Gurbinder Kaur, Bioactive Glasses Potential Biomaterials for Future Therapy, Springer ©2017.

[78] J. C. Knowles, Phosphate based glasses for biomedical applications, J. Mate. Chem. 13 (2003) 2395–2401.

[79] M. Navarro, M. P Ginebra& J. A Planell, Cellular response to calcium phosphate glasses with controlled solubility. J. Biomed. Mate. Res.Part A, 67A (2003b) 1009–1015.

Chapter - 2

Materials and Methods

In this chapter, a comprehensive overview of the melt quenching method for the preparation of phosphate-based bioglass samples is presented. The characterization techniques employed in the present research are also discussed along with relevant theory. The prepared samples, physical properties, density, molar volume and the process adopted for the preparation of the SBF solution for in vitro bioactivity test, variation of pH as well as degradation studies, are also presented. The mode of evaluating the performance of antibacterial and cytocompatibility on the glass samples has been described. The details of the apparatus used and the methodology to study the structural and thermal properties of the prepared samples, such as TG-DTA, XRD, FTIR, SEM-EDS and Hv are included as well.

2. Materials and Methods

2.1 Preparation of bioglass

In this chapter the preparation of bioactive glass technique and characterizations are discussed in detail. Phosphate based bioglasses were prepared by using a normal melt-quenching method of varying the concentration of ZnO, TiO_2, Al_2O_3, and ZrO_2 [1,2]. The nominal values of all glass compositions of the samples are given in Table 2.1. The samples were prepared using high purity of chemicals purchased from Sigma Aldrich with purity of 99.99%. Appropriate chemical compositions of the batches were weighed at 20 grams for each sample, mixed and ground carefully using mortar and pestle to obtain homogenized composition. Then the batch compositions were taken into a platinum crucible and melted at 1000 °C to 1100 °C in an electrical muffle furnace, depending on composition. The synthesis of the prepared glass samples are shown in Fig.2.1.

Fig. 2.1 Brief description of the synthesis of the glass matrix.

While melting, the glass compositions were stirred every 15 minutes to achieve homogeneity, and finally quenched onto a preheated brass moulds and then immediately the samples were transferred to an annealing muffle furnace set at 300-400 °C and kept for 3 to 4 hours. After that the furnace was switched off and allowed to cool slowly to room temperature in order to remove residual stress of the glasses. The samples were then gathered from brass

moulds and then transferred to sealed desiccators to protect glasses from moisture. The prepared bioactive glass samples were crushed to a fine powder in a mortar, for further characterization of the samples using different experimental techniques. The detailed compositions and sample codes of the glasses used in the present study are given in Table 2.1.

Table 2.1 Glass sample code and nominal compositions of the prepared phosphate glasses

Glass Composition (mol%)				
Glass code	**ZnO**	**Na_2O**	**CaO**	**P_2O_5**
Z2	2	22	24	52
Z4	4	22	24	50
Z6	6	22	24	48
Z8	8	22	24	46
Z10	10	22	24	44

Glass Composition (mol%)					
Glass code	**ZnO**	**Na_2O**	**CaO**	**P_2O_5**	**TiO_2**
T0	8	22	24	46	0
T.2	8	22	23.2	46	0.2
T.4	8	22	23.4	46	0.4
T.6	8	22	23.6	46	0.6
T.8	8	22	23.8	46	0.8
T1	8	22	23	46	1

Glass Composition (mol%)					
Glass code	**ZnO**	**Na_2O**	**CaO**	**P_2O_5**	**Al_2O_3**
Al0	8	22	24	46	0
Al2	8	22	22	46	2
Al4	8	22	20	46	4
Al6	8	22	18	46	6
Al8	8	22	16	46	8
Al10	8	22	14	46	10

Glass Composition (mol%)					
Glass code	**ZnO**	**Na_2O**	**CaO**	**P_2O_5**	**ZrO_2**
Zr0	8	22	24	46	0
Zr.1	8	22	23.1	46	0.1
Zr.3	8	22	23.3	46	0.3
Zr.5	8	22	23.8	46	0.5
Zr.7	8	22	23.7	46	0.7

2.2 Physical properties

Physical properties such as density and molar mass play an important role in the structural evaluation of glass materials. The densities of the glass samples prepared were measured to a using electronic digital balance (model: BSA22S-CW: Sartorius) accuracy of ±0.0001g/cc employing the standard Archimedes principle, using Xylene (ρ = 0.86 g/cm^3) an immersion liquid (99.99% pure). The measurements were performed at room temperature where the following equation was used to obtain the densities (ρ) of glasses [3],

$$\text{Density } (\rho) = \frac{W_a}{W_a - W_{Xylene}} \times \rho_{xylene} \qquad \textbf{2.1}$$

Where the masses of samples exposed to air and in Xylene are W_a and W_{Xylene} respectively. The density of Xylene liquid is ρ_{xylene}.

Physical parameters: The other physical properties, molar volume, oxygen molar volume and oxygen packing density values of the bioglass samples were calculated from the experimentally determined densities. Molar volume V_m (cm^3/mol) was calculated as a function of the mole fraction of each component using the following equation:

$$\text{Molar volume(Vm)} = \sum \frac{X_i M_i}{\rho_{glass}} \quad \textbf{2.2}$$

Where X_i is the molar fraction and M_i is the molecular weight of the i^{th} component,

The oxygen molar volume of the glasses V_O (cm^3/mol) was calculated by the following formula:

$$\text{Oxygen molar volume(Vo)} = \left(\sum \frac{X_i M_i}{\rho_{glass}}\right)\left(\frac{1}{\sum X_i n_i}\right) \quad \textbf{2.3}$$

Where n_i is the number of oxygen atoms in each oxide.

The Oxygen packing density (OPD) of the glass samples can be calculated using the following formula

$$\text{Oxygen Packing Density (OPD)} = 1000\ C\left(\frac{\rho}{M}\right) \quad \textbf{2.4}$$

$$\text{Oxygen packing density (OPD)} = 1000\ C\ (\rho/M) \quad \textbf{2.5}$$

Where C is the number of oxygen atoms per composition, M is the molecular weight of the glass sample [3,4].

2.3 Analytical methods

2.3.1 *In vitro* bioactivity study

The in vitro bioactivity of the synthesized glass samples were examined through immersing samples in simulated body fluid (SBF), it can also be prepared employing the procedure detailed by Kokubo and Takadama [5]. The bioactivity test comes in handy to identify the Hydroxyl apatite layer (HAp) formation on the glass samples when they were immersed in SBF solution. Then, the samples were kept at 37 ºC in the incubator, throughout the experiment to simulate the human physical environment. The experiment was carried out

in static condition. The requisite amount of glass powder was soaked in SBF for different time intervals (0, 3, 7, 14, 21days). The samples were then removed from the solution by filtration through use of filter paper and then dried for 24 h at 80 ^{o}C. After drying, the samples surfaces were analysed by X-ray diffraction**,** Fourier transform infrared spectroscopy, Scanning electron microscope-Energy dispersive X-ray spectroscopy, in order to confirm the apatite layer formation purpose.

2.3.2 Preparation of simulated body fluid (SBF)

The simulated body fluid (SBF) solution was prepared by the method suggested by Kokubo and Takadama [5,6]. The various ion concentrations of the prepared SBF solution are given in Table 2.2 which is equal to the human blood plasma (HBL). SBF is a metastable solution containing calcium and phosphate ions which are supersaturated with respect to the hydroxyapatite. The SBF has been prepared by adding the reagent grade (AR grade reagents (Aldrich makes)) NaCl, KCl, $NaHCO_3$, $MgCl_2$ $6H_2O$, $CaCl_2$ and KH_2PO_4 chemicals were dissolved in distilled water with continuous stirring in a polyethylene container and at maintaining the buffer of pH 7.4 at 37 ºC with Tris-(hydroxymethyl aminomethane) and hydrochloric acid 1M.

The SBF preparation process is described as follows. The beakers used for preparation are dipped in hydrochloric acid solution for about 12 h and washed with distilled water. 750 ml of distilled water was taken in 1000 ml polyethylene beaker. The beaker was placed in a hot water bath to raise its temperature to 37 ºC under constant stirring. The beaker is placed on a clean bench to prevent dust. Each reagent given in Table 2.3 was added into distilled water from 1 to 8, one by one in the same order after the earlier added chemical gets completely dissolved. The 9^{th} (Tris) and 10^{th} factors were carefully added, to the pH adjustment and for the pH value of 7.40.

After pH adjustment, the solution was transferred from the poly beaker to glass volumetric flask of 1000 ml. The inside of the poly beaker was washed with distilled water and the same was added to the flask containing the prepared solution. Further, distilled water was added to make up the total volume of the solution to 1000 ml and was stored in a refrigerator kept at 5-10 ºC.

Table 2.2 Concentration of various ions in the SBF solution

Concentration (mmol/L)		
Ion Type	Simulated body fluid (SBF)	Human blood plasma (HBP)
Na^+	142	142
K^+	5	5
Mg^{2+}	1.5	1.5
Ca^{2+}	2.5	2.5
Cl^-	148.8	103.0
HCO_3^-	4.2	4.2
HPO_4^{2-}	1.0	1.0
SO_4^-	0.5	0.5

Table 2.3 Chemical compositions of the prepared SBF solution (1000 mL)

Order	Reagent	Amount
1	NaCl	8.035 g
2	$NaHCO_3$	0.355 g
3	KCl	0.225 g
4	$K_2HPO_4 \cdot 3H_2O$	0.231 g
5	$MgCl_2 \cdot 6H_2O$	0.311 g
6	1.0m-HCl	39 ml
7	$CaCl_2$	0.292 g
8	Na_2SO_4	0.072 g
9	Tris buffer	6.118 g
10	1.0M HCl	0–5 ml

In order to test the stability of the solution, 50 ml of the solution was added to another polyethylene bottle. The Prepared SBF was explored to the presence of sediments was kept in an incubator at 37 ºC for 48 hours. If there is no precipitation in the prepared SBF, it is suitable for *in vitro* studies. *In vitro* bioactivity test was carried out by immersing the glass

powder in 50 ml of SBF at 37 ºC. The surfaces of the samples were investigated by XRD, FTIR and SEM-EDS to determine the advantage of apatite layer formation.

2.3.3 Weight loss measurement

The solubility of glasses was evaluated by the measurement of weight loss in simulating body fluid (SBF) at 37 °C in the incubator. The degradation studies of the bioglass samples in a simulated body fluid solution with pH 7.4 and temperature at 37 °C were obtained by a weight loss measurement method. Initially the glass powder samples were weighed before immersion and then immersed for various time periods (0, 3, 7, 14, and 21days) in SBF solution. Next the samples were taken out of the solution and were dried at room temperature for 48 h. The weight losses after immersion were taken note of each time interval till the point of arrival of percentage of the initial weight according to the following equation [1, 2].

$$\text{Weight loss} = \frac{Wo - Wt}{Wo} \times 100\ \% \qquad \textbf{2.6}$$

Where Wo and W_t stand for initial weight and weight after a specific immersion time respectively.

2.3.4 pH evaluation

The change in pH values of SBF solution containing glass samples for different immersion time 3, 7, 14 and 21 days were measured under identical conditions by using a pH meter (ORION pH 7000) with an error percentage ±0.005. Before reading the pH values, the electrode was calibrated, using the standard pH values of 4.01, 7.00, and 9.20. The measurement of pH of the SBF solution gives the information about the dissolution behaviour of the bioglass samples with time before and after immersion.

2.3.5 Cell cytotoxicity and Proliferation

In vitro cell investigations have been carried out to evaluate the biocompatibility of ZnO, TiO_2, Al_2O_3, and ZrO_2 in the development of bioactive glasses. Cytotoxicity and proliferation were analysed using Cell Counting Kit-8 (CCK-8) viability assay, where $2x10^4$ cells per 96-well plate of rMSC cells were cultured using conditioned media for a period of 24 h and 72 h. The media that was conditioned was replaced every day. The cells cultivated using normal cell media acted as negative control. Cytotoxicity was then recorded precisely using CCK-8 assay by incubating samples with the CCK-8 reagent for 3 h in dark condition at 37 °C. The optical density (OD) values at 450 nm were measured using the iMark microplate

reader (BioRad, USA) and converted into cell viability. Three exact samples of each other (n = 3) were tested for each condition and standard deviation was calculated for each test. The results were expressed in the percentage of average absorbance of controls vs cultured; this means the optical density of control is set to represent 100% viability.

2.3.6 Conditioned media from rMSCs

Stock solutions of conditioned media were prepared by dissolving glass particles in minimum essential medium (α-MEM) to treat with rat mesenchymal stem cells (*rMSCs*). Stock solutions were generated at a concentration of 5 mg/mL and kept in a shaker incubator at 600 rpm at 37 °C for 24 h. Soon after the 24 h incubation period, the solutions were filtered using 0.2 μm syringe filter (Millipore). Solution of media was collected to record stock solution pH values following glass dissolution. The normal buffering of the body as also pH neutralization was concluded by media and storing at 4 °C.

2.3.7 *In vitro* Antibacterial activity test

The antibacterial activity prepared bioglass samples were evaluated by agar disk diffusion assay using bacteria, *Escherichia coli, Staphylococcus aureus* and *Pseudomonas aeruginosa*. The activity exhibit by a substance that can kill bacteria or inhibit its growth is termed as antibacterial activity. The antibacterial activity is indicated by a presence of clear zone around each sample disk. The glass specimens (discs) were sterilized under UV-light for 20 min in aseptic condition. An overnight grown bacterial suspension culture was used for spreading onto the agar plates. 100μL of this suspension culture was introduced onto the agar plates and sample disks were placed at the centre of the agar plates. The agar plates were incubated at 37 ^{o}C in a static incubator. Also, the antibacterial activity was further confirmed by using the optical density (OD) method. According to this procedure, culture media was inoculated with a single species of bacteria in five different test tubes and samples were added (5mg/mL) in the respective test tubes. These culture tubes were kept at 37 ºC at 170 rpm for seven hours. The optical density was measured at different time points (0-7 h) at 600nm in a plate reader. Optical density indicates the concentration of bacterial cells in the suspension culture. All the experiments were performed in triplicates for statistical analysis.

2.4 Materials characterization techniques

2.4.1 Microhardness and Fracture toughness

The microhardness (Hv) test was performed on a highly polished glass sample surfaces (model: SHIMADZU micro hardness tester–HMV-G20S, Japan), at room

temperature with an applied load of 200 gf (1.96 N) as dwell time 15s (Fig. 2.2). For the accuracy in measurement, ten indentations were taken at different points on the surface of the each glass sample. The measurement method involves the use of a diamond micro indenter in shape of a square pyramid (Vickers indenter).

Fig. 2.2 Vickers micro hardness tester (HMV-2000/SHIMADZU)

The resulting impressions of the indents were captured and corresponding length of the indent impression diagonals and length of the cracks originated from the corners of the indent impressions were also recorded by using an optical microscope after unloading. These indentation measurements were carried out at ambient temperature with relative humidity. The microhardness (Hv) and fracture toughness (K_{IC}) were calculated using the formula:

$$\text{Microhardness } (H_v) = 1.854 \frac{F}{d^2} \qquad \textbf{2.7}$$

Where H_v Vickers hardness in GPa, F is the applied force in Newton and d is a length of the diagonals of the indentation in m. The glass fracture toughness K_{IC} (MPa $m^{1/2}$):

$$\text{Fracture toughness } (K_{IC}) = 0.016\, H_v \frac{a^2}{C^{3/2}} \quad \textbf{2.8}$$

Where 'a' is half-length of diagonal of indentation, 'c' is crack length of the centre of indentation to the crack end [6-8].

2.4.2 Differential thermal analysis

Thermal properties of phosphate based bioglasses were analyzed using a Differential thermal analysis (DTA) and Thermo Gravimetric (TG) measurements were carried out on glass powder samples in an air medium from room temperature to 1100 ^{o}C with heating rate of 10 ^{o}C min^{-1} by using NETZSCH-STA 2500 Regulus thermal analysis system, as shown Fig. 2.3. This DTA technique used to examine thermal events in a sample i.e. the crystallization, melting, solidification, decomposition, oxidation etc., by heating or cooling without mass exchange with its surroundings. Thermogravimetry (TG) is a technique which is used for measuring change in mass of a sample with temperature. The glass powders with ~20 mg quantity were taken in an alumina crucible and powdered alumina was used as a reference material to determine the glass transition temperature (Tg), crystallization temperature (Tc) and melting temperatures (Tm). The difference between Tc and Tg representing the thermal stability (ΔT) and the ratio between Tc−Tg and Tm−Tc gives Hruby's criterion (H) of the glass system:

$$\Delta T = T_c - T_g \quad \textbf{2.9}$$

$$H = \frac{T_c - T_g}{T_m - T_c} \quad \textbf{2.10}$$

Fig. 2.4 shows DTA traces, where the upward peaks indicate glass transition temperature (Tg), and crystallization temperature (Tc), which are due to exothermic reaction, while the downward peak indicates melting temperature (Tm) is characterized by endothermic reactions were obtained from the DTA thermographs of all the glasses [9].

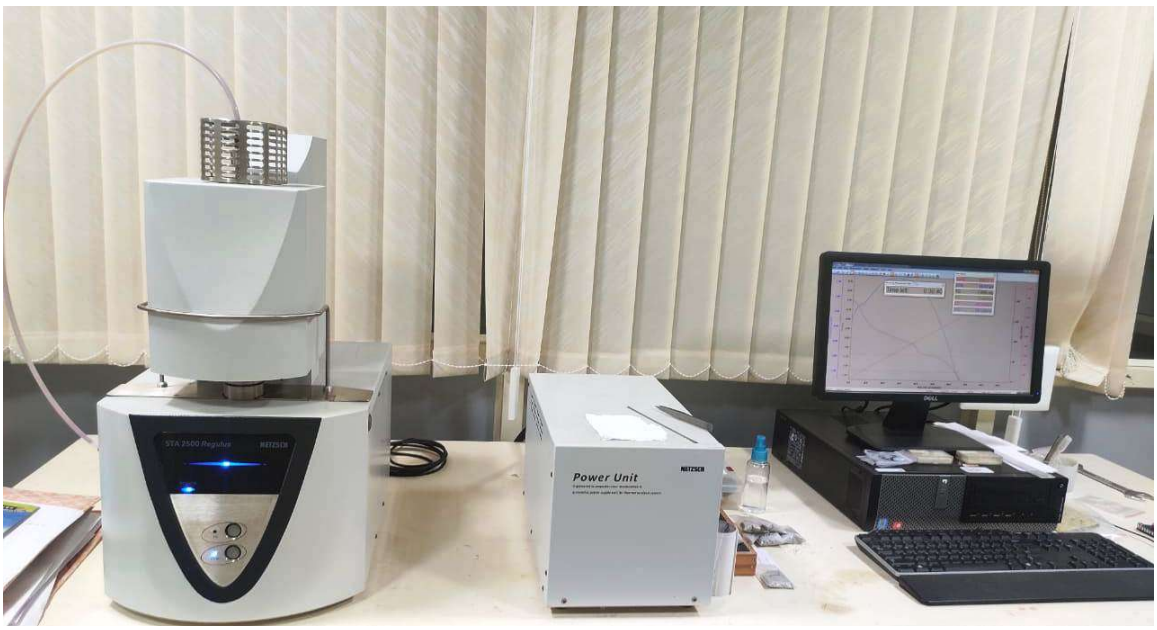

Fig. 2.3 TG-DTA thermal analysis

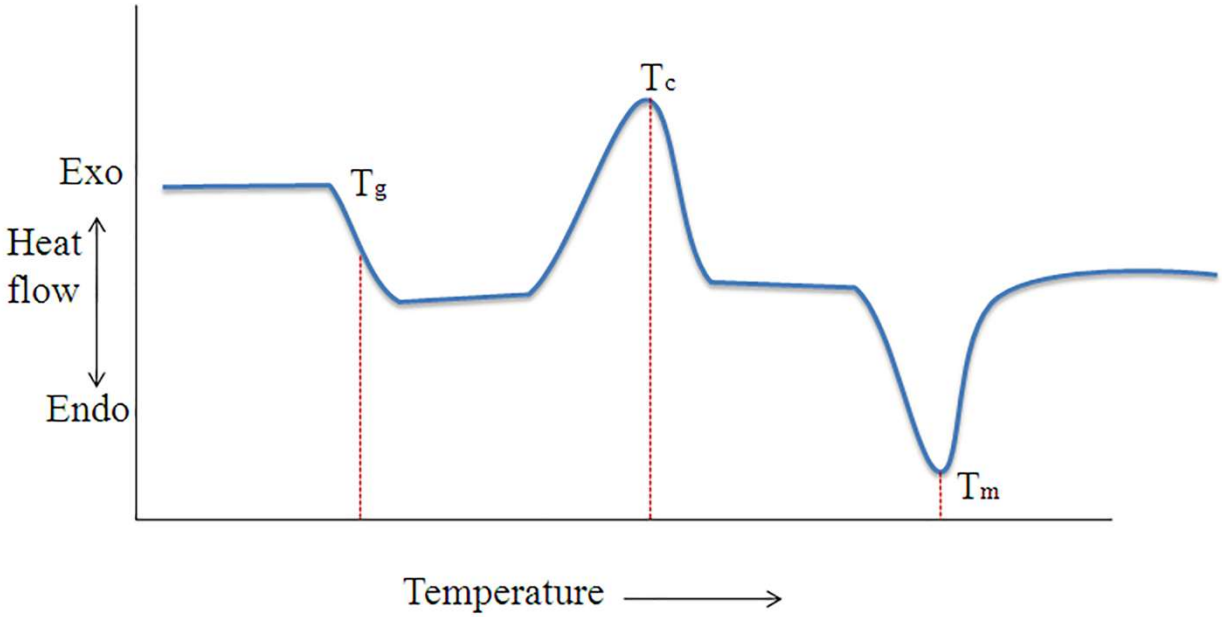

Fig. 2.4 A schematic representation of DTA trace

2.4.3 X-Ray Diffraction Study

X-ray diffraction (XRD) has turned out to be one of the greatest methods for defining atomic structure of solids. XRD technique is commonly used for phase detection and crystal structure of samples. In the present work, Powder X-ray diffraction (Model: PANalytical X'pert Powder) using Cu-Kα as a radiation (λ=1.540598 Å) source at a scanning angle ranging between 10º-80º with a step size of 0.001° and time per step set 20s. In the present work standard data base JCPDS cards (2003) were used as reference data for the interpretation of X-ray patterns obtained. The prepared bioglass samples were characterized by the X-ray

diffraction performances. The presence of a wide hump in the sample indicates the amorphous nature and the pattern of sharp peaks corresponds to crystalline nature of the sample. For the present study this technique was deployed to evaluate the glassy phase after preparation of glass by quenching, and also with the aim of identifying phase formation after it was soaked in SBF solution.

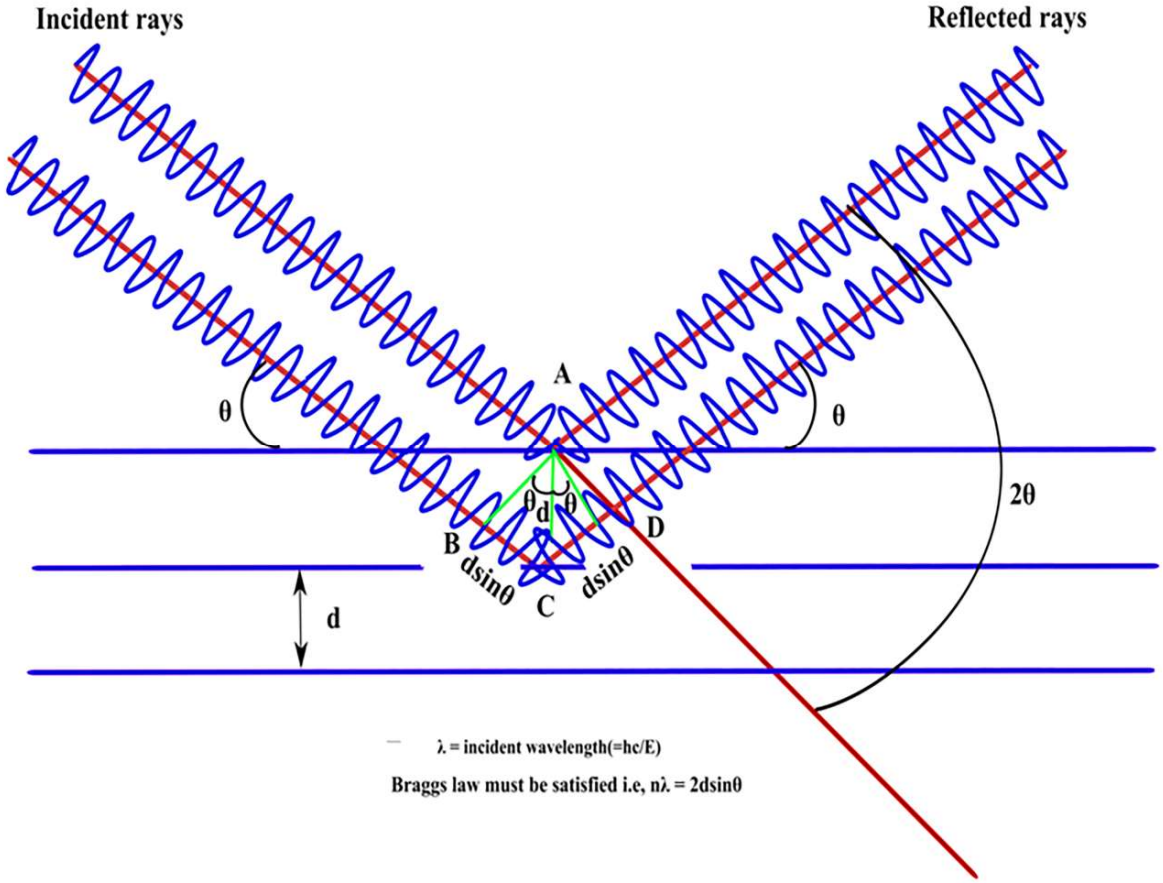

Fig. 2.5 Schematic illustration of Bragg's diffraction

It is a non-contact and non-destructive technique, which is suitable for the classification of any solid samples. When X-rays are incident on the sample, they will interact with the electrons of the atom and scatter the incident radiation. This kind of scattering from the crystal planes takes place only when the lattice spacing (d) is comparable with the wavelength of X-rays. As a result of the scattering, constructive or destructive interference may occur depending on the path difference between the scattered rays as shown in Fig. 2.5.

The condition for conducting a structural interference is that the path difference between the scattered rays is the total number of multiples (n) of wavelength of X-rays, i.e., when conditions satisfy Bragg's Law [10].

$$2d\sin\theta = n\lambda \qquad \textbf{2.11}$$

Where ‘θ’ is the diffraction angle and ‘λ’ is the wavelength of X-rays (λ Cu Kα = 1.54056 Å), *d* is the inter plane distance in the crystalline structure. The position of the diffraction peaks of the same sample changes with change in the wavelength of the X-rays.

Fig. 2.6 PANalytical powder diffractometer

2.4.3.1 XRD-Working principle

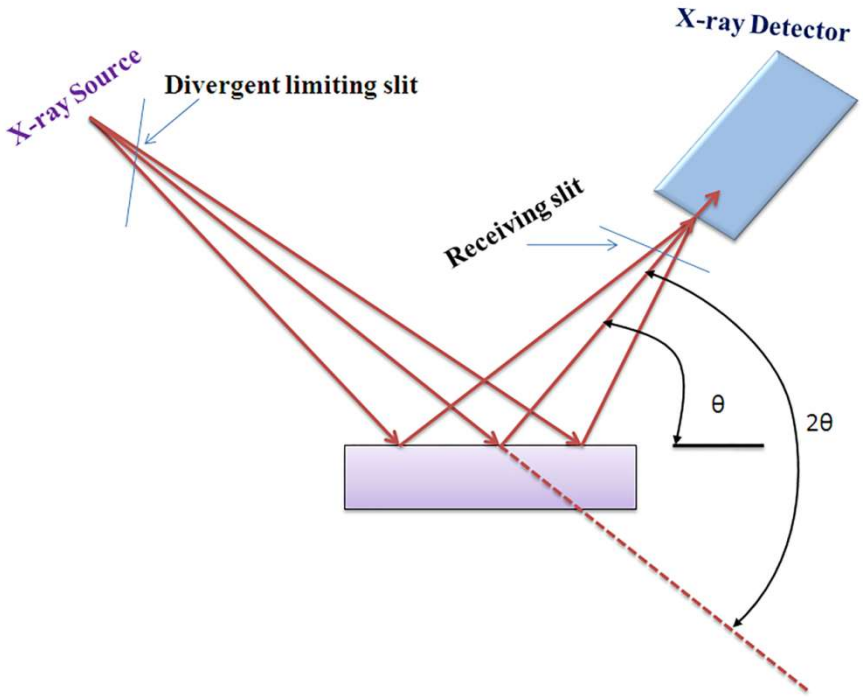

Fig. 2.7 Basic features of an X-ray diffractometer

An X-ray diffractometer comprises three basic units: an X-ray tube, sample holder and an X-ray detector as given in Fig. 2.7. The electrons generated by heating the filament are accelerated toward the target by applying a voltage and made incident on the target material. The electrons possessing sufficient energy hit electrons from the target material resulting in characteristic X-ray emission spectra. The characteristic spectra consist of several components, the most used for X-ray diffraction being Cu-Kα and Cu-Kβ. The monochromatic X-rays are obtained after crossing X-rays with a crystal monochromator. Monochromatic X-rays are collimated and made incident on the sample. X-rays that satisfy Bragg's law interfere constructively forming a bright spot on the detector. The basic characteristic of X-ray diffractometer is shown in Fig.2.7. The setup of the PANalytical powder Diffractometer is shown in Fig 2.6.

2.4.4 Fourier transform infrared spectra

FTIR spectroscopy is a method for obtaining the infrared spectrum of transmission or solid absorption. It is an important tool used to reveal the presences of various structural groups in glasses are present in phosphate-based glasses. The structural properties of bioglass samples were analysed by FTIR spectrometer (FTIR: model S 100; PerkinElmer) as shown in Fig. 2.8. The infrared spectra of the glass sample were noted at room temperature in the spectral range of 400–4000 cm^{-1} at a resolution of 4 cm^{-1}. The pallets were prepared by

mixing sample with KBr (infrared grade-Potassium bromide) in 1:100 ratios by weight and then pressing them using hydraulic press. These pellets were immediately used to record FTIR spectra. From each sample, the FTIR spectrum was normalized with empty KBr pellet. It can be used to analyze organic and inorganic substances. The above studies were done on all glass composition before and after completing *in vitro* studies. Then it helps to determine the chemical bonds or molecular structure of materials in the molecule by producing infrared absorption spectra. Thus the presence of specific functional groups can be monitored by the types of infrared bands, known as group wavenumber.

Fig. 2.8 Perkin Elmer 100SFTIR Spectrophotometer

2.4.4.1 FTIR-Working Principle

The schematic diagram of FTIR spectrophotometer is illustrated in Fig. 2.9. FTIR spectrophotometer has recently replaced the conventional equipment's (dispersing type) due to its superior speed and sensitivity. The FTIR spectrophotometer has consisted of three main basic portions namely, infrared source, an interferometer, and a detector. The interferometer again consists of three parts, namely beam splitter, moving mirror, and fixed mirror. The basic part of the instrument is called the Michelson interferometer.

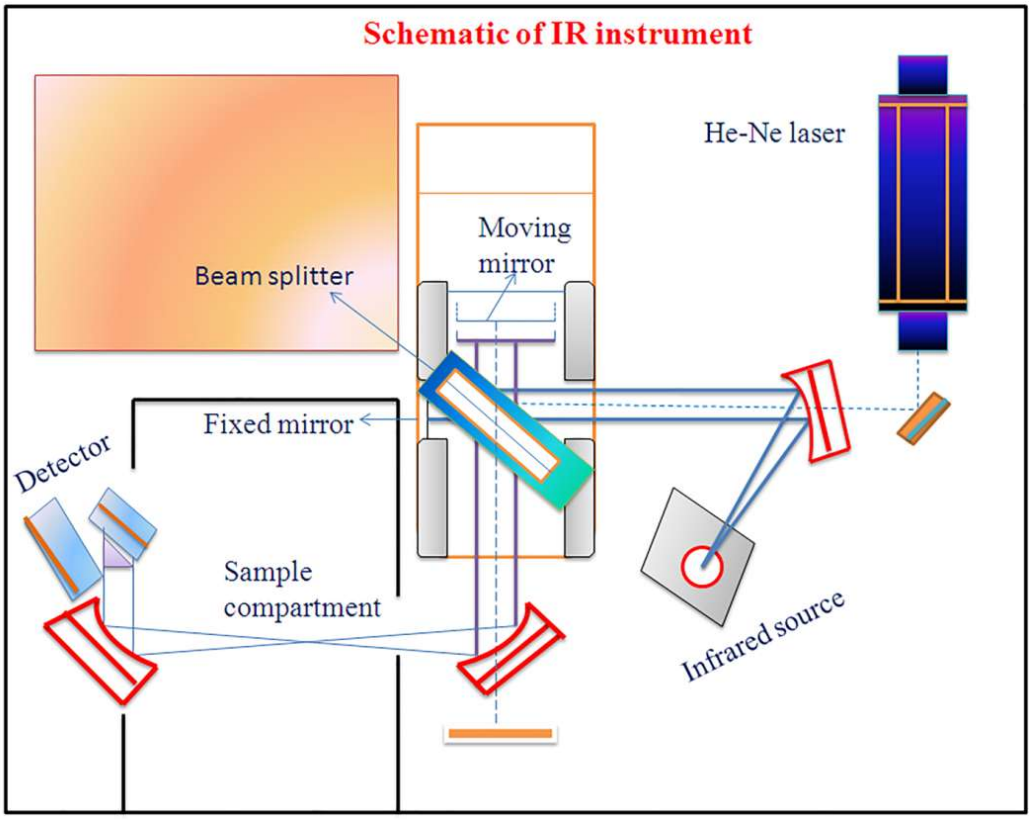

Fig. 2.9 Schematic diagram of Fourier Transform Infrared spectrometer

When the radiation from an IR source is incident on the beam splitter, than half of the radiation is transferred, and half is revealed. The transmitted and reflected beams are made incident on the fixed and moving mirrors respectively from which the beams are reflected rear and incident on the beam splitter. The stable and moving mirror beams interfere constructively and destructively, depending on the mid-path difference. It is the sinusoidal signal at the beam splitter which affects the pattern and focuses on the detector [11].

2.4.5 Scanning electron microscope

The scanning electron microscope (model:VEGA 3 LMU, TESCAN) instrument have been used to investigate the morphologic properties of glass surfaces, which *in vitro* studies explore any precipitation on the surface of the glass nature and the microstructure of glasses as well. On account of the manner in which the image is generated , SEM images bring with them a characteristic three-dimensional appearance and are greatly effective for observing the surface structure of the sample.The photograph of the instrument is shown in Fig.2.10. SEM is one type of electron microscope widely used to produce high-resolution images of a sample surface that is not possible with a light microscope. Thus, from micrographs obtained using the SEM microscope, the Ca-P apatite layer formed on bioactive glasses was identified. In our

case here, we used this microscopy method to analyze the glass phases and layer formation on the glass surface.

Fig. 2.10 Scanning Electron Microscope-Energy Dispersive Spectroscopy (TESCAN, WEGA3 LMU)

2.4.5.1. Working principle of SEM

SEM consists of an electron gun and electromagnetic lenses, and used to study the surface structure and morphology of different materials. A well-defined, when high energy incident electrons strike a specimen, they generate secondary electrons, back scattered electrons, characteristic X-rays, etc. These resultant electrons can be detected with appropriate detectors and provide insight about the surface structure and morphology of the specimens. The characteristic X-rays generated are used to obtain the chemical information from a specimen by using energy dispersive spectrometer (EDS) and wavelength dispersive spectrometer (WDS) techniques. The depth of focus is far larger than that provided by an optical microscope image even at very minute magnifications which is one of the nique selling points of SEM.

2.4.6 Energy dispersive X-ray spectroscopy

The EDS is an analytical method on behalf of elemental analysis or chemical characterization. Each element has a unique atomic structure which would be translated into a particular set of peaks on its X-ray spectrum. When incident high-energy radiations ionized

the atoms in the material, they emit characteristic X-rays. EDS is one of the techniques of X-ray fluorescence spectrometry which analyzes characteristic X-rays from energies. An EDS system comprises a source of high-energy radiation, usually electrons, a sample, a detection system i.e. solid-state detector (usually made from lithium-drifted silicon, Si (Li)), and data collection and processing system. EDS spectrometers are very often attached to electron column instruments. X-rays that enter Si (Li) detector generate a specific number of electron-hole pairs. The characteristic X-rays photons can be separated by their energy levels because high energy photons generate a the number of electron-hole pairs. The X-ray spectrum consists of a series of peaks representing the type and relative amount of each element contained in the sample. The number of columns in each peak may be further converted into elemental weight concentration by comparisons with standard calculations.

2.5. Safety measures needed for handling biomaterials

- When you are working in a research lab or any other place that deals with chemical or biological samples, you may be tasked with preparing these substances for later use. The exact precautions you need to take will vary with the setting and with what kinds of samples you work with, but here are some generally accepted practices help you keep safe.

- Always wear gloves. This may be particularly important in cases where you need to prepare formulations that are free from any contamination. You need to wear these gloves not only to avoid contamination of the substance but also to avoid being burned by some chemical, like an acid, or infected with some dangerous bacterium.

- If necessary, wear a face mask or shield, as well as goggles. A face shield will protect your face from getting burned from a chemical and goggles will protect your eyes. In some instances, you'll be preparing solutions that give off very dangerous and toxic fumes that may make you choke, or gag, or cough. In those cases, you should work in very well-ventilated areas and/or in labs that use fume hoods, which will limit your exposure to toxic fumes.

- Although there is broad evidence that neither bioglass nor PLA is toxic, adequate testing is mandatory for polymers to be used in biological systems. Before the use in humans it must be proved that the material is biocompatible and not cytotoxic.

References

[1] M.M. Babu, P.S. Prasad, P. Venkateswara Rao, N.P. Govindan, R.K. Singh, H.-W. Kim, N. Veeraiah, Titanium incorporated Zinc-Phosphate bioactive glasses for bone tissue repair and regeneration: Impact of Ti^{4+} on physico-mechanical and in vitro bioactivity, Ceram. Int. 45 (2019) 23715–23727.

[2] M.M.Babu, P.S. Prasad, P. Venkateswara Rao, N. Veeraiah,Effect of Al^{3+} ions substitution in novel zinc phosphate glasses on formation of HAp layer for bone graft applications, Colloids and Surfaces B: Biointerfaces 185 (2020) 110591.

[3] V.H.Rao, P.S. Prasad, P.V. Rao, L.F.Santos, N.Veeraiah, Influence of Sb_2O_3on tellurite based glasses for photonic applications, J. Alloys Compd. 687 (2016) 898–905.

[4] O.A. Zamyatin, A.D. Plekhovich, E.V. Zamyatina, A.A. Sibirkin, Glass-forming region and physical properties of the glasses in the TeO_2−MoO_3−Bi_2O_3 system, J. Non. Cryst. Solids. 452 (2016) 130–135.

[5] T. Kokubo, H. Takadama, How useful is SBF in predicting in vivo bone bioactivity?, Biomaterials. 27 (2006) 2907–2915.

[6] H.C. Li, D.G. Wang, X.G. Meng, C.Z. Chen, Effect of ZrO_2 additions on the crystallization, mechanical and biological properties of MgO–CaO–SiO_2–P_2O_5–CaF_2 bioactive glass-ceramics, Colloids Surfaces B Biointerfaces. 118 (2014) 226–233.

[7] S.M. Abo-naf, E.M. Khalil, E.M. El-sayed, H.A. Zayed, R.A. Youness, Spectrochimica Acta Part A : Molecular and Biomolecular Spectroscopy In vitro bioactivity evaluation , mechanical properties and microstructural characterization of Na_2O–CaO–B_2O_3–P_2O_5 glasses, 144 (2015) 88–98.

[8] J.K.M.F. Daguano, P.A. Suzuki, K. Strecker, M.H.F.V. Fernandes, C. Santos, Evaluation of the micro-hardness and fracture toughness of amorphous and partially crystallized 3CaO·P_2O_5–SiO_2–MgO bioglasses, Mater. Sci. Eng. A. 533 (2012) 26–32.

[9] Yangleng “Material characterization: introduction to microscopic and spectroscopic methods”, mar-2009.

[10] W.H. Bragg, The reflection of X-rays by crystals, Philos. Mag. 17 (1914) 428–438.

[11] J.R. Ferraro, and L.J. Basile, Fourier Transform Infrared Spectroscopy, Academic Press, New York-1982.

Chapter-3

Synthesis and characterization of ZnO doped phosphate based bioactive glasses for bone regeneration

This chapter discusses aspects of $Na_2O–CaO–P_2O_5$ glass matrix with Zn^{2+} ions concerning the investigation of phosphate-based bioglass structural properties. The bioglass samples were prepared using a traditional method of melt-quenching technology. In this chapter the physical properties of glass samples, such as density, molar volume, micro hardness and in vitro bioactivity test were conducted after immersing them in SBF solution for 3, 7, 14, and 21days. Then results of structural analysis with the help of X-ray diffraction, SEM-EDS, FTIR-Spectroscopy, TG-DTA and biological studies on cell cytocompatibility and antimicrobial properties are clearly described in this chapter.

3.1 Introduction

Bioactive glasses and glass ceramics are most prominent materials for application in the repair and regeneration of damaged soft and hard tissues. These glasses have potential to solve the transplantation problems occurred due to shortage of living tissues and organs available. In general these bioactive materials undergo specific surface reactions with the tissues and form a HAp layer when implanted into the body. Moreover, this HAp layer is similar to the mineral constituent of bone. This layer acts as an interface and also forms a strong bond between implant and tissue [1,2]. The thickness and strength of the HAp layer depends on chemical composition of choosing glass matrix. Bioactivity is the measure of the material to form apatite layer when the materials in contact with the physiological body fluid in vitro. It also confirms from the *in vitro* bioactivity that the material can show potential bioactivity *in vivo* environment [3]. The first bioactive glass compositions were successfully described by Larry Hench and his co-workers in 1970s [4]. Clinically approved various bioactive glasses like 45S5, 58S, and some silica based glasses are used effectively for bone and dental applications [5,6]. Most of the available commercial bioglasses contain high amount of silica. These silica rich glasses are potential to develop long term implants to replace hard and soft tissues in vivo due to insoluble nature. However, the long term interaction of silica locally and systemically is not yet understood completely and raising the issue about the long-term reaction *in vivo* [7,8]. Most of the clinical reports proved that the glasses with high amount of silica and high network connectivity were accepted by the human body but the rate of degradation was very low and the glass remnants were present in the patient's body for more than 14 years [9,10].

However, as an alternative for rarely absorbed SiO2 glasses for tissue repair, P_2O_5 based glasses were developed by many researchers because of their unusual properties such as lower melting temperature, lower transition temperature, higher thermal expansion coefficient, higher electrical conductivity, higher degradability, higher biocompatibility and lower chemical durability [11,12]. Among the phosphate based glasses, the calcium containing phosphate glasses shows high bioactivity. Moreover, these glasses are the best suits for bone bonding due to the chemical composition which is very close to the natural bone phase [13]. In general, phosphate based glasses have high dissolution and poor chemical durability when compared with silicate and borate based glasses, which limits the applications. The control over degradation rate and improvement of chemical durability can be obtained by adding intermediate network modifiers such as transition metal oxides (Ca^{2+}, Na^{+}, Zn^{2+},Mg^{2+}, Sr^{2+} and K^{+}) [14,15]. The incorporation of these elements modifies the phosphate network and subsequently affect the degradation properties. The rate of

degradation can be selectively controlled by varying the amounts of these constituents incorporated into the glass [15].

Zinc is one of the most abundant trace elements present in bone and it shows the stimulatory effect on the formation of bone mineral phase *in vitro* and in vivo. It is essential for the function of all cells to regulate genetic control of cell proliferation by binding specific deoxyribonucleic acid (DNA) regions. The addition of ZnO to the bioglass system can inspire cell proliferation and differentiation so that the capacity to form a strong bond with the bone. In particular, ZnO improves the bioglass chemical permanence in aqueous solutions such as body fluids and also improves its mechanical strength [16,17]. Besides, it also increases the bone mass, anti-inflammatory, antibacterial, and bone healing properties by increasing the DNA of osteoblasts [18-21]. Abou Neel et.al, reported that the formation of bone bonding enhances on replacing some content of calcium with zinc in bioglass system [10]. On the other hand, a high amount of zinc release can create adverse reactions, so as to avoid this; the rate of release of zinc from implanting must be slow. The release of zinc can be slowdown by incorporating divalent cations with suitable ionic radius [22].

In the present paper, we focused on the development of novel bioglass system ZnO–Na_2O–CaO–P_2O_5 and detailed study on influence of ZnO incorporation on structural, thermal properties, mechanical strength, degradation, pH variation, and formation of HAp layer on the glass surface and cell viability for generation of bone resorbable implants.

3.2 Results and Discussion

3.2.1 Glass conformation test

The glassy nature of the prepared P_2O_5 based bioglass samples was examined by recording X-ray diffraction patterns shown in Fig.3.5 (a). The results obtained show any noticeable sharp intensity peaks present in the diffraction patterns and also the appearance of broad humps over the region 20°–34° for 2θ indicates the no long rage order periodicity in the glass network, which corresponds to diffraction effects due to amorphous portion of the samples. It confirms the amorphous glassy nature of the chosen glass materials [23].

3.2.2 Physical parameters of the bioglasses

The experimental results of various physical parameters such as density, molar volume, oxygen molar volume, and oxygen packing density of the bioglasses are summarised in Table 3.1. The ZnO concentration dependent density, molar volume, and oxygen packing density are shown in Fig. 3.1 (a) & (b). The density and oxygen molar volume are found to increase

and the molar volume and oxygen packing density decreased with increase of ZnO concentration.

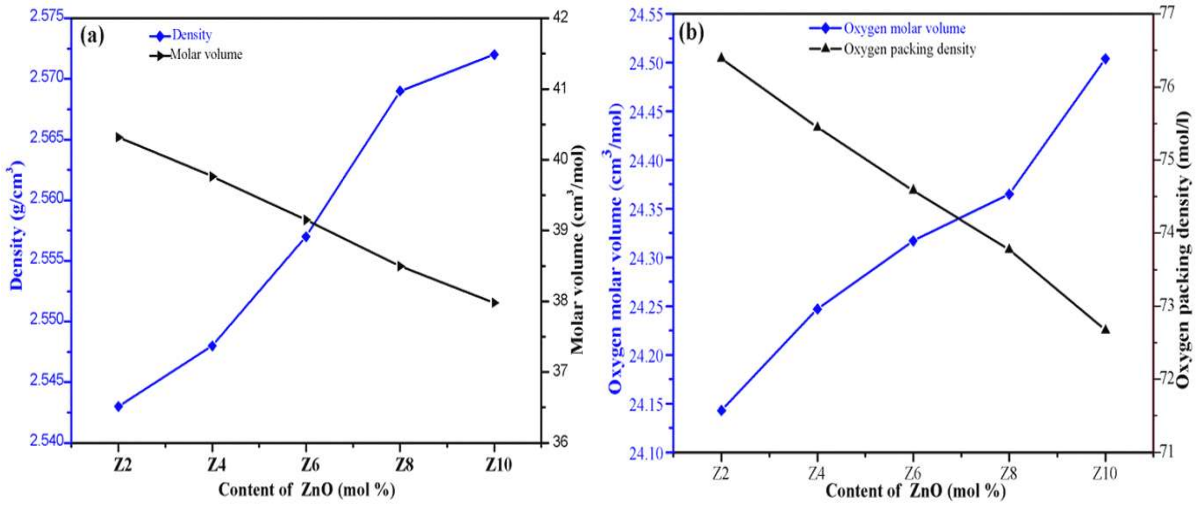

Fig. 3.1 Variation of different physical parameters of studied glasses with increase in content of ZnO (mol%): (a) Density (g/cm^3) and Molar volume (b) Oxygen molar volume and Oxygen packing density.

Table 3.1 Physical and mechanical parameters of the ZnO–Na_2O–CaO–P_2O_5 glass system

Sample code	Molar mass (g/mol)	Molar volume (Vm) (cm^3/mol)	Density (ρ_g) (g/cm^3)	Oxygen molar volume(Vo) (cm^3/mol)	Oxygen packing density (OPD) (mol/1)	Vickers hardness Hv (GPa)	Fracture toughness, K_{IC} (MPa m$^{1/2}$)
Z2	102.532	40.319	2.543	24.143	76.389	2.615(±0.0742)	0.17609
Z4	101.321	39.765	2.548	24.247	75.443	2.652(±0.0744)	0.18365
Z6	100.110	39.151	2.557	24.317	74.582	2.763(±0.0972)	0.19825
Z8	98.898	38.497	2.569	24.365	73.772	3.190(±0.0921)	0.25099
Z10	97.687	37.981	2.572	24.504	72.667	2.781(±0.1003)	0.19682

The density values of glasses varied from 2.543 g/cm^3 to 2.572 g/cm^3, oxygen molar volume (Vo) of the glasses increases slightly from 24.143 cm^3/mol to 24.504 cm^3/mol and inversely the molar volume (Vm) of the glasses decreases from 40.319cm^3/mol to 37.981 cm^3/mol with increase of ZnO mole %. The oxygen molar volume (Vo) of the glasses system showed slight increase from 24.143 cm^3/mol to 24.504 cm^3/mol. The increase in density clearly indicates the presence of more ionic nature of P–O–Zn bonds than P–O–P bonds in the glass network. This leads to the compactness of the glass structure, [27] and also due to the higher density of ZnO (5.61 g cm^{-3}) with respect to P_2O_5 (2.30 g cm^{-3}) [28]. On the other

hand, the decrease in molar volume is due to the reduction in the mole fraction of oxygen ions in the glass [29]. The molar volume decrease can be attributed to strong bond of the Zn–O bond in comparison to P–O and P–O–P bonds which results in smaller bond lengths consequently causing a tightening of the glass network [28,30]. The substitution of P_2O_5 by ZnO is responsible for this orderly decrease because the ionic radii of oxygen ions are higher when compared with radii of both Zn and P ions [29]. Oxygen packing density (OPD) of the glasses varied between 76.389 to 72.667 mol/1 and are found to decrease with content of zinc oxide (2 to10 mol%). Which is attributing the less tightly packing of oxygen atoms in the glass network [23].

3.2.3 Thermo gravimetric-differential thermal analysis

The analysis of various thermal parameters for instance glass transition temperature (Tg), crystallization temperature (Tc), melting temperature (Tm), thermal stability (ΔT) and Hruby's criterion (H) of the glass system is essential to understand the structural transformations with different temperatures. From DTA traces the upward peaks indicates the glass transition temperature (Tg) and crystallization temperature (Tc) are due to exothermic reaction and the downward peak indicates melting temperature (Tm) is characterized by endothermic reactions. The different thermal parameters are labelled in Table 3.2 and DTA traces are shown in Fig. 3.2.

Table 3.2 Thermal properties of ZnO doped bioactive glasses

Sample code	Tg (^oC)	Tc (^oC)	Tm (^oC)	ΔT (^oC)	K_H
Z2	343.31	458.73	716.18	115.42	0.4483
Z4	345.27	456.53	714.11	111.26	0.4319
Z6	346.89	459.12	709.86	112.23	0.4475
Z8	348.52	469.12	704.43	121.19	0.5154
Z10	344.63	458.98	699.75	114.35	0.4749

The glass transition (Tg) values (343.31 ^oC–348.52 ^oC) increases with an increase in up to 8 mol% of ZnO content and then decreases for higher concentration of ZnO. In case of crystallization temperature (Tc) (458.73 ^oC–469.12 ^oC) and melting temperature (Tm) (716.18 ^oC–699.75 ^oC), there is a general decrease in trend with increase of ZnO content up to 10 mol%. The first increase in Tg with an increase of ZnO from 2 to 8 mol% is due to an increase in the average crosslink density through non-bridging oxygen ions (NBO) and the number of bonds per unit volume.

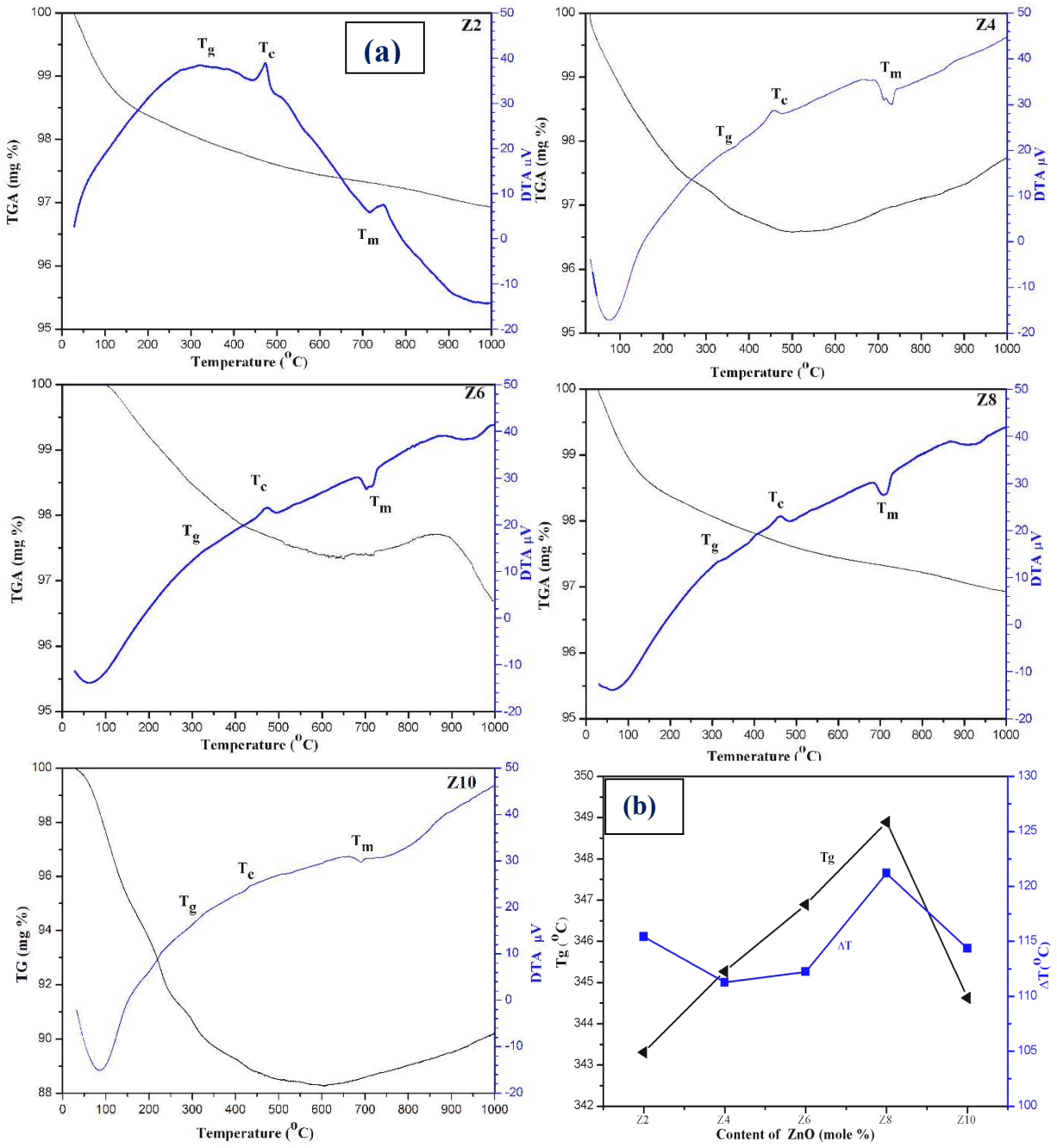

Fig. 3.2 (a) TG-DTA traces of Z2, Z4, Z6, Z8 and Z10 bioglasses and (b) Variation of glass transition (Tg), and thermal stability of all the glasses as a function of ZnO (mol%).

In addition, increase in Tg can also be due to the increasing aggregation effect of ZnO on the glass network and slow mobility of large Zn^{2+} ions, which lead to more rigidity of the glass network [30,31]. Further increasing the ZnO concentration leads to slight decrease in Tg from 348.52 °C to 344.3 °C, which is owing to the breaking of P–O–P bonds in addition of Zn^{2+} ions [30]. It is attributed to the high degree of depolymerisation in the glass network. Thermal stability (ΔT) is a measure of the rigidity of glass network while Hruby criterion (H) shows the glass forming tendency of chosen materials. In the present ZnO doped glasses, the values

of stability (ΔT) increases, from 111.26 °C to121.19 °C and Hruby criterion (H) increases from 0.4483 to 0.5154 with the content of ZnO, which clearly indicates high stability and good glass forming tendency of all glasses. The greater the value of (ΔT) and the smaller the difference of Tm–Tc the more the deceleration of crystallization against devirtification of the glass network, which leads to glass formation [32]. In the present system, Z8 is confirmed as the best glass because of its high thermal stability (ΔT) and Hruby criterion (H) values.

A significantly slight weight loss is observed at two regions of the TG curves shown in the Fig.3.2 along with DTA traces. The first weight loss of ~1.59% of Z2 sample appeared from the room temperature to ~128 °C and the second weight loss is around ~2.64%, from the temperature between ~128 °C to ~ 626 °C. In the Z4 sample the first weight loss of the ~1.93 % found from room temperature to 166°C and the second weight loss is ~3.25% from the 166 °C to 449 °C. The TG curve of Z6 sample is observed from the room temperature to 325 °C with a first weight loss of ~2.42% and a second weight loss of 3.18% from 325 °C to 623 °C. Similarly, for Z8 and Z10 samples the first weight loss of ~1.35% (from room temperature to 120 °C) and ~5.21% (159 °C) respectively. The second weight loss of ~2.51% from 120 °C to 610 °C and ~9.59% from 159 °C to 340 °C of samples Z8 and Z10 respectively. The first stage of weight loss at around 76 ^{o}C to 250 ^{o}C is owing to the loss of hydrated, and coordinated water molecules, which is coming into the ambient environment and the second stage of weight loss at around 300 ^{o}C to 600 ^{o}C is attributed to residual precursor phosphorus from the glass composition. After this there is no significant weight loss is observed with rise in temperature up to 1000 °C. The low loss of weight indicates the high rigidity of the glass network of as-developed samples [33].

3.2.4 Mechanical properties

The mechanical properties such as hardness, and fracture toughness are very essential for any material to establish structural compactness. Calcium phosphate glasses gain reasonably better improvement in mechanical properties with the addition of ZnO. The variation of Vickers microhardness and fracture toughness as a function of ZnO content of prepared bioglasses are shown in Fig.3.3 (a) and (b) the related values are summarised in Table 3.1. It is observed that Vickers microhardness and fracture toughness values gradually increases from 2.615 (±0.0742) to 3.190 (±0.0921) GPa and from 0.17609 to 0.25099 (MPa $m^{1/2}$) respectively with growing content of ZnO in the glass network.

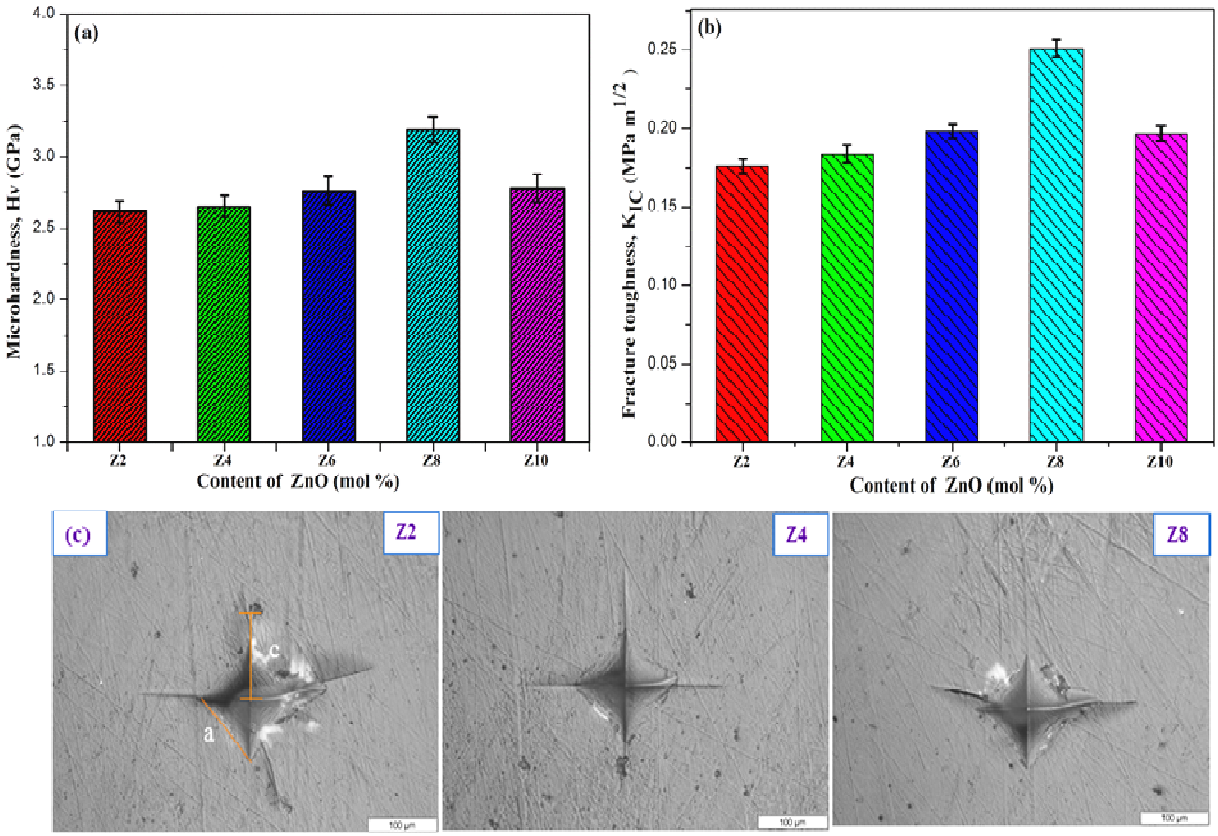

Fig. 3.3 (a) Microhardness and (b) fracture toughness of the Z2, Z4, Z6, Z8 and Z10 glasses as a function of the ZnO (mol%) and (c) Optical images of vickers indentation from Z2, Z4 and Z8 glass samples.

Fig. 3.3 (c) shows the optical microscopic Vickers indent impressions for Z2, Z4 and Z8 glasses. The fracture toughness of the bioglasses is calculated by using Hv values and measured the crack length from the optical microscopic Vickers indent impressions of the samples. A gradual increase in the measured microhardness and toughness values of the bioglasses, with increasing an ZnO content is due to the expansion of the glass network in harmony with the enhance in the bond length or inter-atomic spacing linking the atoms. Zn^{2+} ions enter interstitially in the glass network to form more P–O–Zn linkages by breaking the P–O–P bonds. Which in turn reduces the number of non bridgingoxygens (NBO's) and increases cross-linking density, compactness and rigidity of the glass network [34]. In the present as-prepared glasses Z8 has highest Hv and K_{IC} values. It is found that there is an increase in hardness and the toughness from Z2 (2 mol%) to Z8 (8 mol%) and then decreases slightly for Z10 (10 mol%), which is apparently due to the decrease in packing density [35,36]. It means breaking of some P–O–Zn bonds per volume in the glass network during the application of load, which leads to decrease the resistance to deformation.

3.3. *In vitro* bioactivity evaluation in SBF

3.3.1 X- ray diffraction analysis

The X-ray diffraction results of the glass samples (Z2, Z4, Z6, Z8 & Z10) after immersion in SBF for various time periods (3, 7, 14 and 21 days) are shown in Fig. 3.4 (a, b, c, d & e). The samples show any noticeable crystalline sharp peaks before immersion in SBF, which confirms the amorphous nature of all glasses (Fig. 3.4 (a)). After immersion in SBF for different days, the XRD patterns show intense crystalline peaks. It is signifying the formation of a crystalline hydroxy apatite ($Ca_{10}(PO_4)_6(OH)_2$) layer on the surface of the glasses. The observed peaks for present glasses at different diffracted angles (2θ) subsequent to HAp reflections 10.82 (110), 15.28 (021), 21.73 (200), 22.82 (111), 23.50 (231), 25.87 (002), 27.56 (131), 31.74 (211), 32.17 (112), 32.86 (300), 40.81 (103), 41.80 (032), 45.32 (203), 56.27 (500), 66.36 (143), 75.56 (215) (indexed using the JCPDS card No 72-1243) are shown in Fig. 3.4 (b, c, d, e). The HAp layer is developed on the surface of the glasses due to chemical reaction of the glass surface with the simulated body fluid [37,38].

After 3days of immersion in SBF, the diffraction pattern shows development of four prominent peaks at 2θ values of 10.82, 21.73, 31.74 and 45.32 corresponding to crystal planes (110), (200), (211) and (203) respectively shown in Fig. 3.4. It is observed that, the peak intensity of HAp reflections (203) and (211) increases, while for (110) and (200) decreases at 2θ with increase in content of ZnO. Additional peaks are observed along with the above mentioned four reflections after 7, 14 and 21 days of incubation period in SBF. The intensities of the reflections at different values of 2θ increase gradually with increase in incubation time (7, 14 and 21days) and also with change in ZnO content Fig. 3.4 (b, c, d, e & f). After 21 days of immersion time, a clear dense apatite layer is detected on all glass surfaces. Accumulation of the HAp layer over the glass surfaces signals the bioactive nature of as-prepared glasses. The evolution of the crystalline HAp layer as a function of incubating time in SBF is confirmed by the gradual intensification and reduction of individual HAp reflections at diffracted angles 2θ and also thinning of the peak width. In all samples, there is an increase in intensity of two prominent reflections at 31.74 (211) and 45.32 (203) with a variation of immersion time is observed due to the increase of Ca^{2+} and PO_4^{3-} ions concentration on the surface of the glass by ion leaching, which initiate the development of amorphous calcium phosphate ($CaO–P_2O_5$) rich layer and then it can be instigate to development of crystalline HAp layer on glass surface [2,38]

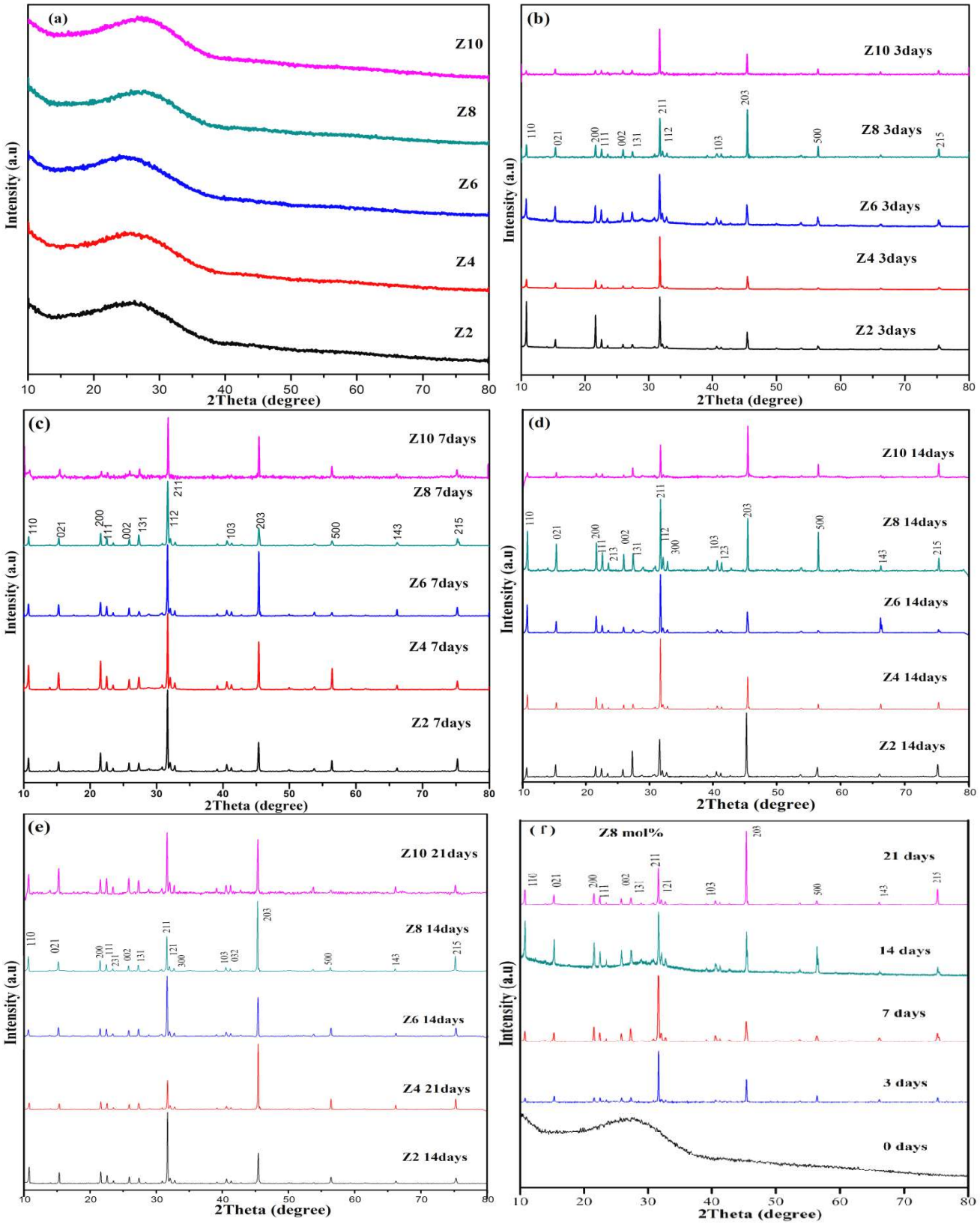

Fig. 3.4 XRD patterns of Z2, Z4, Z6, Z8 and Z10 glasses before and after immersion in a SBF solution for different time periods: (a) 0 days, (b) 3 days, (c) 7 days, (d) 14 days and (e) 21 days and (f) Variation of reflection intensities with different immersion points of Z8 (8 mol% ZnO) glass.

The addition of ZnO to glass network, enhances the crystallization of the $CaO–P_2O_5$ layer with the interaction of the SBF solution to shape the HAp layer by entering into the SBF solution as $Zn(OH)_2$ to create a large number of OH^- ions required for conversion of the amorphous layer to crystalline HAp layer [39]. The XRD results reveal that, the present chosen glasses showing high apatite layer forming ability to increase of ZnO content at the expense of the major constituent P_2O_5 in the glass matrix without disturbing the concentration of CaO and Na_2O.

3.3.2 FT-IR spectroscopic analysis

Fig. 3.5 Shows the FTIR spectroscopic pattern of the bio glass samples Z2, Z4, Z6, Z8 and Z10 before, and after immersion in SBF for 3, 7, 14, and 21 days. The spectrum before the immersion shows some intense absorption bands at 526, 720, 900, 1105 and 1270 cm^{-1} and weak absorption at 1643, 2382 and broad band of absorption peak around 3470 cm^{-1}. These bands are evident of phosphate group's occurrence in the glass network. FTIR spectra of the bioglass samples before immersion are displayed in Fig.3.5 (a). The absorption band at around 526 cm^{-1} may be assigned by the harmonics of P–O–P bending vibration and also due to the deformation mode of PO^- groups [30,40]. The peaks at 720 cm^{-1} and 900 cm^{-1} are due to symmetric and asymmetric stretching mode of vibrations attributed to P–O–P bands, respectively [40,41]. A peak at 1105 cm^{-1} is observed due to vibrations of a phosphate group ($P–O^–$) or might be P–O–Zn linkages [16-18]. Here there is a little intense band at around ~1270 cm^{-1} ascribed to (O–P–O), which is asymmetric stretching vibration of O–P–O bonds [41]. Nearly at around 1643 cm^{-1}, a weak intense band is assigned due to P–O–H bridge. These groups form the strongest hydrogen bonding with non-bridging oxygens [42]. From the IR band located in the range of 2382 cm^{-1} is very weak intense band and due to the assigned by the different structural sites as a stretching vibration of P–O–H group or stretching of CO_2 [30]. A broad band absorption peak at around 3470 cm^{-1} is due to the presence of water molecules in the glass structure. The presence of water is probably due to the absorption of atmospheric moisture by the phosphate glass sample or pellet resulting in the appearance of the H–O–H band belonging to water molecules, because the sample as such does not contain water as a unit in the network [43]. The FTIR spectra of the bioactive glass (Z2, Z4, Z6, Z8 and Z10) after immersion in SBF solution for 3, 7, 14 and 21days are shown in Fig. 3.5 (b–e).The functional groups of different bands confirming the HAp layer formation with comparison to literature are summarised in Table 5. After immersion in SBF for different time periods (3, 7, 14 & 21 days), new bands at around 556 to 665 cm^{-1}, 1035 to 1060 cm^{-1}, 1402

to 1552 cm^{-1}, 2088 to 3237 cm^{-1} are established along with the existing bands. This indicates the formation of HAp layer over the surfaces of the glass samples.

The peaks identified at around 556 to 665 cm^{-1} are ascribed to P–O stretching vibration modes of hydroxy apatite group [16,18,19,21] appeared in all glass samples shown in Fig. 3.5 (b–e). The intensity of these peaks decreases for the incubation of 3 to 7 days with the increase in content of ZnO and then rises from 14 to 21 days of incubation. The absorption bands at 744–740 cm^{-1} attributed to the symmetric stretching of the P–O–P groups [40,44]. These bands slightly shifted to higher wave number and the intensity increases with the incubation time and also with the concentration of Zn^{2+} ions in the glass network. It is observed in all these IR spectra near at 920–925 cm^{-1} absorption peaks ascribed to asymmetric stretching band (P–O–P) by asymmetric bridging oxygen atoms bonded to a phosphorus atom in a Q^2 phosphate tetrahedron [41]. From the Fig. 3.5 (b–e), the bands appeared at around 1035 cm^{-1} and 1060 cm^{-1} are the characteristic of P–O symmetric and asymmetric stretching vibration of phosphate groups, respectively [42]. It is found that, no change in intensity and shifting of the weak band at 1036 cm^{-1} with increase in concentration but disappears at 7 days of incubation, which might be overlapped with 1060 cm^{-1} band. The peaks at 1130 to 1142 cm^{-1} are assigned due to PO_2 symmetric stretching mode [45]. A stable band at 1295 cm^{-1} is ascribed to asymmetric stretching mode PO_2 shifted toward a lower frequency [42,45]. The intensity of this band increases with immersion from 3days to 14days and then decreases. It may be due to decrease in crystalline nature of Ca–P layer with an increase in ZnO concentration [22,46,47].

The presence of above mentioned significant phosphate bands in all bioglass samples for various incubation periods in SBF provides the evidence of rich HAp layer formation on glass surfaces. The development of bands at 1402 to 1404 cm^{-1} and a weak band at 1464 cm^{-1} confirms the presence of the carbonate CO_3^{2-} group. On the other hand the bands ranging from 1400–1512 cm^{-1} is related to substation of carbonate in the glass structure [30,48–51]. As a result, the growth of HAp layer on the glass surfaces is in the form of new hydroxy carbonate apatite (HCA) layer after immersion in SBF [12,30]. Along with CO_3^{2-} group bands, a sharp peak at ~1552 cm^{-1} authenticates the presence of A-type HCA [50,51]. Fig. 3.5 (b, c, d, e) show little broad absorption bands following a decrease in intensity with incubation and content of ZnO at 2088–2095 cm^{-1} which are attributed to P–O(H) stretching in HPO_4^{2-} groups [42]. The absorption bands at 3225–3237 cm^{-1} and 3409–3441 cm^{-1}, both corresponding to the stretching mode of vibration of –OH hydroxyl group. 3 days of

immersion shows abroad band located at 3438 cm^{-1} and with an increase in immersion time (7, 14 and 21 days), it splits into two sharp bands which peak at around 3225 cm^{-1} and 3441 cm^{-1}.

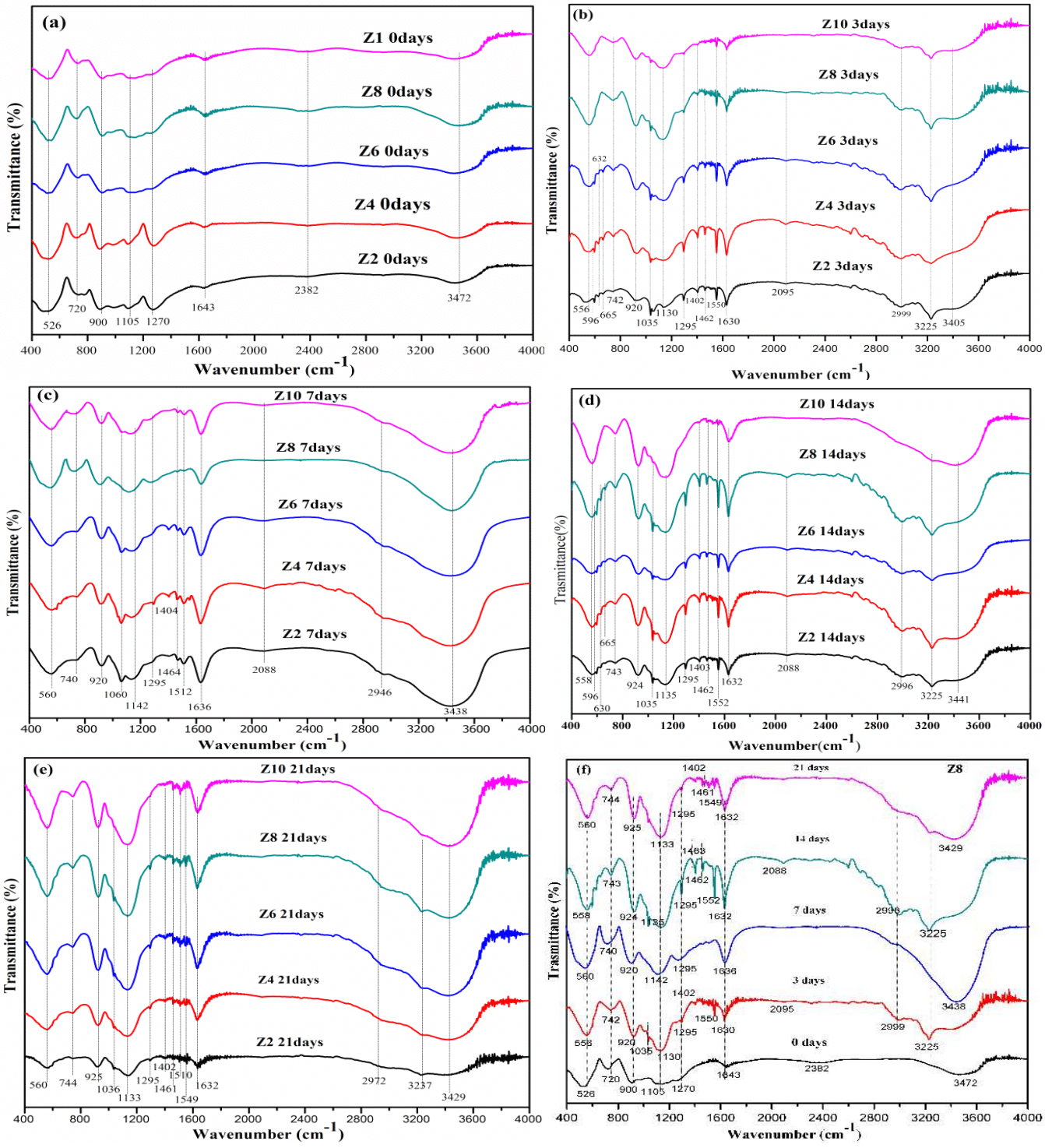

Fig. 3.5 FTIR spectra of Z2, Z4, Z6, Z8 and Z10 glasses before and after immersion in a SBF solution for different time periods: (a) 0 days, (b) 3 days, (c) 7 days, (d) 14 days and (e) 21 days and (f) Variation of band intensities with different immersion periods of Z8 (8 mol% ZnO) glass.

Table 3.3 Assignment of various FTIR bands before and after immersion of glass samples in SBF for 3,7,14 and 21 days.

Wave number(cm^{-1})	Assignment of FTIR bands	References
525	P–O–P bending Vib./Deformation mode of PO^{-}	[28,41]
556-560	P–O band (crystal)	[16,18,19,21]
594-596	P–O band	[16,18]
632-665	OH- HAp group	[19,20]
720	P–O–P stretching vibrations	[41,42]
740-743	P–O–P symmetric stretching	[41,46]
900	asymmetric stretching vibration of P–O–P linkages, ν_{as}(P–O–P),	[41,42]
1105	Symmetric stretching vibration ν_s (P–O–P)	[16,18,18]
920-925	P–O–P asymmetric stretching	[42]
1035-1060	PO_4 asymmetric stretching	[41,42,43]
1130-1142	1130 P= O asymmetric stretching 1142 PO_2 symmetric stretching	[47,48]
1270	ν_s (O–P–O) group	[42]
1295	(O–P–O) asymmetric stretching	[44,47]
1402-1404	1402–1404 OH group	[28]
1464	1470 C–O vibration in CO_3^{2-}	[48,53,54,55]
1552-1512	CO_3^{2-} Stretching vibration	[54,55]
1630-1636	OH^{-}	[28,56]
1643	P–O–H bridge	[43,44]
2088-2095	PO–OH stretching PO_4^{2-}	[44,57]
2382	stretching of CO_2 / stretching vibration of P–O–H group	[28,34]
2946-2999	PO–H stretching in HP_4^{2-} group	[44,57]
3225-3237	O−H stretching vibrational mode	[44,57]
3405-3441	hydroxyl (-OH) group	[42]
3472	H_2O or P–O–H vibration	[45]

Therefore, mentioned bands at around 1035, 1402, 2095, 2996 and 3225 cm^{-1} were completely missing *in vitro* tests. The above absorption peaks related to OH^{-} group of bonds confirms, the existence of hydroxyl components that originated from water molecules after *in*

vitro treatment and Fig. 3.5(f) clearly shows the variation of band intensities with different immersion periods of Z8 (8 mol% ZnO) glass sample. This discussion concludes, with the increase of zinc content and immersion time the intensity of absorption peaks related to apatite is pronounced more, confirming the development of the crystallized apatite layer (HAp) over the glass surfaces. These results are in good agreement with the XRD analysis.

3.3.3 SEM-EDS micrographs analysis

Fig. 3.6 shows the SEM micrographs and respective EDS spectra of Z8 and Z10 bioactive glass surfaces before (0days) and after being immersed in SBF solution for 3, 7, 14 and 21 days. The surfaces of Z8 and Z10 glass samples are appearing like more plane and smooth with a good compactness before immersion in SBF solution. This indicates no morphological change of the as-prepared glasses. After 3 days of immersion, the surface is mostly covered with flakes or foam type of structure, confirming the development of Ca–P apatite layer over glass surfaces. From the EDS spectra, it is clearly observed that, after immersion in SBF, there is a prominent increase in the intensities of existing peaks of calcium and phosphorous when compared with untreated samples. The EDS results confirm the formation of new HAp layer over glass surface with association to visual evidence from SEM micrographs. In addition to Ca and P, the EDS spectra reveals the presence of elements O, Mg, Cl, S, K and Zn on the surfaces of the treated all samples in SBF. The existence of these elements is due to ion exchange between the glass and the simulated body fluid. Moreover, these elements are responsible for growth of bone-like apatite precipitates over glass surface (shown in Fig. 3.6). After 7 days and 14 days of immersion, the glass surfaces of Z8 and Z10 are all most covered with cotton foam like a well precipitated apatite layer. It is also observed from Fig. 3.6 after 21days of immersion, a complete dense layer of HAp is produced on the surfaces of Z8 and Z10 glasses. In addition, the gradual increase in Ca and P concentrations with the increase in immersion time from 3days to 21 days identified from intensity peaks obtained in EDS spectra. In accordance with the SEM–EDS results, the thickness of the developed HAp layer on the glass surface strongly depends on the Ca/P ratio. In order to use the glass material as implant material, the Ca/P ratio of HAp of that material must be greater than 1 (for human bone ~1.67) [15,35]. However, the Ca/P ratios of the as-prepared glasses varying in between 1.46-1.85, these values are very close to Ca/P ratios of the human bone [36].

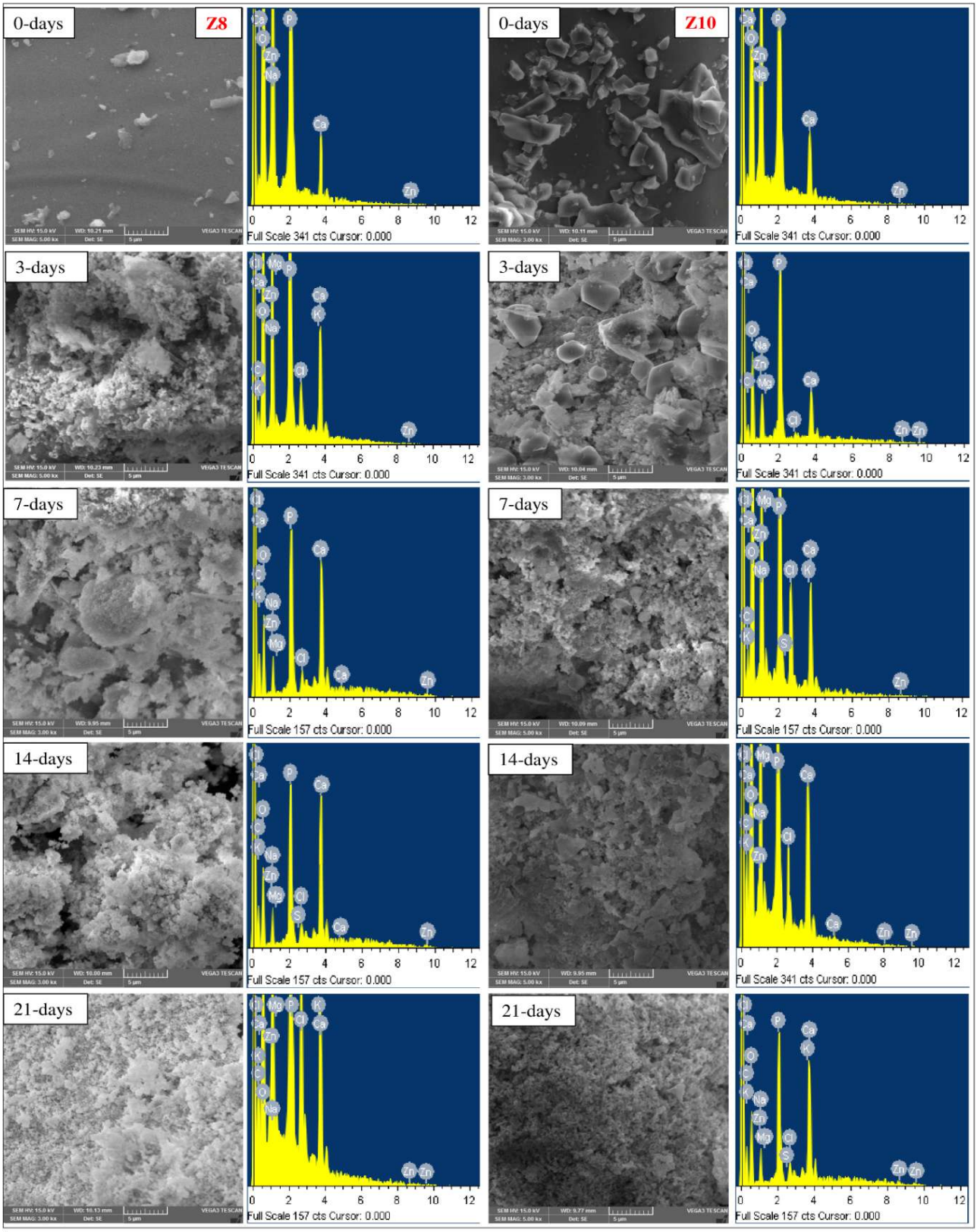
0-days
Z8
0-days
Z10
3-days
3-days
7-days
7-days
14-days
14-days
21-days
21-days
Full Scale 341 cts Cursor: 0.000
Full Scale 157 cts Cursor: 0.000

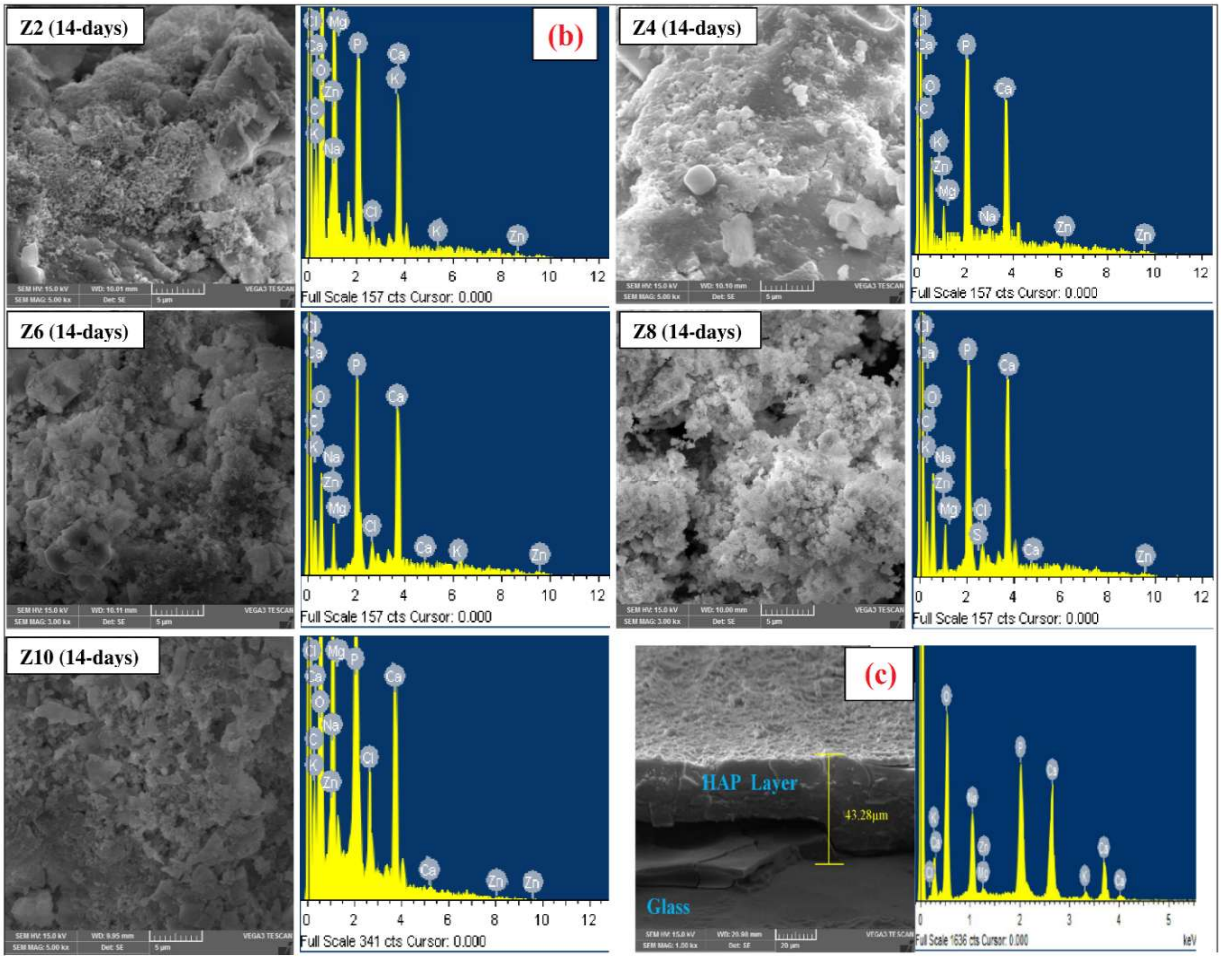

Fig. 3.6 (a) SEM micrographs and EDS spectra of the Z8 and Z10 bioglass samples before and after immersion in SBF for different incubation time 0, 3, 7, 14 and 21 days, (b) SEM–EDS spectra of all glasses after immersion in SBF solution for 14 days and (c) The cross-sectional view of SEM micrograph and EDS elemental mapping of Z8 glass after 21 days of immersion in SBF.

Moreover, Fig. 3.6 (b) illustrates the effect on the HAp layer formation on the surface of the samples with a variation of ZnO content for 14days of immersion in SBF. With increase in concentration of ZnO from 2 mol% to 8 mol%, a slight increase in the formation of HAp layer over the glass surface is noticed after that (Z10) a slight decrease in apatite layer density is noticed. This is in good agreement with the results obtained from XRD and FTIR analysis (shown in Fig. 3.4 & 3.5). Most of the previous reported research results reveal the inhibition of the HAp formation with increase the content of ZnO in SiO_2 based bioglasses due to uncontrolled releases of zinc ion [53]. On the contrary to previous results, the present system of glasses showing an increase in crystalline nature of HAp with ZnO addition. This might be slow release of Zn^{2+} ions. It is also confirmed from Ca/P ratio values obtained from EDS data.

Fig. 3.6 (c) explains the cross-sectional view of SEM micrograph and EDS elemental mapping of Z8 glass after 21days of immersion in SBF. The cross-sectional micrograph of the Z8 sample is divided into two regions. The top region is HAp layer and underneath to HAp layer is the glass. The thickness of apatite layer formed on Z8 glass for 21days of incubation is around 43.28 mm. In the present system of glasses the thickness of HAp layer enhances up to 8 mol% ZnO and then decreased further increase of ZnO content. However, the addition of ZnO does not inhibit HAp formation up to certain mol%, but it may slowdown the degree of HAp formation due to the unsolvable nature of ZnO. It is good that, the chosen system of glass composition acquiring the controlled zinc release and high apatite is forming ability *in vitro*.

3.3.4 Weight loss during the conversion reaction

This measurement of weight loss of glasses provides information about the dissolution kinetics and insight about dissolving amount of glass in SBF solution. Fig.3.7 illustrates the weight loss of the bioglasses as a function of immersion time. The weight loss of all the samples is found to be increased with the increase in immersion time from 3days to 21 days. A sudden increase in weight loss within 3days of immersion takes place due to rapid ion exchange from sample to SBF solution. Later, it follows very slight increase in trend with immersion periods 7, 14, and 21 days. Moreover, with the increase in content of ZnO the degradation of all glass samples also increases slightly. So there is a considerable low weight loss due to reduction of ion release from the samples. During the dissolution processes, the amorphous regions will dissolve and increases the release of Na^{+}, Ca^{2+} and Zn^{2+} ions leads formation of an amorphous Ca–P layer and then over a period, the degradation decreases and rapid degradation of crystallized regions takes place [5,54]. Most of the previous reports on zinc phosphate based glasses showed high degradation rate with high content of zinc present in glasses [25,47]. This is because of increase of release of phosphate anions with increase of ZnO content due to the formation of Zn–O–P weak bonds. Moreover, Ca^{2+} ions release is higher for low content of ZnO [46,54]. Conversely, in the present system of glasses evidencing the controlled degradation behaviour with increase in content of ZnO, this may be due to a fixed percentage of CaO and Na_2O, presence of high content of P_2O_5 which is replaced with a small amount of ZnO in the chosen glass matrices. This degradation gives very clear indication that, there is not much deviation of the degradation curves with immersion time after 3days and also with the content of ZnO. This reveals the deposition of rich HAp layer over the glass surface; on the other hand, the glasses show high bone forming ability.

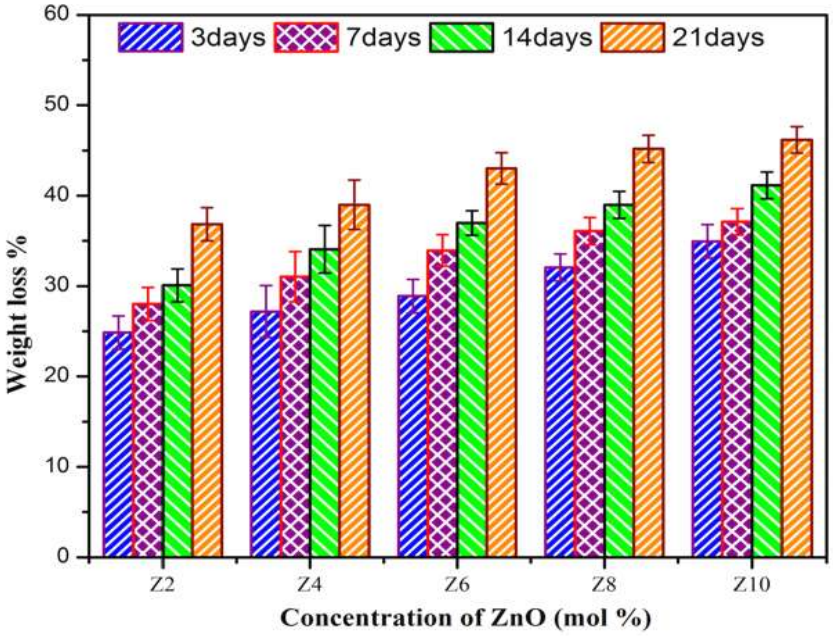

Fig. 3.7 The weight loss of all bioglasses during immersion time (0, 3, 7, 14 and 21 days) in SBF solution at 37 ^{o}C. The error bars represent the standard deviation (as mean ± SD): n=3).

3.3.5 pH evaluation

The variation of pH values in the SBF solution after immersion of the glass samples for different time periods are shown in Fig.3.8. There is a noticeable change in pH values of all glass samples are observed with different days (0, 3, 7, 14 and 21days) of immersion is due to ion leaching. A sudden increase in pH values from 7.4 to 7.56 within 3days of immersion for all samples. Moreover, within 3days of incubation the pH values also increases with the increase in content of ZnO from 2 mol% to 10 mol%. After that there is a decrease in the trend of pH values is pronounced with 7 days, 14 days and 21 days of incubation time. The pH value decreases and approaches to 7.45 within 7days of incubation and then further decrease to 7.42 within 14 days. This is almost equal to the initial value of the pH of SBF at 0days. It is found that, here also the values of pH increases with ZnO content, but Z4 and Z6 values coincide with each other. Furthermore, the pH decreases to 7.25 within 21days of long immersion. The initial increase in pH values of SBF of all glasses, when compared with the pH value at 0days of SBF may be due to the release of Na^{+} and Ca^{2+} ions through exchange with H^{+} or OH^{-} ions in the simulated body fluid (SBF) solution. The released cations Na^{+} and Ca^{2+} initiate the formation of HAp layer over the surface of glasses [55,56]. Afterwards, a slight decrease in pH value with the increase in immersion period is observed due to increase in dissolution rate of glasses and decrease in sodium ion content. On the other hand, the formation of calcium phosphates and carbonates by precipitation of Ca^{2+} ions from the SBF solution leads to decrease in pH values and also the movement of zinc ions into solution

makes it towards acidic nature [57]. Moreover, with increase in ZnO content, the dissolution rate and pH values are found to increase. The stabilization of pH of the medium can be achieved by the precipitation of Zn ions as $Zn(OH)_2$ in SBF [58]. The development of HAp layer strongly depends on the pH variation and the rate of dissolution of Ca^{2+} and PO_4^{3-} ions [56]. In the current study, the obtained pH values of 7.25 to 7.56 are very close to the value of physiological fluid (7.4). These results are in close agreement with SEM analysis (Fig. 3.6). It confirms the bioglasses prepared very are more suitable for cellular activity and bone formation. Their high degradation rate leads to a higher pH value and favour an early development of hydroxy carbonate apatite layer on the sample surface with more crystallinity evident from SEM image.

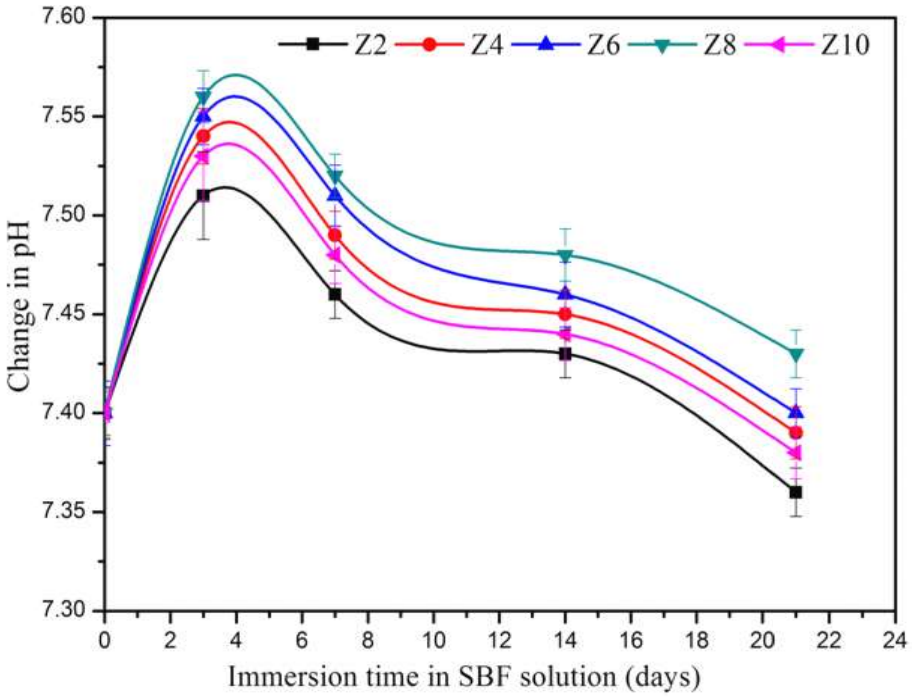

Fig. 3.8 pH changes of SBF solution containing all bioglasses with different immersion times as the initial value of pH is 7.4 at 37 ^{o}C. (Error bars indicate the standard deviation: n=3).

3.3.6 Cell cytotoxicity and Proliferation

The cytocompatibility and cell Proliferation analysis are very crucial to know about the *in vitro* biological activity of the bioglass samples before going to test *in vivo* as bone regenerative implant. The main interest of the present study is, how the viability and functional activity of *rMSCs* cells seeded on surfaces of as-prepared bioglasses are affected by ions released from glasses. For this cell growth study, rat mesenchymal stem cells (*rMSCs*) are used because of their multi potent and self-renewal capacity. Moreover, it acts as a potential source for regenerative treatment of bone tissues. Fig. 3.9 demonstrates the cell

viability on the ZnO dope bioglasses (Z2, Z4, Z6, Z8 and Z10) and control during rMSCs culture for 1day and 3days and is as assessed by a CCK-8 method. Interestingly, glass samples from Z2 to Z8 showing considerable high cell viability when compared with the control except Z10 for 1day and 3days. It is observed that, the cell viability enhances with increases in ZnO content up to 8 mol% (Z8) with respect to control, implying the possible ionic effects on rMSCs viability. Afterwards, it is found to reduce slightly with an increase in concentration of ZnO at 10 mol% (Z10) for 1day and further decreases in case of 3days culturing as shown clearly in the Fig. 3.9.

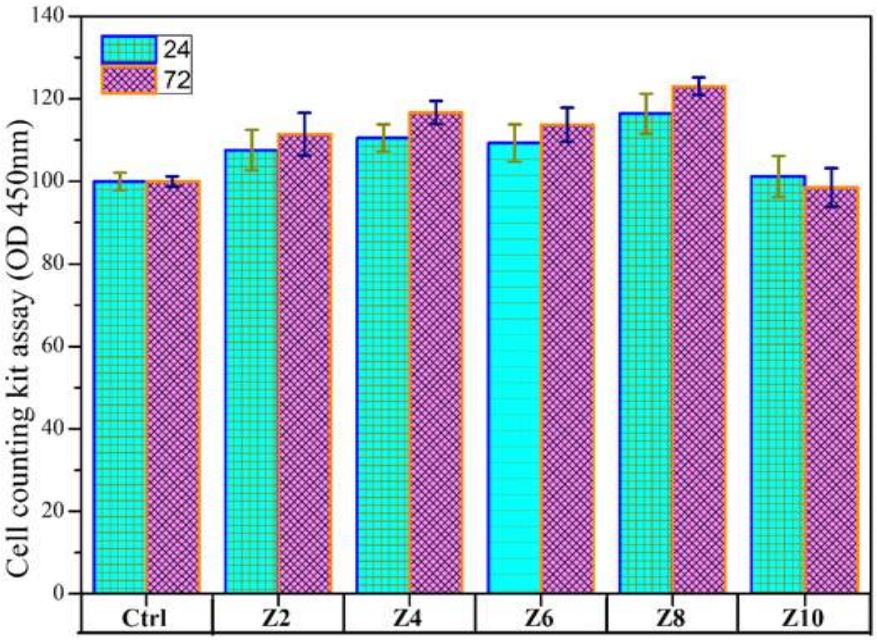

Fig. 3.9. Cell cytotoxicity and Proliferation analysis of rMSCs on different content of ZnO doped glasses by CCK-8 method.

The viability and cell proliferation of Z8 (8 mol%) sample is showing significantly higher values compare to other samples. Moreover, the rate of cell proliferation of Z8 improved after culturing for 3days. However, this decrease in proliferation is attributed to high zinc release from Z10 glass sample. In other words the reduction in cell proliferation with an increase in ZnO mol% after 3days may be due to the quantity of ZnO present in the glass [29,58]. Most of the available previous literature reports on ZnO doped glasses suggesting that, the inhibition nature of HAp layer formation due to high release of Zn^{2+} ions. Moreover, increase in ZnO concentration higher than ~2 ppm in conditioned medium can show toxic effects and leads to cell death [29,59].Similar reports from various researchers Atsuo Ito et al., showed that, at 10 mol% of ZnO in composite ceramic of tricalcium phosphate and HAP enhanced osteoblastic cell proliferation and differentiation *in vitro* within

a nontoxic level [22], Abou Neel et al., demonstrate that, 10–20 mol% of ZnO showed lower compatibility with MG63 cells due to reduction in the surrounding pH to acidic level [6], Aina et al., observed that, 45S5 Bioglass doped with 5 wt% ZnO enhanced cell proliferation, later increasing zinc concentration caused to significant release of lactate dehydrogenase , which resulting in cell death [47]and Saurabh Kapoor et al., reported that, the glass ceramics 4 mol% of ZnO contained glass ceramics displays the highest levels of mesenchymal cell proliferation, further increasing ZnO contents led to a significant decrease in viability [28]. Conversely to the earlier studies on different ZnO doped glass systems, the present results of Zinc-phosphate based glasses confirming the effectively controlled the release of Zn^{2+} ions. This leads to enhanced cell proliferation and cytocompatibility. Out of all glasses the viability of Z8 (8 mol%) is significantly high. Moreover, the rate of cell proliferation of Z8 improved after culturing for 3days. So the material can stimulate the bone growth effectively and these glasses can be suitable for bone repair implants.

3.3.7 Evaluation of antibacterial activity

The antibacterial effect of ZnO bioglass samples is assessed by the perceived zone of inhibition against *E. coli* and *S. aureus* as shown in Fig. 3.10. This study is conducted to determine the amount of ZnO-doped samples exhibiting antibacterial activity by the presence of a zone of inhibition around each sample disk. It is clearly visualised that, the samples Z2, Z4, Z6, Z8 and Z10 have shown clear inhibitory zone as indicated by transparent zone against *E. coli* (Fig. 3.11a) and *S. aureus* (Fig. 3.11b). And also noticed that the antibacterial activity of *E.Coli* is more porn as compared *S. aureus* for given glass samples. This trend is in good agreement with the earlier reports describing the high antibacterial activity of the Zn^{2+} ions containing bioglasses [11,60,61]. Moreover, the Zn^{2+} ions from ZnO-doped glasses showing better antibacterial activity compared to the TiO_2–Al_2O_3/ZrO_2 doped glasses [11,62,63]. The growth of inhibition zone indicates the improved antibacterial activity, which is mainly due to release of Zn^{2+} ions. These ions subsidise to intense disorder of bacterial membrane potential and consequently, which leads to increase the ZnO concentration inside of the cell where it induces oxidative stress. The increase oxidative stress inside the cell causes the destruction in the bacterial cell wall [60,64]. Along with agar method, optical densities also measured at various timing points from 0 h–7 h at 600nm to confirm the antibacterial activity.

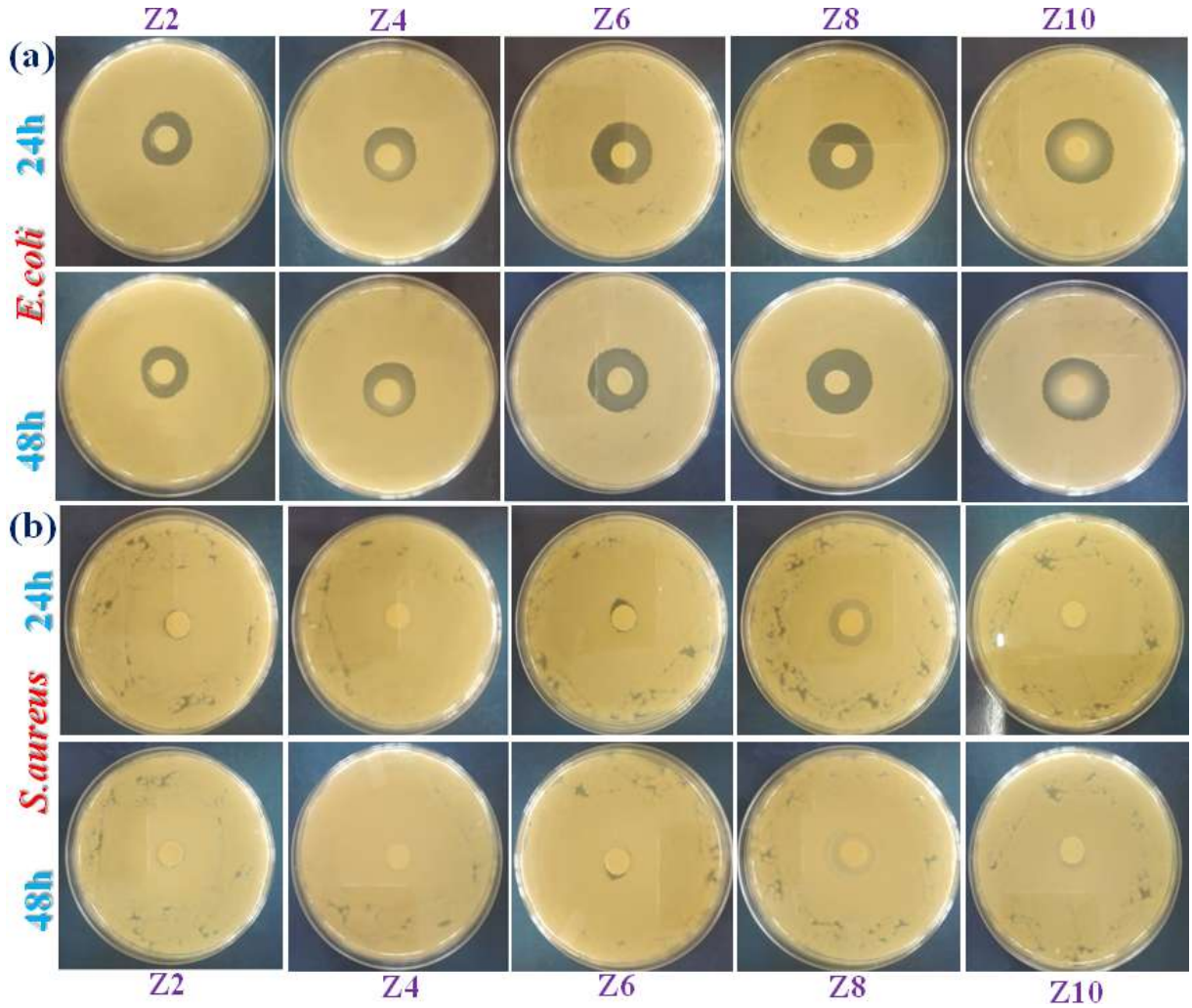

Fig. 3.10 Antibacterial activity by agar disk-diffusion assay against *E. coli* and *S. aureus* at 24 and 48 h for sample Z2, Z4, Z6, Z8 and Z10.

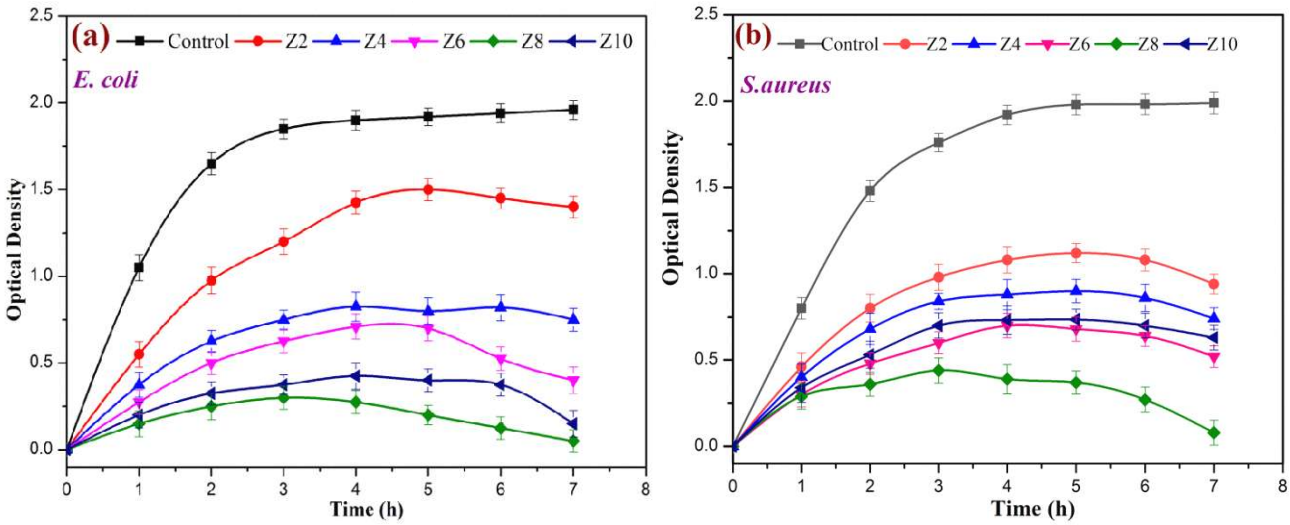

Fig. 3.11 Optical density measurement against (a) *E. coli* and (b) *S. aureus* at different time points.

Fig. 11(a & b) is showing the optical density measurement traces of bioglasses at different time points against *E. coli*, and *S. aureus* respectively. *E. coli* strain has relatively improved growth compared to *S. aureus* in terms of optical density. The results obtained from optical density measurement showed that the OD values decreases when the bacterial species are treated with samples. The low OD value indicates that the antibacterial properties of the samples given against gram-negative bacteria formation are high. Both, agar disk diffusion assay and optical density measurements confirms the ZnO doped samples are exhibited good antibacterial effect against *E.coli*.

4. Conclusions

In the current work, we have developed enhanced bioactivity and improved mechanical strength of ZnO incorporated P_2O_5 based bioglasses for bone regeneration applications. The main conclusions which can be drawn from the results are:

1. The density and oxygen molar volumes are found to enhance and the molar volume and oxygen packing density are reduced with increase in ZnO concentration. The increase in density visibly indicates the presence of more ionic nature of P–O–Zn bonds than P–O–P bonds in glass network, which leads to compactness of the glass structure.

2. The glass transition temperature (Tg) increases with increase in content of ZnO up to 8 mol% and then decreases for higher concentration of ZnO. The increase in Tg can be due to increasing aggregation effect of ZnO on the glass system, and slow mobility of the large Zn^{2+} ions, which lead to more rigidity of glass network. The values of stability (ΔT) increase from 111.26 °C to 121.19 °C and Hruby criterion (H) increases from 0.4319 to 0.5154 with the content of ZnO, which clearly designate the high strength and as a good glass forming tendency of all glasses.

3. Vickers microhardness and toughness values of the as-prepared bioglasses increase with increasing ZnO content due to expansion of the glass network in harmony with the increase in the bond length or inter-atomic spacing. Zn^{2+} ions enter interstitially in the glass network to form more P–O–Zn linkages by breaking P–O–P bonds. These, in turn lead to reduction of number of nonbridging oxygens (NBO's) and increases cross-linking density, compactness and rigidity of the glass network. In the present as-prepared glasses Z8 has highest Hv and K_{IC} values.

4. Correlation between the presence of additional intensity reflections from XRD, intensity of absorption bands of FTIR, change in surface morphology of SEM and ratio of Ca and P values from EDS results after incubation periods of 3, 7, 14 and 21days in SBF strongly confirms the development of the rich HAp layer with incubation time. The addition of ZnO to glass network, enhances the crystallization of the $CaO–P_2O_5$ layer by creating a large number of OH^- ions required for conversion of the amorphous layer to crystalline HAp layer through SBF solution as $Zn(OH)_2$.

5. Unlike, previous results on ZnO doped glasses, the present system of glasses evidencing the controlled degradation behaviour and stable pH variation very close to the value of physiological fluid (pH 7.4) with the increase in content of ZnO and incubation time, this might be due to a fixed percentage of CaO and presence of high content of P_2O_5 and is replaced with small amount of ZnO in the chosen glass matrices.

6. Enhanced cell proliferation and cytocompatibility indicate the release of Zn^{2+} ions was controlled effectively in all glass samples.

7. Advanced antibacterial activity is also detected, which is due to synergistic 'contact-killing' effect of Ca^{2+} and Zn^{2+}release. In summary, Zn^{2+} positively affects the cellular reaction and antibacterial activity, given that an attractive bone filler alternative.

From the above mentioned final conclusions, it is noteworthy that, out of all glasses Z8 (8 mol%) exhibiting all enhanced properties might to be used in the development of bone resorbable implants.

References

[1] D.E. Day, A.P. Tomsia, S.B. Jung, B. Sonny Bal, Q. Fu, M.N. Rahaman, L.F. Bonewald, Bioactive glass in tissue engineering, Acta Biomater. 7 (2011) 2355–2373.

[2] T. Kokubo, H. Takadama, How useful is SBF in predicting in vivo bone bioactivity?, Biomaterials. 27 (2006) 2907–2915.

[3] T. Kokubo, H. Kushitani, S. Sakka, T. Kitsugi, T. Yamamum, Solutions able to reproduce in vivo surface-structure changes in bioactive glass-ceramic A-W[3,] Biomed. Mater. 24 (1990) 721–734.

[4] L.L. Hench, H.A. Paschall, Direct chemical bond of bioactive glass-ceramic materials to bone and muscle, J. Biomed. Mater. Res. 7 (1973) 25–42.

[5] L.L. Hench, Bioceramics: From Concept to Clinic Larry, J. Am. Ceram. Soc. 74 (1991) 1487–1510.

[6] E.A. Abou Neel, J.C. Knowles, Physical and biocompatibility studies of novel titanium dioxide doped phosphate-based glasses for bone tissue engineering applications, J. Mater. Sci. Mater. Med. 19 (2008) 377–386.

[7] G. Jordan, S. Clarke, J. Glenn, S. Nazhat, S. Valappil, K. Skelton, J. Knowles, G. Georgiou, Effect of ternary phosphate-based glass compositions on osteoblast and osteoblast-like proliferation, differentiation and death in vitro, Acta Biomater. 3 (2007) 563–572.

[8] I. Ahmed, M. Lewis, I. Olsen, J.C. Knowles, Phosphate glasses for tissue engineering: Part 1. Processing and characterisation of a ternary-based P_2O_5–CaO–Na_2O glass system, Biomaterials. 25 (2004) 491–499.

[9] D. Groh, F. Döhler, D.S. Brauer, Bioactive glasses with improved processing. Part 1. Thermal properties, ion release and apatite formation, Acta Biomater. 10 (2014) 4465–4473.

[10] S.P. and N. Abou Neel, Ensanya A. and Pickup, David M. and Valappil, J.C. Robert J.and Knowles, Bioactive functional materials: a perspective on Phosphate-based glasses, J. Mater. Chem. 19 (2008) 690–701.

[11] A.A. Ahmed, A.A. Ali, D.A.R. Mahmoud, A.M. El-Fiqi, Study on the preparation and properties of silver-doped phosphate antibacterial glasses (Part I), Solid State Sci. 13 (2011) 981–992.

[12] H.Z. Mingwei Lu, Fu Wang, Kuiru Chen, Yunya Dai, Qilong Liao, The crystallization and structure features of barium-iron phosphate glasses Mingwei, Spectrochim. Acta Part A Mol. Biomol. Spectrosc. 148 1–6 Contents. 148 (2015) 1–6.

[13] R.C. Lucacel, M. Maier, V. Simon, Structural and in vitro characterization of TiO_2–CaO–P_2O_5bioglasses, J. Non. Cryst. Solids. 356 (2010) 2869–2874.

[14] H.A. Othman, G.M. Arzumanyan, D. Möncke, The influence of different alkaline earth oxides on the structural and optical properties of undoped, Ce-doped, Sm-doped, and Sm/Ce co-doped lithium alumino-phosphate glasses, Opt. Mater. (Amst). 62 (2016) 689–696.

[15] J.C. Knowles, Phosphate based glasses for biomedical applications, J. Mater. Chem. 13 (2003) 2395–2401.

[16] S. Chajri, S. Bouhazma, S. Herradi, H. Barkai, S. Elabed, S.I. Koraichi, B. El Bali, M. Lachkar, Studies on preparation and characterization of SiO_2–CaO–$P_2O_5$and SiO_2–CaO–P_2O_5–Na_2O bioglasses subtituted with ZnO, J. Mater. Environ. Sci. 6 (Y) (2015)1882-1897.

[17]. M.A. Ouis, Effect of ZnO on the Bioactivity of Hench's Derived Glasses and Corresponding Glass-Ceramic Derivatives, Silicon.3 (2011)177–183.

[18] B. Resorption, Role of Zinc in Bone Formation and Bone resorption, J. Trace Elem. Exp. Med. 11 (1998) 119–135.

[19] G. Perozzi, C. Murgia, C. Lang, M. Leong, P. Zalewski, D. Knight, R. Ruffin, L.-W. Tan, Anti-inflammatory effects of zinc and alterations in zinc transporter mRNA in mouse models of allergic inflammation, Am. J. Physiol. Cell. Mol. Physiol. 292 (2006) L577–L584.

[20]. J. Ovesen, L. Mosekilde, B. MØller-Madsen, J.S. Thomsen, G. Danscher, The positive effects of zinc on skeletal strength in growing rats, Bone. 29 (2002) 565–570.

[21] D. Boyd, H. Li, D.A. Tanner, M.R. Towler, J.G. Wall, The antibacterial effects of zinc ion migration from zinc-based glass polyalkenoate cements, J. Mater. Sci. Mater. Med. 17 (2006) 489–494.

[22] P. Layrolle, T. Tateishi, K. Hayashi, K. Ojima, A. Ito, N. Ichinose, K. Kawamura, Zinc-Releasing Calcium Phosphate Ceramics Stimulating Bone Formation, Bioceramics**,**22 (2013) 567–570.

[23] V.H. Rao, P.S. Prasad, P.V. Rao, L.F. Santos, N. Veeraiah, In fl uence of Sb_2O_3 on tellurite based glasses for photonic applications, J. Alloys Compd. 687 (2016) 898–905.

[24] M.M. Babu, P.S. Prasad, P. Venkateswara Rao, N.P. Govindan, R.K. Singh, H.W.Kim, N. Veeraiah, Titanium incorporated Zinc-Phosphate bioactive glasses for bone tissue repair and regeneration: Impact of Ti^{4+}on physico-mechanical and in vitro bioactivity, Ceram. Int. 45 (2019) 23715–23727.

[25] S.M. Abo-naf, E.M. Khalil, E.M. El-sayed, H.A. Zayed, R.A. Youness, In vitro bioactivity evaluation , mechanical properties and microstructural characterization of

$Na_2O–CaO–B_2O_3–P_2O_5$ glasses, Spect.Acta. Part A: Mol. and Biom.Spect. 144 (2015) 88–98.

[26] A.W. Bauer, W.M. Kirby, J.C. Sherris, M. Turck, Antibiotic susceptibility testing by a standardized single disk method, Am. J. Clin. Pathol. 45 (1966) 493–496.

[27]. M. Jemal, I. Khattech, R.O. Omrani, J.J. Videau, S. Krimi, A. El Jazouli, Structural and thermochemical study of $Na_2O–ZnO–P_2O_5$ glasses, J. Non. Cryst. Solids. 390 (2014)5–12.

[28] S. Kapoor, A. Goel, A.F. Correia, M.J. Pascual, H.Y. Lee, H.W. Kim, J.M.F. Ferreira, Influence of ZnO/MgO substitution on sintering, crystallisation, and bio-activity of alkali-freeglass-ceramics,Mater.Sci.Eng.C. 53 (2015) 252–261.

[29] P. Anigrahawati, M.R. Sahar, S.K. Ghoshal, Influence of Fe_3O_4 nanoparticles on structural, optical and magnetic properties of erbium doped zinc phosphate glass, Mater. Chem. Phys. 155 (2015) 155–161.

[30] G. Rajkumar, S. Aravindan, V. Rajendran, Structural analysis of zirconia-doped calciumphosphateglases, J.Non.Cryst.Solids. 356 (2010) 1432–1438.

[31] L. Zhang, S. Liu, Structure and crystallization behavior of $50CuO–xTiO_2–(50-x)P_2O_5$ (x =5–20)glasses,J.Non.Cryst.Solids.473(2017)108113.

[32] K.F. Ahmed, S.O. Ibrahim, M.R. Sahar, S.Q. Mawlud, H.A. Khizir, Thermal analyses, spectral characterization and structural interpretation of Nd^{3+}/Er^{3+}ions co-doped TeO_2-$ZnCl_2$ glasses system, AIP Conf. Proc. 1888 (2017) 020008–10.

[33] H. Kalita, B.N. Prashanth Kumar, S. Konar, S. Tantubay, M. Kr. Mahto, M. Mandal, A. Pathak, Sonochemically synthesized biocompatible zirconium phosphate nanoparticles for pH sensitive drug delivery application, Mater. Sci. Eng. C. 60 (2016) 84–91.

[34] K. Amin Matori, M.H. Mohd Zaid, H.J. Quah, S.H. Abdul Aziz, Z. Abdul Wahab, M.S. Mohd Ghazali, Studying the Effect of ZnO on Physical and Elastic Properties of $(ZnO)_x$ $(P_2O_5)_{1-x}$ Glasses Using Nondestructive Ultrasonic Method, Adv. Mater. Sci. Eng. 2015 (2015) 1–6.

[35] K. Januchta, R.E. Youngman, A. Goel, M. Bauchy, S.J. Rzoska, M. Bockowski, M.M. Smedskjaer, Structural origin of high crack resistance in sodium aluminoborate glasses, J. Non. Cryst. Solids. 460 (2017) 54–65.

[36] D. Yang, Y. Lu, X. Liang, Y. Sun, K. Yuan, D. Tian, X. Ma, Comparison on mechanical properties of heavily phosphorus and arsenic doped Czochralski silicon wafers, AIP Adv. 8 (2018) 045301.

[37] M. Ashok, N. Meenakshi Sundaram, S. Narayana Kalkura, Crystallization of hydroxyapatite at physiological temperature, Mater. Lett. 57 (2003) 2066–2070.

[38] R.K. Singh, G.P. Kothiyal, A. Srinivasan, In vitro evaluation of bioactivity of CaO–SiO_2–P_2O_5–Na_2O–Fe_2O_3 glasses, Appl. Surf. Sci. 255 (2009) 6827–6831.

[39] R.K. Singh, A. Srinivasan, Bioactivity of SiO_2–CaO–P_2O_5–Na_2O glasses containing zinc–iron oxide, Appl. Surf. Sci. 256 (2009) 1725–1730.

[40] H.S. Liu, T.S. Chin, S.W. Yung, FTIR and XPS studies of low-melting PbO–ZnO–P_2O_5 glasses, Mater. Chem. Phys. 50 (1997) 1–10.

[41] P.Y. Shih, S.W. Yung, T.S. Chin, FTIR and XPS studies of P_2O_5–Na_2O–CuO glasses, J. Non. Cryst. Solids. 244 (1999) 211–222.

[42] M. Kamitakahara, C. Ohtsuki, H. Inada, M. Tanihara, T. Miyazaki, Effect of ZnO addition on bioactive CaO–SiO_2–P_2O_5–CaF_2 glass-ceramics containing apatite and wollastonite, Acta Biomater. 2 (2006) 467–471.

[43] L. Müller, F.A. Müller, Preparation of SBF with different HCO^{3-} content and its influence on the composition of biomimetic apatites, Acta Biomater. 2 (2006) 181–189.

[44] A.C. Tas, Synthesis of biomimetic Ca-hydroxyapatite powders at 37 ^{o}C in synthetic body fluids., Biomaterials. 21 (2000) 1429–1438.

[45] Y.C. Hsiao, C.H. Chen, J.C. Kung, C.S. Chien, C.J. Shih, W.C. Chen, Effects of bioactive glass with and without mesoporous structures on desensitization in dentinal tubule occlusion, Appl. Surf. Sci. 283 (2013) 833–842.

[46] M. Al Qaysi, A. Petrie, R. Shah, J.C. Knowles, Degradation of zinc containing phosphate-based glass as a material for orthopedic tissue engineering, J. Mater. Sci. Mater. Med. 27 (2016) 157.

[47] A. Fiorio Pla, L. Munaron, C. Morterra, V. Aina, G. Malavasi, Zinc-containing bioactive glasses: Surface reactivity and behaviour towards endothelial cells, Acta Biomater. 5 (2008) 1211–1222.

[48] P.Y. Shih, J.Y. Ding, S.Y. Lee, 31P MAS-NMR and FTIR analyses on the structure of CuO-containing sodium poly- and meta-phosphate glasses, Mater. Chem. Phys. 80 (2003) 391–396.

[49] A. Krajewski, M. Mazzocchi, P.L. Buldini, A. Ravaglioli, A. Tinti, P. Taddei, C. Fagnano, Synthesis of carbonated hydroxyapatites: Efficiency of the substitution and critical evaluation of analytical methods, J. Mol. Struct. 744–747 (2005) 221–228.

[50] A. Ślósarczyk, Z. Paszkiewicz, C. Paluszkiewicz, FTIR and XRD evaluation of carbonated hydroxyapatite powders synthesized by wet methods, J. Mol. Struct. 744–747 (2005) 657–661.

[51] L. Medvecky, M. Giretova, J. Durisin, V. Girman, M. Faberova, T. Sopcak, R. Stulajterova, Effect of phase composition of calcium silicate phosphate component on

properties of brushite based composite cements, Mater. Charact. 117 (2016) 17–29.

[52] W. Jiang, S. Cai, D.M. Wang, G.H. Xu, J.Y. Li, W.J. Zhang, Microstructural characteristics and crystallization of $CaO–P_2O_5–Na_2O–ZnO$ glass ceramics prepared by sol–gel method, J. Non. Cryst. Solids. 355 (2008) 273–279.

[53] K. Sharma, A. Dixit, S. Bhattacharya, Jagannath, M.N. Deo, G.P. Kothiyal, Effect of ZnO on phase emergence, microstructure and surface modifications of calcium phosphosilicate glass/glass-ceramics having iron oxide, Appl. Surf. Sci. 256 (2010) 3107–3115.

[54] T. Kokubo, S. Ito, Z.T. Huang, T. Hayashi, S. Sakka, T. Kitsugi, T. Yamamuro, Ca,P-rich layer formed on high-strength bioactive glass-ceramic A-W, J Biomed Mater Res. 24 (1990) 331–343.

[55] A. Oki, B. Parveen, S. Hossain, S. Adeniji, H. Donahue, Preparation and in vitro bioactivity of zinc containing sol-gel-derived bioglass materials, J. Biomed. Mater. Res. - Part A. 69 (2004) 216–221.

[56] L.L. Hench, D.E. Clark, North-tlolland Publishing Company Physical Chemistryof Glass Surfaces,J. Non. Cryst. Solids. 28 (1978) 83–105.

[57] J.M.F. Ferreira, G. Balossier, S. Kannan, J. Michel, A. Balamurugan, A.H.S. Rebelo, Development and in vitro characterization of sol–gel derived $CaO–P_2O_5–SiO_2–ZnO$ bioglass, Acta Biomater. 3 (2006) 255–262.

[58] F. Chai, A.Q. Truong-Tran, L.H. Ho, P.D. Zalewski, Regulation of caspase activation and apoptosis by cellular zinc fluxes and zinc deprivation: A review, Immunol. Cell Biol. 77 (1999) 272–278.

[59] A. Hoppe, N.S. Güldal, A.R. Boccaccini, A review of the biological response to ionic dissolution products from bioactive glasses and glass-ceramics, Biomaterials. 32 (2011) 2757–2774.

[60] M. Eltohamy, B. Kundu, J. Moon, H.-Y. Lee, H.-W. Kim, Anti-bacterial zinc-doped calcium silicate cements: Bone filler, Ceram. Int. 44 (2018) 13031–13038.

[61] Farah N.S. Rajaa, T. Worthingtona, Mark A. Isaacsb, Karan S. Ranaa, Richard A. Martin, The antimicrobial efficacy of zinc doped phosphate-based glass for treatingcatheter associated urinary tract infections, Mate. Sci. & Eng. C 103 (2019) 109–868.

[62] P. Li, C. Ohtsuki, T. Kokubo et al., “Effects of ions in aqueous media on hydroxyapatite induction by silica gel and its relevance to bioactivity of bioactive glasses and glass-ceramics,” J. Appl. Biomat. 4 (1993) 221–229.

[63] V.V. Anusha Thampia, M. Prabhua, K. Kavithaa, P. Manivasakana, P. Prabua, V. Rajendrana,n, S. Shankarc, P. Kulandaivelu, Hydroxyapatite, alumina/zirconia,

andnanobioactive glass cement for tooth-restoring applications, Ceram. Int. 40 (2014) 14355–14365.

[64] L. Esteban-Tejeda, C. Prado, B. Cabal, J. Sanz, R. Torrecillas, J.S. Moya, Antibacterial and Antifungal Activity of ZnO Containing Glasses, plos one, 10 (7) (2015) 1–7

Chapter-4

Influence of Ti^{4+} ions on physico-mechanical and *in vitro* bioactivity of $ZnO–Na_2O–CaO–P_2O_5$ glass system

This chapter has systematically analysed structural and biological properties as well as dissolution behavior aspects of $ZnO–Na_2O–CaO–P_2O_5$ *glass matrix with* Ti^{4+} *ions. This chapter also delineates physical properties of density, molar volume, microhardness, and thermal. In vitro bioactivity test were carried out on glass matrix immersed in SBF solution for 3, 7, 14 and 21days, and the resulting pH variation as well as degradation rate, were discussed. Structural analysis which was performed with the help of X-ray diffraction, SEM-EDS, FTIR-Spectroscopy, Biological studies on Cell cytocompatibility and antimicrobial results are also briefly described in the chapter.*

4.1 Introduction

The necessity of development of new biocompatible and bioactive materials with superior properties has driven research in the field of bioactive glass synthesis. These glasses are investigated for their excellent properties such as resorbability, osteoproductivity, osteoconductivity and osteoinductivity. They have multiple advantages over traditional materials used in medicine including functions ranging from grafting to augmentation as well as implantation and repair [1]. Phosphate bioactive glasses are of great interest in particular, because of their biocompatibility, bioresorbable nature and because of inorganic phase of the bone. Moreover, phosphate glasses contain elements that are natural constituents of the human body, so it is suitable for various potential applications in soft and hard tissue engineering [1,2,3,4]. The phosphate enters the glass network by forming PO_4 tetrahedra structural units. These units are the main building blocks of phosphate glass structure. Nominally phosphorus has a charge of 5^+. The glassy structure of phosphate comprises only orthophosphate tetrahedra that form a three-dimensional network by sharing three covalently bonded bridging oxygens (BOs) with neighbouring PO_4^{3-} tetrahedral, but the oxygen atoms that are not shared between phosphate tetrahedra might distribute their two unpaired electrons with the P^{5+} ions to form a terminal double bond [5,6,7]. Moreover the addition of modifying metal oxides lead to depolymerisation of the glass network by means of the splitting of P–O–P bonds with the formation of negatively charged NBOs at the expense of BOs [7]. Several studies conducted on bioactivity of phosphate glasses biocompatibility showed that, there are no adverse effects found on craniofacial osteoblasts, when the degradation rates are considerably low [8,9]. Therefore, the controlled the dissolution rate of the glasses can be achieved by inclusion of appropriate amounts of various transition metal oxides. Introduction of ZnO in small quantity is expected to act as a modifier and increases the molar volume through weak linkages with the network former. ZnO has also been investigated for its antimicrobial properties in bioactive glasses. It is expected that the antibacterial properties of the glass will improved with the concentration of ZnO. In other hand , the addition of ZnO shows inhibitory effects on the formation of apatite layer on glass surfaces, which causes reduction in bioactivity [1,10]. The presence of calcium oxide (CaO) and phosphorous pentoxide (P_2O_5) is expected to produce amorphous calcium phosphate clusters that accumulate at the surface of glass leading to the formation of hydroxyapatite (HAp) layer. These heterogeneities are expected to improve the bioactivity of glass [11]. Phosphate is a good network former with a high dissolution rate. It has also been shown that glasses with lower Ca/P ratio induce more rapid production of apatite layer [12]. Sodium oxide is expected

to play an important role as a network modifier in the glass composition. Since Na^+ ions produce non bridging oxygens and are expected to reduce rigidity of the network, it leads to reduction of glass hardness [13]. Low network connectivity is also correlated to higher bioactivity, however and high concentrations of Na^+ are also known to trigger a cytotoxicity response [10,14].

However, phosphate based glasses displayed exceptional bioactivity and poor mechanical strength, when compared to other bioactive glasses. This is mainly due to higher dissolution rate of phosphate glasses both *in vitro* and *in vivo* [15,16,17]. The formation rate of HAp layer depends on degradation rate. Higher the degradation rate, better and faster the apatite layer formation but lower is the compactness of the glass structure. In other hand, there is a mismatching between the rate of conversion of HAp layer to the growth of new bone has been occurred. Attaining balance between these two parameters is most important in case of bone regeneration applications. It is also well established that degradation rate can be controlled by modifying glass composition, with some metallic oxides in the glass network, such as TiO_2 [18].

Titanium oxide is a very special and useful transition metal oxide and a well-known nucleating agent for any glass system. Titanium dioxide (TiO_2), unlike sodium, is an intermediate glass forming oxide. Previous studies have shown that sodium and titanium ions produce opposite effects in the rate of dissolution of silicate based bioactive glasses. Na increases the rate of dissolution of Si ions while Ti reduces dissolution rate [19]. Titanium ions enter glass network both as [TiO_6] and [TiO_5]/[TiO_4] structural units depending on the concentration of TiO_2 [18,20,21]. Many research reports revealed that the addition of TiO_2 to phosphate based glasses enhances physic-chemical (density, molar volume, durability etc.), thermal (thermal expansion coefficient, glass transition temperature, etc.), mechanical (hardness, fracture toughness etc.) properties along with improved biocompatibility and bioactivity both *in vitro* and *in vivo* [11]. In addition, the formation of Ti–OH groups on the glass sample is reported, which is due to great affinity of TiO_2 absorb the water molecules, when immersed in SBF solution. These elementary Ti–OH groups stimulate to develop crystalline HAp layer [22]. However, the influence of TiO_2 on structural and in vitro bioactivity of zinc phosphate based bioglasses is not reported yet. But most of the researchers have focused on calcium phosphate and silicate based bioactive glasses only. Furthermore, the main role of TiO_2 in bioactive glasses and glass ceramics is still under debate.

In the present work, titanium incorporated novel Zinc-Phosphate bioactive glasses are fabricated by melt quenching technique. The effect of TiO_2 on physico-mechanical, chemical and biological properties that influence the formation of quality of HAp layer to bind soft and hard tissues for the development of resorbable implants in the field of bone tissue engineering is investigated in detail.

4.2 Results and Discussion

4.2.1 Physical properties of the bioglasses

Physical parameters of bioglasses such as density, molar mass, molar volume, oxygen packing density and oxygen molar volume (Chanshetti *et al.,* 2011) were calculated and the values recorded in Table 4.1.

4.2.1.1 Density

Fig.4.1 shows the density of phosphate glasses, as a function of TiO_2 content. The bulk bioglass clearly shows density increasing (Table 4.1) linearly with increased TiO_2 content. This increase is probably due to the dense closely packed glass structure formed by the strong P–O–Ti bonds and also due to formation of structural units TiO_5 or TiO_4 of titanium [27,28]. Moreover, the bioglass density is also dependent on the compactness of the structural groups. We also notice that the density of the samples increases with the increasing TiO_2 concentration and decreasing CaO content and of 23 mol% CaO sample shows significantly higher density. In other words, the detected increase in density is attributed to replacement of CaO with TiO_2 which is ascribed to the replacement of a light element (Ca) with a heavier one (Ti) [29].

4.2.1.2 Molar mass and Molar volume

The molar volume of the samples was calculated from their densities and the range noted in Table 4.1 The bioglass series (T0, T.2, T.4, T.6, and T.8 and T1) showed a decrease in molar volume with an increasing density (inset of Fig. 4.1), due to the incorporation of titania. The decrease in molar volume is due to the reduction of oxygen atoms by means of replacement of Ca–O bonds with Ti–O bonds [16,29].

4.2.1.3 Oxygen molar volume and oxygen packing density

The oxygen molar volume of the prepared samples was found to increase with increasing mol% of titanium oxide in place of calcium oxide content (Table 2). The values of oxygen packing density also increased with increasing content of TiO_2 as shown in inset of Fig. 4.1. This behaviour of the glass sample reveal crucial facts about increase in the ratio of

the number of oxygen atoms [23]. In the present studies, the oxygen molar volume decreased indicates that the glass structure became denser as mol% of TiO_2 increases, with decreasing content of CaO at constant mol% of NaO, ZnO and P_2O_5 which is due to the intensity of Ti^{4+} ions.

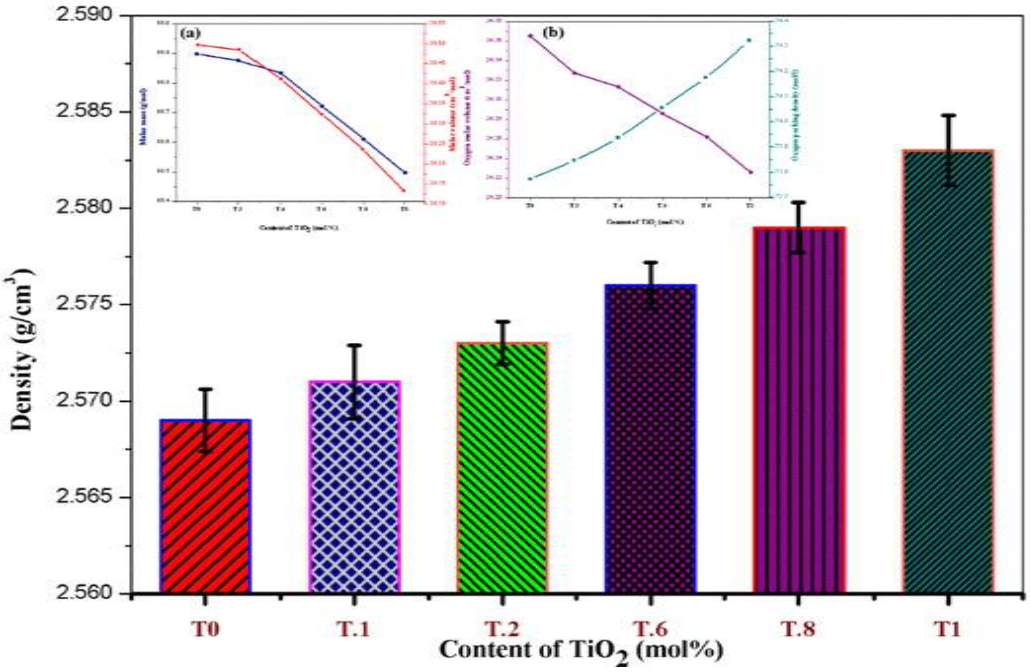

Fig. 4.1 Dependence of density with change in TiO_2 content on $ZnO–Na_2O–CaO–P_2O_5–TiO_2$ bioactive glasses and inset shows the variation of molar mass, molar volume and oxygen packing density and molar volume with content of titanium.

Table 4.1 Density, Molar mass, Molar volume, Oxygen molar volume, Oxygen Packing density and Micro hardness of the TiO_2 doped Phosphate based bioglasses.

S.No	Physical Parameters	T0	T.2	T.4	T.6	T.8	T1
1	Density, ρ(g/cm³)	2.569	2.571	2.573	2.576	2.579	2.583
2	Molar Mass, M(g/mol)	98.898	98.946	98.834	98.722	98.610	98.497
3	Molar volume,Vm(cm³/mol)	38.497	38.485	38.412	38.323	38.236	38.133
4	Oxygen Molar volume,Vo(cm³/mol)	24.365	24.327	24.313	24.286	24.262	24.226
5	Oxygen Packing density,OPD(mol/1)	73.772	73.846	73.935	74.053	74.172	74.318
6	Microhardness (Hv)	325.3 (±9.40)	336.1 (±8.27)	347.2 (±9.23)	363.9 (±6.04)	373.7 (±9.31)	379.7 (±7.35)

The values of oxygen packing density also increased with increasing content of TiO_2as shown in inset of Fig. 4.1. This behaviour of the glass sample reveal crucial facts about increase in the ratio of the number of oxygen atoms [23]. In the present studies, the oxygen

molar volume decreased indicates that the glass structure became denser as mol% of TiO_2 increases, with decreasing content of CaO at constant mol% of NaO, ZnO and P_2O_5 which is due to the intensity of Ti^{4+} ions.

4.2.1.4 Microhardness

Vickers Hardness test gives us very useful information about the surface structural behaviour of bioglass. From Table 4.1, it is shown that an increase from 0 up to 1 mol% of TiO_2 content leads to micro hardness increasing gradually, also observed in Fig. 4.2. Therefore, it seems that the substitution of a part of calcium ions with titanium ions improved the mechanical properties. Among the prepared samples micro hardness value is greater for glass sample T1 (1 mol%), which is the higher concentration of TiO_2 doped glasses as shown in Fig. 4.2. This is attributed to very close packing of atoms by the formation of strong bonds of P–O–Ti. On the other hand, it is easily understood that the higher density of glass leads to more compact glass structure, consequently confirming higher microhardness and mechanical strength [28].

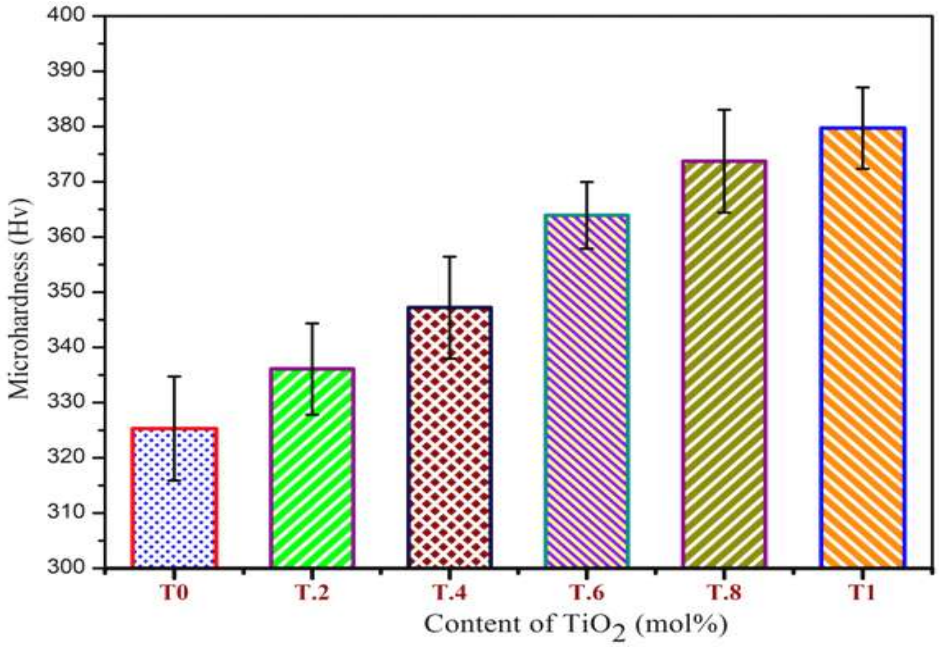

Fig. 4.2 Microhardness (Hv) as a function of content of TiO_2 (mol %) doped glass samples.

4.2.1.5 Differential thermal analysis

Fig. 4.3 illustrates differential thermal analysis of T.6 glass sample corresponding to exothermic and endothermic peak positions from DTA curve (reaming samples are not shown in Fig. 4.3). Thermal parameters like glass transition temperature (Tg), crystallization temperature (Tc) and melting temperature (Tm) obtained during exothermic, endothermic heat

changes are suitable for qualitative assessment of thermal stability of glasses and the ability to produce quality glasses for better applications.

Table 4.2 Thermal parameters of the bio glasses obtained from DTA analysis

sample	Tg (°C)	Tc (°C)	Tm (°C)	ΔT (°C)	K_H
T0	339.58	512.46	681.93	173.28	1.0249
T.2	340.96	517.23	682.89	178.27	1.0761
T.4	341.89	524.39	689.56	182.50	1.1049
T.6	344.97	529.79	693.59	184.82	1.1283
T.8	349.65	536.85	695.93	187.20	1.1767
T1	358.69	549.83	701.53	191.14	1.2599

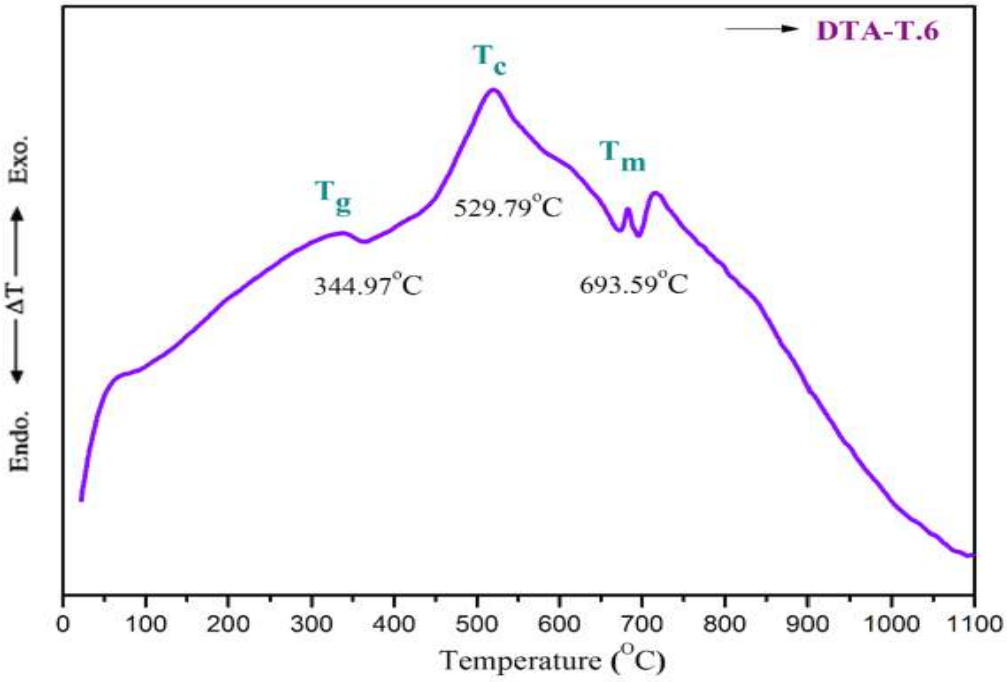

Fig. 4.3 DTA trace of 0.6 mol % (T.6) of ZnO–Na_2O–CaO–P_2O_5–TiO_2 glass system.

The thermal results have shown that, the values of Tg increases for all glass samples with increasing content of $TiO_2$and it is also well pronounced up to 1 mol%. The DTA results are summarized in Table 4.2. The Tg values rises from 339.58 to 358.69 °C. The values of glass transition (Tg) from 339.58 to 358.69 °C, crystallization temperature (Tc) from 512.46 to 549.83 °C and melting temperature (Tm) from 681.93 to 701.53 °C increases with increase in content of TiO_2 from 0.2 to 1 mol%. Parameters such as stability (ΔT= (Tc−Tg)) from 173.28 to191.14 °C and Hruby criterion (K_H= (Tc−Tg)/(Tm−Tc)) from 1.0249 to 1.2599 of as-prepared bioglasses following the same increasing trend with increase in content of TiO_2,

confirming the structure formation and thermal stability of the bioglasses [30]. The increase in these parameters with TiO_2 content is due to growing TiO_2 aggregation on the phosphate structural network to form new linkages and enter into the network in the form of either TiO_4 or $TiO_{5/6}$ structural units [20,31,32]. Moreover, the increase in density and Tg of the samples with TiO_2 is ascribed to formation of P–O–Ti bonds, which reinforce the glass structure by forming ionic cross-linking between the non-bridging oxygen (NBOs) of two different chains [15,28]. This leads to increase in glass viscosity and subsequently the glass transition temperature increases [33]. Therefore, the results obtained support earlier phosphate glass results, which indicates that Tg, Tc and Tm temperatures increase with increase in TiO_2 content [32,34].

X-ray diffraction analysis Fig. 4.4 illustrates XRD patterns of bioglass samples before and after immersion in SBF solution for various time points (0, 3, 7, 14and 21days). Before being soaked, the patterns of all glasses show a broad hump at around 25^o-35^o, which is related to glass network. It is obvious that the prepared bioactive glasses are amorphous in nature before immersed in SBF solution (Fig. 4.4 (a)). After incubation of samples for 3, 7, 14 and 21days in SBF, it is found to observe the formation crystalline peaks in the patterns of all samples due to structural changes as shown in the Fig. 4.4 (b, c, d, e). The development of HAp layer is clearly seen even after 3days of immersion and from Fig. 4.4 (b), it is observed that the glass sample with a surface apatite layer emerged after 3 days of immersion time and the evolution of HAp layer is confirmed from XRD patterns processing intensity peaks at 31.73^o and 45.46^o corresponding to reflections at (211) and (203) respectively. However, XRD data reveal that all the samples exhibited very low crystallization of apatite layer after 3 days of immersion in SBF. Further increasing the immersion time for 7, 14 and 21 days, there is increasing intensity of reflection along with the formation of new intensity peaks at diffracted angles (2θ) and related reflections at 31.73(211), 32.112(300), 45.46(203), 56.53(500) and 66.18(422), 75.86(215), 27.48(112), 40.76(103), 25.92(003), 22.68(111), 21.67(200), 15.32(021) and 10.78(100) respectively. The phases of all peaks matched standard JCPDS data card No. 89–4405 and 40–0008. The XRD patterns confirmed rich crystalline layer formation on the surface of all glasses investigated after a maximum of 21days of immersion in simulated body fluid shown in Fig. 4.4 (e). This crystalline layer could be identified as a high hydroxyl apatite layer. The formation of HAp layer on the surface of the glass samples signifies the capacity to form a strong bond between the implant and natural bone [17,33]

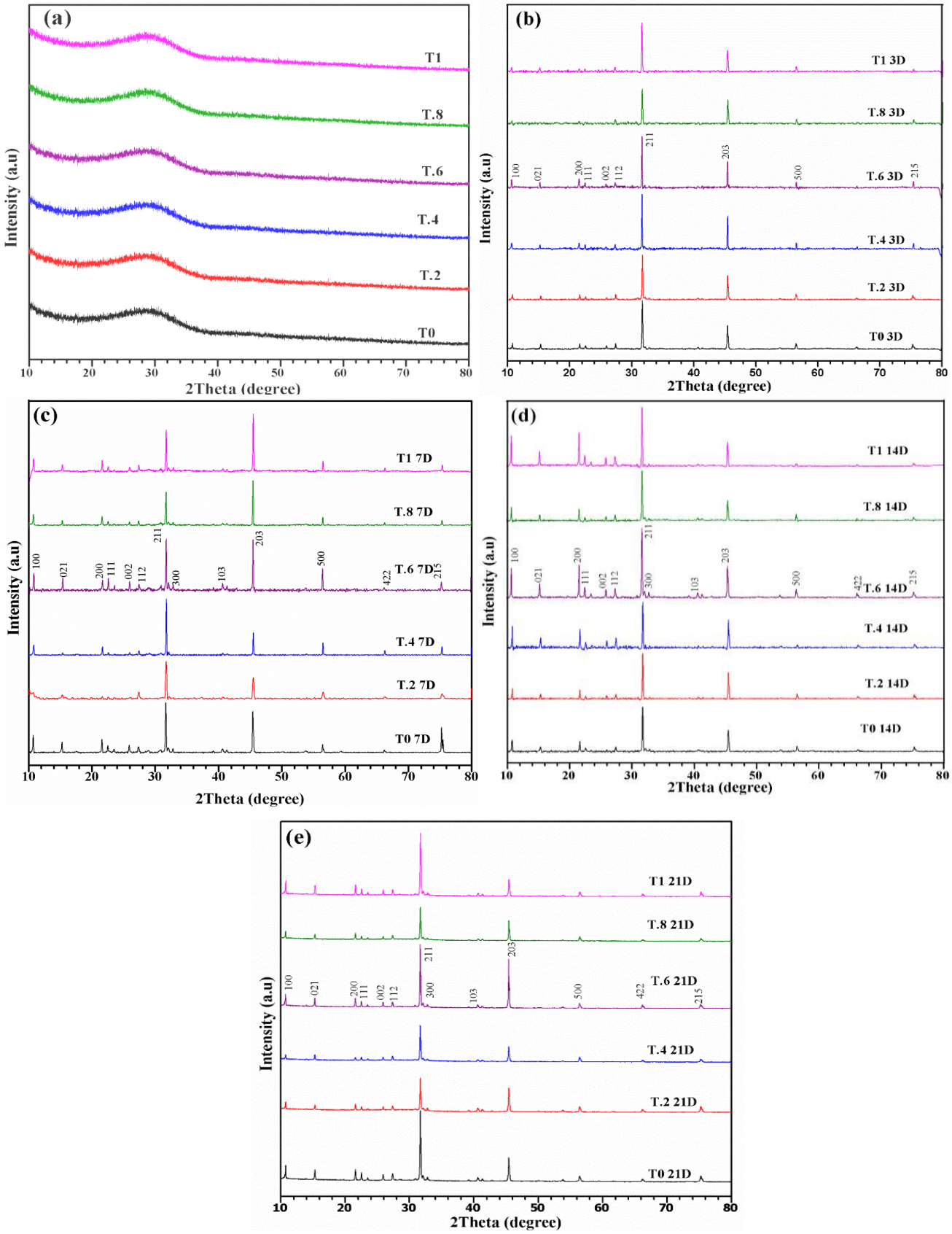

Fig. 4.4 XRD patterns of bioglass samples: before (a-0days) and after (b-3, c-7, d-14, and e-21days) immersion in a SBF solution.

The formation of HAp layer on the surface of the glass samples signifies the capacity to form a strong bond between the implant and natural bone [17,33]. This reaction happens mostly by ion leaching and network dissolution in SBF. In addition the HAp layer growth and nucleation were mainly influenced by Ca^{2+} and P ions from physiological body fluid. In the present TiO_2 doped bioglass system, the growth and crystallisation of apatite layer takes place due to chemical reaction between CaO and H_3O^+ ions, when the sample is immersed in SBF solution. Moreover, the presence of Ti–OH groups and dissolution of bioglass increases the calcium and phosphate ions in SBF solution [17,35,36]. As-prepared TiO_2 glasses are displayed considerably higher peak intensities, which confirm their tendency to form complete crystalline hydroxyapatite (HAp) layer. Among all samples, the reflection intensities related to HAp of T.6 (0.6 mol%) glass sample is predominating. These results attest to the prominence of as prepared bioglasses as being suitable for bone repair and regeneration implant application. In an effort to obtain additional information on the rate of formation of Ca–P layer, the surfaces of samples T0, T.2, T.4, T.6, T.8 and T1 were analysed by FTIR and SEM-EDS (Fig. 4.5 & Fig. 4.6) after immersion in SBF solution.

4.3 FTIR spectroscopy analysis

Fourier transform infrared spectra were investigated for all glass samples (T0, T.2, T.4, T.6, T.8, and T1), at room temperature, before and after immersion in SBF solution for different intervals of time (0, 3, 7, 14, and 21days) as shown in Fig. 4.5 (a, b, c, d, and e). From Fig. 4.5 (a), before immersion all the glass samples exhibit a spectrum characterized by the presence of bands in the regions showing intense absorption bands at ~525 cm^{-1} assigned to fundamental frequencies (the harmonics O=P–O) of PO^3_4 [21]. The centre of the bond at 736 cm^{-1} is assigned to symmetric stretching vibration of (P–O–P) bonds which is characteristic of metaphosphate group $Q^2([P(OP)_2(O^-)_2])$ [20,37]. The vibrations of PO_4^{3-} can be recognized by the main region at 968 cm^{-1}, which is a weak band corresponding to the symmetric stretching. The transmittance of the spectral band in the range 1075 cm^{-1} corresponds to the P–O vibrations, may be due to the deposition of PO_4^{2-} ions indicating the initiation of the phosphate group [38]. The band at 1158 cm^{-1} is assigned to symmetrical stretching vibration mode of PO_2 and the observed absorption peak at 1645 cm^{-1} is attributed to the deformation mode of water molecule –OH(H_2O) [26,39]. The bands at 2375 cm^{-1} and 3453 cm^{-1} are ascribed to O–H symmetric stretching vibration of hydrogen bonded O–H groups [38, 40,41]

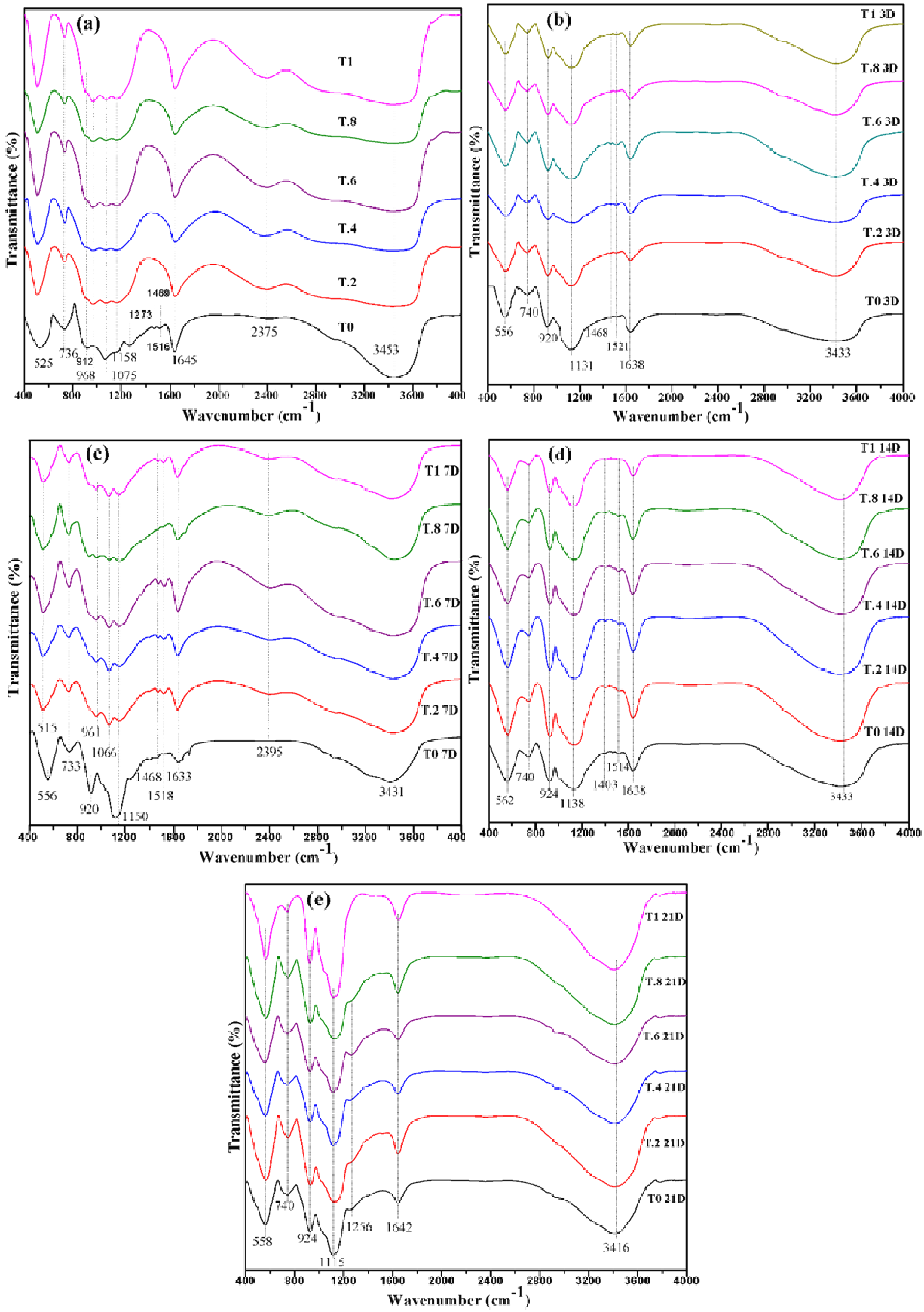

Fig. 4.5 FTIR spectra of bioglasses: before (a-0days) and after (b-3, c-7, d-14 and e-21days) immersion in SBF solution.

After immersion, almost precisely, strong absorption peaks from 556 to 562 cm^{-1} are evident by the presence of calcium pyrophosphate P–O bending mode, which are characteristic bands present in hydroxyl apatite after in vitro studies (of 3, 7, 14, and 21days) [42,43]. The bands between 733–740 cm^{-1} are established due to the formation of P–O–P symmetric stretching vibrations, which is a good indicator of the establishment of pyrophosphate units [43,44]. From Fig. 4.5 (b, c, d, e), the distinct bands at around 920 to 924 cm^{-1} are related to P–O symmetrical stretching vibrations in tetra calcium phosphate [45].

From Fig. 4.5 (c) the bands at 961 cm^{-1} and 1066 cm^{-1} are ascribed to vibrational mode of PO_4^{3-} group representing a HAp precipitation after 7 days of incubation [34,45]. The band may have shifted to a lower wavenumber with respect to immersion time due to the addition of TiO_2. Similar changes in structural peaks splits, through the absorption spectra from 1115 to 1155 cm^{-1}(as asymmetric stretching of $(PO_3)^{2-}$ in Q^1 units) the formation of HA was confirmed by broad bands, which are characteristic of P–O in HAp [43,27]. A low intensity of absorption band appeared at 1256 cm^{-1}, which is assigned by asymmetric stretching mode of PO_2 terminal groups (in the Q_2 units) [46]. The FTIR characteristics of the simultaneous enrichment of other bands situated in between 1403 to 1468 cm^{-1} (it's a B-type carbonate HAp;Ca_9 $(HPO_4)_{0:5}(CO_3)_{0:5}(PO_4)_5OH$, in the system was bone-like apatite) and 1514–1521 cm^{-1} which are characteristic of carbonate group (C–O), confirms the apatite layer formed is a carbonate-substituted hydroxyapatite [34,47,48]. Due to P–O–H stretching vibrations, the bands located at (7days) 2395 cm^{-1} correspond to atmospheric CO_2 traces while bands at 3416 cm^{-1} are due to O–H stretching mode of vibrations, respectively. The low sharp bands between 1638–1642 cm^{-1} and broad bands between 3416–3433 cm^{-1} indicate adsorbed H_2O in bioglass samples from a large surface area [36]. In fact, due to atmospheric moisture in the pellet pressing time, on the bioglass surfaces, there is water molecule absorption. It is clearly observed from Fig. 4.5 that the intensities of absorption bands for 0.6 mol% of TiO_2 increase with incubation time, along with some bands which slightly shift towards lower wavenumber. The band shift is ascribed to changes in the force constants of stretching vibration of P–O bonds, which influences the depolymerisation affinity of glasses during incubation in SBF [21]. The FTIR results revealed the development and enhancement of HAp layer on the glass surfaces with immersion time and proper titanium concentration. Moreover, interestingly, the FTIR results obtained are in good agreement with XRD results of as-synthesized bioactive glass samples.

4.4 SEM-EDS analysis

The SEM micrograph of bioglass samples containing 0.6 (T.6) and 1 (T1) mol% of TiO_2, before and after immersion in SBF at physiological conditions pH 7.4 at 37 ^oC (up to 21days), after evidence of bioactivity morphological changes are shown in Fig. 4.6. Before immersion of bioglass samples in SBF, the micrograph structure of the sample surfaces clearly showed without any layer formation at 0 days and EDS analysis shows nominal presence of elements P, Ca, Zn, Na, Ti, O in the glass and there is no trace of apatite composition. After 3 and 7 days of immersion (T.6 and T1 samples), the surface precipitation increased and new foam like structure appeared or apatite cluster formation on the bioactive glass surfaces was conspicuous. The formation of cation type layer on the surface of T.6, T1 samples (Fig. 4.6) increases with exposure time 14 and 21 days in SBF and supports previous reports [49]. Apatite development can be observed by observing the thickness of layer formed and complete coverage of the surface of the samples, which is mainly due to nucleation and crystal growth of apatite layer process as the incubation period expands [50]. Moreover, it is easy for Ca^{2+} and PO_4^{3-} to be supersaturated in some regions and favourable for HA to nucleate and grow [25]. The formation of HAp layer was also confirmed by EDS spectra before and after immersion in SBF for various time intervals. Before immersion, EDS analysis gives nominal elements P, Ca, Zn, Na, Ti, O only are present in the glass and there are no traces of apatite composition. After treatment in SBF new elements (P, Ca, Zn, Na, Ti, O, Cl, K, Mg) along with the actual glass compositional elements are present [51]. Moreover, the Ca/P atomic ratios determined (between 1.8 and 2.3 for T.6 and T1) from intensity peaks also confirmed the formation of HAp layer. The increase in CaO content increases Ca^{2+} ion release into SBF solution and it leads to increase in HA layer formation on the sample surface. Hench et al. explained this in detail based on the analysis of XRD, FTIR and SEM-EDS experiments [52]. From SEM analysis, we come to a conclusion that the dynamics of the growth of the bioactive layer on the surface of the bioactive glass can be controlled by altering the concentration of TiO_2. That is, TiO_2 doping causes depolymerisation of $(PO_4)^{3-}$ and produces short phosphate network through the formation of Ti–O–P bonds [28,53]. Moreover, the Ca/P atomic ratios determined (between 1.8 and 2.3 for T.6 and T1) from intensity peaks also confirmed the formation of HAp layer. The increase in CaO content increases Ca^{2+} ion release into SBF solution and it leads to increase in HAp layer formation on the sample surface. Hench et al., explained this in detail based on the analysis of XRD, FTIR and SEM-EDS experiments [52].

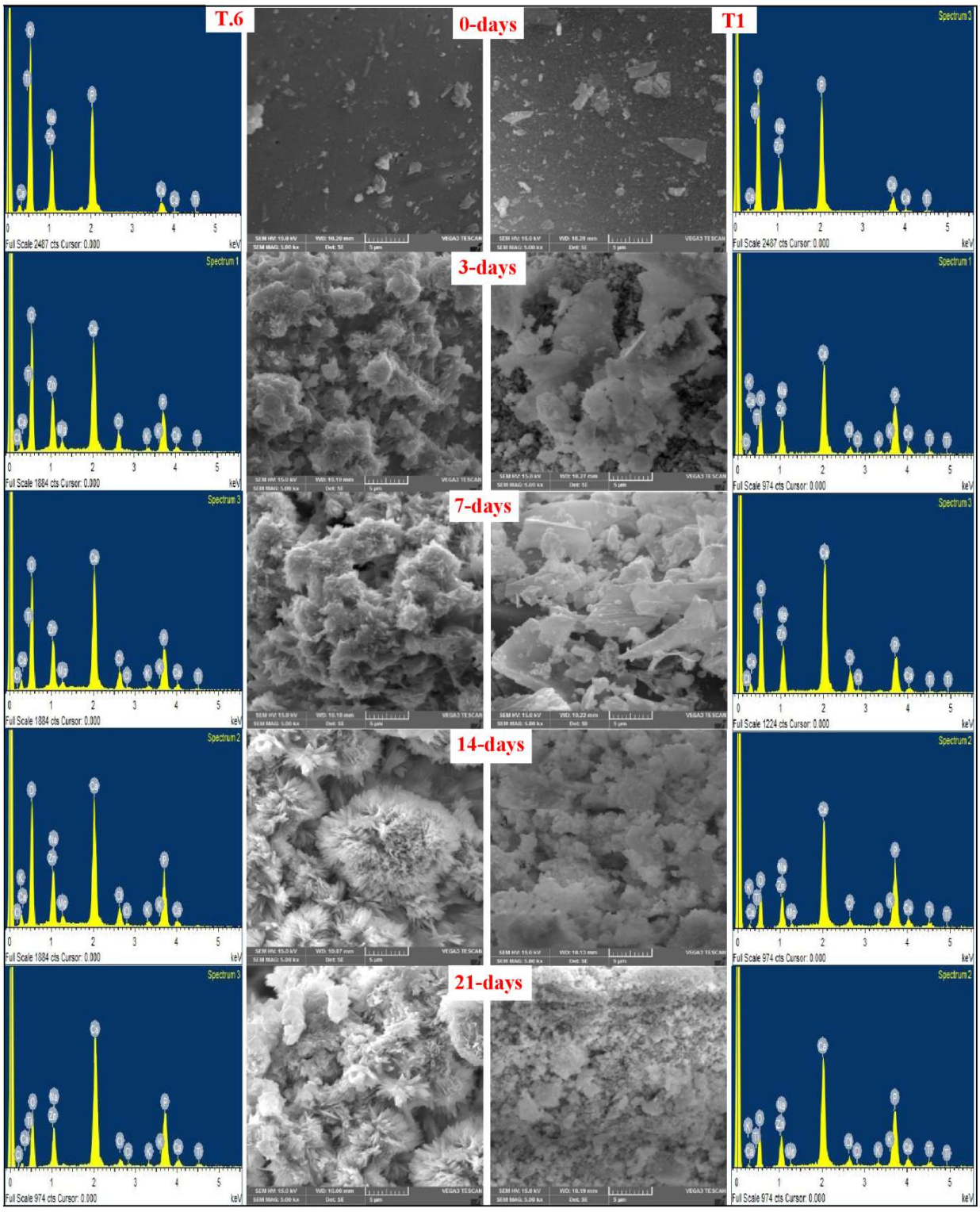

Fig. 4.6 SEM micrographs and EDS spectra of T.6 and T1 glass samples immersed SBF for various time periods (0, 3, 7, 14 and 21days).

From SEM analysis, we come to a conclusion that the dynamics of the growth of the bioactive layer on the surface of the bioactive glass can be controlled by altering the concentration of TiO_2. That is, TiO_2 doping causes depolymerisation of $(PO_4)^{3-}$ and produces short phosphate network through the formation of Ti–O–P bonds [28,53]. Out of all samples

0.6 mol% TiO_2 doped $ZnO–P_2O_5$ bioactive glass confirm high growth of HAp layer. From the results of SEM and EDS, it is very clear that a hydroxyapatite layer formed on all sample surfaces which tallied with XRD and FTIR results discussed in above mentioned sections (4.3 and 4.4).

4.5 Weight loss measurements

The weight loss and pH measurements are very important to know the amount of active ions released during the dissolution process of the glasses which are suitable for repair and regeneration of tissues, when these materials are implanted in the body. It is well known that, simple phosphate based glasses possess poor chemical durability than multicomponent phosphate glasses. In addition to being of network modifiers, ions in these glasses can slowdown the release of dissolution behaviour and lead to formation of rigid network [17,28]. The degradation process takes place, once water gets absorbed by glass and forms gel type layer on glass sample containing PO_4^{3-} ions. Later these phosphate chains leak into the surrounding physiological medium and make the medium acidic by forming phosphoric acid (H_3PO_4). This leads to decrease in pH values of easily dissolvable Ti-free glasses. The addition of Ti^{4+} ions to glass network can slowdown the hydration process by increasing cross link density between phosphate chains by forming P–O–Ti bonds [29]. Therefore, these measurements are necessary for as-prepared bioactive glasses. Fig. 4.7 shows the change in weight loss as a function of immersion time. It is clearfrom that Fig. 4.7 the percentage of weight loss of all the samples increases with increase in immersion time from 3days to 21days. A rapid increase in weight loss occured initially within 3days of immersion due to suddenleaching of ions from sample to SBF solution. Later, it follows very slight increase in trend with immersion periods of 7 days, 14 days and 21 days. On the other hand, decrease in solubility with increase in content of TiO_2 from 0.2 mol% to 1 mol% is detected.It is also observed that the dissolution rate of TiO_2 doped glasses is low compared to TiO_2–free glasses. In general phosphate based glasses contain more P–O–P bonds and can easily dissolve in SBF, but incorporation of TiO_2in glass network leads to gradual breaking of P–O–P bonds and the formation of P–O–Ti bonds [34]. Due to large electric charge and small ionic radii of Ti^{4+}, ions can easily enter phosphate network and forms strong covalent bonds (P–O–Ti), which resist dissolution when compared to P–O–P bonds [17,26,54]

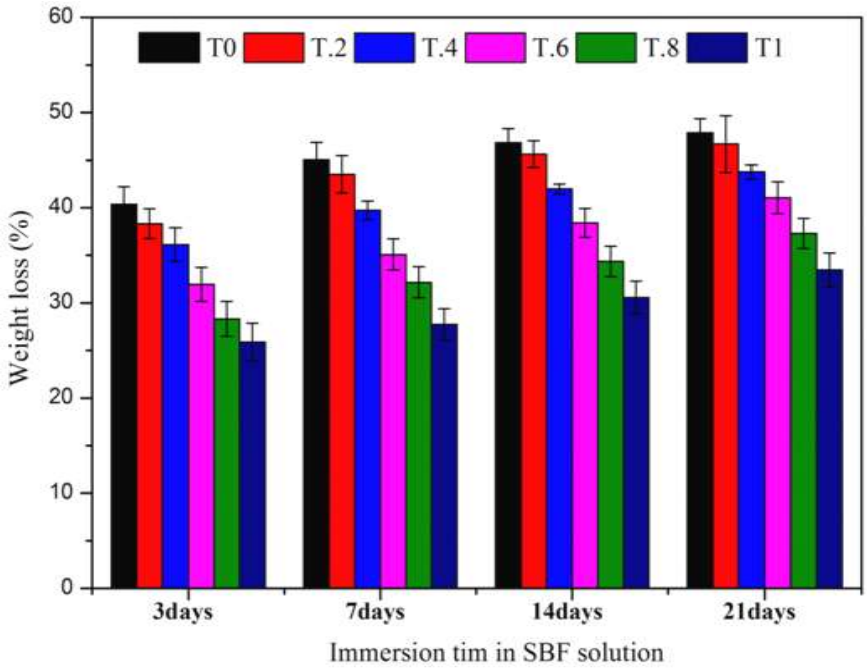

Fig. 4.7 Weight loss of the bioglass samples during the immersion time (3, 7, 14 and 21days) in SBF solution at 37 ^{o}C.

On the other hand, the decrease in dissolution with increase in content of TiO_2 is attributed to increase of leaching ion strength and leads to decrease of interaction with hydrated layers, which in turn decreases dissolution rate [17,34]. The results reveal that the control rate of dissolution can be achieved in phosphate based glasses by appropriate inclusion of TiO_2.

4.6 pH measurements

The apatite layer formation or bioactivity of as-prepared glass samples are tested by measuring changes in pH values of SBF solution. Fig. 4.8 demonstrates the variation of pH values of SBF solution, when the glass samples are treated for different immersion time intervals (0, 3, 7, 14 and 21 days).It is observed that the pH values of all glass samples increase rapidly after 3 days of incubation with reference to the initial starting value of pH at 0days (pH=7.4 at 37 ^{o}C). After that a gradual decrease in pH is noticed with immersion time. Furthermore, the pH values of glasses T.8, T1 and T.2, T.4, T.8 and T1 for incubation of 7 days and 14 days respectively, showing below the starting value (pH=7.4). After 21 days of immersion all TiO_2 doped glasses show low pH values when compared with starting value except TiO_2-free glasses. The sudden rise of pH values after 3 days of immersion is due to quick release of Ca^{2+} and Na^{2+} ions from glass and exchange with H^{+} ions from SBF solutions [41,55,56]. Later the pH values were found to decrease with immersion time and also with

increase in content of TiO_2 for all glasses, which might be attributed to formation of phosphoric acid by the release of phosphate ions in physiological solution (SBF). Already it has been discussed that the increase in structural compactness is in accordance with the formation of TiO_5 and TiO_6 units, which enter into the glass network to form strong P–O–Ti bonds [57]. The pH values obtained are likely to register low weight loss values except T.6 (0.6 mol% TiO_2), which attains highest pH value when compared to other glasses containing TiO_2, as shown in Fig. 4.8. Moreover, the decreases in pH and degradation results were found to be in congruence with increased density, glass transition temperature (Tg) values.

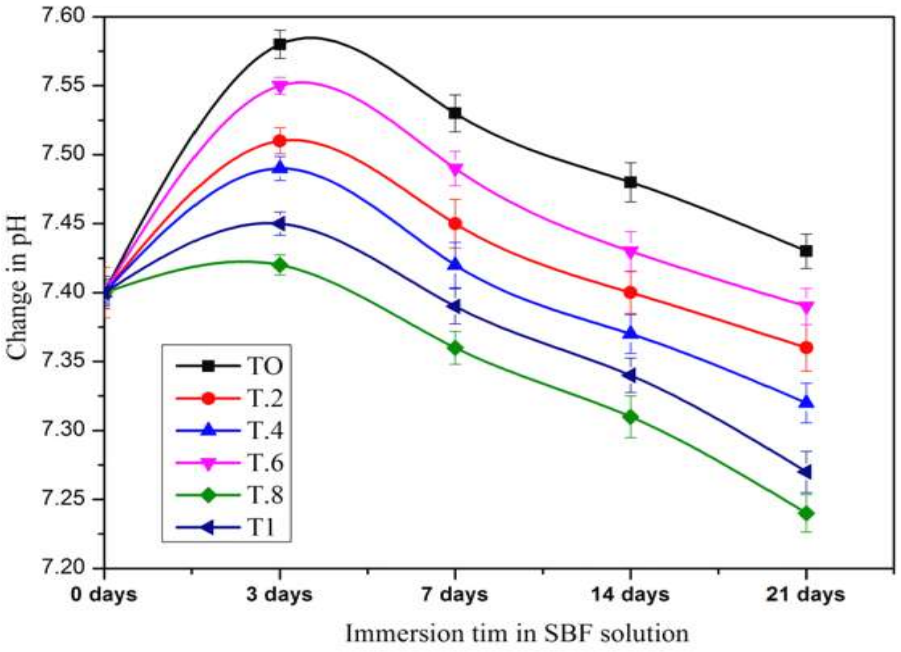

Fig. 4.8 Variation of pH in SBF with the soaking period (0, 3, 7, 14 and 21days) of bioglasses.

4.7 Cell Cytotoxicity and Proliferation assays

The effects of bolus on cellbehaviors were examined. The rMSCs cells were used to know the bone formation ability of the bioglasses. In particular, we focused on ions released from bioglass that might affect the viability and functional activity of the cells. The indirect culture assay was used, where ionic extracts conditioned media were used to treat cells. A conditioned media were first treated at room temperature for 24 and 72 hours and the cell viability were measured by CCK assay, highest rate exhibited in cell proliferation. Fig.4.9 shows cell viability assays on bioglass samples (T0, T.2, T.4, T.6, T.8, and T1) and the control during cell culture for 24 h, and 72 h and is evaluated using cell counting kit (CCK-8) method. It is observed that the cell growth kinetics of all samples was found to be enhanced

significantly when compared with plastic control except T.8 (0.8 mol% of TiO_2) glass sample. Among all samples, 0.6 mol% of TiO_2 (T.6) doped bioglass showed high cell growth.

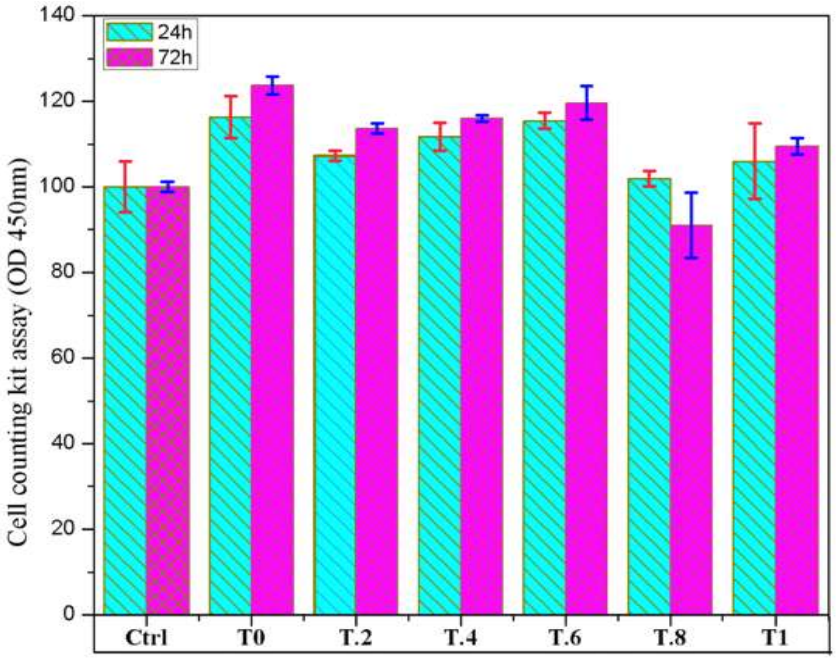

Fig. 4.9 Evaluation of *rMSCs* cells growth on TiO_2 doped phosphate glasses culturing for 24 h and 72 h by the CCK-8 method.

Moreover, all samples showed absorbance values greater than 90% with respect to plastic control as base line (assumed to be 100%). It means as-prepared bioglasses are not inducing any toxic effects. If the viability assay values were less than 70% they were treated as toxic [58]. Furthermore, the seeded rMSCs cells proliferate on the TiO_2 doped glasses with incubation time. The proliferation enhances with time and also in TiO_2 content of up to 0.6 mol%; later it decreases slightly compared with control. Therefore, the correct ligand of the cell form a covalent bond due to TiO_2 content increases and develops the certain bactericidal properties and the effect leads to higher cell viability when compared with other samples discussed by researchers (Lakhkar et al., 2012, Mozumder, Zhu, & Perinpanayagam et al, 2011; Verket et al., 2012); this showed low cytotoxicity and good bioactivity [59,60]. The resulting expansion of cell proliferation assays should have a titanium oxide effect of molar densities and dependence on bone cell functions. While substituting TiO_2 for CaO would enhance cell proliferation efficiency of glass sample containing titanium by up to 0.6 mol%, further increase in TiO_2 creates inhibitory effects on cell growth and HAp layer formation, an observation which is in good agreement with the XRD, FTIR, SEM and controlled dissolution analysis.

4.8 Antibacterial analysis

The antibacterial activity of T0, T.2, T.6 and T1 bioglass samples was tested against Gram-negative bacteria, *E. coli*, by optical density method (ODM).

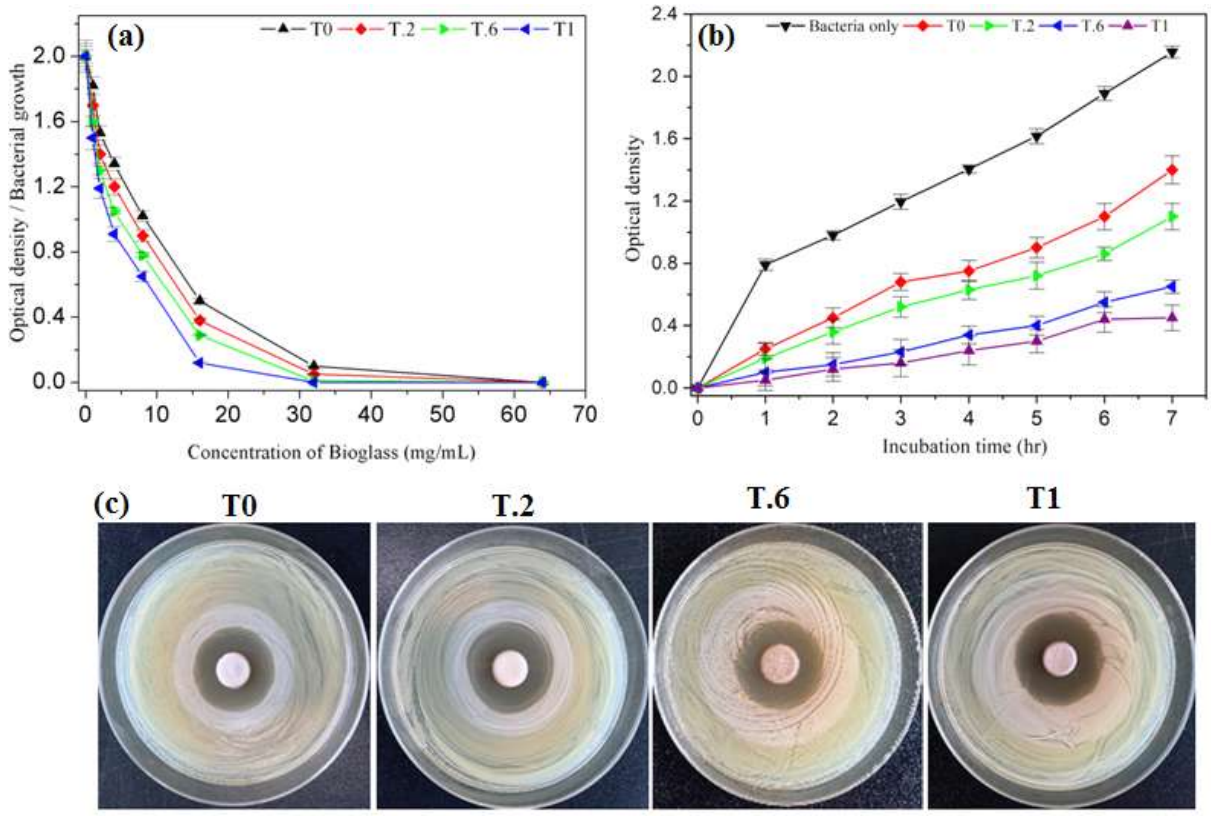

Fig. 4.10 Antibacterial activity of the TiO_2 doped zinc-phosphate bioglasses against bacteria *Escherichia coli.* (a) The bacteria viability during culture with bioglass with different concentrations monitored at 12 h (b) The bacteria viability during culture with bioglass monitored up to 7 h at fixed concentration 10mg/mL by Presto Blue assay (n=3), (c) Antibacterial tests using an agar diffusion plate.

Fig. 4.10 shows the antibacterial activity of TiO_2 doped zinc- phosphate bioglasses against bacteria *Escherichia coli.* It is a well-known fact and many available reports revealed that, Zn and Ti are a potent antibiotic against many bacterial species [6,62,63]. The results obtained showed that OD values decrease when bioglass samples are treated with bacterial species at different time intervals with fixed amount of bioglass (10 mg/mL) and also with the different amounts of bioglass samples (Fig. 4.10 a & b). On the other hand, the suppression of the growth of *E. coli* with increase in Ti concentration leads to decrease in OD of the bacterial solution. The decrease in OD designates antibacterial activity of as-prepared glasses [63,64]. However, the increase of Ti significantly inhibits the growth of bacteria species. Moreover, the antibacterial tests of bioglass against *E. coli* using an agar diffusion plate confirm the

formation of antibacterial effective zone around the sample observed after 7 h, shown in Fig. 10(c). This difference may be due to the release of tiny amounts of ions Zn and Ti. As a consequence, the Zn and Ti co-delivery ions sufficiently inhibit the growth of bacterial species.

5. Conclusions

Titanium incorporated zinc phosphate based glasses were successfully developed by conventional melt quenching process and detailed investigations were carried out to know the influence on structural, mechanical, and biological properties for the fabrication of resorbable orthopaedic implants. The density, glass transition temperature and mechanical strength of as-prepared glasses increase with increase in TiO_2 content which is attributed to cross link densification of glass structure formed by strong P–O–Ti bonds. In vitro studies confirmed the development of rich crystalline HAp layer on the samples with incubation time (3, 7, 14 and 21 days) and content of TiO_2 up to 0.6 mol% in SBF. The glass samples turned more resistant to hydration, indicating reduced dissolution rate and pH values. Moreover, a controlled degradation with increase in Ti^{4+} was observed. High cell attachments and biocompatibility were noticed by cell proliferation and cytotoxicity tests were conducted using CCK-8 method on *rMSCs* cells. Furthermore, inhibition of bacteria species growth significantly with increase of TiO_2 confirmed good antibacterial activity of the glasses. The results concluded that there was no inhibitory effect on HAp layer formation which is useful for generation of new bone tissues. Among all TiO_2 doped samples, 0.6 mol% glass showed high mechanical strength, controlled pH and degradation behaviour along with in vitro bioactivity in vitro and is suitable for in vivo evaluation for bone resorbable implant development.

References

[1] I.Ahmed, C.A.Collins, M.P. Lewis, I. Olsen, J.C.Knowles, Processing, characterisation and biocompatibility of iron-phosphate glass fibres for tissue engineering, Biomaterials. 25 (2004) 3223–3232.

[2] M. Bitar, V. Salih, V. Mudera, J.C. Knowles, M.P. Lewis, Soluble phosphate glasses: In vitro studies using human cells of hard and soft tissue origin, Biomaterials. 25 (2004) 2283–2292.

[3] M. Bitar, JC Knowles, V Salih,Soluble phosphate glass fibres for repair of bone-ligament interface, J. Mater. Sci. Mater. Med. 16 (2005) 1131–1136.

[4] R. Shah, A.C.M. Sinanan, J.C. Knowles, N.P. Hunt, M.P. Lewis, Craniofacial muscle engineering using a 3-dimensional phosphate glass fibre construct, Biomaterials. 26 (2005) 1497–1505.

[5] E.A. Abou Neel, D.M. Pickup, S.P. Valappil, R.J. Newport, J.C. Knowles, Bioactive functional materials: A perspective on phosphate-based glasses, J. Mater. Chem. 19 (2009) 690–701.

[6] O.Bretcanu1, F. Baino, E. Verne, C. Vitale-Brovarone, Novel resorbable glass-ceramicscaffolds for hard tissue engineering: from the parent phosphate glass to its bone-like macroporous derivatives, J. Biomater. Appl. 28 (2014) 1287–1303.

[7] U.Hoppe, G. Walter, R. Kranold and D. Stachel, Structural specifies of phosphateglasses probed by diffraction methods: A review, J. Non. Cryst. Solids. 263–264 (2000) 29–47.

[8] P. Haque, I. Ahmed, A. Parsons, R. Felfel, G. Walker, C.Rudd, Degradation properties and microstructural analysis of $40P_2O_5$–$24MgO$–$16CaO$–$16Na_2O$–$4Fe_2O_3$phosphate glass fibres, J. Non. Cryst. Solids. 375 (2013) 99–109.

[9] A. Hoppe, N.S. Güldal, A.R.Boccaccini, A review of the biological response to ionic dissolution products from bioactive glasses and glass-ceramics, Biomaterials. 32(2011) 2757–2774.

[10] I. Atkinson, E.M. Anghel, L. Predoana, O.C. Mocioiu, L. Jecu, I. Raut, C. Munteanu, D. Culita, M. Zaharescu, Influence of ZnO addition on the structural, in vitro behavior and antimicrobial activity of sol–gel derived CaO–P_2O_5–SiO_2 bioactive glasses, Ceram. Int. 42 (2016) 3033–3045.

[11] A. García, M. Cicuéndez, I. Izquierdo-Barba, D. Arcos, M. Vallet-Regi, Essential role of calcium phosphate heterogeneities in 2D-hexagonal and 3D-cubic SiO_2–CaO–P_2O_5 mesoporous bioactive glasses, Chem. Mater. 21 (2009) 5474–5484.

[12] M. Araújo, M. Miola, G. Baldi, J. Perez, E. Verné, Bioactive glasses with low Ca/P ratio and enhanced bioactivity, Materials 9 (2016) 226.

[13] I. Farooq, M. Tylkowski, S. Müller, T. Janicki, D.S. Brauer, R.G. Hill, Influence of sodium content on the properties of bioactive glasses for use in air abrasion, Biomed. Mater. 8 (2013) 065008.

[14] K.E. Wallace, R.G. Hill, J.T. Pembroke, C.J. Brown, P.V. Hatton, Influence of sodium oxide content on bioactive glass properties, J. Mater. Sci. Mater. Med. 10 (1999) 697–701.

[15] V. Rajendran, A. V. Gayathri Devi, M. Azooz, F.H. El-Batal, Physicochemical studies of phosphate based P_2O_5–Na_2O–CaO–TiO_2 glasses for biomedical applications, J. Non. Cryst. Solids. 353 (2007) 77–84.

[16] A.S. Monem, H.A. ElBatal, E.M.A. Khalil, M.A. Azooz, Y.M. Hamdy, In vivo behavior of bioactive phosphate glass-ceramics from the system P_2O_5–Na_2O–CaO containing TiO_2, J. Mater. Sci. Mater. Med. 19 (2007) 1097–1108.

[17] A. V. Gayathri Devi, V. Rajendran, N. Rajendran, Structure, solubility and bioactivity in TiO_2-doped phosphate-based bioglasses and glass-ceramics, Mater. Chem. Phys. 124 (2010) 312–318.

[18] G. Jagan Mohini, G. Sahaya Baskaran, V. Ravi Kumar, M. Piasecki, N. Veeraiah, Bioactivity studies on TiO_2-bearing Na_2O–CaO–SiO_2–B_2O_3 glasses, Mater. Sci. Eng. C. 57 (2015) 240–248.

[19] X. Chen, Y. Meng, Y. Li, N. Zhao, Investigation on bio-mineralization of melt and sol-gel derived bioactive glasses, Appl. Surf. Sci. 255 (2008) 562–564.

[20] H.A. ElBatal, E.M.A. Khalil, Y.M. Hamdy, In vitro behavior of bioactive phosphate glass-ceramics from the system P_2O_5–Na_2O–CaO containing titania, Ceram. Int. 35 (2009) 1195–1204.

[21] R.C. Lucacel, M. Maier, V. Simon, Structural and in vitro characterization of TiO_2–CaO–P_2O_5 bioglasses, J. Non. Cryst. Solids. 356 (2010) 2869–2874.

[22] C. Ohtsuki, H. Iida, S. Hayakawa, A. Osaka, Bioactivity of titanium treated with hydrogen peroxide solutions containing metal chlorides,J. Biomed. Mater. Res 35 (1997) 39–47.

[23] V.H. Rao, P.S. Prasad, P.V. Rao, L.F. Santos, N. Veeraiah, Influence of Sb_2O_3on tellurite based glasses for photonic applications, J. Alloys Compd. 687 (2016) 898–905.

[24] O.A. Zamyatin, A.D. Plekhovich, E. V. Zamyatina, A.A. Sibirkin, Glass-forming region and physical properties of the glasses in the TeO_2−MoO_3−Bi_2O_3 system, J. Non. Cryst.

Solids. 452 (2016) 130–135.

[25] T. Kokubo, H. Takadama, How useful is SBF in predicting in vivo bone bioactivity?, Biomaterials. 27 (2006) 2907–2915.

[26] R. Samudrala, P. Abdul Azeem, V. Penugurti, B. Manavathi, Cytocompatibility studies of titania-doped calcium borosilicate bioactive glasses in-vitro, Mater. Sci. Eng. C. 77 (2017) 772–779.

[27] R.O. Omrani, A.b. Kaoutar, A. El, S. Krimi, I. Khattech, M. Jemal, J. Videau, M. Couzi, Structural and thermochemical properties of sodium magnesium phosphate glasses, J. Alloys .Comp. 632 (2015) 766–771.

[28] E.A. Abou Neel, J.C. Knowles, Physical and biocompatibility studies of novel titanium dioxide doped phosphate-based glasses for bone tissue engineering applications, J. Mater. Sci. Mater. Med. 19 (2008) 377–386.

[29] E.A. Abou Neel, W. Chrzanowski, S.P. Valappil, L.A.O'Dell, D.M. Pickup, M.E. Smith, R.J. Newport, J.C. Knowles, Doping of a high calcium oxide metaphosphate glass with titanium dioxide, J. Non. Cryst. Solids. 355 (2009) 991–1000.

[30] F.A. Santos, J.R.J. Delben, A.A.S.T. Delben, L.H.C. Andrade, S.M. Lima, Thermal stability and crystallization behavior of TiO_2 doped ZBLAN glasses, J. Non. Cryst. Solids. 357 (2011) 2907–2910.

[31] R.K. Brow, D.R. Tallant, W.L. Warren, A. McIntyre, D.E. Day, Spectroscopic studies of the structure of titanophosphate and calcium titanophosphate glasses, Phys. Chem. Glas. 38 (1997) 300–306.

[32] L. Koudelka, P. Mošner, M. Zeyer, C. Jäger, Lead borophosphate glasses doped with titanium dioxide, in: J. Non. Cryst. Solids. 326 & 327 (2003) 72–76.

[33] S. Liu, H. Liu, T. Wang, H. Huang, Structure and crystallization of $(1-x)(33.33Li_2O–33.33Fe_2O_3–33.33P_2O_5)–xB_2O_3$ glasses, J. Non. Cryst. Solids. 450 (2016) 38–41.

[34] A. Kiani, J. V. Hanna, S.P. King, G.J. Rees, M.E. Smith, N. Roohpour, V. Salih, J.C. Knowles, Structural characterization and physical properties of $P_2O_5–CaO–Na_2O–TiO_2$ glasses by Fourier transform infrared, Raman and solid-state magic angle spinning nuclear magnetic resonance spectroscopies, Acta Biomater. 8 (2012) 333–340.

[35] D.S.L. Weiss, R.D. Torres, S. Buchner, S. Blunk, P. Soares, Effect of Ti and Mg dopants on the mechanical properties, solubility, and bioactivity in vitro of a Sr-containing phosphate based glass, J. Non. Cryst. Solids. 386 (2014) 34–38.

[36] R. Koohkan, T. Hooshmand, M. Tahriri, D. Mohebbi-Kalhori, Synthesis, characterization and in vitro bioactivity of mesoporous copper silicate bioactive glasses,

Ceram. Int. 44 (2018) 2390–2399.

[37] A. Shaim, M. Et-Tabirou, L. Montagne, G. Palavit, Role of bismuth and titanium in $Na_2O–Bi_2O_3–TiO_2–P_2O_5$ glasses and a model of structural units, Mater. Res. Bull. 37 (2002) 2459–2466.

[38] I.R. Gibson, I. Rehman, S.M. Best, W. Bonfield, Characterization of the transformation from calcium-deficient apatite to β-tricalcium phosphate, J. Mater. Sci. Mater. Med. 11 (2000) 533–539.

[39] P.Y. Shih, S.W. Yung, T.S. Chin, FTIR and XPS studies of $P_2O_5–Na_2O–CuO$ glasses, J. Non. Cryst. Solids. 244 (2003) 211–222.

[40] J. Ma, C.Z. Chen, D.G. Wang, J.Z. Shi, Textural and structural studies of sol-gel derived $SiO_2–CaO–P_2O_5–MgO$ glasses by substitution of MgO for CaO, Mater. Sci. Eng. C. 30 (2010) 886–890.

[41] M. Cerruti, D. Greenspan, K. Powers, Effect of pH and ionic strength on the reactivity of Bioglass® 45S5, Biomaterials. 26 (2005) 1665–1674.

[42] C.Y. Kim, A.E. Clark, L.L. Hench, Compositional dependence of calcium phosphate layer formation in fluoride bioglasses®, J. Biomed. Mater. Res. 26 (1992) 1147–1161.

[43] A. Cüneyt Tas, Synthesis of biomimetic Ca-hydroxyapatite powders at 37°C in synthetic body fluids, Biomaterials. 21 (2000) 1429–1438.

[44] M.Lu, F. Wang, Q. Liao, K. Chen, J. Qin, S. Pan, FTIR spectra and thermal properties of TiO_2-doped iron phosphate glasses, J. Mol. Struct. 1081 (2015) 187–192.

[45] C. Ohtsuki, T. Kokubo, T. Yamamuro, Mechanism of apatite formation on $CaO–SiO_2–P_2O_5$ glasses in a simulated body fluid, J. Non. Cryst. Solids. 143 (1992) 84–92.

[46] J.C. Elliott, Structure and Chemistry of the Apatites and Other Calcium Orthophosphates, 1994.

[47] H. Tripathi, S. Kumar Hira, A. Sampath Kumar, U. Gupta, P. Pratim Manna, S.P. Singh, Structural characterization and in vitro bioactivity assessment of $SiO_2–CaO–P_2O_5–K_2O–Al_2O_3$ glass as bioactive ceramic material, Ceram. Int. 41 (2015) 11756–11769.

[48] J. Barralet, S. Best, W. Bonfield, Carbonate substitution in precipitated hydroxyapatite: An investigation into the effects of reaction temperature and bicarbonate ion concentration, J. Biomed. Mater. Res. 41(1998) 79–86.

[49] R.K. Singh, G.P. Kothiyal, A. Srinivasan, In vitro evaluation of bioactivity of $CaO–SiO_2–P_2O_5–Na_2O–Fe_2O_3$ glasses, Appl. Surf. Sci. 255 (2009) 6827–6831.

[50] X. Chen, Y. Meng, Y. Li, N. Zhao, Investigation on bio-mineralization of melt and sol-gel derived bioactive glasses, Appl. Surf. Sci. 255 (2008) 562–564.

[51] T. Kokubo, H.M. Kim, M. Kawashita, Novel bioactive materials with different mechanical properties, Biomaterials. 24 (2003) 2161–2175.

[52] L.L. Hench, The story of Bioglass, J. Mater. Sci. Mater. Med. 17 (2006) 967–978.

[53] E.A. Abou Neel, W. Chrzanowski, J.C. Knowles, Effect of increasing titanium dioxide content on bulk and surface properties of phosphate-based glasses, Acta Biomater. 4 (2008) 523–534.

[54] M. Navarro, M.P. Ginebra, J. Clément, S. Martínez, G. Avila, J.A. Planell, Physicochemical degradation of titania-stabilized soluble phosphate glasses for medical applications, J. Am. Ceram. Soc. 86 (2003) 1345–1352.

[55] M. Karabulut, E. Melnik, R. Stefan, G.K. Marasinghe, C.S. Ray, C.R. Kurkjian, D.E. Day, Mechanical and structural properties of phosphate glasses, J. Non. Cryst. Solids. 288 (2001) 8–17.

[56] L.L. Hench, Bioceramics: From Concept to Clinic Larry, J. Am. Ceram. Soc. 74 (1991) 1487–1510.

[57] N.J. Lakhkar, J.-H. Park, N.J. Mordan, V. Salih, I.B. Wall, H.-W. Kim, S.P. King, J. V Hanna, R.A. Martin, O. Addison, F. Mosslemans, J.C.Knowles, Titanium phosphate glass microspheres for bone tissue engineering Division of Biomaterials and Tissue Engineering, Acta Biomater. 8 (2012) 4181–4190.

[58] S. Kapoor, A. Goel, A.F. Correia, M.J. Pascual, H.Y. Lee, H.W. Kim, J.M.F. Ferreira, Influence of ZnO/MgO substitution on sintering, crystallisation, and bio-activity of alkali-free glass-ceramics, Mater. Sci. Eng. C. 53 (2015) 252–261.

[59] P.C. Maness, S. Smolinski, D.M. Blake, Z. Huang, E.J. Wolfrum, W.A. Jacoby, Bactericidal activity of photocatalytic TiO_2reaction: Toward an understanding of its killing mechanism, Appl. Environ. Microbiol. 65 (1999) 4094–4098.

[60] J. Zhou, L. Zhao, Hypoxia-mimicking Co doped TiO_2microporous coating on titanium with enhanced angiogenic and osteogenic activities, Acta Biomater.43 (2016) 358–368.

[61] H. Hu , W. Zhang, Y. Qiao, X. Jiang, X. Liu, C. Ding, Antibacterial activity and increased bone marrow stem cell functions of Zn-incorporated TiO_2 coatings on titanium, Acta Biomater. 8 (2012) 904–915.

[62] L. Zhang, J. Guo, T. Yan, Y. Han, Fibroblast responses and antibacterial activity of Cu and Zn co-doped TiO_2 for percutaneous implants, Appl. Surf. Sci.434 (2018) 633-642.

[63] M.N. Capela, D.M. Tobaldi, C.Oliveira, A. Pereira, A.S. Duarte, M.P. Seabra, M.H.V.Fernandes, Bioactivity and antibacterial activity against E-coli of calcium-phosphate based glasses: Effect of silver content and crystallinity, Ceram. Int.43 (2017) 13800–13809.

[64] X. K. Naresh,A.T. Pawar,R.V.N. Gundloori, Polyesteramide of Neem Oil and Its Blends as an Active Nanomaterial for Tissue Regeneration, ACS Appl. Bio Mater, 8 (2019) 3341-3351.

Chapter -5

Evaluation of HAp layer formation over Al^{3+} ions doped novel zinc-phosphate glasses for bone repair implant applications

This chapter covers the structural aspects of $ZnO–CaO–Na_2O–P_2O_5$ glasses mixed with Al_2O_3 ions, and results based on biological response and dissolution behaviour. In this chapter, physical properties such as density, molar volume, micro hardness and in vitro bioactivity test of glasses with Al_2O_3 content immersed in SBF solution for several of 3, 7, 14, and 21days, due to the pH variation as well as degradation rate, are also discussed. Structural analysis was carried out with the help of X-ray diffraction, SEM-EDS, and FTIR-spectroscopy, and Biological studies on cell cytocompatibility and antimicrobial of results also figure in the chapter.

5.1 Introduction

Bioglasses and glass ceramics are crucial biomaterials employed in biomedical tissue repair and regeneration applications than metals and metal related composites due to their nontoxic behaviour, better corrosion resistance and improved mechanical properties [1]. The main advantage of these bioglasses is ability to form bone like mineral phase or crystalline HAp layer, when in contact with simulated body fluid (SBF). The formation of apatite layer confirms bioactivity of the materials *in vitro* and *in vivo*. The crystalline apatite layer formed can enhance cell proliferation and cell attachment, which leads to repair of defected bone tissues or generation of new soft or hard tissues [2]. Various types of bioglass implant materials have been developed for the purpose of repair and regeneration of defected hard and soft bone tissues. However, some materials show high mechanical strength and low bioactivity and others show poor strength and high bioactivity. Particularly, silica free calcium phosphate based glasses have great advantages, because of their chemical composition is quite similar to natural bone phase [3]. Moreover, phosphate based bioactive glasses can stimulate to form new bone due to their osteoinductive nature [4]. The main disadvantage of these glasses is high solubility rate and low fracture toughness. This limits the potential use of bio implants suitable for load bearing applications. Recently, numerous attempts have been made by researchers, in order to improve mechanical properties and achieve the controlled degradation by varying bioglass composition with suitable metal oxides such as ZnO, TiO_2, SrO, MgO, Al_2O_3 etc. These metal oxides act as network modifiers and enable the release of non-bridging oxygen atoms (NBO's) by breaking the continuity of glass network. As a result, the reactivity of the glass enhances when it interacts with aqueous medium and also leads to apatite formation on bioglasses [5,6].

Out of various metal oxides, strong and stable aluminium oxide can improve the fracture toughness and control the release of metal ions suitable for the development of phosphate based bioglass stable implants [5]. Besides, improvement of mechanical strength and control of solubility, the chemical durability of glasses was also found to increase enormously with the incorporation of Alumina oxide [7]. Pure Al_2O_3 acts as a Bioinert and also exhibits biocompatibility with living organs. The mechanical strength of Al_2O_3 is considerably high when compared with the bioglass materials [8]. It has been reported that the addition of Al_2O_3 to bioglasses improves the mechanical strength without degrading biocompatibility and also restrains hydroxyapatite layer formation depending on the glass composition and the content of Al_2O_3 [9,10]. According to McMillan, if the ionic field

strength (Z/r^2) of metal ion is less than 5 $Å^{-2}$, it acts as network modifier, where Z is in cation valence state and r is the radius of ion. If it is greater than 5 $Å^{-2}$ then it act as network former, but for Al^{3+} it is ≈11.53 $Å^{-2}$ [1]. Alumina enters glass network as AlO_4 tetrahedra for higher concentrations, which makes the glass network very rigid and leads to improvement in mechanical properties. At lower concentrations the Alumina enters the network as AlO_6 octahedra causing intense bioactivity [3,7,11,12]. Al_2O_3 act as network stabilizer and forms strong covalent bonds (P–O–Al) with the P_2O_5 glass network [7]. Furthermore, Al_2O_3 plays the role of network former and slows down the rate of dissolution of bioglasses. The controlled release of Aluminium ions leads to the formation of Al^{3+} ion based apatite layer. On the other hand, the reduction of bioactivity and inhibition of hydroxyapatite (HAp) layer formation of the glasses in contact with the simulated body fluid (SBF) is observed due to increase in ionic field strength from the addition of a network of Aluminium oxide to the glass system [13]. At the same time, there is carcinogenicity and adverse impact on the bioactivity of glasses with the incorporation of huge amount of Al_2O_3 [14,15]. Most of the available earlier research reports focused on the effect of Al_2O_3 doped silicate based bioglasses only. There are very few reports are available on physico-chemical, mechanical and bioactive properties of Al_2O_3 incorporated phosphate based glasses. J.M. Smith et al studied in detail about the structural properties of Al_2O_3–Na_2O–CaO–P_2O_5 glass as a function of aluminium content by neutron diffraction data analysis method [3]. Moreover, many researchers varied Aluminium oxide content in the glass system from 0 mol% to 5 mol% [1,5,7,16]. This study varied Al_2O_3 concentration from 0 to 10 mol% in silica free ZnO–P_2O_5 based glasses in order to enhance the bioactivity along with hardness. Still, there is a lack of reliable information about the influence of Al_2O_3 on biological and mechanical properties of P_2O_5 based glasses. So it is most essential to explore in detail in vitro biocompatibility, cell culture, cell proliferation and mechanical properties of alumina doped zinc phosphate glasses in particular.

In the current report, we have fabricated novel Al_2O_3 doped 8ZnO–22Na_2O–24CaO–46P_2O_5 bioglass system. To the best of our knowledge, it is new and no one has reported studies on the glass system yet. The main objective of the present investigation is to study the effect of Al_2O_3 substitution by CaO on structural, physical, mechanical, thermal properties and in vitro bioactivity, cell viability and proliferation for the generation of resorbable implant material for bone repair and regeneration applications.

5.2 Results and Discussion

5.2.1 Physical and Mechanical Properties

Table 5.1 summarises, the various physical parameters and Vickers micro hardness of the as-prepared bioglass samples with the addition of Al_2O_3, density, oxygen molar volume and oxygen packing density appeared to increase and there was a decrease in molar volume of the glasses. The variation of different physical parameters as a function of Al_2O_3 concentration is shown in Fig.5.1 (a) & (b). An increase in density is observed with Al_2O_3 content.

Table 5.1 Physical and mechanical properties of the ZnO–CaO–Na_2O–P_2O_5–Al_2O_3 glass system.

Sample code	Molar mass (M) (g/mol)	Molar volume (Vm) (cm^3 /mol)	Density (ρ_g) (g/cm^3)	Oxygen molar volume (Vo) (cm^3/mol)	Oxygen packing density (OPD) (mol/1)	Vickers hardness (Hv)
Al0	98.898	38.497	2.569	24.365	73.772	325(±09.40)
Al2	99.816	38.688	2.580	24.332	74.440	329(±16.52)
Al4	100.734	38.953	2.586	24.346	74.960	349(±15.81)
Al6	101.651	38.917	2.612	24.172	76.059	368(±13.23)
Al8	102.569	39.163	2.619	24.175	76.601	396(±16.32)
Al10	103.487	39.274	2.635	24.094	77.404	429(±12.83)

The Aluminium enters glass network in the form of [AlO_4] and [AlO_6], when it replaces phosphate. In general phosphate contains a large number of P–O–P bonds. By the introduction of Al_2O_3 to the glass network, the breaking of P–O–P linkages occurs, leading to formation of new P–O–Al bonds. Moreover, these newly formed bonds are more stable than P–O–P and which lead to the more compactness of the glass structure [20,21]. On the other hand, the decrease in molar volume is attributed to the reduction in mole fraction of oxygen ions in the glass network [22]. The variation of Vickers microhardness as a function of Al_2O_3 content of bioglasses is shown in Fig. 5.1 (c). The microhardness of glass samples increases from 325(±09.40) to 429(±12.83) Hv with increasing Al_2O_3 content in the glass network. On the same grounds as of density, a steady increment in the measured Vickers microhardness of bioglasses with increasing Al_2O_3 content is due to the strengthening of glass structure by increasing bond strength of P–O–Al ionic linkages [23]

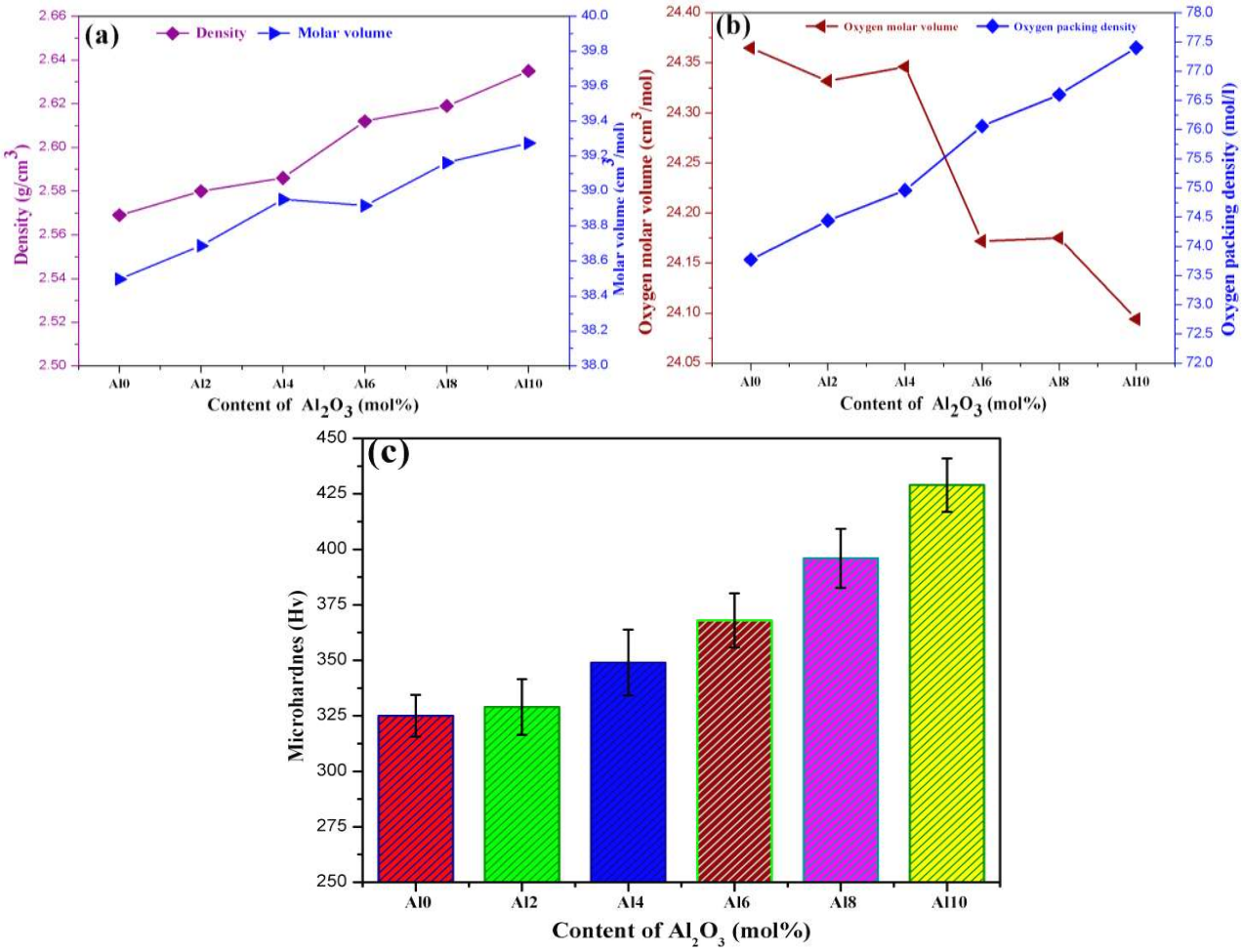

Fig. 5.1 The variations of physical parameters (a) Density (g/cm^3) and molar volume (b) Oxygen molar volume and Oxygen packing density values (c) Micro hardness as a function of Al_2O_3 content.

In other words, it can also be explained that, there is a slight increase in the number of octahedrally coordinated Al^{3+} ions and stronger ionic cross linkages due to insertion of Al^{3+} ions between phosphate networks [5]. This in turn reduces the number of nonbridging oxygen atoms (NBO's) and increases cross-linking density, compactness and rigidity of the glass network. Out of all prepared glasses, Al10 had highest Hv value.

5.2.2 Differential thermal analysis

Fig. 5.2 shows DTA graph for Al4 bioglass and Fig. 5.2 is presented in order to compare the variation of thermal parameters with increase of Al_2O_3 doping in bioglasses. Thermal properties such as glass transition temperature (Tg), crystallization temperature (Tc), melting temperature (Tm), ΔT and Hruby parameter are assessed from DTA graphs and are presented in Table 5.2.

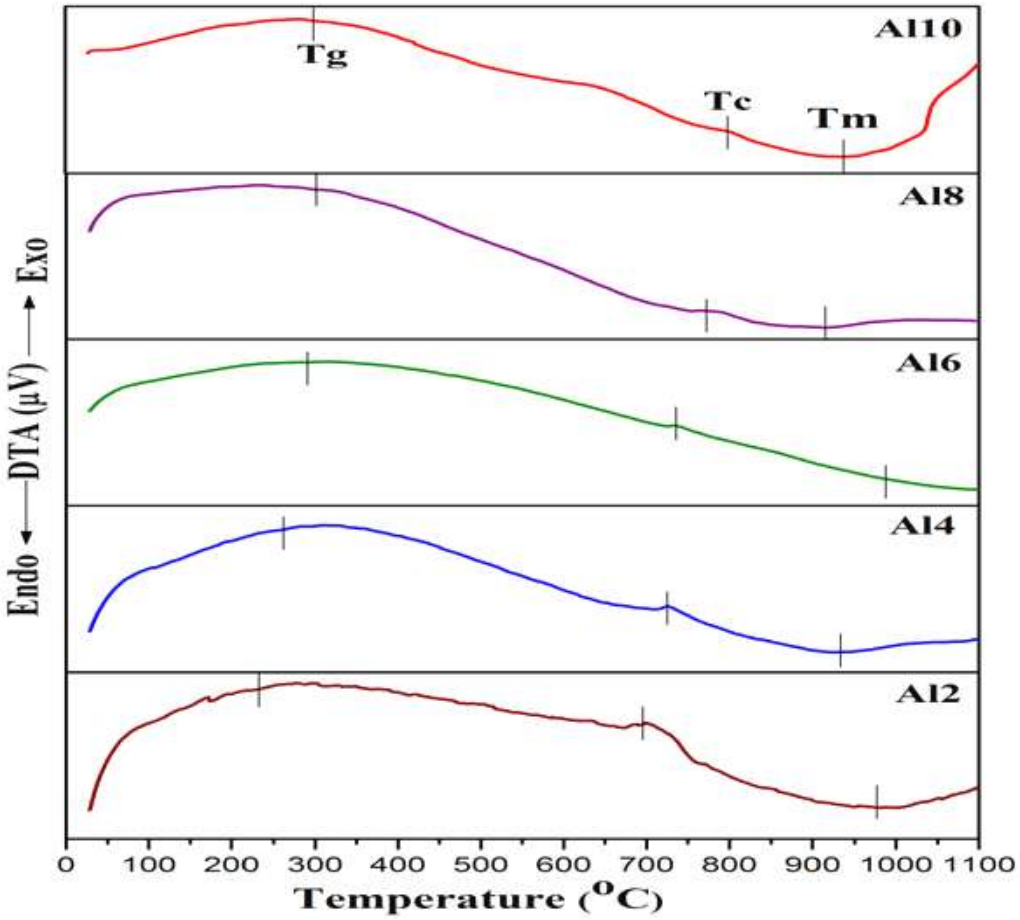

Fig. 5.2 Variation of thermal properties of the Al_2O_3 doped bioglass samples.

Table 5.2 Thermal properties of aluminium doped bioactive glasses

Sample Code	Tg (°C)	Tc (°C)	Tm (°C)	ΔT (°C)	K_H
Al2	223.42	698.71	980.49	475.29	1.68
Al4	258.53	724.42	936.89	465.89	2.19
Al6	293.61	737.27	927.87	443.66	2.33
Al8	302.82	779.16	918.12	476.34	3.49
Al0	308.35	796.17	915.45	487.87	4.08

DTA curves in Fig. 5.2, the glass transmission temperature (Tg) an endothermic effect is found in the range of 223.42–308.35 °C, crystallization temperature (Tc), exothermic effect in the range of 698.71–796.17 °C, and melting temperature (Tm), endothermic effect in the range of 980.49–915.45 °C. These results are in agreement with reports elsewhere for similar

glasses. The results revealed that the incorporation of Al_2O_3 and the decrease in CaO content causes increase in glass transition and crystallization temperatures, and decrease in melting temperature. From Table 5.2 it is also observed that the stability of the glasses ΔT is not varying much with the variation of Al_2O_3 content in the glass. The highest Al_2O_3 content glass Al8 is found to have high Tg and Tc along with high stability (487.87) among all the glasses. Further, the glass shows good bioactivity [24].To examine the glass-forming potential of the study materials, Hruby parameter (1.68-4.08) was also measured. When Al_2O_3 ions are substituted for calcium ions, they form a strong covalent Al-O bond than Ca-O. This is because the electro negativity of Al_2O_3 is higher than that of calcium. These evolutions are presented in Table 5.2 [25]. Our results are in good agreement with those in previous studies on alumina phosphate glasses [24,26]. Tiwari et al., reported that initial rise in glass transition temperature and crystallization temperature may be the effect of glass network strengthening by Al_2O_3-induced cross-linking among phosphate chains [27]. In general, Tg and Tc reflect structure compactness in the glass structure arrangement. The more the degree of structural compactness in glass construction, the higher the value of Tg and Tc. Therefore, it is a lot easier to obtain glass when the structure is very compact. As the amount of Al_2O_3 rises with decrease in CaO, Al_2O_3 takes part in forming Al^{3+} glass structure and renders the glass structure far more compact as [AlO_4] and [AlO_6]. This is the principal reason that makes Tg grow steadily [28].

The Al_2O_3 in the glass structure can acquire the new P–O–Al instead of P–O. This enables the glass structure to become more solid. Moreover, Al_2O_3 can break the glass structure and the bond of P–O–Al instead of P–O–P, which is more stable compared to P–O–P [28,29]. Therefore, as the content of Al_2O_3 increases, the glass structure becomes more compact, leading to an increase of Tg, Tc and Tm. Furthermore, in the melting region, even though the initial temperature is almost unchanging for all composite samples, the melting process varies in each composition of different alumina percentage [30].

5.3 *In vitro* bioactivity analysis

5.3.1 X- ray diffraction analysis

The XRD patterns of Alumina doped phosphate bioactive glasses before and after immersion in SBF solution for various time periods (0, 3, 7, 14 days) are shown in Fig. 5.3(a) and 5.3(b, c, d, e & f) respectively. From Fig. 5.3 (a), it is found that a broad hallo hump over the region 18°–34° for 2θ and the presence of any significant sharp intensity peaks in the diffraction patterns.

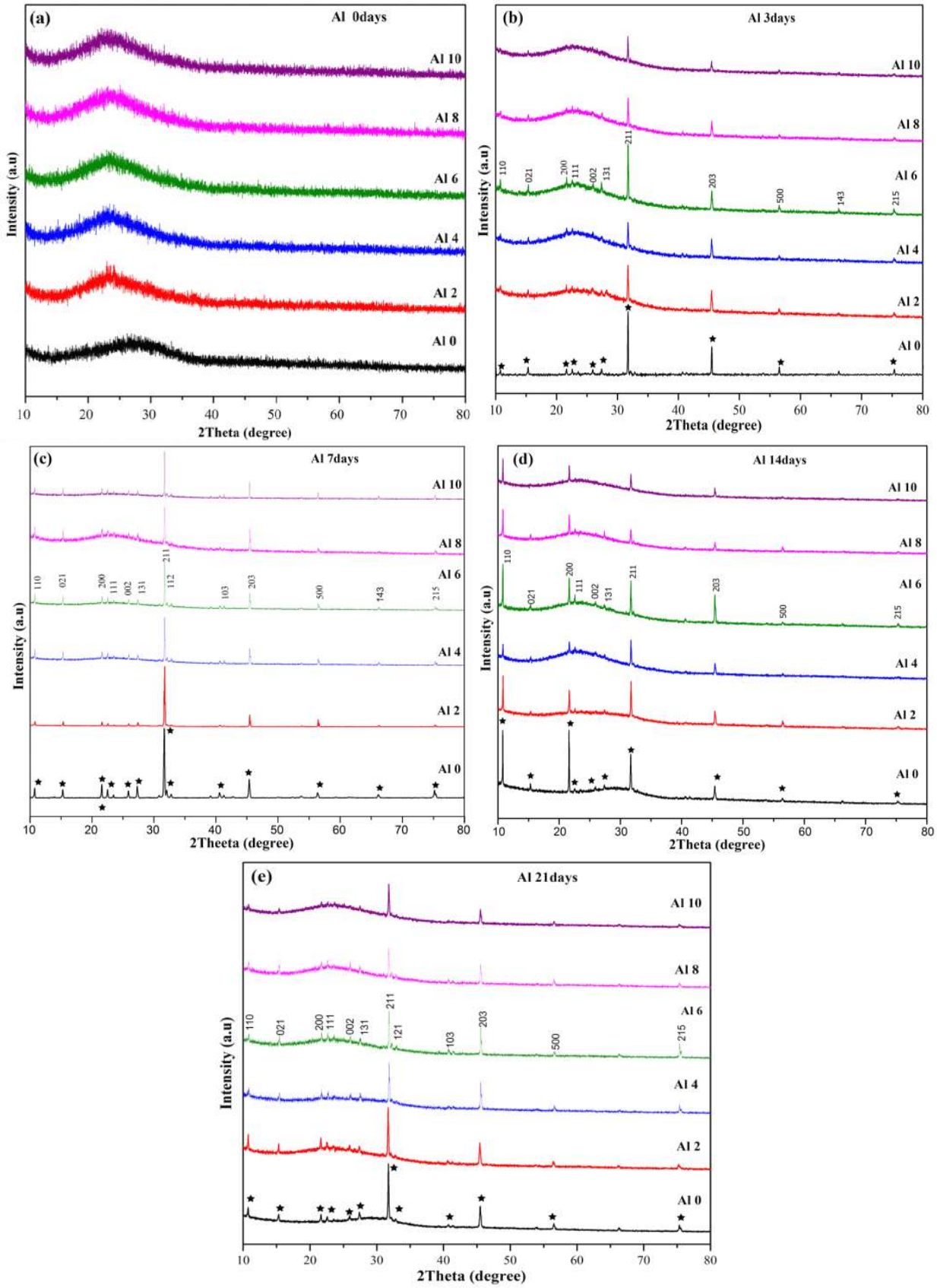

Fig. 5.3 XRD patterns of the glasses before and after immersion in SBF solution for different time intervals: (a) 0days, (b) 3days, (c) 7days, (d) 14days and (e) 21days (Hydroxyapatite; ✦72-1243).

This corresponds to the diffraction effects due to the amorphous portion of the samples. Which evidencing the amorphous glassy nature of the as-prepared glasses [19]. The samples show no noticeable crystalline sharp peaks before immersion in SBF, which confirms the amorphous nature of all glasses (Fig. 5.3(a)). The well-defined intense crystalline peaks appeared after immersion of all bioglass samples in SBF for various time periods (3, 7, 14 and 21days).It is a clear indication of crystalline hydroxyapatite ($Ca_{10}(PO_4)_6(OH)_2$) layer development over the surface of all glasses. Moreover, the broadening of hallo humps symmetrically without disappearing completely also confirms the crystalline HAp layer formation on glass samples. The intensity peaks observed for present glasses at various diffracted angles (2θ) consequent to HAp reflections 10.82(110), 15.28(021), 21.73(200), 22.82(111), 25.87(002), 27.56(131), 31.74(211), 32.17(112), 40.81(103), 45.31(203), 56.29(500), 66.31(143), 75.52(215) (indexed using the JCPDS card No ✦72-1243) are shown in Fig. 5.3(b, c, d, e). After 3 days of immersion in SBF, the diffraction patterns show the development of two prominent peaks at 2θ values of 31.74 and 45.32 corresponding to crystal planes (211) and (203) respectively, shown in Fig. 5.3. It is observed that, the peak intensity of HAp reflections (211) and (203) increases at 2θ with increase in content of Al_2O_3 from Al2 to Al6 (2 to 6 mol% Al_2O_3) and then decreases from Al8 to Al10. The same trend is continued after 7, 14 and 21 days of immersion time in SBF solution but additional peaks are present along with the above mentioned two reflections at 2θ.

Moreover, the intensities of the reflections at different values of 2θ increases gradually with an increase in incubation time up to 7days and then decrease slightly in 14 and 21 days shown in Fig. 5.3 (b, c, d, e & f). But all samples (Al2 to Al10) possess an excellent capability of HAp layer formation on the surfaces even for 3days of immersion to 21 days. The deposition of HAp layer over the bioglass samples indicates the bioactivity of the as-synthesized glasses *in vitro*. Furthermore, *in vitro* analysis in SBF solution authenticates the bioactive potential of the glasses in vivo [31,32]. The formation of apatite layer is mainly due to increase of Ca^{2+} and PO_4^{3-} ions concentration on the surface of glass by ion leaching from SBF, which initiate the development of amorphous calcium phosphate ($CaO–P_2O_5$) rich layer. The amorphous nature of HAp layer can be confirmed by the existence of broad humps centred at $2\theta = 32^{\circ}$ from XRD patterns of bioglass samples [33]. Later it can be converted into a crystalline HAp layer on bioglass surface [32]. Therefore, XRD results disclosed the enhancement in apatite layer formation capacity with Al_2O_3 content at the expense of major constituent CaO in the glass matrix without disturbing the concentration of ZnO, P_2O_5, and Na_2O. Further the apatite layer formation is confirmed by FTIR and SEM analysis.

5.3.2 FTIR-Spectrometry

Fig. 5.4 (a, b, c, d, e) shows FTIR spectral bands of as-prepared bioactive glasses (Al2, Al4, Al6, Al8 and Al10) before and after immersion in SBF for different time periods (3, 7, 14, and 21 days). Fig. 5.4a shows the absorption spectral bands of bioglasses before being soaked in SBF solution. These untreated glass samples exhibit vibrational bands at 509, 545, 740, 902, 1133, 1292, 1648, 2358, 2931 and 3438 cm^{-1}. Most of these absorption bands in between 500–1400 cm^{-1} are assigned due to presence of phosphate in the glass network. After immersion in SBF for different time periods (3, 7, 14 & 21days), new bands at around 548 to 636 cm^{-1}, 852 to 882 cm^{-1}, 958 to 1070 cm^{-1}, 1302 to 1526 cm^{-1}, 2880 to 2893 cm^{-1}, 3211 cm^{-1} and 3712 to 3724 cm^{-1} emerge along with the existing bands of untreated samples. The presence of new vibrations, shifting of existing bands and change in peak intensities confirms the formation of a crystalline HAp layer on the surfaces of bioglass samples. It is well known that, aluminium enters the phosphate glass network as [AlO_6] and [AlO_4]. Octahedral units [AlO_6] exist for small amounts of aluminium while it can be converted into tetrahedral units [AlO_4] for higher amounts of Al_2O_3. This can enhance the glass stability by forming P–O–Al linkages, when [PO_4] bonds with [AlO_4] units [21,34,35]. The absorption bands at around545 to 636 cm^{-1} are attributed to stretching vibration modes of P–O bonds [36-38] or ascribed to [AlO_6] vibrations [21], which indicates the establishment of $CaO–P_2O_5$ apatite layer on as-prepared glasses (Fig. 5.4 (b–e)). Initially a broad band centred at 545 cm^{-1} is appearing before immersion in SBF and then shifted to higher wavenumber following 3days of immersion on further increasing the incubation time from 7 days to 21 days, it is observed that the broad band split into two prominent bands (545 and 636 cm^{-1}) centred by a small kink at 549 cm^{-1}. The absorption peaks at around 740 to 748 cm^{-1} and 852 to 882 cm^{-1} are due to symmetric and asymmetric stretching of P–O–P vibrations, respectively [5,39,40]. The intensity of these peaks gradually decreases as the content of Al_2O_3 increases, which is due to replacement of P–O–P by P–O–Al linkage within the glass network, resulting in decrease in P–O–P linkage [21]. Moreover, these bands moved a little bit towards the lower wavenumber side with immersion time ranging from 3 days to 21 days. Before immersion, a little broad band appeared at 902 cm^{-1} and it turned into a doublet with small peaks at 882 and 968 cm^{-1} after immersion in SBF for 3days, which is assigned due to P–O symmetrical stretching vibrations in tetra calcium phosphate ($Ca_4(PO_4)_2O$). It symbolises presence of a crystalline HAp layer [41,42]. Moreover, these bands become sharper and shifted to higher frequency with increase in incubation time.

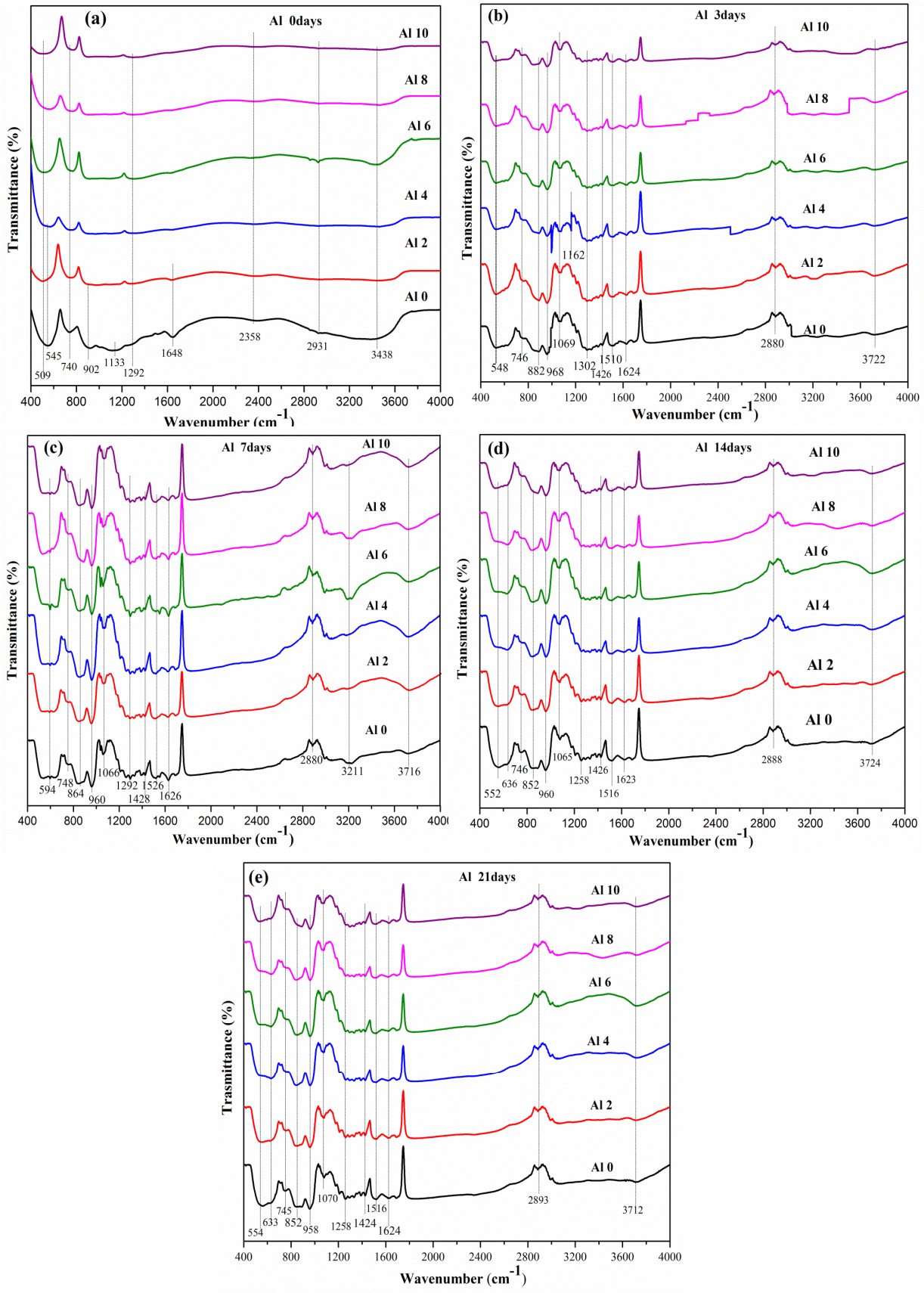

Fig. 5.4 FTIR spectra of the glass samples before and after immersion in SBF for different incubation times: (a) 0 days, (b) 3 days, (c) 7 days, (d) 14 days and (e) 21 days.

From Fig. 5.4(b–e), the bands which appeared at around 1065 cm^{-1} to 1070 cm^{-1} are the characteristic vibration modes of PO_4^{3-} groups, which is clear sign of precipitation of hydroxyl apatite from SBF solution [41,42]. It is found that, there is no change in intensity increment between 3days and 7days of immersion while there is decrease with increase in incubation time. Moreover, there is no considerable shift in wavenumber with content of aluminium and also the immersed time. The band at about 1258–1302 cm^{-1} is assigned to asymmetric stretching modes of O–P–O bond [40,43]. Along with the presence of phosphate groups, the bands at around 1424 to 1526 cm^{-1} are attributed to carbonate groups (C–O), indicating the precipitation of B-type hydroxy carbonate apatite. The presence of these groups confirms the formation of HCA layer from HAp layer [44,45]. HCA layer is responsible for the bonding between bioactive material and the bone tissue for repairing and regeneration of new bone tissues. The occurrence of FTIR absorption bands from 1623 to 1648 cm^{-1} and 3438 to 3722 cm^{-1}may be ascribed to O–H bending and stretching vibrations, respectively, which indicate the hygroscopic nature of phosphate glass [46]. The bands located at around 2358 to 2931cm^{-1} are assigned to stretching vibrations of P–O–H group /C–H stretching vibrations [46,47]. These results strongly point to the formation of HCA layer on as-prepared Al_2O_3 doped phosphate bioglasses. Moreover, we can observe the influence of replacing small amounts of CaO by Al_2O_3 on the formation of HCA layer on the surface of the bioactive glasses and also the increase in life time of the HCA layer with immersion time from stable absorption peaks which appear in FTIR spectra (Fig. 5.4). Furthermore, the obtained FTIR results are supported strongly by the XRD results of bioactive glass samples.

5.3.3 SEM-EDS Analysis

The SEM micrographs and EDS spectra of bioactive glasses (Al6 and Al10) before and after soaking in SBF for 0, 3, 7, 14 and 21 days are shown in Fig. 5.5. The untreated sample surfaces show the homogeneous plane surface without any cracks, which indicates that no morphological changes occurred before immersion. After 3 days of incubation in SBF, some remarkable changes in the microstructure of the surfaces of all samples are enclosed typically with flake type of construction, which is evidence of formation of HAp layer on the glass surfaces. It is also confirmed from additional peaks that appear in EDS spectra, compared with spectra of untreated samples. In addition to Ca and P, EDS spectra reveals the presence of elements O, Zn, Mg, Cl, K and Al on the surfaces of all samples soaked in SBF. The existence of these elements is due to ion leaching between the glass and the simulated body fluid. Moreover, these elements are responsible for the growth of bone-like apatite precipitates over the glass surface (shown in Fig. 5.5). After 7 days, 14 days and 21 days of

immersion, the glass surfaces of Al6 and Al10 are all mostly covered with highly dens cotton foam like precipitated HCA layer. Moreover, these cotton foam or flake like HCA transformed into finer structure with increase in immersion time due to partial dissolution and re-precipitation phenomena in SBF solution [48].

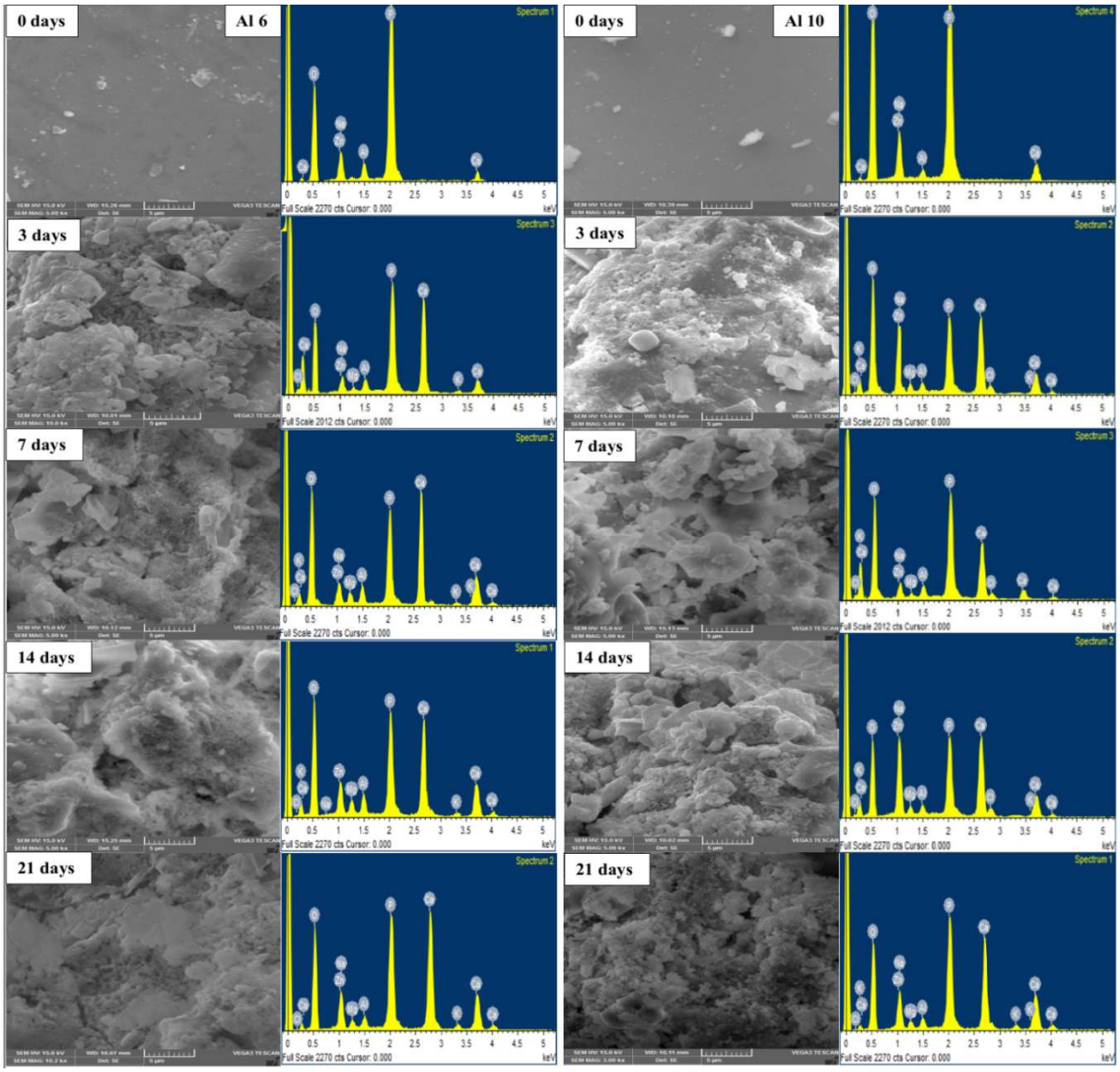

Fig. 5.5 SEM-EDS of Al6 and Al10 bioglass samples before and after immersion for different incubation time periods: (a) 0 days, (b) 3 days, (c) 7 days, (d) 14 days and (e) 21 days.

However, it is very clear from the SEM micrographs and EDS spectral peak intensities that there increase in the formation of HAp layer over the glass surface with increase in concentration of Al_2O_3 from 2 mol% to 6 mol% and then decrease in apatite layer density slightly from Al8 to Al10. This is due to the establishment of AlO_6 octahedra up to 6 mol%, which leads to improvement of bioactivity of as-prepared glass sample by increasing the number of non-bridging oxygens. On the other hand, a slight decrease in HAC layer

formation beyond 6 mol% due to AlO_4 tetrahedra formation in the glass network [49,50]. Himanshu Tripathi et al., observed the adverse effect on the bioactivity of the glasses with the inclusion of Al_2O_3 more than 1.5 mol% of Al_2O_3 or higher quantities in SiO_2–CaO–P_2O_5–SrO–Al_2O_3 glass system [7]. Most of the earlier reported research results disclose the inhibition of HAp formation with increase the content of Al_2O_3content in SiO_2 and P_2O_5 based bioglasses due to the formation of strong covalent bonds (Si–O–Al) and (P–O–Al) bonds respectively, with the glass network, which results in the compactness of the glass structure [7]. Contrary to previous results, the present system of glasses showed an increase in the crystalline nature of HAp with Al_2O_3 addition of up to 6 mol% and then slight decrease followed by further increase in Al_2O_3. SEM micrographs and EDS spectral analysis are in good agreement with the results obtained from XRD and FTIR analysis.

5.3.4 pH measurement

The evaluation of pH values gives the hydrolytical stability to all glasses in SBF solution. Fig.5.6 shows the variation of pH values in SBF solution after incubation of bioglasses for different time periods (0, 3, 7, 14 and 21 days). It is observed that there is an appreciable change in pH values during immersion time, which is due to ion leaching from the glasses to the SBF solution. After 3days of immersion there is an abrupt rise in pH values of glasses Al0, Al2, Al4, and Al6 from an initial value of SBF (pH=7.4 at 0days) and decreases for Al8 and Al10, when compared with base glass Al0 (pH=7.51). After that there is a decrease in the trend of pH values with 7 days, 14 days and 21 days of incubation time.

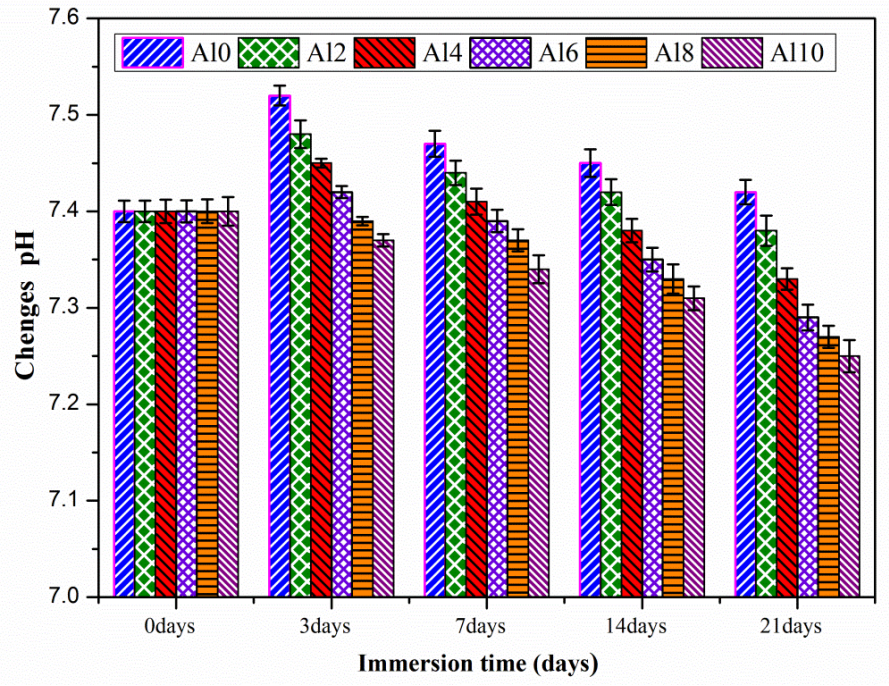

Fig. 5.6 pH variation of bioglasses with immersion time at initial pH 7.4 at 37 ^oC.

The initial increase in pH values of SBF of all glasses, when compared with pH value at 0days of SBF may be due to the release of Na^+ and Ca^{2+} ions through exchange with H^+ or OH^- ions in the simulated body fluid (SBF) solution. The cations Na^+ and Ca^{2+}released initiate the formation of HAp layer over the surface of glasses [51,52]. Afterwards, a slight decrease in pH value with increase in immersion period is observed due to increase in dissolution rate of glasses and decrease in sodium ion content. On the other hand, the formation of calcium phosphates and carbonates by precipitation of Ca^{2+} ions from the SBF solution leads to decrease in pH values and also the movement of Aluminium ions into solution makes it acidic in nature [53]. From Fig .5.6 it is very clear that, pH values increase by up to 6 mol% of Al_2O_3 and then decrease to 10 mol% of Al_2O_3 for 3 days of immersion. This increase in pH up to Al6 indicates increase in bioactivity up to 6 mol% Al_2O_3, which is due to formation of AlO_6 octahedral units and creates more of non-bridging oxygens. Further, the decrease in bioactivity beyond 6 mol% of Al_2O_3 addition is due to formation of AlO_4 tetrahedral units in the glass network. In other words, it can be explained that, a little drop in pH with increase in Al_2O_3 content is due to increase in glass strength with the addition of stabilizer cations to glass network, which leads to control of dissolution of the glass sample in SBF solution [7]. In other words, the addition of Al_2O_3 decreases the release of phosphate ions in SBF solution due to its absorption in HCA layer formation and to the reduction of glass solubility [5]. These results are evidence of controlled release of ions from glasses, leading to the formation of a rich HCA layer. Further, these are supported by micrographs of SEM. So these bioglasses can form interfacial bonds with living bone due to formation of rich HCA layer on glass surfaces.

5.3.5 Degradation measurement

Fig. 5.7 shows the degradation behaviour of bioglasses as a function of soaking time in SBF. After 3days of immersion a sudden increase in weight loss is noticed, which is due to rapid release of ions from the glass sample to SBF solution. Later, a slight weight loss of all samples is found to increase for 7, 14 and 21 days of incubation periods. Moreover, it is clearly seen from Fig.5.7 that, the degradation of the all glass samples decreases with the increase of Al_2O_3 content from 2 mol% to 10 mol% in the glass system. The minimal weight loss of the sample is found to be Al10. So there is a considerable low weight loss due to reduction of ion release from the samples. During dissolution processes, there is release of $Ca^{2+}$and PO_4^{3-} ions which in form increases the release of Na^+, Ca^{2+} and Al^{3+} ions into the surrounding SBF solution and causes degradation of the glass, which results in super

saturation of calcium and phosphate, helping to formation of HAp layer. It is well known that the release rates of Ca^{2+} and PO_4^{3-} from biomaterials are associated with bioactivity [3,54].

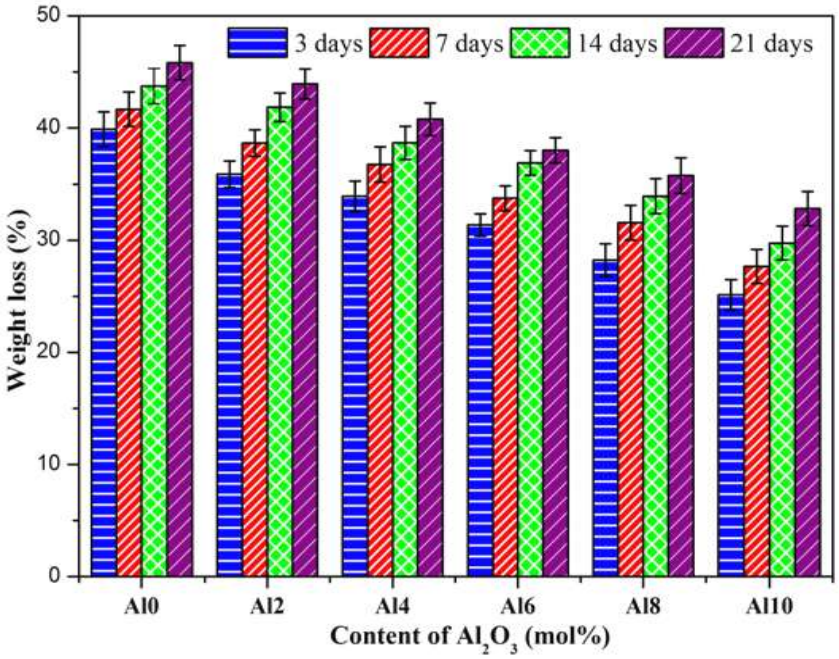

Fig. 5.7 Weight loss (%) of undoped and Al_2O_3 doped glasses as a function of immersion time.

Most of the previous reports on aluminium doped phosphate based glasses showed low degradation rate with high amount of aluminium present in glasses [4,5,7]. The decrease in weight loss with an increase of Al_2O_3 content is due to decrease in the number of P–O–P bonds and the formation of strong P–O–Al bonds, which weaken the connectivity of phosphate network and also replacing of Na^+ with Al^{3+} ions take place, which results in decrease in bioactivity. Conversely, the present system of glasses is showing high bioactivity and mechanical strength. This is possible only when there is controlled degradation of the glasses with increase in content of Al_2O_3. It is well known fact that ZnO doped glasses shows high degradation, while Al_2O_3 doped glasses show very low degradation in phosphate based bioglasses. In the present study, the base glass (0 mol% Al_2O_3) has high degradation due to the presence of ZnO and addition of Al_2O_3 may stabilize the degradation rate of ZnO–P_2O_5 glass to retain bioactivity. This explanation is supported experimentally by pH analysis and visually by SEM micrographs. These results report the formation of a rich HCA layer on as prepared aluminium incorporated bioglasses, which are more suitable for in vitro cell culture and bone regeneration.

5.3.6 Cytocompatibility and Proliferation

Fig. 5.8 exhibits the cell viability on Al_2O_3 doped bioglasses (Al2, Al4, Al6, Al8 and Al10) and control during *rMSCs* culture for 24 h and 72 h and is as assessed by a CCK-8 method. Interestingly, glass samples from Al2 to Al8 showed considerable high cell viability when compared with control except Al10 for 24 h and 72 h. It is observed that, cell viability enhances with an increase in Al_2O_3 content up to 6 mol% (Al6) with respect to control, implying the possible ionic effects on rMSCs viability. Afterwards, it is found to decrease slightly with an increase in concentration of Al_2O_3 at 10 mol% (Al10) for 24 h and further decreases in case of 72 h culturing as shown clearly in Fig. 5.8. The viability and cell proliferation of Al6 (6 mol%) sample is show significantly higher values compared to other Al_2O_3 doped samples except the base sample (Al0 or 0 mol% Al_2O_3). Moreover, the rate of cell proliferation of Al6 improved after culturing it for 72 hours. A slight decrease in proliferation is observed for Al8 and Al10, which is ascribed to very low degradation of the glass. In other words the slight reduction in cell proliferation with an increase in Al_2O_3 mol% after 3 days may be due to the network forming action of Al_2O_3 in the glass system. Recently, Himanshu Tripathi et al. studied in vitro bioactivity and structural properties of the SiO_2–CaO–P_2O_5–SrO–Al_2O_3 bioactive glasses and reported the inhibition of cell viability and proliferation beyond 1.5 mol% of Al_2O_3 addition [7].

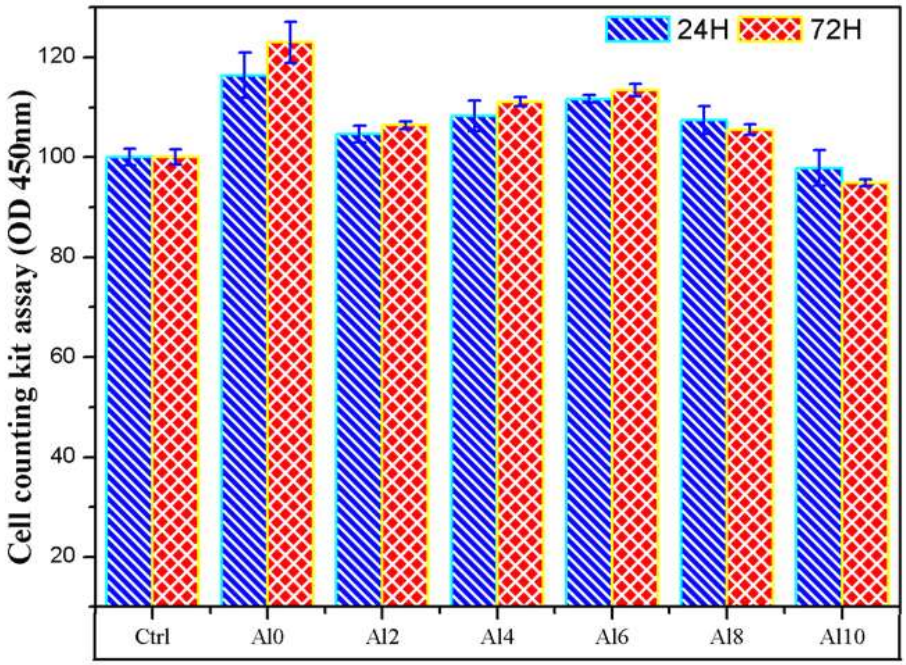

Fig. 5.8 Cytocompatibility and Proliferation analysis of the bioglasses assessed by *rMSCs* cells and CCK-8 method.

Many researchers have reported reduced bioactivity and increased mechanical strength of Al_2O_3 doped silicate and phosphate based bioglasses with increase in content of Al_2O_3 on account of very low dissolution rate of ions and formation of more number of strong P–O–Al covalent bonds with an increase of alumina content in the glass network [5,7,10]. On the contrary with regard to previous research reports on Al_2O_3 doped phosphate glass systems, the present results of zinc-phosphate based glasses containing aluminium confirmed effectively controlled the release of Al^{3+} ions. This leads to enhancement in cell viability and cell proliferation. Out of all glasses, the viability of Al6 (6 mol% Al_2O_3) is significantly high. Moreover, the rate of cell proliferation of Al6 improved after culturing for 72 h. So the material can stimulate the bone growth effectively and these glasses can be suitable for bone repair implants.

3. Conclusions

Aluminium doped phosphate based bioactive glasses were developed using melt quenching method and the influence of Al_2O_3 on structural and bioactivity behaviour of phosphate glasses was investigated for bone regeneration implant applications. The results showed that the density and microhardness, thermal properties (Tg, Tc & Tm) of glass samples increases with increasing Al_2O_3 content due to the strengthening of glass structure by increasing bond strength of P–O–Al ionic linkages. Sample Al10 is showed high mechanical strength among them. The formation of a rich HCA layer on the surface of sample immersed in SBF solution enhanced with incubation time and also with increase in content of Al_2O_3 by up to 6 mol% of alumina and then decreased slightly as confirmed from XRD, FTIR, SEM and EDS, which indicates good bioactivity of as-prepared samples. Besides, bioactivity is also confirmed by a decrease in pH values and controlled dissolution of bioglasses in SBF with increase content of Al_2O_3. Moreover, the HCA layer formed might live longer time on phosphate glasses due to controlled decrease in solubility by the inclusion of alumina. The growth of rMSCs cells on glass samples indicates enhancement in cell viability and cell proliferation. The biocompatibility of Al6 (6 mol% Al_2O_3) is significantly higher compared to remaining glasses. Moreover, it is observed that the rate of cell proliferation of Al6 improved after culturing it for 72 h of all samples A6 showed enhanced bioactivity and high mechanical strength. So this glass sample (6 mol% Al_2O_3) can effectively stimulate bone growth and also can be appropriate for development of bone repair resorbable implants.

References

[1] G. Kaur, P. Sharma, V. Kumar, K. Singh, Assessment of in vitro bioactivity of SiO_2–BaO–ZnO–B_2O_3–Al_2O_3 glasses: An optico-analytical approach, Mater. Sci. Eng. C.32 (2012) 1941–1947.

[2] P.H. Kumar, V.K. Singh, P. Kumar, G. Yadav, R.K. Chaturvedi, Effect of Al_2O_3 on leucite based bioactive glass ceramic composite for dental veneering, Ceram. Int. 42 (2016) 3591–3597.

[3] J.M. Smith, S.P. King, E.R. Barney, J. V. Hanna, R.J. Newport, D.M. Pickup, Structural study of Al_2O_3–Na_2O–CaO–P_2O_5 bioactive glasses as a function of aluminium content, J. Chem. Phys. 138 (2013) 034501.

[4] D. Shi, G. Jiang, X. Wen, In vitro bioactive behavior of hydroxylapatite-coated porous Al_2O_3, J. Biomed. Mater. Res. 53 (2000) 457–466.

[5] A.A. El-Kheshen, F.A. Khaliafa, E.A. Saad, R.L. Elwan, Effect of Al_2O_3 addition on bioactivity, thermal and mechanical properties of some bioactive glasses, Ceram. Int. 34 (2008) 1667–1673.

[6] V.-R. María, R. C. Victoria, S. Antonio J., Glasses with Medical Applications, Eur. J. Inorg. Chem. 2003 (2003) 1029–1042.

[7] H. Tripathi, C. Rath, A.S. Kumar, P.P. Manna, S.P. Singh, Structural, physico-mechanical and in-vitro bioactivity studies on SiO_2–CaO–P_2O_5–SrO–Al_2O_3 bioactive glasses, Mater. Sci. Eng. C. 94 (2019) 279–290.

[8] X. Chatzistavrou, N. Kantiranis, E. Kontonasaki, K. Chrissafis, L. Papadopoulou, P. Koidis, A.R. Boccaccini, K.M. Paraskevopoulos, Thermal analysis and in vitro bioactivity of bioactive glass-alumina composites, Mater. Charact. 62 (2011) 118–129.

[9] M.E. Lines, Can the minimum attenuation of fused silica be significantly reduced by small compositional variations? II. Combined fluorine and alkali metal dopants, J. Non. Cryst. Solids.171 (1994) 219-227.

[10] S.H. Hong, Fabrication and mechanical properties of al-cnt, 2 (2016) 77–81.

[11] L. van Wüllen, G. Tricot, S. Wegner, An advanced NMR protocol for the structural characterization of aluminophosphate glasses, Solid State Nucl. Magn. Reson. 32 (2007) 44–52.

[12] J.M. Egan, R.M. Wenslow, K.T. Mueller, Mapping aluminum/phosphorus connectivities in aluminophosphate glasses, J. Non. Cryst. Solids. 261 (2000) 115–126.

[13] A.M. and B.M. Mujtaba, Effect of Al_2O_3 on Crystallization Behavior and Microstructure of Na_2O–CaO–P_2O_5–SiO_2 Glass-ceramic System, J. Korean Ceram. Soc. 49 (2012) 146–150.

[14] C. Ohtsuki, T. Kokubo, T. Yamauro, Compositional dependence of bioactivity of glasses in the system CaO–SiO_2–Al_2O_3: its in vitro evaluation, J. Mater. Sci. Mater.

Med. 3(1992) 119–125.

[15] U. Gross, V. Strunz, The interface of various glasses and glass ceramics with a bony implantation bed, J. Biomed. Mater. Res. 19 (1985) 251–271.

[16] N. Lahl, K. Singh, L. Singheiser, K. Hilpert, D. Bahadur, Crystallisation kinetics in $AO–Al_2O_3–SiO_2–B_2O_3$ glasses (A=Ba, Ca, Mg), J. Mater. Sci. 35 (2000) 3089–3096.

[17] T. Kokubo, H. Takadama, How useful is SBF in predicting in vivo bone bioactivity?, Biomaterials. 27 (2006) 2907–2915.

[18]. H.-M. Kim, F. Miyaji, T. Nakamura, M. Uchida, T. Kokubo, Bonelike Apatite Formation Induced on Zirconia Gel in a Simulated Body Fluid and Its Modified Solutions, J. Am. Ceram. Soc. 84 (2010) 2041–2044.

[19] V.H. Rao, P.S. Prasad, P.V.Rao, L.F. Santos, N. Veeraiah, Influence of Sb_2O_3 on tellurite based glasses for photonic applications, J.Alloys.Compd. 687 (2016) 898–905.

[20] M. Jemal, I. Khattech, R.O. Omrani, J.J. Videau, S. Krimi, A. El Jazouli, Structural and thermochemical study of $Na_2O–ZnO–P_2O_5$ glasses, J. Non. Cryst. Solids. 390 (2014) 5–12.

[21] H. Liu, Y. Lu, Y. Qu, H. Lu, Y. Yue, Effect of the content of Al_2O_3 on structure and properties of calcium-phosphate glasses: Two experimental case studies, J. Non. Cryst. Solids. 450 (2016) 95–102.

[22] P. Anigrahawati, M.R. Sahar, S.K. Ghoshal, Influence of Fe_3O_4 nanoparticles on structural, optical and magnetic properties of erbium doped zinc phosphate glass, Mater. Chem. Phys. 155 (2015) 155–161.

[23] S.N. Salama, H.A. El-Batal, Microhardness of phosphate glasses, J. Non. Cryst. Solids. 168 (1994) 179–185.

[24]. AA. El-Kheshen, FA. Khaliafa, EA. Saad, Effect of Al2O3 addition on bioactivity, thermal and mechanical properties of some bioactive glasses. *Ceram. Int.* 34(7) (2008) 1667-1673.

[25] Hongting Liu, Yadong Lu, Ya Qu, Hao Lu, Yunlong Yue, Effect of the content of Al_2O_3 on structure and properties of calcium-phosphate glasses: Two experimental case studies, Journal of Non-Crystalline Solids 450 (2016) 95–102.

[26] Brow RK. Nature of Alumina in Phosphate Glass: I, Properties of Sodium Aluminophosphate Glass. J.Am.Cer.Soc, 76(4) (1993) 913-918.

[27] Tiwari B, Dixit A, Kothiyal GP, et al. Preparation and characterization of phosphate glasses containg titanium. *Barc Newsletter*, 285 (2007):167-173

[28] J. Schneider, S.L. Oliveira, L.A.O. Nunes, A.F. Bonk, H. Panepucci†, Short-range structure and cation bonding in calcium−aluminum metaphosphate glasses, Inorg. Chem. 44 (2005) 423–430.

[29] J. Tsuchida, J. Schneider, M.T. Rinke, H. Eckert, Structure of ternary aluminum metaphosphate glasses, J. Phys. Chem. C 115 (2011) 21927–2194.

[30] X. Chatzistavrou, N. Kantiranis, E. Kontonasaki, K. Chrissafis, L. Papadopoulou, P.Koidis, A. R. Boccaccini, M. K. Paraskevopoulos, Thermal analysis and in vitro bioactivity of bioactive glass–alumina composites, Materials Characterization 62 (2011) 118–129.

[31] M. Ashok, N. Meenakshi Sundaram, S. Narayana Kalkura, Crystallization of hydroxyapatite at physiological temperature, Mater. Lett. 57 (2003) 2066–2070.

[32] R.K. Singh, G.P. Kothiyal, A. Srinivasan, In vitro evaluation of bioactivity of CaO–SiO_2–P_2O_5–Na_2O–Fe_2O_3 glasses, Appl. Surf. Sci. 255 (2009) 6827–6831.

[33] C.V.B.E. Vern, P. Appendino, Macroporous bioactive glass-ceramic scaffolds for tissue engineering, 17 (2006) 1069–1078.

[34] R.K. Brow, Nature of Alumina in Phosphate Glass: I, Properties of Sodium Aluminophosphate Glass, J. Am. Ceram. Soc. 76 (1993) 913-918.

[35] R. Abd-allah, Chemical cleaning of soiled deposits and encrustations on archaeological glass : A diagnostic and practical study, J. Cultural Heritage.14 (2013) 97–108.

[36] H.A. Elbatal, M.A. Azooz, E.M.A. Khalil, A.S. Monem, Y.M. Hamdy, Characterization of some bioglass – ceramics, J. Mate. Chem. Phy. 80 (2003) 599–609.

[37] M.Yamaguchi, B. Resorption, Role of Zinc in Bone Formation and Bone Resorption, J.Trace Elements in Experimental Medicine, 135 (1998) 119–135.

[38] G. Perozzi, C. Murgia, C. Lang, M. Leong, P. Zalewski, D. Knight, R. Ruffin, L.-W. Tan, Anti-inflammatory effects of zinc and alterations in zinc transporter mRNA in mouse models of allergic inflammation, Am. J. Physiol. Cell. Mol. Physiol. 292 (2006) L577–L584.

[39] H.S. Liu, T.S. Chin, S.W. Yung, FTIR and XPS studies of low-melting PbO–ZnO–P_2O_5 glasses, Mater. Chem. Phys. 50 (1997) 1–10.

[40] P.Y. Shih, S.W. Yung, T.S. Chin, FTIR and XPS studies of P_2O_5–Na_2O–CuO glasses, J. Non. Cryst. Solids. 244 (1999) 211–222.

[41] C. Ohtsuki, T. Kokubo, T. Yamamuro, Mechanism of apatite formation on CaO–SiO_2–P_2O_5 glasses in a simulated body fluid, J. Non. Cryst. Solids. 143 (1992) 84–92.

[42] A. Kiani, J. V. Hanna, S.P. King, G.J. Rees, M.E. Smith, N. Roohpour, V. Salih, J.C. Knowles, Structural characterization and physical properties of P_2O_5–CaO–Na_2O–TiO_2 glasses by Fourier transform infrared, Raman and solid-state magic angle spinning nuclear magnetic resonance spectroscopies, Acta Biomater. 8 (2012) 333–340.

[43] F.H. ElBatal, Y.M. Hamdy, S.Y. Marzouk, Gamma ray interactions with V_2O_5-doped sodium phosphate glasses, Mater. Chem. Phys. 112 (2008) 991–1000.

[44] M.R.T. Filgueiras, G. La Torre, L.L. Hench, Solution effects on the surface reactions of three bioactive glass compositions, J. Biomed. Mater. Res. 27 (1993) 1485–1493.

[45] O.P. Filho, G.P. Latorre, L.L. Hench, Effect of crystallization on apatite-layer formation of bioactive glass 45S5, J. Biomed. Mater. Res. 30 (1996) 509–514.

[46] L. Radev, V. Hristov, I. Michailova, H. Fernandes, M. Salvado, In vitro bioactivity of biphasic calcium phosphate silicate glass-ceramic in $CaO–SiO_2–P_2O_5$ system, Process. Appl. Ceram. 4 (2013) 15–24.

[47] I.R. Gibson, I. Rehman, S.M. Best, W. Bonfield, Characterization of the transformation from calcium-deficient apatite to β-tricalcium phosphate, J. Mater. Sci. Mater. Med. 11 (2000) 533–539.

[48] E. Vernè, S. Di Nunzio, M. Bosetti, P. Appendino, C. Vitale Brovarone, G. Maina, M. Cannas, Surface characterization of silver-doped bioactive glass, Biomaterials. 26 (2005) 5111–5119.

[49] A. Belkébir, J. Rocha, A.P. Esculcas, P. Berthet, B. Gilbert, Z. Gabelica, G. Llabres, F. Wijzen, A. Rulmont, Structural characterisation of glassy phases in the system $Na_2O–Al_2O_3–P_2O_5$ by MAS and solution NMR, EXAFS and vibrational spectroscopy, Spectrochim. Acta - Part A Mol. Biomol. Spectrosc. 55 (1999) 1323–1336.

[50] D. Zhao, W. Huang, M.N. Rahaman, D.E. Day, D. Wang, Mechanism for converting Al_2O_3-containing borate glass to hydroxyapatite in aqueous phosphate solution, Acta Biomater. 5 (2009) 1265–1273.

[51] A. Oki, B. Parveen, S. Hossain, S. Adeniji, H. Donahue, Preparation and in vitro bioactivity of zinc containing sol-gel-derived bioglass materials, J. Biomed. Mater. Res. - Part A. 69 (2004) 216–221.

[52] L.L. Hench, D.E. Clark, Physical Chemistry Of Glass Surfaces, J.Non-Cryst. Soli. 28 (1978) 83–105.

[53] A. Balamurugan, G. Balossier, S. Kannan, J. Michel, A.H.S. Rebelo, J.M.F. Ferreira, Development and in vitro characterization of sol-gel derived $CaO–P_2O_5–SiO_2–ZnO$ bioglass, Acta Biomater. 3 (2007) 255–262.

[54] T. Kokubo, S. Ito, Z.T. Huang, T. Hayashi, S. Sakka, T. Kitsugi, T. Yamamuro, Ca,P-rich layer formed on high-strength bioactive glass-ceramic A-W, J Biomed Mater Res. 24 (1990) 331–343.

Chapter - 6

In vitro bioactivity, antibacterial activity and functionality of zirconia doped zinc phosphate bioglasses for application in dental and orthopedics

This chapter has systematically studied the structural aspects of $ZnO–Na_2O–CaO–P_2O_5$ glas$_s$ matrix with Zr^{4+} ions. In this chapter physical properties of density, molar volume, micro hardness and in vitro bioactivity of the matrix immersed in SBF solution for several of 3, 7, 14, and 21days, further were tested pH variation as well as degradation rates, are also discussed. Then structural analysis done with the help of X-ray Diffraction SEM-EDS, FTIR-Spectroscopy, TG-DTA and Biological studies on cell cytocompatibility and antimicrobial of results are briefly detailed in this chapter.

6.1 Introduction

Zirconium containing glasses and glass ceramics have been identified as prospective bioactive materials for use in dental and orthopaedic implant applications [1-3]. The first bioactive glass was formulated as 45S5 by Prof. Larry Hench in 1969 and is used successfully in many clinical applications such as bone defect repair, regeneration of new bone, bone filler materials, dental, and orthopaedic implants [4-6]. These aforementioned potential applications of bioglasses are possible only because of their exceptional properties like biocompatibility, bioactivity, osteoconductivity, antibacterial, and angiogenesis etc., [2,3]. The uniqueness of the bioglasses is to form new bone bond with living tissues, when it comes to physical contact as a biological response. The chemical bond formed or interface is nothing but biologically active apatite known as hydroxyl carbonate apatite (HCA). This apatite layer ties strongly the implant material and host tissue chemically [4,7]. A variety of oxide based bioglasses, such as SiO_2, B_2O_3 and P_2O_5 etc., are available. Out of which P_2O_5 based bioactive glasses have been attracted significant attention as materials to be used in the field of tissue engineering, because of high bioactivity, easily dissolvable nature and low mechanical strength. Moreover phosphate enters glass network as PO_4 structural units. However, these phosphate based bioactive glasses are not suitable for load bearing applications due to poor mechanical strength and low fracture toughness and high degradation rate, which might be ascribed to high amorphous nature of the glasses [4]. It is a well-known fact that improved bioactivity and other functional properties of the bioglasses can be achieved by choosing the initial composition and incorporation of other oxide materials to host composition [4-6]. Additionally, several therapeutically active ions such as zinc, titanium, strontium, zirconia, cobalt, fluoride and magnesia etc., have been included by incorporating them into various glass systems to improve bioactivity along with functionality. Nevertheless, zirconia incorporation in bioglasses have attracted many researchers because of its special features which are functionality most suited in the fields of orthopaedic and dentistry [8].

The addition of zirconia (ZrO_2) to phosphate glass network can enhance bioactivity along with mechanical strength. ZrO_2 enters glass network in the form of ZrO_6 octahedra structural units and forms Zr–O–Si and Zr–O–P covalent bonds in silica and phosphate glass networks respectively, in order to reinforce glass network [9,10]. Zirconium oxide exists mainly in three crystalline phase structures; monoclinic phase (m-ZrO_2), tetragonal phase (t-ZrO_2) and cubic phase (c-ZrO_2), and their structural stability depends on the temperature. Based on the stability, the mechanical properties also alter. The tetragonal phase of ZrO_2 ensures a stable structure at a high temperature of around 1170–2370 ^{o}C with good

mechanical strength in comparison with other two crystalline phases. The stabilization of tetragonal phase at room temperature can also be attained by adding metal oxides like CaO, MgO, Na_2O, CeO_2 and Y_2O_3 etc., in order to fabricate high strength implants [11-13]**.** Along with these extraordinary mechanical properties, zirconia doped bioglasses showed good biological properties. Zirconia is a biocompatible and bioinert ceramic material. It is unable to form any direct bond with bone or show any osteoconduction environment. Significantly small amounts of zirconia might reduce the rate of crystallization or enhance the amorphous microstructure, which leads to increase in degradation and that makes bioglass as more bioactive [10]. Glasses containing zirconia can't induce cytotoxicity side effects with soft and hard tissues and it also displays favourable antibacterial effects. Moreover, it does not release any harmful constituents in the human body during dissolution processes. This is also confirmed by the earlier reports related to *in vitro* and *in vivo* toxicity tests [8,14,15]. Besides having good biological properties, zirconia based glasses and glass ceramics also have the mechanical properties of them almost close to those of strong metals and alloys such as stainless steel etc., [16]. Zirconia based ceramics are being used in place of titanium and alumina based implants in orthopaedic and dentistry due to their comparable mechanical strength and nontoxic behaviour, titanium implants showed some cytotoxicity effect on tissues. Because of these superior qualities, Zirconia based glasses and glass ceramics are considered as ideal choice of material for development of biomedical implants for orthopaedic and dentistry [8]. D.G. Wang et al., studied the influence of ZnO and ZrO_2 on structure, mechanical properties, degradability and *in vitro* bioactivity of wollastonite and they also developed and characterized $MgO–CaO–SiO_2–P_2O_5–CaF_2$ bioactive glass-ceramics doped with ZrO_2 [17,18]. Ting Lei et al., investigated the effect of small amounts of ZrO_2 on the dissolution behaviour, pH variation, and in vitro bioactivity along with mechanical properties of $CaO–P_2O_5–SiO_2–SrO$ glass system by sol-gel method, and they found enhanced bioactivity and controlled dissolution [19]. V. K. Marghussian et al., developed $CaO–TiO_2–P_2O_5$ micro porous glass-ceramic by adding zirconia and also observed the improvement in chemical durability and mechanical strength in the presence of ZrO_2 [20]. Jin cheng Du et al., discussed the effect of ZrO_2 on the local environment and medium-range structure of the soda-lime silicate glasses by using molecular dynamics simulation method by means of pair distribution function and bond angle distribution calculations [9]. V. Rajendran et al., fabricated $P_2O_5–Na_2O–CaO–ZrO_2$ glasses by varying of ZrO_2 contents upto1.0 mol% in place of Na_2O and they pointed out that 0.75 mol% of ZrO_2 containg glass displaying higher bioactivity and good mechanical strength out of other compositions [21]. The aforementioned

studies are related to ZrO_2 incorporated high silica based bioglasses and glass ceramics [9,17-20]. Most of the researchers have looked at structural, mechanical and bioactivity of SiO_2 based bioglasses influenced by zirconia content and the research reports revealed that, mechanical properties enhance tremendously and bioactivity decreases with increase in ZrO_2 content.

However, very few reports are available on zirconia contain P_2O_5 based bioglasses and glass ceramics [20,21]. Moreover, there is no unblemished and ample evidence about the impact of Zr^{4+} ions in the phosphate glass structure, which leads to modify the degradation rate, bioactivity, mechanical strength cell proliferation and antibacterial activity of bioglasses used for tissue engineering applications. In view of such lack of information about the effect of zirconia on phosphate network and their applications, we made an attempt to explore these gaps by choosing a novel zinc phosphate bioglass system by the inclusion of small amounts of ZrO_2 without compromising the mechanical strength on rate of bioactivity.

In the present study, we have reported in detail about the HAp layer formation, cytocompatibility, rMSCs proliferation, antibacterial activity against three strains *E.coli*, *S.aureus* and *P. Aeruginosa* and structural and mechanical properties altered by the addition of small amounts of zirconia and also the suitability of as-developed glasses for dental and orthopaedic implant applications.

6.2 Results and Discussions

6.2.1 Physical parameters

The structural changes that occurred by the inclusion of metal oxides to bioglasses can be studied by measuring physical parameters like density, molar volume, oxygen packing density and oxygen molar volume of the as-prepared glasses. The values of various physical parameters are presented in Table 6.1. From Fig. 6.1(a) & (b) the density and molar volume of as-prepared ZrO_2 doped bioglasses showed opposite behavior. It is clearly noticed that, the density of glasses increases from 2.569 to 2.588 gcm^{-3}, while molar volume decreases from 38.496 to 38.389 cm^3 /mol with increase in the content of ZrO_2 (0.1 to 0.7 mol%). Likewise, with the addition of ZrO_2, oxygen packing density appeared to increase from 73.772 to 74.148, while the oxygen molar volume of the glasses decreased from 24.365 to 24.194 cm^3/mol. This increase in density and decrease in volume with the addition of zirconia in place of CaO at constant mol% of Na_2O, ZnO, and P_2O_5 is attributed to the formation of terminal oxygen by demolishing P–O–P bonds. Consequently, Zr^{4+} ions are interconnected to

PO_4 tetrahedral by non-bridging oxygen (NBOs). In other words the establishment of ionic cross-linking between NBOs of two different chains may lead to glass structure reinforcement [3,21].

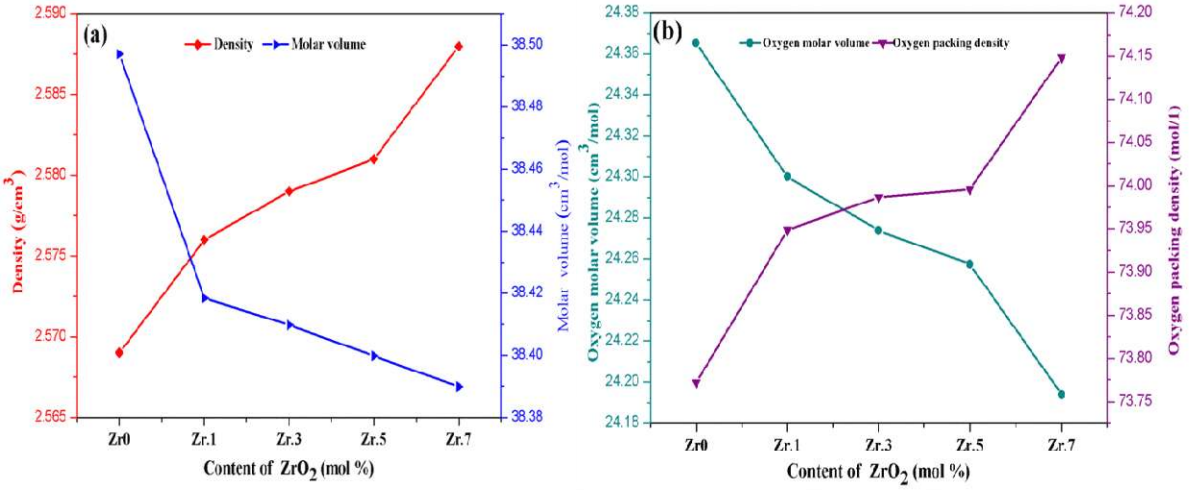

Fig. 6.1 Variation of physical parameters (a) Density, Molar volume, (b) Oxygen molar volume and oxygen packing density as a function of ZrO_2 (mol%) content.

Table 6.1 Physical and mechanical parameters of the ZrO_2 doped bioglasses

Sample code	Molar mass(M) (g/mol)	Molar volume (Vm) (cm^3/mo)	Density (ρ_g) (g/cm^3)	Oxygen molar volume (Vo) (cm^3/mol)	Oxygen packing density (OPD) (mol/1)	Vickers hardness Hv (GPa)	Fracture toughness K_{IC} (MPa $m^{1/2}$)
Zr0	98.898	38.496	2.569	24.365	73.772	3.19 (±0.0921)	0.251
Zr.1	98.965	38.418	2.576	24.300	73.948	3.42 (±0.1001)	0.259
Zr.3	99.101	38.409	2.579	24.274	73.986	3.60 (±0.1088)	0.262
Zr.5	99.234	38.399	2.581	24.257	73.995	3.75 (±0.0895)	0.273
Zr.7	99.368	38.389	2.588	24.194	74.148	3.95 (±0.0807)	0.313

6.2.2 Microhardness and Fracture toughness

The variation of vickers microhardness and fracture toughness as a function of ZrO_2 content of zinc phosphate bioglasses are shown in Fig. 6.2 (a) & (b) and the related values are summarised in Table 6.1. The values of Vickers microhardness and fracture toughness increased gradually from 3.42 (±0.1001) to 3.95 (±0.0807) GPa and from 0.259 to 0.313 (MPa $m^{1/2}$) respectively, with increasing the ZrO_2 content in the glass network. It is clearly noticed that, there is considerable increment in the microhardness and fracture toughness

values, when compared with Zirconia free bioglasses [26,27]. The optical microscopic images of Vickers indentation impressions of Zr.1, Zr.3, Zr.5, and Zr.7 glasses are illustrated in Fig. 6.2(c).

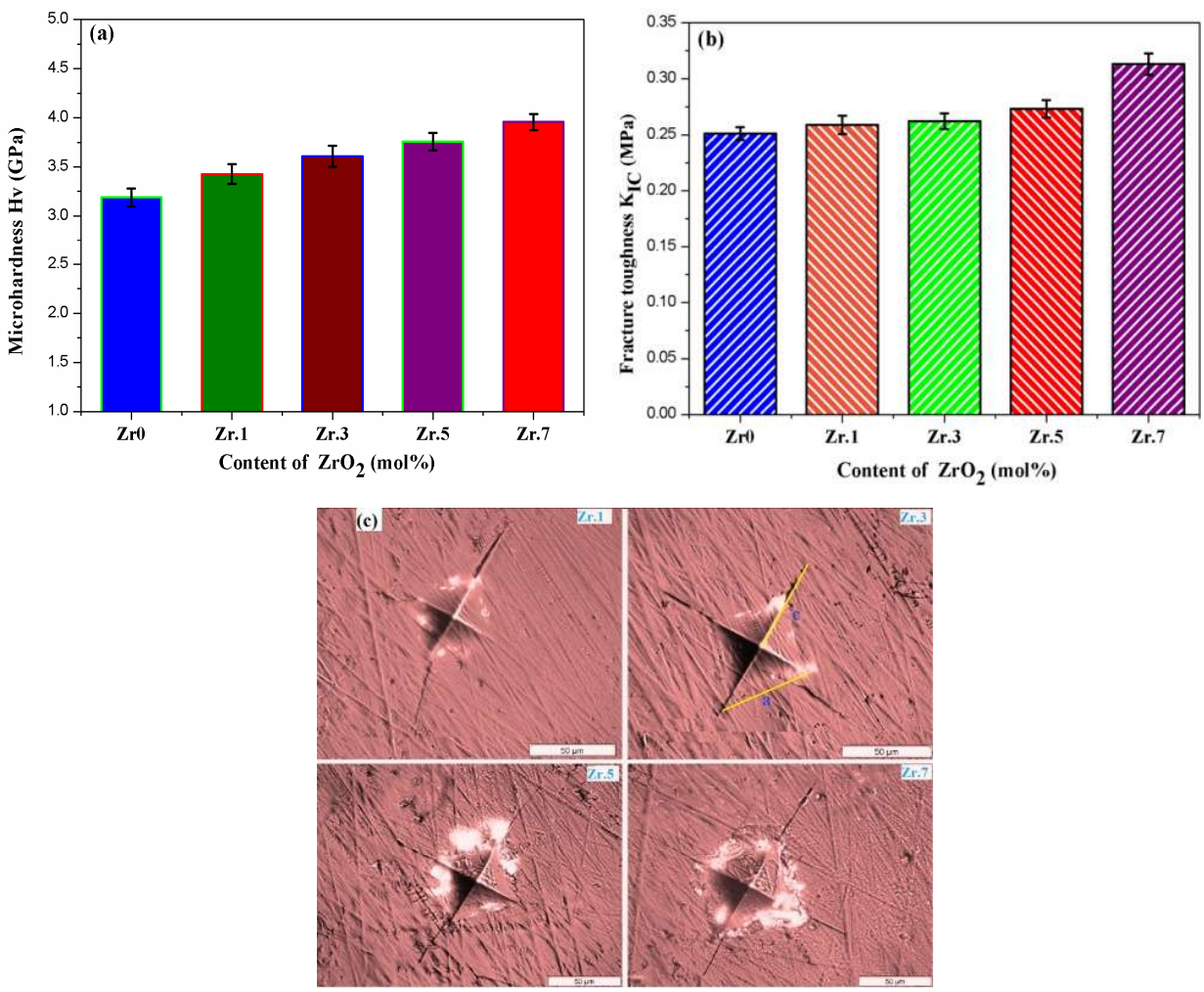

Fig. 6.2 Mechanical parameters as a function of ZrO_2 (mol%) concentration, (a) Micro hardness vs ZrO_2 (mol%) (b) Fracture toughness vs ZrO_2 (mol%) and (c) Optical images of vickers indentation for Zr.1, Zr.3, Zr.5 and Zr.7 glass samples.

The fracture toughness of bioglasses are calculated using Hv values and from measuring the crack length from optical microscopic Vickers indent impressions of the samples. A significant enhancement in hardness values with ZrO_2 content is due to the establishment of new P–O–Zr bonds by breaking P–O–P bonds, which leads to densification of phosphate glass network [21]. In other words, with increase in the amount of ZrO_2, during the heating process, the ions present in the precursors attracted by Zr^{4+} might be devitrified in complex and dense glassy network, which leads to decrease in porosity and strengthen the glass network [3].

6.2.3 Thermal properties

The results of thermal analyses (DTA) are shown in Fig. 6.3 and Table 6.2. The temperature values Tg, Tc, and Tm of ZrO_2 doped glass samples are summarized in Table 6.2. The values of glass transition temperature (Tg) from 262.211 to 301.156 ^oC, crystallization temperature (Tc) from 335.675 to 386.324 ^oC and melting temperature (Tm) from 672.676 to 697.495 ^oC increases with increase in content of ZrO_2 from 0.1 to 0.7 mol%. The increase in Tg with an increase of ZrO_2 from 0.1 to 0.7 mol% is due to an increase in the average crosslink density through non-bridging oxygen ions (NBO) and the number of bonds per unit volume. In addition, increase in Tg can also be due to the increasing aggregation effect of ZrO_2 on the glass network and slow mobility of large Zr^{4+} ions, which lead to more rigidity of the glass network. The exothermic Tc and endothermic Tm peaks are also increase gradually with the addition of ZrO_2 (of Zr^{+4} ions (0.72 A˚)). Furthermore, there is a rising glass viscosity with increasing ZrO_2, through the reduction of non-bridging oxides and/or high ionic field strength [1,15,3].

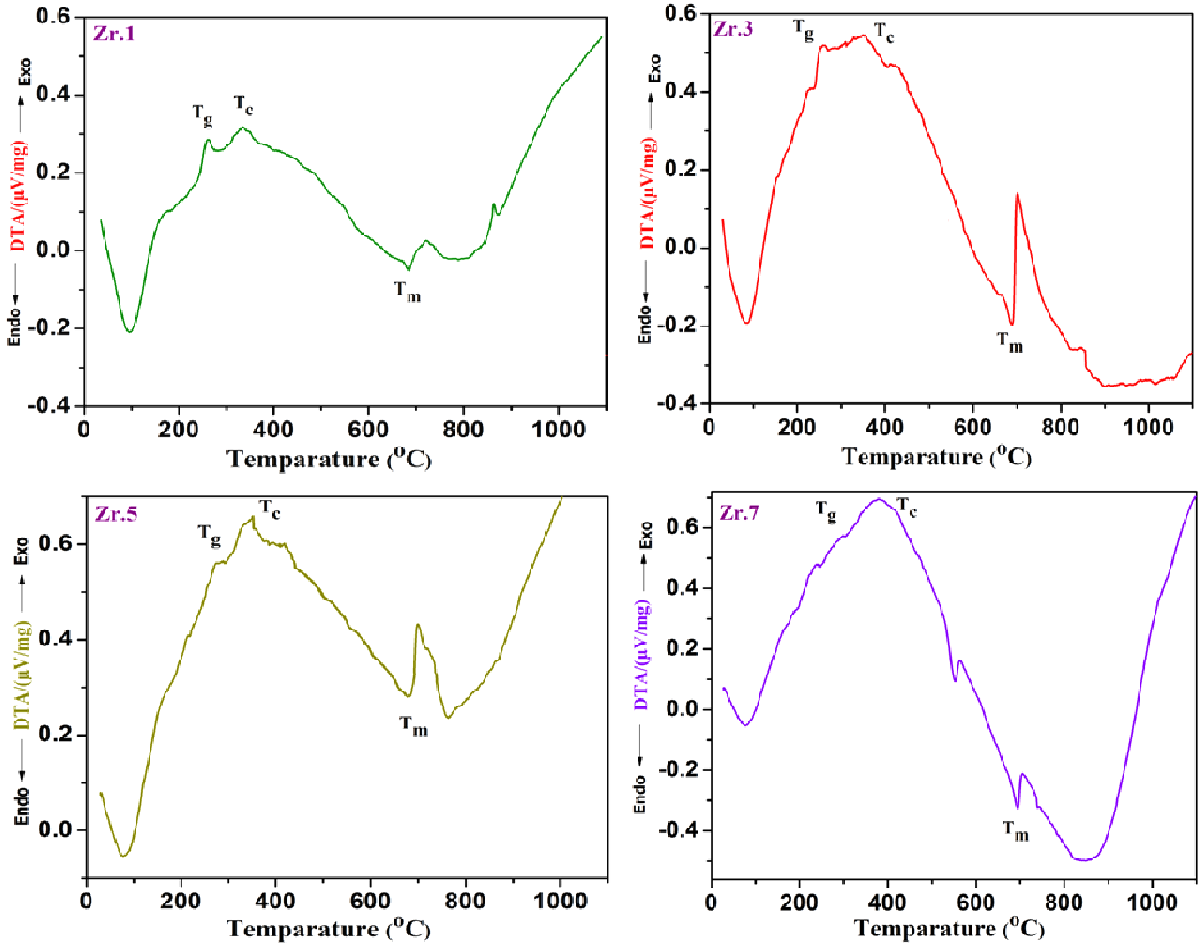

Fig. 6.3. DTA-TGA analysis curves of ZrO_2 doped bioglasses

Table 6.2 Thermal properties of the ZrO_2 containg bioglasses

Sample code	Tg (^oC)	Tc (^oC)	Tm (^oC)	ΔT (^oC)	K_H
Zr.1	262.211	335.675	672.676	73.465	0.220
Zr.3	271.102	349.210	686.926	78.108	0.231
Zr.5	280.404	362.875	691.843	82.471	0.250
Zr.7	301.156	386.324	697.495	85.168	0.273

In the current ZrO_2 doped glasses, the glass stability (ΔT) values increases, from 73.465 °C to 85.168 °C and Hruby criterion (H) increases from 0.220 to 0.273 with the content of ZrO_2, which undoubtedly designates the high stability and the good glass-forming tendency of as-prepared glasses. The abstained results confirming the structure formation and thermal stability of the zirconia incorporated bioglasses.

6.3 *In vitro* HAp layer conformation

6.3.1 X-ray diffraction (XRD) analysis

Fig. 6.4 illustrates XRD traces of all bioactive glass samples before and after immersion in SBF solution for various time intervals (0, 3, 7, 14 and 21days). A clear broad hump is detected between 20-35° (2θ) of XRD patterns before incubation in SBF. It indicates the amorphous nature of the as-synthesized glass samples and is shown in Fig. 6.4(a). Moreover, addition of zirconia could not create any crystalline signals in the homogeneous phosphate glass network [28]. The in vitro bioactivity of bioglass samples post-immersed in SBF solution for 3, 7, 14, and 21 days are shown in Fig. 6.4(b, c, d, e). The presence of crystalline peaks in XRD traces confirms the development of microstructure hydroxyapatite ($Ca_{10}(PO_4)_6(OH)_2$) layer on glass surfaces [22,29]. This is evident from the peaks observed at diffracted angles (2θ): 10.83^o, 15.27^o, 21.73^o, 22.82^o, 25.86^o, 27.56^o, 31.75^o, 40.69^o, 45.32^o, 56.28^o, 66.35^o and 75.56^o corresponding to the reflections 110, 021, 200, 111, 002, 112, 211, 221, 203, 500, 143 and 215 respectively. These intense crystalline peaks of the XRD pattern were indexed using JCPDS card No: *72-1243, @40-0008, ◈76-0694. It is detected that incubation time plays a crucial role to enhance HAp layer formation on bioglass surfaces based on ratios of calcium and phosphate, when compared with the initial phase [22,30,31]. After 3 days of immersion (Fig. 6.4b), the appearance of new strong peaks at 31.74^o (211) and 45.32^o (203) in the XRD patterns indicates the development of crystalline phases of calcium phosphate hydroxide (HAp) [32].

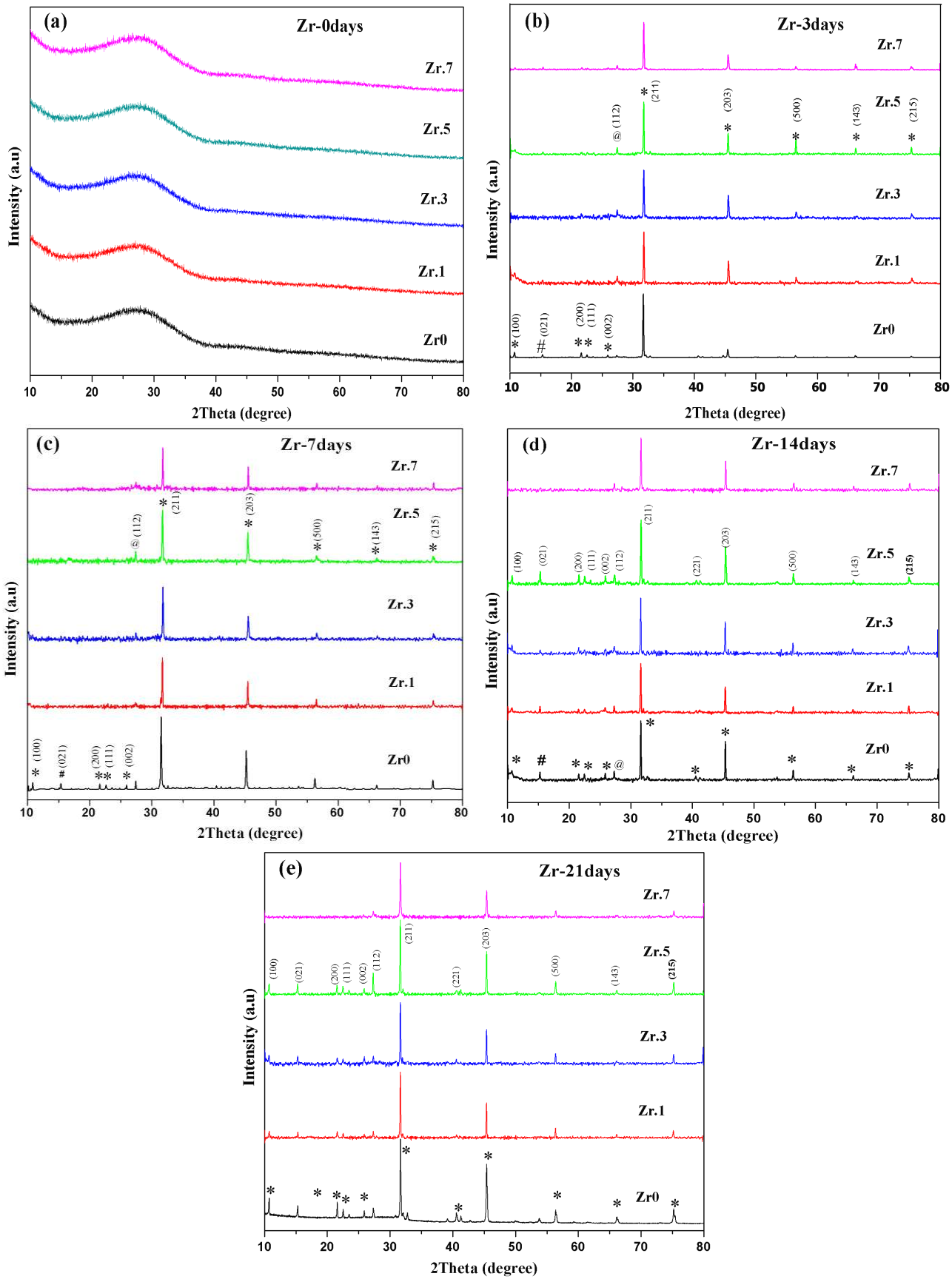

Fig. 6.4 XRD patterns of the bioglasses before and after immersion in SBF solution for different (**a**-0days, **b**-3days, **c**-7days, **d**-14days and **e**-21days) time intervals.

Further, increasing the incubation time for 7, 14 and 21days, entering of additions peaks along with the prominent intense peaks presented during 3days of incubation is observed. It is found that, all the reflections related to HAp increase with the incubation time. In addition the intensities of reflections increase with the content of ZrO_2 from 0.1 mol% to 0.5 mol% and then decreases further increase in the concentration of zirconia (for 0.7 mol%) in the glass network after immersion, shown clearly in Fig. 6.4(b,c,d,e). The formation of calcium phosphate layer attributed to ions leaching from the bioglass to SBF solution and this ion leaching is more prone towards amorphous glass structure than the crystalline structure [33]. This is the added advantage of the glasses to possess high bioactivity. Montezarian et al.,[34] Observed that, the substitution of ZrO_2 in replacement of CaO might enhance the density of Zr^{4+} ions near the $[PO_4]^{3-}$ units. Due to this formation of the glass network increases in the form of ZrO_4 structural units [19]

In the present system of as–prepared bioglasses follows the same trend with the addition of ZrO_2 to the base glass, which results in reducing the crystallization affinity in the glass network. This confirms the chosen zirconia doped phosphate bioglasses have great capacity to form HAp layer. Further, these obtained XRD results are verified and supported in detail by the FTIR and SEM-EDS analysis.

6.3.2 FTIR spectroscopy analysis

Fig. 6.5 designates the structural properties of bioglasses assessed using FTIR spectra before and after immersion for various time periods (0, 3, 7, 14 and 21 days) and corresponding various absorption bonds are summarised in Table 6.3. From Fig. 6.5(a) it is observed that various absorption band intensities of all glass samples as a function of wave number are noticed at ~506, 749, 910, 986, and 1066, 1269, 1640, 2364, and 3349 cm^{-1}. These are in accordance with the available previous FTIR spectroscopic studies available on phosphate-based glasses. The absorption band at 506 cm^{-1} can be assigned by P–O bending amorphous while at 749 $cm^{-1,}$ it is due to symmetric stretching of P–O–P bridges [35,36]. The intensity peaks at 910 and 986 cm^{-1} are ascribed to asymmetrical stretching υ_{as}(P–O–P) bonds (Q^2 phosphate units), and while the other shifts to higher shoulder centred peak at 986 cm^{-1} are due to symmetrical stretching $\upsilon_s(PO_3)^{2-}$ in Q^1 units, respectively [37,38]. Around 1066 cm^{-1} the band is assigned by asymmetric stretching vibration of the meta phosphate group $\upsilon_{as}(PO_3)$. Here, band at ~1269 cm^{-1} is ascribed to asymmetric stretching vibration of O–P–O groups (Q^2 phosphate tetrahedron) [39-41]. At the absorption bands, 1640 cm^{-1} is ascribed due to P–O–H water molecule. The weak band at 2364 cm^{-1} is due to various construction sites of P–O–H

group vibration or attributed to stretching of CO_2 [42-44]. The broad intensity peak at 3449 cm^{-1} is ascribed to O–H symmetric stretching groups [40]. From Fig. 6.5, we have observed in all glass samples that band intensity is slightly increased along with increase in Zirconium content [42]. After immersion of glasses for 3, 7, 14 and 21days in SBF solution, an additional prominent absorption bands representing hydroxyapatite layer (556 to 560, 664, 734 to 739, 914 to 920, 1114 to 1120, 1274, 1290 cm^{-1}), carbonate (C) and hydroxyl (OH) groups (1404–1406, 1460, 1552, 1636–1641, 1650, 2096, 2850, 2928–2930, 3230, 3410–3426 cm^{-1}) are emerged along with the fore mentioned bands in untreated glass samples as shown in Fig. 6.5(b,c,d,e). The bands are concentrated at 556–560 cm^{-1}, 664 cm^{-1} and shift towards higher wavenumber with immersion time ascribed to P–O bending vibrations of apatite PO_4^{3-} tetrahedral [45]. The absorption peak in the range of 734 to 739 cm^{-1} can be assigned to the symmetric stretching υ_s(P–O–P) mode [35,37,38,46]. This is a good sign of establishment of pyrophosphate units in the glass network? The spectral bands between 914–920 cm^{-1} are attributed to asymmetric stretching mode of P–O–P linkages [41,44,47]. A broad peak noticed at 1116 to 1120 cm^{-1} is attributed to asymmetric stretching mode of $(PO_3)^{2-}$ in Q^1 units. The presence of broad peaks in FTIR spectra is associated with the formation (α-$Ca_2P_2O_7$) of Hydroxy apatite [21,35,37]. The characteristic phosphate group representing absorption bands in the range 1274 $cm^{-1}$is assigned due to asymmetric stretching modes of O–P–O linkages or $\upsilon_{as}(PO_2)$ units of two nonbridging oxygen atoms [35,41]. The band at around ~1290 cm^{-1} is due to initiating from HPO_4 group [48]. New significant hydroxy apatite bands are evolved after 7, 14 and 21days of incubation of glasses in SBF solution shown in Fig. 6.5(c,d,e). The weak absorption peak at 1460 cm^{-1} is split into two peaks (1404 to 1406 cm^{-1} B-type and 1460 cm^{-1} A-type) and the peak intensities increase with increase in immersion time and increase in the content of ZrO_2,which may be attributed to stretching vibration mode of carbonate (C–O) group. From the characteristic wave numbers of ~1406, 1460 cm^{-1} confirmed by related to A-type and B-type CHA [45]. In addition, the specific bands of C–O resonance of CO_3^{2-} are located at 1552 cm^{-1}, which endorses the occurrence of A-type HCA layer (hydroxyl is substituted by carbonate group) [49]. The intensity peak at 1636–1650 cm^{-1} and a broad band between 3230–3410 cm^{-1} are attributed to symmetric stretching of O–H groups (instigated by absorbing water molecules) [42,50].

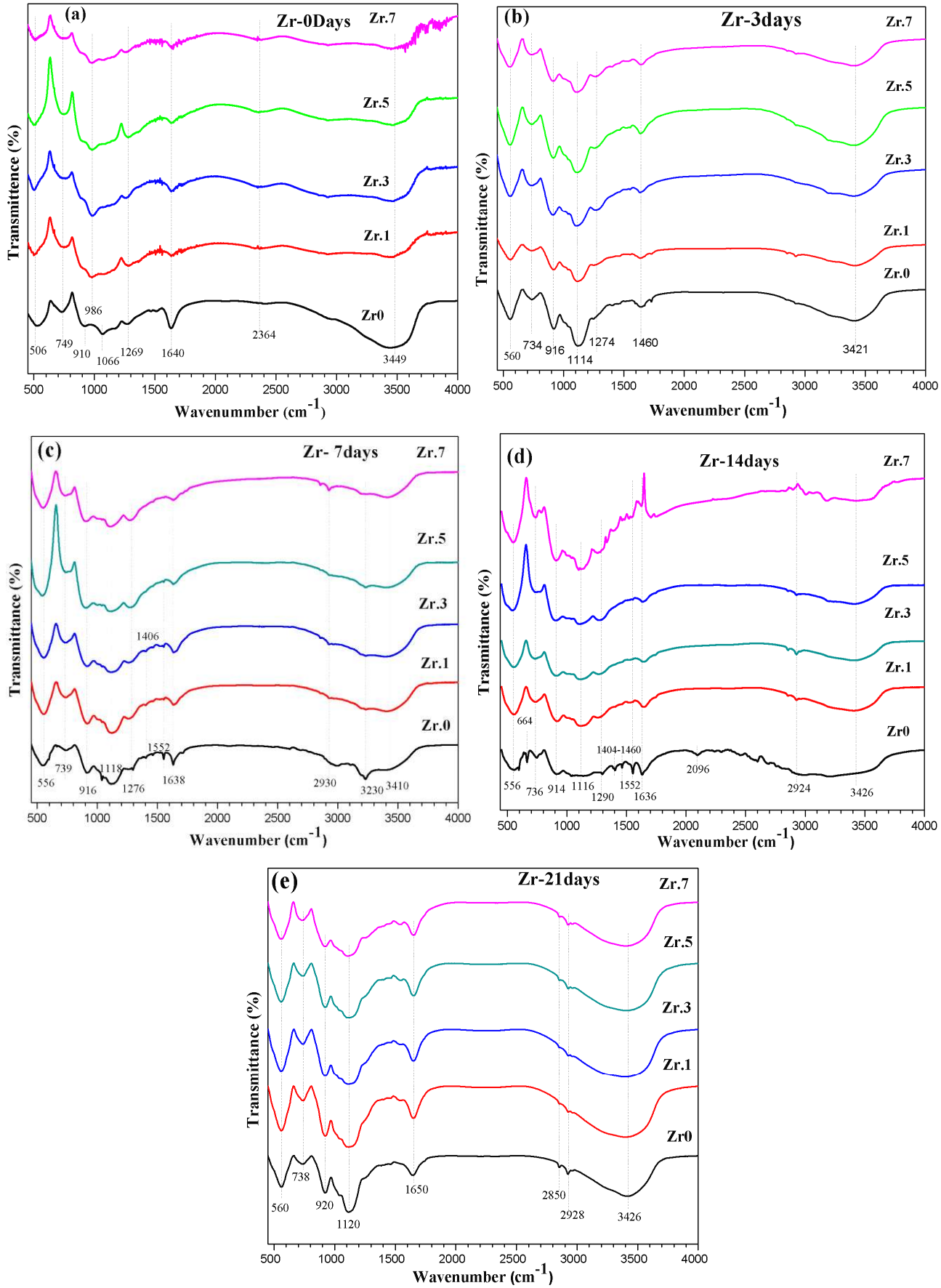

Fig. 6.5 FTIR spectra of bioglass samples before and after immersion in SBF solution for different time periods: (a) 0 days, (b) 3 days, (c) 7 days, (d) 14 days and (e) 21 days.

The absorption bands observed at 2096 cm^{-1} show characteristic peaks of –OH group (Dumas and Miller 2003) and the bands noticed at 2850–2930 cm^{-1} are assigned to the C–H stretching vibrations [44,51]. The appearance of PO_3^{2-}, CO_3^{2-} and OH groups in FTIR spectra of all as-synthesized bioglasses confirm the development of rich crystalline HCA layer. Ping Yin et al., [19] and N. Veeraiah et al., [3] reported that increase in ZrO_2 content might reduce the rate of formation of HAp layer formation. Contrary to earlier available reports, in the present system of glasses, apatite layer formation is found to be enhanced with increase in content of ZrO_2 and also with immersion time. The FTIR results are in good agreement with XRD analysis (shown in section 6.3.2).

Table 6.3 FTIR Spectroscopic absorption bands of Zirconia doped bioglasses

FTIR Spectroscopy absorption bonds of bioglass samples before and after immersion in SBF (cm^{-1}).						
0days	**3days**	**7days**	**14days**	**21days**	**Assignments**	**References**
506	560	556	556	560	~506 P–O amorphous	[36,37]
					556–560 HAp PO_4^{3-}	[46]
--	--	--	664	--	Apatite PO_4^3 tetrahedral	[46]
749	734	739	736	738	υ_s(P–O–P) bridges	[36,38,39,47]
910	916	916	914	920	υ_{as}(P–O–P) (Q^2 units).	[42,45,48]
986	--	--	--	--	υ_s $(PO_3)^{2-}$ in a Q^1units	[38,40]
1066	--	--	--	--	$\upsilon_{as}(PO_3)$ group	[40]
--	1114	1118	1116	1120	υ_{as} $(PO_3)^{2-}$ in Q^1 units	[22,36,38]
1269	1274	1276	1290	--	$\upsilon_{as}(PO_2)$ units (NBOs)/	[36,40-42]
					~1290 HPO_4 group	[49]
--	--	1406	1404	--	B-type of CHA	[46]
--	1460	--	1460	--	A-type of CHA	[46]
--	--	1552	1552	--	CO_3^{2-} are A-type HCA	[50]
1640	--	1638	1636	1650	P–O–H group	[43]
2364	--	--	2096	--	P–OH/CO_2 group	[44,45,52]
--	--	--	--	2850	C–OH stretching	[45,52]
--	--	2930	2924	2928	C–OH stretching	[45,52]
--	--	3230	--	--	O–H group	[51,43]
3449	3421	3410	3426	3426	H_2O /O–H groups	[41,43]

6.3.3 SEM-EDS analysis

Hydroxyapatite layer formation of all zirconia doped bioglass samples are analysed by using SEM micrographs and the EDS spectra. Fig. 6.6 shows the surface morphology of Zr.3 (0.3 mol%) and Zr.5 (0.5 mol%) bioglass samples before and after soaking in SBF for 3,7,14 and 21days. It is clearly noticed that, before immersion the glass samples exhibited smooth surfaces with dense glass morphology (Fig. 6.6(a-0days)). This is also confirmed by the intensity peaks appeared in EDS spectra related to the elements (Zn, Ca, Na, Zr, P, and O) of glass chosen bioglass system (Fig. 6.6(a-0days)). After 3days of immersion a new layer containing white flakes type of structure is formed on the glass surface and is known as hydroxyapatite layer, which is the main building block to bond the bone and implant material in the body as illustrated in Fig. 6.6(a-3days). The crystalline hydroxyapatite layer formation was confirmed by XRD and FTIR results. As immersion time increases (Fig. 6.6. shows at (a) 7days and (b) 14, 21days), the morphology on the surface of glasses has also changed. We can see the conversion of flake type structure to dense foam type of structure and after 14 days and 21 days of immersion time (Fig. 6.6(b-14, 21days)), the glass surfaces are completely covered by uniformly formed apatite layer. This is due to the leaching of Ca^{2+}, Na^{+} and P^{5+} ions from glass to solution, migration of ions from solution to surface of the glasses and in addition, establishment of Zr–OH groups on the surface of glasses by exchange mechanism due to interaction with water molecules. Moreover, the higher reactivity of glass in aqueous medium depends on the disordered structure of glass [52]. Finally it leads to nucleation and evolution of HAp layer on the glass surface [53].

Supporting SEM data, the HAp layer development on as-prepared bioglasses is analysed by EDS spectra shown in Fig. 6.6. The results attained confirm increase in Ca and P concentrations to soaking time in SBF solution and Ca–P ratios along with the development of the apatite layer. In addition, the presence of Mg, Cl and K ions after SBF treatment along with glass ions are a clear indication of the formation of apatite layer. According to N. Zarifah, et al., the bioglasses processing Ca/P ratios greater than 1 can be most suitable for bone implant applications, because of good solubility [53,54]. The calculated stoichiometric ratios (Ca/P) is ranging from 1.65 to 1.89 for the chosen bioglass samples associated with the SBF solution, which are almost equivalent to bone composition [54-56]. Along with incubation time, the content of zirconia also influences the formation of apatite layer over the surfaces of glass samples. The formation of HAp layer increase with increases in content of ZrO_2 from 0.1mol% to 0.5 mol% after which there is a slight decrease in layer formation from intensity peaks of EDS and SEM morphology.

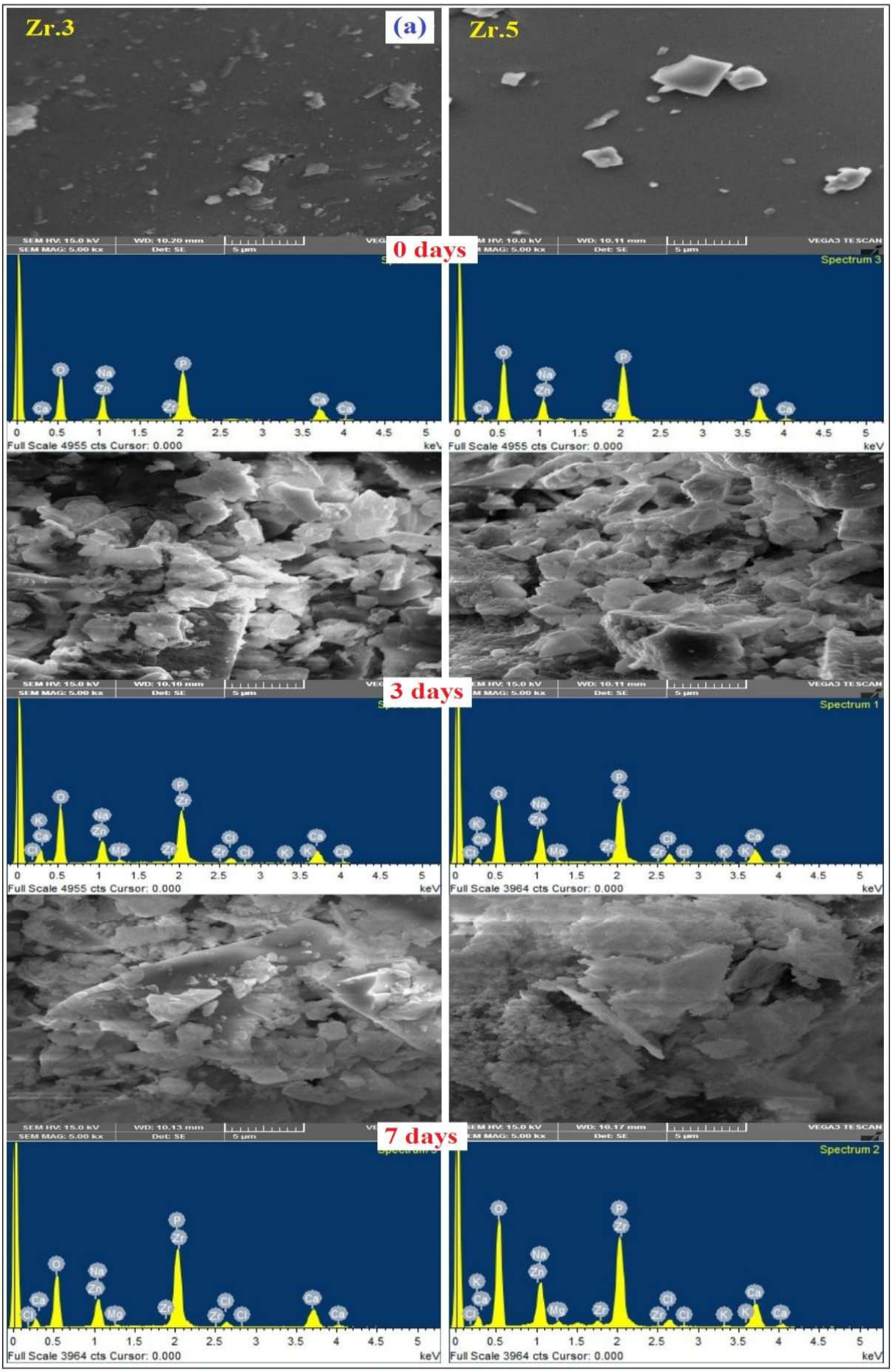
Zr.3
(a)
Zr.5
0 days
3 days
7 days
Spectrum 3
Spectrum 1
Spectrum 2
Full Scale 4955 cts Cursor: 0.000
Full Scale 3964 cts Cursor: 0.000
keV

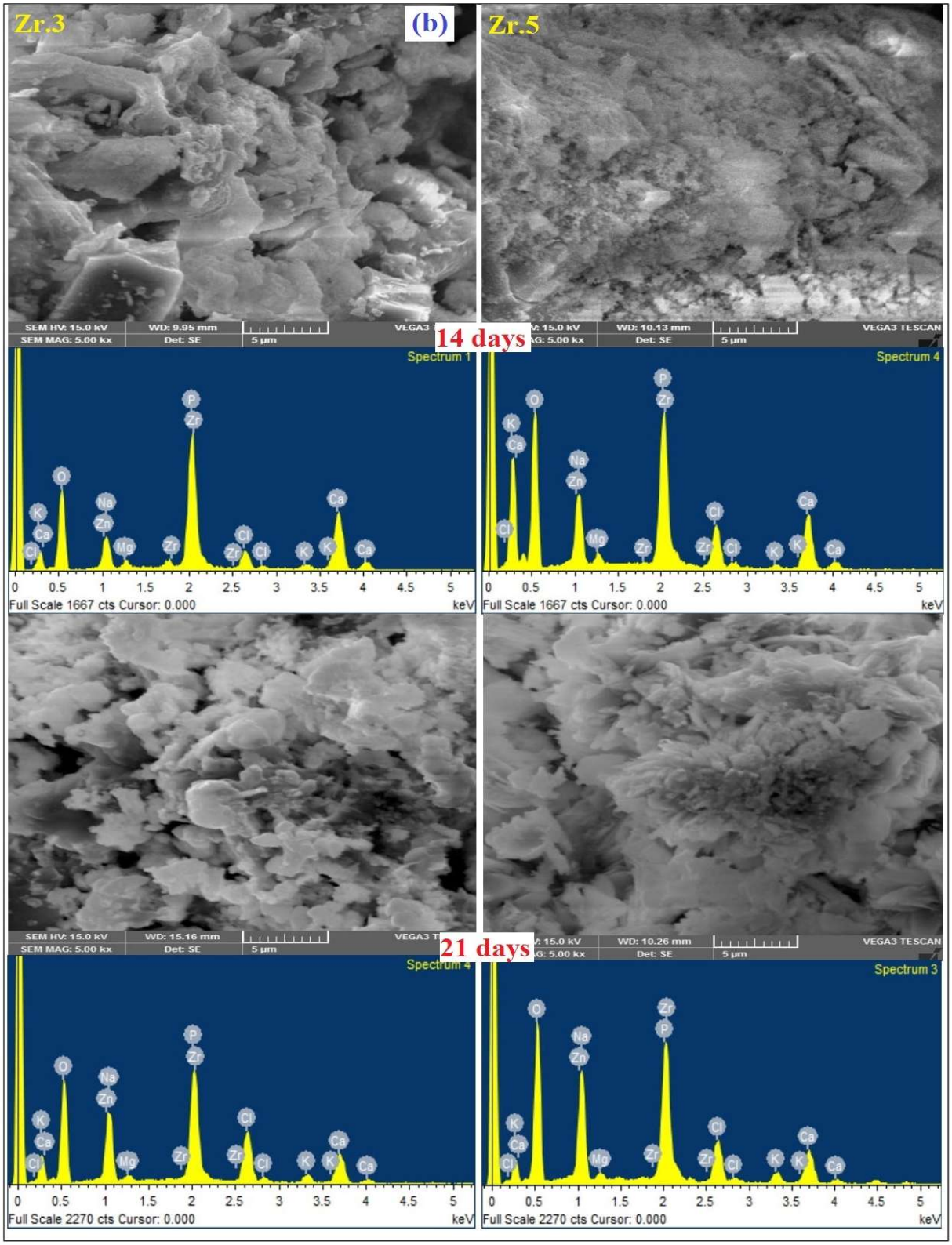

Fig. 6.6 SEM micrographs and EDS spectra of the Zr.3 and Zr.5 bioglass samples before and after immersion in SBF solution for different time periods (**a**) 0 days, 3 days and 7 days, (**b**) 14 days and 21 days.

This is due to decrease in solubility with the presence of zirconia, in other words, the release of Ca^{2+} ions increases initially up to 0.5 mol% ZrO_2 and then decrease with increase in ZrO_2 (0.7 mol% onwards), it leads to decrease in HAp layer formation in full agreement with the study by Montazerian et al.[34]. Fig. 6.7 explains the cross-sectional view of SEM micrograph and EDS elemental mapping of base glass (Zr-free (Zr0)) and Zr.5 glass after 21days of immersion in SBF. We can see clearly two regions from cross-sectional micrographs, the top region is HAp layer and beneath to HAp layer is the glass.

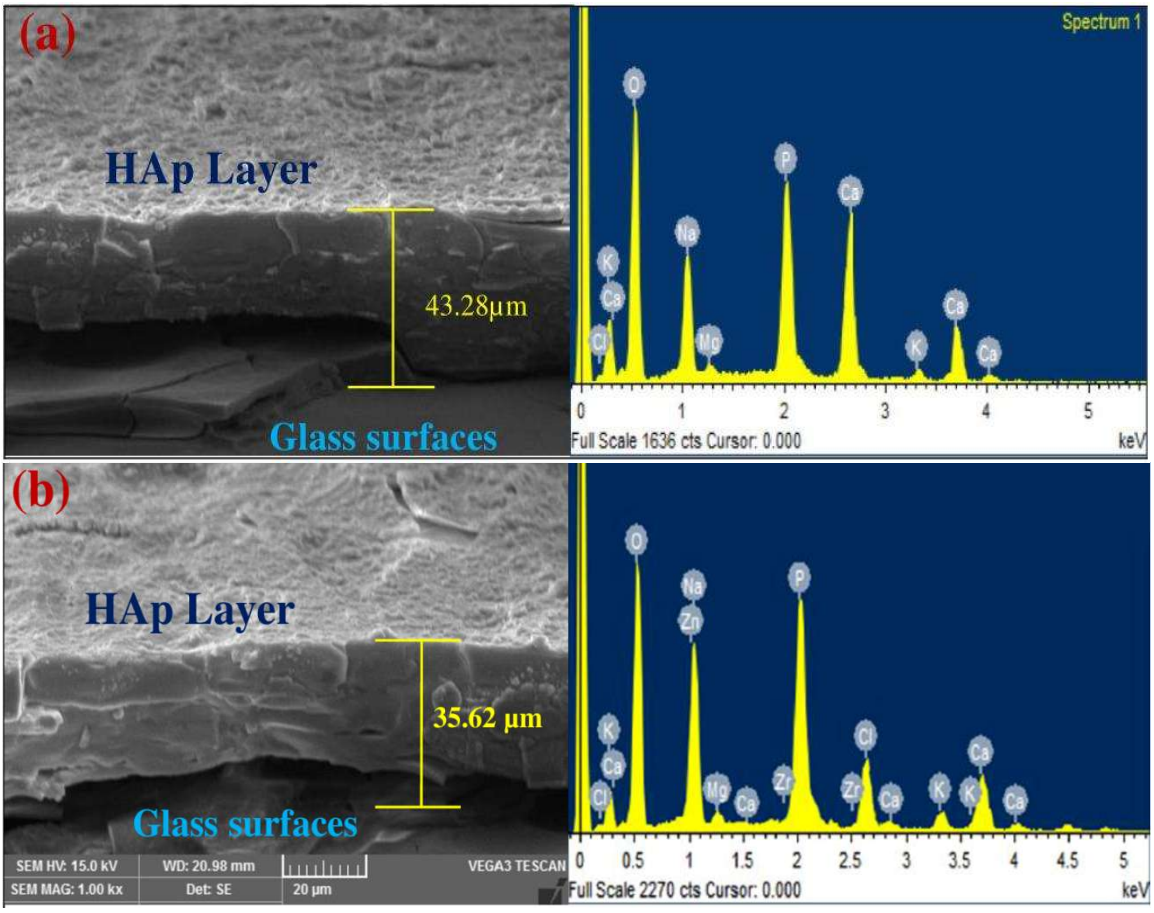

Fig. 6.7 The cross-sectional outlook of SEM micrograph and EDS elemental mapping of (a) base glass (Zr0) and (b) Zr.5 glass after 21 days of immersion in SBF.

The thickness of apatite layer formed on Zr.5 and Zr0 glass is around 35.62 and 43.28 microns respectively; for 21days of incubation in SBF. Zr-free glass shows thick layer formation than Zr-doped glasses, but the thickness of HAp layer formation increases with ZrO_2 content. This confirms the rich layer formation and leads to high bioactivity of chosen glasses. These results fit perfectly with XRD and FTIR results.

6.3.4 Degradation Analysis

The rate of degradation or dissolution behavior of bioglasses is estimated by measuring the weight of glasses before and after immersion in SBF solution for various time intervals, because the measurements of weight loss gives straight evaluation of degradation of glasses in solution. Fig. 6.8.shows the weight loss of Zr doped bioglasses before and after immersion in SBF solution for 3, 7, 14 and 21 days. The weight loss of all bioglasses was observed to decrease with increase in immersion time (Fig. 6.8). Zirconia free base glass (ZrO_2) displays high dissolution rate when compared with ZrO_2 doped glasses. Out of all glasses 0.7 mol% ZrO_2 doped glass (Zr.7) exhibited low weight loss. This considerable low weight loss is due to reduction of ion release from the samples. For the duration of degradation procedures, the release of Ca^{2+}, PO_4^{3-}, Na^+ and Zr^{4+} ions into the surrounding SBF medium causes the dissolution of the glass, which results in super saturation of calcium and phosphate and leading to the formation of HAp layer. It is well known that the release rates of Ca^{2+} and PO_4^{3-} from biomaterials are associated with bioactivity [57].

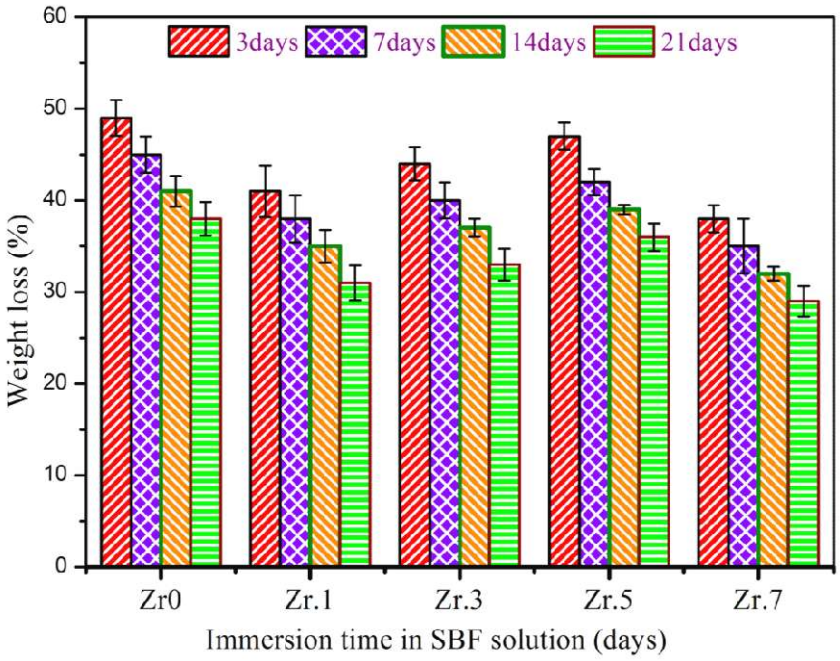

Fig. 6.8 Variation in weight loss of glass samples as a function of ZrO_2 concentration and soaking time in SBF solution.

It is very clearly visualized in the figure that, the dissolution rate slightly increases with increase in the content of ZrO_2 for up to 0.5 mol% and beyond that it decreases (0.7 mol%), which might be due to the formation of highly cross-linked dense structures that prevent degradation. This increase in solubility of Zr.1, Zr.3 and Zr.5 glasses lead to rich HAp layer formation. It's a well-known fact that apatite enhancement depends on the solubility of glass

in SBF solution higher the solubility greater the layer initiation. Contrary to previous reports on Zr-doped glasses [3,19,21], the present system of bioglasses shows a reverse trend as the gradual increase of zirconia up to 0.5 mol% leads to increase in degradation rate slightly. This might be attributed to the presence of low concentrations of ZrO_2 in phosphate glass network and controlled release of Ca^{2+} ions as replacement of CaO by ZrO_2. Furthermore, the rise in pH values of the residual SBF solution strongly supports degradation behavior of ZrO_2 doped bioglasses along with previously discussed XRD, FTIR and SEM-EDS results.

6.3.5 pH evaluation

Fig. 6.9 depicts the variation of pH values of SBF solution containing bioglasses as a function of incubation time (0, 3, 7, 14 and 21days). A sudden rise in pH of the solution (around 7.55) after 3days of immersion from initial pH 7.4, at 37 ^{o}C.

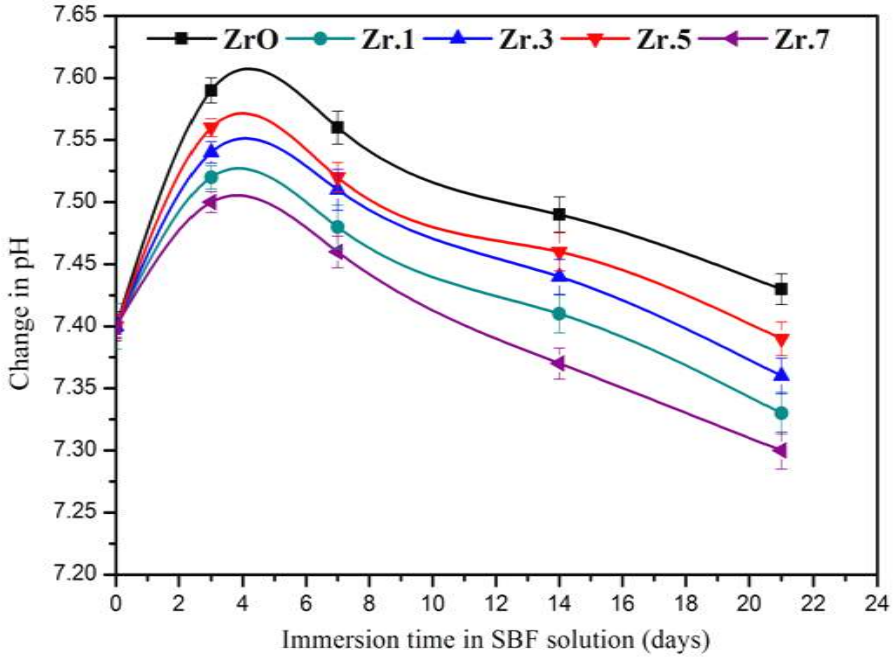

Fig. 6.9 The evaluation of the pH variation of glass samples immersed in SBF solution for different time intervals at 37 ^{o}C.

After an increase in immersion time from 7days to 21days, a gradual decrease in pH is noticed in all samples immersed in SBF solution. The increase in pH values are due to release of Ca^{2+}, PO_4^{3-}, Na^{+} and Zr^{4+} ions from the surface of glasses which then react with H_3O^{+} or H^{+} ions in SBF solution triggering OH^{-1} ions resulting the rapid rise in pH values [57]. In other hand, this is due to dissolution of cations from the surface of bioactive glass. After 7, 14 and 21 days of immersion, the decrease in pH values of all samples is due to the absorption of

phosphate and calcium ions in the SBF [48,58]. Moreover, with the addition of ZrO_2 from 0.1 to 0.5 mol%, there is a slight increase in pH and beyond this decrease. The changes that appeared in pH variation of Zr-doped glasses are very small compared to the base glass. Furthermore, it follows the same trend as that of weight loss. Sample Zr.5 displays a high pH value due to high dissolution rate. Therefore, the results obtained endorse controlled solubility of as–developed Zr glasses, which is an indication of high quality HAp layer growth [19,57]. This nature is highly advantageous and welcome towards cell adhesion and growth [34].

6.3.6 Cell cytotoxicity and Cell proliferation

Cell proliferation evaluation on as-prepared zirconia doped phosphate bioglasses was done by using cell counting kit (CCK-8) method. Fig. 6.10 shows the growth of rat mesenchymal cells (rMSC) along with ZrO_2 bioglass samples for one and three days of incubation. Interestingly, the cell viability enhances for all bioglass samples compared with the plastic control.

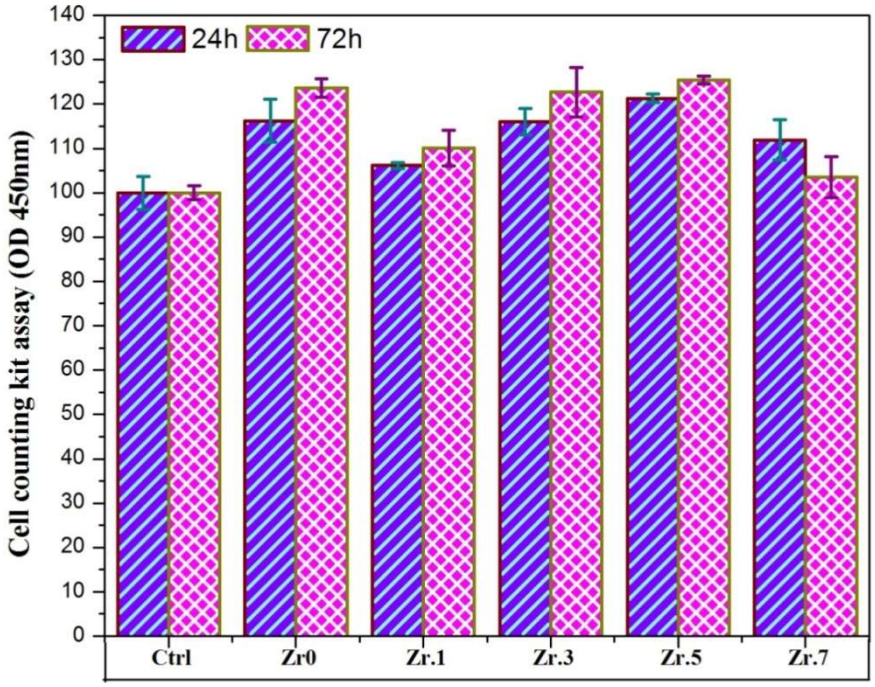

Fig. 6.10 Cytocompatibility and Proliferation analysis of the bioglasses assessed by *rMSCs* cells and CCK-8 method.

The glass samples Zr.1, Zr.3 and Zr.5 showed significantly higher cell viability at 24 h and 72 h of culture except Zr.7. It was also noticed clearly that the addition of up to 0.5 mol% of ZrO_2 (Zr.5) improved the cell viability, which then reduced gradually on further increase in content of ZrO_2. Among all zirconia doped bioglasses Zr.5 (0.5 mol% ZrO_2) glass possessing highest cell viability and proliferation. However, Fig. 6.10 it can observed that, the growth of

the rMSCs cells on the surface of Zr0 (ZnO containing base glass) without Zirconia also increases significantly, even higher than that of Zr.1, Zr.3, Zr.5 and Zr.7, which shows the enhancement in cell viability and proliferation. It may be due to ionic effect indicating cell viability with the rat mesenchymal cells. The increase in proliferation is ascribed to the release of Zr^{4+} ions effectively regulated by glass network with increase in ZrO_2 content by up to 0.5 mol%. There was decrease in cell proliferation after 3 days of 0.7% ZrO_2, due to gradual densification of ZrO_2 glass network [59,60]. For a specific doping ion concentration, the responses of osteoblasts, bone marrow stroma stem cells or fibroblasts can be gradually enhanced by the increased amount of ZnO. However, at excess concentration, Zn can induce cellular toxicity via production of reactive oxygen species and disruption of energy metabolism. Moreover, the amounts of Zn^{2+} and Zr^{4+} incorporated in zirconia doped bioglasses or released into medium are much lower than their threshold values which can induce cytotoxicity (Figs. 1 and 5). It means that if ZnO or ZrO_2 is doped separately in the glass system, should not reduce the cell viability. The decrease in numbers and viability of cells might be due to the comprehensive effect of ZrO_2 and ZnO, even though the concentrations of Zn and Zr are much lower than their inhibitory concentrations [61]. In other words, the increase in cell proliferation depends on stabilization of pH variations. In the present chosen categories of glasses pH variation was between 7.35 to 7.55, which is desirable for cell metabolism and thus for cell proliferation [62]. Moreover, all samples showed absorbance values greater than 100% with respect to plastic control as base line (assumed to be 100%). It means the as-prepared bioglasses were not inducing any toxic effects, assuming the viability assay values less than 70% were treated as toxic [63,64]. These results confirm enhancement in cell proliferation and cytocompatibility of as-prepared bioglasses. Lee et al., [65] reported that the cell culture studies are an alternative approach to SBF test and they confirmed the development of similar type of HAp layer under cell culture environments. The cell culture results are correlated detailed analysis of XRD, FTIR, SEM and pH data. So it is concluded that ZrO_2 incorporated bioglasses show stimulatory effect on bone growth and leads to development of orthopaedic implants.

6.3.7 Antibacterial activity

Fig.6.11 describes the studies of agar disk-diffusion assays conducted against *E. coli, S. aureus* and *P. aeruginosa* for 24 h and 48 h at 37 ˚C [66]. The antibacterial activity of the given samples was confirmed by the presence of a zone of inhibition around each sample disk. The zone of inhibition was obtained by subtracting the diameter of sample disk from the total zone of inhibition given in Table 6.4.

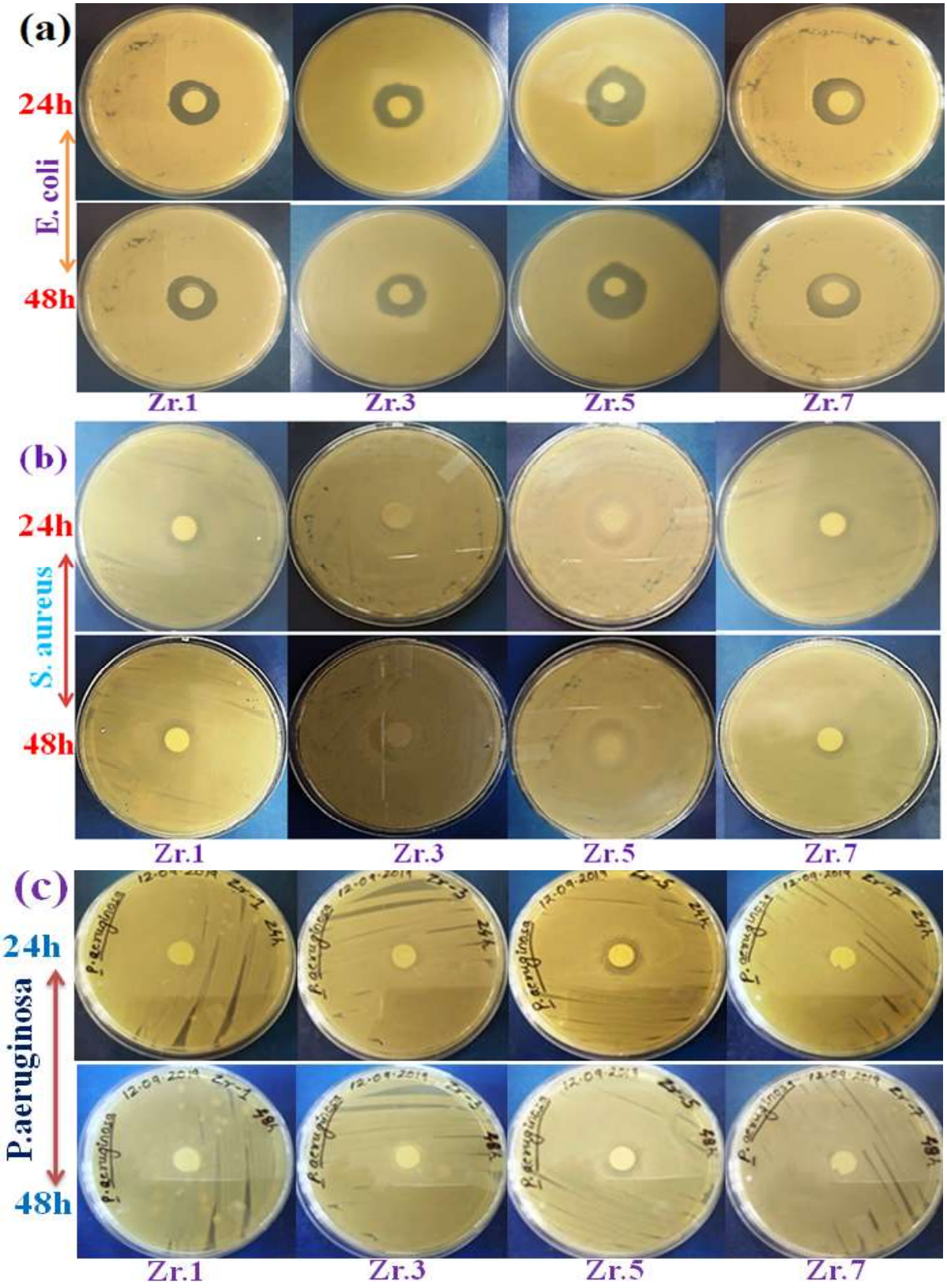

Fig. 6.11 Antibacterial assay using agar plate of disk diffusion assay against (a) *E. coli*, (b) *S.aureus* and (c) *P. aeruginosa* at different time intervals, 24 h and 48 h.

Table 6.4 Antibacterial activity of glass samples based on zone of inhibition

Sample code	Inhibition zone diameter* (in mm)					
	E. coli		*S.aureus*		*P. aeruginosa*	
	24 h	**48 h**	**24 h**	**48 h**	24 h	**48 h**
Zr.1	9.25	6.19	7.36	5.21	00	00
Zr.3	12	8	9.23	6.10	2	0
Zr.5	17	14	10.13	7.85	7	2
Zr.7	9.52	7.49	7.62	5.34	00	00

* All the calculations are made by subtracting the diameter of the glass sample disk i.e. 10mm.

It can be clearly visualised that samples Zr.1, Zr.3, Zr.5 and Zr.7 have shown clear inhibitory zone against *E. coli, S. aureus* and *P. aeruginosa* was not clear. *E. coli* was found to be more susceptible compared to *S. aureus* and *P. aeruginosa* against the given glass samples. From these micrographs, the bacterial growth of *E. coli* was inhibited significantly, as indicated by the transparent zone. Fig. 6.11 (a b & c) are show the inhibition efficiency of samples against *E. coli* at 24 h and 48 h, respectively which clearly indicates inhibition zone by sample Zr.3 and Zr.5. It is observed that, antibacterial activity was found to rise with increasing content of ZrO_2 from 0.1 mol% to 0.5 mol% and then decreases. This might be due to rise in release of Zr^{4+} ions. The results obtained are in good agreement with earlier reports describing antimicrobial activity of zirconia and other metal oxides [67,70]. The results obtained from antibacterial studies suggested that sample disks (Zr.3 and Zr.5) can greatly inhibit the growth of both gram negative bacteria shown in Table 6.4. The highest zone of inhibition was shown by Zr.3 and Zr.5 against *P. aeruginosa*, *S. aureus* and *E. coli* respectively after 24 & 48 hours.

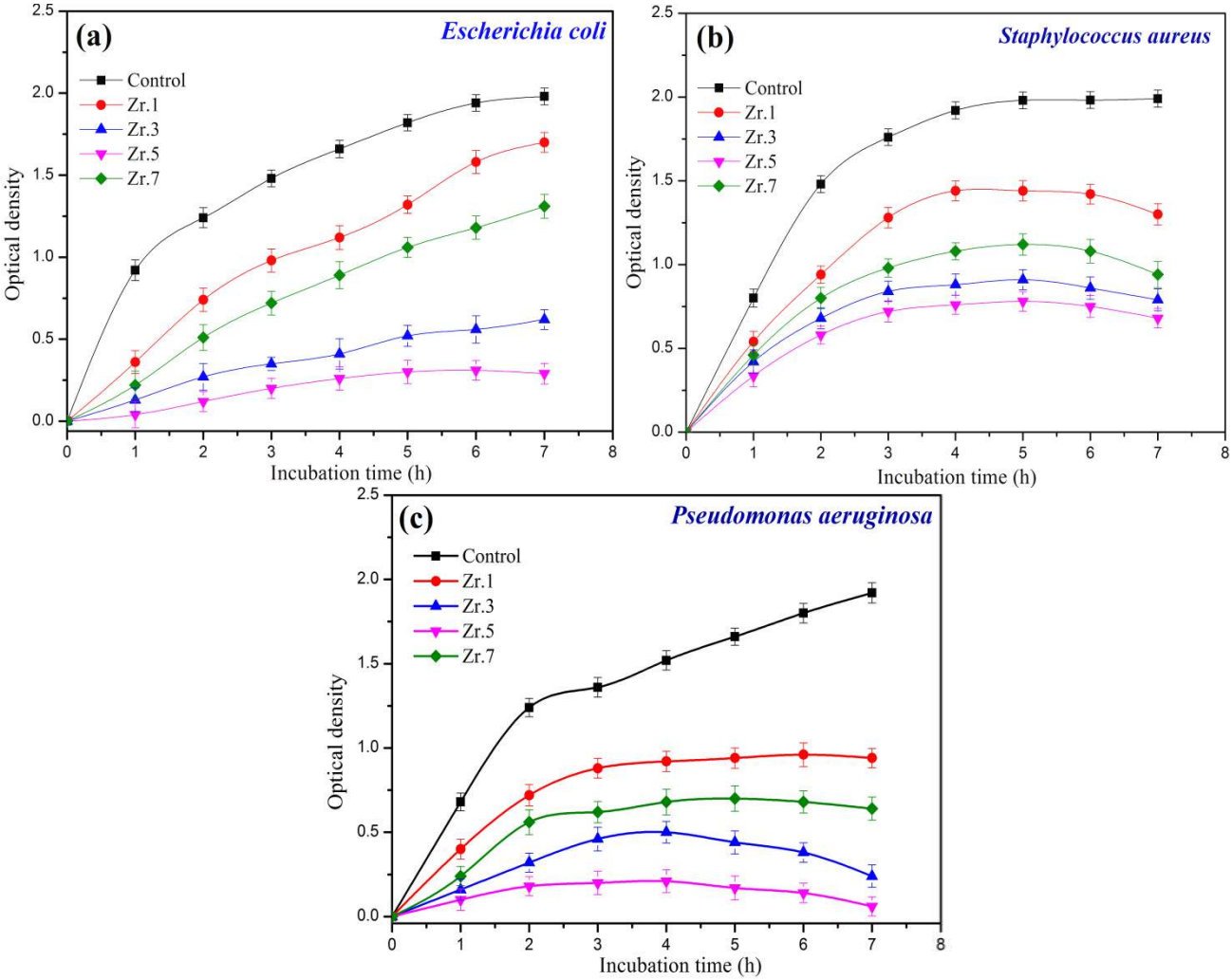

Fig. 6.12 Optical density measurement of samples at different time points against (a) *E. coli* (b) *S.aureus* and (c) *P. aeruginosa*.

Further, the antibacterial activity also confirmed by the optical density measured at eight different time points from 0h-7h at 600nm. Samples were individually incubated with both the bacterial cultures and OD measurement was recorded from the Fig. 6.12 (a, b and c). The results obtained from optical density measurement showed that the OD values decreases when the bacterial species were treated with samples. A low OD value indicates the antibacterial properties of given samples against gram negative bacteria. Fig. 6.12 (a, b and c) is showing the optical density measurement graphs of different samples at different time points against *E. coli*, *S. aureus* and *P. aeruginosa* respectively. Both agar disk diffusion assay and optical density measurements clearly indicate that sample Zr.5 has more potential against *E. coli* and *S. aureus* whereas, sample Zr.3 showed highest potency against *P. aeruginosa*. Therefore Zr.5 could be taken for future use for various medical purposes because of its superior bioactivity and antibacterial activity.

6.4 Conclusions

In the present study, HAp layer formation, cytocompatibility, rMSCs proliferation, structural and mechanical properties influenced by small quantity of ZrO_2 incorporation on 8ZnO–22Na_2O–24CaO–46P_2O_5 bioglass system have been investigated. The results obtained revealed that, the physical properties such as density and mechanical strength escalation with increasing content of ZrO_2, attributed to the establishment of new P–O–Zr bonds. The XRD, FTIR, and SEM-EDS results after immersing them in SBF for various durations strongly confirms the development of rich hydroxyapatite layer over as-synthesised glass surfaces. It is found that the layer formation enhances with immersion time and also ZrO_2 content up to 0.5 mol%. The controlled degradation rate and stable pH variations showed the release of Ca^{2+} and Zr^{4+} ions required for thick HAp layer. In addition, the growth of *rMSCs* cells on the surface of all bioactive glasses increases significantly, which shows increase cell proliferation and biocompatibility. Moreover, these glasses do not exhibit any toxic effects on rMSCs cells evaluated by CCK-8 assay. Furthermore, ZrO_2 doped phosphate bioglasses showed better antibacterial effect against three strains *E. coli*, *S.aureus* and *P. aeruginosa*; subsequently, among all glasses Z.5 (0.5 mol%) bioactive glass showed enhanced bioactivity with better mechanical strength and antibacterial activity; hence this could be suitable for the development of clinical implants.

Reference

[1] L. Saldana, A. Mendez-Vilas, L. Jiang, M. Multigner, J.L. Gonzalez-Carrasco, In vitro biocompatibility of an ultrafine grained zirconium, Biomaterials 28 (2007) 4343–4354.

[2] F.Y. Zhou, B.L. Wang, K.J. Qiu, L. Li, J.P. Lin, H.F. Li, Y.F. Zheng, Microstructure, mechanical property, corrosion behavior, and in vitro biocompatibility of Zr-Mo alloys, J. Biomed. Mater. Res. Part B Appl. Biomater. 101 B (2013) 237–246.

[3] N. Krishnamacharyulu, G.J. Mohini, G.S. Baskaran, V.R. Kumar, N. Veeraiah, Effect of ZrO_2 on the bioactive properties of B_2O_3–SiO_2–P_2O_5–Na_2O–CaO glass system, J. Non. Cryst. Solids. 452 (2016) 23–29.

[4] L.L. Hench, R.J. Splinter, W.C. Allen, T.K. Greenlee, Bonding mechanisms at the interface of ceramic prosthetic materials, J. Biomed. Mater. Res. 5 (1971) 117–141.

[5] L.L. Hench, Bioceramics from concept to clinic, J. Am. Ceram. Soc. 74 (1991) 1487–1510.

[6] T. Kokubo, Apatite formation on surfaces of ceramics, metals and polymers in body environment, Acta Mater. 46 (1998) 2519–2527.

[7] R.Z. LeGeros, Properties of osteoconductive biomaterials: Calcium phosphates, Clin. Orthop. Relat. Res. 395 (2002) 81–98.

[8] F.Bollino, E.Armenia, E.Tranquillo, Zirconia/hydroxyapatite composites synthesized via sol-gel: Influence of hydroxyapatite content and heating on their biological properties, Materials. 10 (2017) 757.

[9] X. Lu, L. Deng, J. Du, Effect of ZrO_2 on the structure and properties of soda-lime silicate glasses from molecular dynamics simulations, J. Non. Cryst. Solids. 491 (2018) 141–150.

[10] D. Mondal, S. So-Ra, B.T. Lee, Fabrication and characterization of ZrO_2–CaO–P_2O_5–Na_2O–SiO_2 bioactive glass ceramics, J. Mater. Sci. 48 (2013) 1863–1872.

[11] R.H.J. Hannink, P.M. Kelly, B.C. Muddle, Transformation Toughening in Zirconia-Containing Ceramics, J. Am. Ceram. Soc. 83 (2000) 461–487.

[12] W. Burger, H.G. Richter, C. Piconi, R. Vatteroni, A. Cittadini, M. Boccalari, New Y-TZP powders for medical grade zirconia, J. Mater. Sci. Mater. Med. 8 (1997) 113–118.

[13] L. Ruiz, M.J. Readey, Effect of heat treatment on grain size, phase assemblage, and mechanical properties of 3 mol% Y-TZP, J. Am. Ceram. Soc. 79 (1996) 2331–2340.

[14] H. Harianawala, M. Kheur, A. Bal, Biocompatibility of Zirconia, J. Adv. Med. Dent.

Scie. Res. 4 (2016) 35–39.

[15] T.R. Ramesh, M. Gangaiah, P. V. Harish, U. Krishnakumar, B. Nandakishore, Zirconia ceramics as a dental biomaterial-An over view, Trends Biomater. Artif. Organs. 26 (2012) 154–160.

[16] C. Piconi, G. Maccauro, Zirconia as a ceramic biomaterial, Biomate. 20 (1999) 1–25.

[17] H.C. Li, D.G. Wang, C.Z. Chen, Effect of zinc oxide and zirconia on structure, degradability and in vitro bioactivity of wollastonite, Ceram. Int. 41 (2015) 10160–10169.

[18] H.C. Li, D.G. Wang, X.G. Meng, C.Z. Chen, Effect of ZrO_2 additions on the crystallization, mechanical and biological properties of $MgO–CaO–SiO_2–P_2O_5–CaF_2$ bioactive glass-ceramics, Colloids Surfaces B Biointerfaces. 118 (2014) 226–233

[19] P. Yin, J.W. Yuan, L.H. Liu, T. Xiao, T. Lei, Effect of ZrO_2 on the bioactivity properties of gel-derived $CaO–P_2O_5–SiO_2–SrO$ glasses, Ceram. Int. 43 (2017) 9691–9698.

[20] M. Kord, V.K. Marghussian, B. Eftekhari-yekta, A. Bahrami, Effect of ZrO_2 addition on crystallization behaviour, porosity and chemical-mechanical properties of a $CaO–TiO_2–P_2O_5$ microporous glass ceramic, Mater. Res. Bull. 44 (2009) 1670–1675.

[21] G. Rajkumar, S. Aravindan, V. Rajendran, Structural analysis of zirconia-doped calcium phosphate glasses, J. Non. Cryst. Solids. 356 (2010) 1432–1438.

[22] T. Kokubo, H. Takadama, How useful is SBF in predicting in vivo bone bioactivity?, Biomaterials. 27 (2006) 2907–2915.

[23] M. Uchida, H.-M. Kim, T. Kokubo, F. Miyaji, T. Nakamura, Bonelike Apatite Formation Induced on Zirconia Gel in a Simulated Body Fluid and Its Modified Solutions, J. Am. Ceram. Soc. 84 (2004) 2041–2044.

[24] V.H. Rao, P.S. Prasad, M.M. Babu, P.V. Rao, L.F. Santos, G.N. Raju, N. Veeraiah, Luminescence properties of Sm^{3+} ions doped heavy metal oxide tellurite-tungstate-antimonate glasses, Ceram. Int. 43 (2017) 16467–16473.

[25] M.M. Babu, P.S. Prasad, P.V. Rao, N.P. Govindan, R.K. Singh, H.W. Kim, N. Veeraiah, Titanium incorporated Zinc-Phosphate bioactive glasses for bone tissue repair and regeneration: Impact of Ti^{4+} on physico-mechanical and in vitro bioactivity, Ceram. Int. 45 (2019) 23715–2327.

[26] S.M. Abo-naf, E.M. Khalil, E.M. El-sayed, H.A. Zayed, R.A. Youness, Spectrochimica Acta Part A : Molecular and Biomolecular Spectroscopy In vitro bioactivity evaluation ,

mechanical properties and microstructural characterization of $Na_2O–CaO–B_2O_3–P_2O_5$ glasses, 144 (2015) 88–98.

[27] J.K.M.F. Daguano, P.A. Suzuki, K. Strecker, M.H.F.V. Fernandes, C. Santos, Evaluation of the micro-hardness and fracture toughness of amorphous and partially crystallized $3CaO·P_2O_5–SiO_2–MgO$ bioglasses, Mater. Sci. Eng. A. 533 (2012) 26–32.

[28] J. Liu, S.C.F. Rawlinson, R.G. Hill, F. Fortune, Fluoride incorporation in high phosphate containing bioactive glasses and in vitro osteogenic, angiogenic and antibacterial effects, Dent. Mater. (2016) 1–17.

[29] X. Chen, Y. Meng, Y. Li, N. Zhao, Investigation on bio-mineralization of melt and sol-gel derived bioactive glasses, Appl. Surf. Sci. 255 (2008) 562–564.

[30] L.L. Hench, I.D. Xynos, J.M. Polak, L.L. Hench, I.D. Xynos, J.M. Polak, Bioactive glasses for in situ tissue regeneration, J. Biomat. Sci. 15 (2004) 543–562.

[31] T. Kokubo, H. Kushitani, C. Ohtsuki, S. Sakka, T.Yamamuro, O.F. Materials, I.N. Medicine, Chemical reaction of bioactive glass and glass-ceramics with a simulated body fluid, J. Materi. Sci.: Mater.Medi. 3 (1992) 79–83.

[32] D.L. Wheeler, E.J. Eschbach, R.G. Hoellrich, T.M.J. Lmontfort, L. Chamberland, Assessment of Resorbable Bioactive Material for Grafting of Critical-size Cancellous Defects, J. Orthop. Res. 18 (2000) 140–148.

[33] A.K. Srivastava, R. Pyare, Characterization of ZnO substituted 45S5 Bioactive Glasses and Glass-Ceramics, J. Mater. Sci.Res. 1 (2012) 207–220.

[34] M. Montazerian, B.E. Yekta, V.K. Marghussian, C.F. Bellani, R.L. Siqueira, E.D. Zanott,Bioactivity and cell proliferation in radiopaque gel-derived $CaO–P_2O_5–SiO_2–ZrO_2$ glass and glass–ceramic powders.J. Mater. Sci. Eng. C, 55 (2015) 436–447.

[35] A.A. El-Kheshen, F.A. Khaliafa, E.A. Saad, R.L. Elwan, Effect of Al_2O_3 addition on bioactivity, thermal and mechanical properties of some bioactive glasses, Ceram. Int. 34 (2008) 1667–1673.

[36] D. Ilieva, B. Jivov, G. Bogachev, C. Petkov, I. Penkov, Infrared and Raman spectra of $Ga_2O_3–P_2O_5$ glasses, J. Non. Cryst. Solids. 283 (2001) 195–202.

[37] D. Carta, D.M. Pickup, J.C. Knowles, I. Ahmed, M.E. Smith, R.J. Newport, A structural study of sol-gel and melt-quenched phosphate-based glasses, J. Non. Cryst. Solids. 353 (2007) 1759–1765.

[38] N.F. Ibrahim, H. Mohamad, S.N.F. Mohd Noor, N. Ahmad, Apatite formation on melt-derived bioactive glass powder based on $SiO_2–CaO–Na_2O–P_2O_5$ system, Ceram. Int. 43 (2017) 11676–11685.

[39] P.Y. Shih, S.W. Yung, T.S. Chin, FTIR and XPS studies of P_2O_5–Na_2O–CuO glasses, J. Non. Cryst. Solids. 244 (1999) 211–222.

[40] A. Kiani, J. V. Hanna, S.P. King, G.J. Rees, M.E. Smith, N. Roohpour, V. Salih, J.C. Knowles, Structural characterization and physical properties of P_2O_5–CaO–Na_2O–TiO_2 glasses by Fourier transform infrared, Raman and solid-state magic angle spinning nuclear magnetic resonance spectroscopies, Acta Biomater. 8 (2012) 333–340.

[41] S.P. Valappil, D. Ready, E.A. Abou Neel, D.M. Pickup, W. Chrzanowski, L.A. O'Dell, R.J. Newport, M.E. Smith, M. Wilson, J.C. Knowles, Antimicrobial gallium-doped phosphate-based glasses, Adv. Funct. Mater. 18 (2008) 732–741.

[42] R.L. Ciceo, D.L. Trandafir, T. Radu, O. Ponta, V. Simon, Synthesis, characterisation and in vitro evaluation of sol-gel derived SiO_2–P_2O_5–CaO–B_2O_3 bioactive system, Ceram. Int. 40 (2014) 9517–9524.

[43] R. Samudrala, G.V.N. Reddy, B. Manavathi, P.A. Azeem, Synthesis , characterization and cytocompatibility of ZrO_2 doped borosilicate bioglasses, J. Non. Cryst. Solids. 447 (2016) 150–155.

[44] S. Cai, W.J. Zhang, G.H. Xu, J.Y. Li, D.M. Wang, W. Jiang, Microstructural characteristics and crystallization of CaO–P_2O_5–Na_2O–ZnO glass ceramics prepared by sol-gel method, J. Non. Cryst. Solids. 355 (2009) 273–279.

[45] D.S. Brauer, N. Karpukhina, M.D.O. Donnell, R. V Law, R.G. Hill, Acta Biomaterialia Fluoride-containing bioactive glasses: Effect of glass design and structure on degradation, pH and apatite formation in simulated body fluid, Acta Biomater. 6 (2010) 3275–3282.

[46] D.M. Pickup, P. Guerry, R.M. Moss, J.C. Knowles, E. Smith, R.J. Newport, New sol–gel synthesis of a $(CaO)_{0.3}(Na_2O)_{0.2}(P_2O_5)_{0.5}$ bioresorbable glass and its structural characterisation, J. Mater. Chem.17 (2007) 4777–4784.

[47] P.Y. Shih, Properties and FTIR spectra of lead phosphate glasses for nuclear waste immobilization, J. Mater. Chem. Phy. 80 (2003) 299–304.

[48] G. Kaur, P. Sharma, V. Kumar, K. Singh, Assessment of in vitro bioactivity of SiO_2–BaO–ZnO–B_2O_3–Al_2O_3 glasses: An optico-analytical approach, J. Mater. Sci. Eng. C. 32 (2012) 1941–1947.

[49] R. Koohkan, T. Hooshmand, M. Tahriri, D. Mohebbi-Kalhori, Synthesis, characterization and in vitro bioactivity of mesoporous copper silicate bioactive glasses, Ceram. Int. 44 (2018) 2390–2399.

[50] H. Tripathi, S. Kumar Hira, A. Sampath Kumar, U. Gupta, P. Pratim Manna, S.P. Singh, Structural characterization and in vitro bioactivity assessment of SiO_2–CaO–P_2O_5–K_2O–

Al_2O_3 glass as bioactive ceramic material, Ceram. Int. 41 (2015) 11756–11769.

[51] Y. Goh, A.Z. Alshemary, M. Akram, M. Rafiq, A. Kadir, Bioactive Glass : An In-vitro Comparative Study of Doping with Nanoscale Copper and Silver Particles, J. Appl. Glass. Sci. 12 (2014) 1–12

[52] S.M. Best, A.E. Porter, E.S. Thian, J. Huang, Bioceramics: Past, present and for the future, J. Eur. Ceram. Soc. 28 (2008) 1319–1327.

[53] J. Ajita, S. Saravanan, N. Selvamurugan, Effect of size of bioactive glass nanoparticles on mesenchymal stem cell proliferation for dental and orthopedic applications, Mater. Sci. Eng. C. 53 (2015) 142–149.

[54]. N.A. Zarifah, W.F. Lim, K.A. Matori, H.A.A. Sidek, Z.A. Wahab, N. Zainuddin, M.A. Salleh, B.N. Fadilah, A.N. Fauzana, An elucidating study on physical and structural properties of 45S5 glass at different sintering temperatures, J. Non. Cryst. Solids. 412 (2015) 24–29.

[55] N. Farhana, H. Mohamad, S. Noor, F. Mohd, N. Ahmad, Apatite formation on melt-derived bioactive glass powder based, Ceram. Int. 43 (2017) 11676–11685.

[56] T. Kokubo, H.M. Kim, M. Kawashita, Novel bioactive materials with different mechanical properties, Biomaterials. 24 (2003) 2161–2175.

[57] Y. Abe, T. Kokubo, T. Yamamuro, Apatite coating on ceramics, metals and polymers utilizing a biological process, J. Mater. Sci. Mater. Med. 1 (1990) 233–238.

[58] X. Lu, Y.L. Ã, Theoretical analysis of calcium phosphate precipitation in simulated body fluid, 26 (2005) 1097–1108.

[59] J. Li, Y. Liu, L. Hermansson, R. Soremark, Evaluation o biocompatibility of various ceramic powders with human fibroblasts in vitro, Clin. Mater. (1993) 197-201.

[60] H.A. Abo-mosallam, D. Kim, H. Kim, H. Lee, In fl uence of ZrO_2 oxide on the properties and crystallization of calcium fl uoro-alumino-silicate glasses, 42 (2016) 5107–5112.

[61] Lan Zhang, Jiaqi Guo, Ting Yan, Yong Han, Fibroblast responses and antibacterial activity of Cu and Zn co-doped TiO_2 for percutaneous implants, Applied Surface Science 434 (2018) 633–642.

[62] B. Alberts, D. Bray, J. Lewis, M. Raff, K. Roberts, J.D.Watson, Molecular Biology of the Cell, 4th edition Garland Publishing, New York, 2003.

[63] S. Kapoor, A. Goel, A.F. Correia, M.J. Pascual, H.Y. Lee, H.W. Kim, J.M.F. Ferreira, Influence of ZnO/MgO substitution on sintering, crystallisation, and bio-activity of alkali-free glass-ceramics, Mater. Sci. Eng. C. 53 (2015) 252–261.

[64] N.J. Lakhkar, I.H. Lee, H.W. Kim, V. Salih, I.B. Wall, J.C. Knowles, Bone formation controlled by biologically relevant inorganic ions: Role and controlled delivery from phosphate-based glasses, Adv. Drug Deliv. Rev. 65 (2013) 405–420.

[65] J.T.Y. Lee, Y. Leng, K.L. Chow, F. Ren, X. Ge, K. Wang, X. Lu, Acta Biomaterialia

Cell culture medium as an alternative to conventional simulated body fluid, 7 (2011) 2615–2622.

[66] A.W.Bauer,W.M.Kirby, J.C.Sherris, and M.Turck, "Antibiotic susceptibility testing by a standardized single disk method," American Journal of Clinical Pathology. 45 (1966) 493– 496.

[67] P. Li, C. Ohtsuki, T. Kokubo et al., "Effects of ions in aqueous media on hydroxyapatite induction by silica gel and its relevance to bioactivity of bioactive glasses and glass-ceramics," J. Appl. Biomat., 4 (1993) 221–229

[68] K. C. Kavya, R. Jayakumar, S. Nair, and K. P. Chennazhi, "Fabrication and characterization of chitosan/gelatin/n SiO_2 composite scaffold for bone tissue engineering," Int.J. Biolog. Macromole., 59 (2013) 255–263.

[69] A.A. Ahmed, A.A Ali, D. Mahmoud, AM.El-Fiqi, Study on the preparation and properties of silver-doped phosphate antibacterial glasses. Sol. State. Sic 13 (2011) 981–992.

[70] V.V. Anusha Thampia, M. Prabhua, K. Kavithaa, P. Manivasakana, P. Prabua, V. Rajendrana, S. Shankarc, P. Kulandaivelu, Hydroxyapatite, alumina/zirconia, and nanobioactive glass cement for tooth-restoring applications, Ceram. Int. 40 (2014) 14355–14365.

Chapter -7

Summary and Conclusions

This chapter reports the summary and main conclusions of structural and dissolution behaviour, in vitro bioactivity and antibacterial activity of undoped and transition metal oxides (ZnO, TiO_2, Al_2O_3 and ZrO_2) doped high phosphate bioglasses developed by conventional melt quenching method. It is also discussed bone mineral phases like rich HAp layer formation over the surfaces of glass samples suitable for bone regeneration tissue engineering applications. The scope of future work is also discussed in this study.

7.1 Summary

In the present study, high phosphate bioactive glass systems with chemical compositions xZnO–22Na_2O–24CaO–(54-x)P_2O_5 (x = 2, 4, 6, 8 and 10 mol%), 8ZnO–8ZnO–22Na_2O–(24-x)CaO–46P_2O_5–$x$$TiO_2$ (x =0.2, 0.4, 0.6, 0.8 and 1mol%), 8ZnO–22Na_2O–(24-x)CaO–46P_2O_5–$x$$Al_2O_3$ (x = 2, 4, 6, 8 and 10 mol%), 8ZnO–22Na_2O–(24-x)CaO–46P_2O_5–$x$$ZrO_2$ (x = 0.1, 0.3, 0.5 and 0.7mol%) have been synthesized by melt quenching technique. The bioactive glasses thus prepared were characterized by employing various techniques like XRD, FTIR, SEM, DTA etc., to know structural changes such as physical parameters, mechanical properties and thermal properties with the inclusion of various transition metal ions (Zn^+, Ti^+, Al^+ and Zr^+). The biological activity of as prepared bioglasses was explored *in vitro* by measuring biocompatibility, bioactivity, cytocompatibility, cell proliferation and antibacterial activity. Besides, the chemical behavior such as weight loss and pH variation of glass samples when they come in physical contact with artificial blood plasma or simulated body fluid (SBF) solution was studied. XRD and FTIR studies provide the information about the amorphous or crystalline nature and various vibrational bonds of the bioglasses respectively, before and after immersion in SBF solution at 37 °C with pH 7.4. The formation of bone like hydroxy apatite layer (HAp) over the surface of glass samples can be identified by observing surface morphology and elemental analysis from SEM-EDS data before and after immersion of bioglass samples at various time intervals (0, 3, 7, 14, 21days). To know the glass dissolution behavior in order to estimate the bioactive capacity of the bioglasses, weight loss measurements were done as a function of incubation time. At the same time pH variation was also noticed in support of the degradation of glass samples in SBF solution. Cell viability, Cell cytotoxicity and proliferation were analyzed by seeding Rat Mesenchymal Stem Cells (r*MSC*s) on bioglasses using cell counting kit (CCK-8). The antibacterial activity against gram negative bacteria *Escherichia coli, Staphylococcus aureus,* and *Pseudomonas aeruginosa* was tested by agar disk diffusion assay and optical density (OD) methods for 24 h and 72 h of incubation. The results obtained confirm the appropriateness of as-developed phosphate bioactive glasses for application in bone regeneration tissue engineering.

7.2 Conclusion

The main conclusions drawn from the results of the above studies are summarized below:

The **physical parameters** such as density, molar volume, oxygen molar volume and oxygen packing density of bioglasses change with incorporation of different concentrations of ZnO, TiO_2, Al_2O_3 and ZrO_2 transition metal oxides. The density and oxygen molar volume are

found to increase and the molar volume and oxygen packing density decrease with increase in ZnO concentration. The increase in density clearly indicates the presence of the highly ionic nature of P–O–Zn bonds than P–O–P bonds in glass network, which leads to compactness of the glass structure. The density, glass transition temperature and mechanical strength of as-prepared glass specimens report an increase with an increase in TiO_2 content which could be attributed to cross link densification of glass structure following the formation of powerful P–O–Ti bonds. The density as well as microhardness of glass samples increases with an increase in Al_2O_3 content thanks to the strengthening of glass structure because of corresponding enhancement in bond strength of P–O–Al ionic linkages. Density and mechanical strength escalation with increasing content of ZrO_2 could be attributed to the establishment of new P–O–Zr bonds.

The **XRD traces** of all glass samples before immersion showed that the prepared samples are non-crystalline in nature. After immersion in SBF for various time periods (3, 7, 14 and 21days), the traces displayed sharp crystalline peaks in all phosphate glasses doped with ZnO, TiO_2, Al_2O_3 and ZrO_2 transition metal oxides. The presence of crystalline peaks in XRD traces confirms development of micro structured hydroxyapatite ($Ca_{10}(PO_4)_6$ $(OH)_2$) layer on the glass surfaces. This is the evident from the peaks observed at diffracted angles (2θ): 10.83^o, 15.27^o, 21.73^o, 22.82^o, 25.86^o, 27.56^o, 31.75^o, 40.69^o, 45.32^o, 56.28^o, 66.35^o and 75.56^o corresponding to the reflections 110, 021, 200, 111, 002, 112, 211, 221, 203, 500, 143 and 215 respectively. It is found that, additional peaks appeared with incubation time and also the intensities of reflections were related to HAp increase with incubation time. In addition the intensities of reflections increase with increase in the content of ZnO from 0 mol% to 8 mol%, TiO_2 from 0.2 to 0.6 mol%, Al_2O_3 from 2 to 6 mol% , ZrO_2 from 0.1 mol% to 0.5 mol%, and it then decreases further with increase in the concentration of these dopents in the glass network. The XRD results reveal that the glasses chosen for the present study show high apatite layer forming ability to increase dopent content while reducing major constituent P_2O_5 in the glass matrix without affecting the concentration of CaO and Na_2O.

The **FTIR spectrum** before immersion shows some intense absorption bands at 526, 720, 900, 1105 and 1270 cm^{-1} and weak absorption at 1643, 2382 cm^{-1} and broad band of absorption peak around 3470 cm^{-1}. These bands are indicative of phosphate group occurrence in the glass network. The absorption band at around 526 cm^{-1} may be assigned by the harmonics of P–O–P bending vibration and also due to the deformation mode of PO^- groups. The peaks at 720 $cm^{-1}$and 900 cm^{-1} are due to symmetric and asymmetric stretching mode of

vibrations attributed to P–O–P bands, respectively. A peak at 1105 cm^{-1} is observed due to vibrations of the phosphate group (P–O) it might be because of P–O–Zn linkages. Here, a little intense band at around ~1270 cm^{-1} is ascribed to (O–P–O), which is the asymmetric stretching vibration of O–P–O bonds. Nearly, at around 1643 cm^{-1}, a weak intense band is assigned due to the presence of P–O–H bridge. These groups form the strongest hydrogen bonding with non-bridging oxygens. The IR band located in the range of 2382 cm^{-1} is weak due to a stretching vibration of P–O–H group or stretching of CO_2. A broad band absorption peak at around 3470 cm^{-1} is due to the presence of water molecules in the glass structure. The presence of water is probably due to the absorption of atmospheric moisture by the phosphate glass sample or pellet resulting in the appearance of H–O–H band belonging to water molecules, because the sample per se has no water as a unit in the network. After immersion of glasses for 3, 7, 14 and 21days in SBF solution, an additional prominent absorption band representing hydroxyapatite layer (556 to 560, 664,734 to 739, 914 to 920, 1114 to 1120, 1274, 1290 cm^{-1}), carbonate (C) and hydroxyl (OH) groups (1404–1406, 1460, 1552, 1636-1641, 1650, 2096, 2850, 2928–2930, 3230, 3410–3426 cm^{-1}) emerges along with the fore mentioned bands in untreated glass samples. This indicates the formation of HAp layer over the surfaces of glass samples. Moreover, it is also observed that with the increase of dopent content and immersion time the intensity of absorption peaks related to apatite is pronounced, confirming the development of crystallized apatite layer over glass surfaces. These results tally very well with XRD analysis.

The **SEM-EDS** of ZnO, TiO_2, Al_2O_3 and ZrO_2 doped phosphate based bioglasses are clearly visualised and before immersion all glass samples exhibited smooth surfaces with dense glass morphology. This is also confirmed by the intensity peaks related to the elements (Zn, Ti, Al, Ca, Na, Zr, P and O) present in the EDS spectra matches with the chosen bioglass system constituents with maximum ratios. After 3days of immersion, a new layer containing white flakes type of structure is formed on the glass surface and is known as hydroxyapatite layer, which is the main building block to bond the bone and implant material in the body. The crystalline hydroxyapatite layer formation was confirmed by XRD and FTIR results. As immersion time increases, the morphology on the surface of the glasses has also changed. We can see the conversion of flake type structure to dense foam type of structure after 14days and 21days of immersion time where the glass surface is completely covered by uniformly formed apatite layer. This is due to the leaching of Ca^{2+}, Na^{+} and P^{5+} ions from glass to solution, migration of ions from solution to surface of the glasses. From EDS, the stoichiometric ratios (Ca/P) calculated range from 1.65 to 1.89 for the chosen bioglass samples associated with

SBF solution, which are almost equivalent to bone composition. This confirms the rich layer formation and leads to high bioactivity of the chosen glasses. These results are in agreement with the XRD and FTIR results.

The **degradation or weight loss** of all bioglasses is found to decrease with increase in immersion time and it also changes with doping concentration of transition metal oxides. An abrupt increase in weight loss is detected following three days of immersion of the sample in water, which is due to rapid release of ions from the glass sample to SBF solution. Much later though, a tiny weight loss of all samples was found to increase at 7, 14 and 21 days of incubation period. Base glass (ZnO doped) displays high dissolution rate when compared with TiO_2, Al_2O_3 and ZrO_2 doped glasses. Out of all glasses 0.7 mol% ZrO_2, 0.6 mol% TiO_2 and 10 mol% Al_2O_3 doped glasses exhibited low weight loss. This considerable low weight loss is due to reduction of ion release from the samples. For the duration of degradation procedures the release of Ca^{2+}, PO_4^{3-}, Na^+ and Zr^{4+} , Ti^{4+}, Al^{3+} ions into the surrounding SBF medium causes dissolution of glass, which results in super saturation of calcium and phosphate and leads to the formation of HAp layer. It is well known that the release rates of Ca^{2+} and PO_4^{3-} from biomaterials are associated with bioactivity.

There is a noticeable change in pH values of all glass samples with different days observed between (0, 3,7,14 and 21days) of immersion due to ion leaching. A sudden increase in pH values is 7.4 (0days of initial SBF) and 7.56 of immersion of all samples. Moreover, within 3days of incubation the pH values also increase with increase in content of ZnO, TiO_2, Al_2O_3 and ZrO_2. Noticeable decrease in pH values becomes conspicuous at 7 days, 14 days and 21 days of incubation time. The pH value of residual SBF solution measured at regular intervals of immersion time reported a trend similar to that of weight loss for all glasses on which research was carried out.

The cell cultural studies confirmed that, cell viability enhances for all bioglass samples compared with the plastic control. The cell viability enhances with increase in ZnO content up to 8 mol% with respect to control, implying the possible ionic effects on *rMSCs* viability. Afterwards, it is found to decrease slightly with an increase in concentration of ZnO at 10 mol% for 1 day and further decreases in case of 3 days of culturing. The viability and proliferation of cells in 6 mol% sample bestowed significantly higher values compared to other Al_2O_3 doped samples. Moreover, proliferation rate of cells at a concentration of 6 mol% showed alleviation after culturing it for 72 hours. Proliferation enhances with time and also based on TiO_2 content of 0.6 mol% in the solution; later, it decreases slightly. ZrO_2 doped

glasses showed significantly higher cell viability at 24 h and 72 h of culture except Zr.7. It was also noticed clearly that in addition to ZrO_2, up to 0.5 mol% cell viability improved and then reduced gradually with further increase in content of ZrO_2. Among all Zirconia doped bioglasses 0.5 mol% ZrO_2 glass possessed highest cell viability and proliferation. It may be due to ionic effect indicating cell viability with the rat mesenchymal cells. The increase in proliferation is ascribed to the release of Zr^{4+}, Ti^{4+}, $Al^{3+}$and Zn^{2+} ions effectively regulated by glass network and the decreasing rate of cell proliferation after 3 days might be due to gradual densification of glass network.

The **antibacterial activity** of ZnO, TiO_2 and ZrO_2 doped phosphate based glasses were tested against bacteria *E. coli*, *S. aureus* and *P.* aeruginosa using agar diffusion disc and optical density (OD) methods. ZnO doped glasses showed clear inhibitory zone indicated by transparent zone against *E. coli* and S. aureus. It was also noticed that the antibacterial activity of *E.Coli* was more pronounced compared to *S. aureus* for the given glass samples. The antibacterial tests of TiO_2 doped bioglass against *E. coli employing* an agar diffusion plate attest to the formation of antibacterial effective zone around the sample, which is observed after 7h. On the other hand, stifling the growth of *E.coli* with increase in Ti concentration reduces OD of the bacterial solution. The decrease in OD dictates antibacterial activity of as-prepared glasses. In case of ZrO_2 doped glasses, the bacterial growth of *E. coli* was inhibited significantly, as indicated by the transparent zone. The highest zone of inhibition was shown by Zr.3 and Zr.5 against S. Aureus and *E. coli* respectively after 24 and 48 hours respectively. Both agar disk diffusion assay and optical density measurements confirm ZnO, TiO_2 and ZrO_2 doped samples exhibited good antibacterial effects.

7.3 Scope for future work:

✓The prepared phosphate-based glasses made by controlled heat-treatment can be converted to their glass-ceramics.

✓ The phosphate glasses developed further can be investigated more comprehensively in terms of mechanical behavior.

✓ In a detailed study on biocompatibility, we can experiment more deeply with in-vivo animal models.

✓ Finally, based on in-vitro and in-vivo results, clinical trials for tissue-related engineering applications will be implemented on more proximal animals in the future.